July 2012

An Anatomical and Functional Characterisation of the Avian Centrifugal Visual System:

A feedback pathway from the brain to the retina

Christopher Mark Dillingham

Visual Neuroscience and Molecular Biology Group

Submitted to Cardiff University for the Degree of Doctor of Philosophy

Cardiff University School of Optometry and Vision Sciences

CARDIFF UNIVERSITY
PRIFYSGOL CAERDYDD

Acknowledgements

First and foremost, I would like to acknowledge the great contributions and support of my supervisors Jon Erichsen and Jez Guggenheim and thank them for giving me this opportunity.

Secondly, I thank Nick Wright and Jane Heath for taking the time out to introduce me to a number of techniques.

Thirdly, I would like to acknowledge joint OPTOM and BBSRC funding as well as additional support from the OPTOM research council for my trip to Cold Spring Harbor Labs, Stony Brook University and the Gordon Conference on eye movements in the University of New England.

Forthly, I would like to thank Debbie Mason, Jim Ralphs and Alvin Kwan for such a positive introduction to academia. In addition, for various reasons, I would like to thank John Wild, Paul Murphy, Carsten Müller, Craig Evinger, Wayne Kuenzel, Dom Miceli and remember Walter Woodson and Josh Wallman.

Finally I would like to thank Freyja, the chicks, the pigeons (particularly pigeon-117), and my Parents, for one, or more, of the following:

- Being patient.
- Being helpful.
- Being well-behaved.
- Being supportive.
- Keeping your eyes open.

Summary

The centrifugal visual system (CVS) is a feedback pathway of predominantly visual information from the brain to both eyes, but principally to the contralateral retina. The CVS is often considered to be something of a peculiarity, regarded as being specific to birds (*Aves*). Indeed, so-called 'higher' vertebrate species are assumed not to even possess such a centrifugal pathway when, in fact, an efferent projection to the retina has been conclusively demonstrated in all vertebrate groups (including humans).

Perhaps this point of view reflects the lack of progress made in the elucidation of function in the bird, the dominant model for CVS research in the 120 years since being first described. In the series of experiments presented here, I have begun to investigate the role of the CVS in the modulation of eye growth. In addition, I have addressed a number of unknowns that exist regarding the midbrain connectivity of the CVS.

In a series of four parallel lesion experiments, the centrifugal efferent pathway to the retina was unilaterally disrupted in post hatch chicks, raised under different developmental conditions. Under normal visual conditions but in the absence of centrifugal efferents, eyes contralateral to the lesion developed shorter eyes and moderate, relative hyperopia (long-sightedness). In contrast, under constant light conditions, *ipsilateral* eyes became significantly shorter than fellow (i.e. contralateral) eyes. Compensation for, and recovery from, plus and minus lens-imposed defocus in contralateral eyes was largely unaffected.

Centrifugal efferents emanate from two distinct midbrain populations: the isthmo-optic nucleus (ION) and the surrounding scattered cells within the ectopic area (EA). From experiments using pathway tracing techniques, I have demonstrated that, unlike cells of the ION, EA cells do not receive input from primary visual areas. In addition I present evidence for a possible 'cross-talk' pathway between centrifugal cells on either side of the midbrain, and discuss its potential involvement in the normally symmetrical eye growth.

Contents

List of figures

Chapter 01

Chapter 02

Chapter 03

Chapter 05

Chapter 06

Chapter 07

Chapter 08

Chapter 09

List of Tables

Chapter 5

Chapter 6

Chapter 7

Chapter 8

Abbreviations

5-HT	serotonin
AAC	association amacrine cells (of Cajal)
AC	anterior commissure
ACD	anterior chamber depth
ANOVA	analysis of variance
AOS	accessory optic system
AP	area pretectalis
AP	anterior-posterior axis
Aq	aqueduct
AXL	axial length
BC	brachium conjunctivum
CI	confidence interval
CL	constant light
CNIV	trochlear nerve
CNS	ciliary nerve section
CR	corneal radius of curvature
CtB	cholera toxin subunit B
CtB-488	cholera toxin subunit B conjugated to Alexa-fluor 488
CVS	centrifugal visual system
D	Dioptres
DAB	3,3' diaminobenzidine
dCNIV	decussation of the trochlear nerve
dH2O	distilled water
dLGN	dorsal lateral geniculate nucleus
DPT	days post treatment
dRGC	displaced retinal ganglion cell
DSGC	direction sensitive ganglion cell
DV	dorsal-ventral axis
DW	Dekalb White
EA	ectopic area
FB	Fast Blue
FDM	form deprivation myopia
FLM	fasciculus longitudinalis medialis
GABA	gamma aminobutyric acid
GCt	substantia grisea centralis
GLd	nucleus geniculatus lateralis pars dorsalis
HRP	horseradish peroxidase
Imc	nucleus isthmi magnocellularis
INL	inner nuclear layer
ION	isthmo-optic nucleus
IOTC	isthmo-optic target cell
IOTr	isthmo-optic tract
Ipc	nucleus isthmi parvocellularis
IPL	inner plexiform layer
IR	infra-red
LC	nucleus linearis caudalis
LED	light emitting diode
LLd	nucleus lemnisci lateralis pars dorsalis
LMmc	nucleus lentiformis mesencephalic, pars magnocellularis
LoC	locus ceruleus

LT	lens thickness
ML	medial-lateral axis
NADPH	nicotinamide adenine dinucleotide phosphate
nBOR	nucleus of the basal optic root
NHS	normal hose serum
NL	normal light
NO	nitric oxide
NOS	nitric oxide synthase
nIV	trochlear nucleus
OLM	outer limiting membrane
ONL	outer nuclear layer
ONS	optic nerve section
OPL	outer plexiform layer
OPT	nucleus opticus principalis thalami
PB	phosphate buffer
PBS	phosphate buffered saline
PC	posterior commissure
PC	personal computer
Q (1-4)	quartile
RGC	retinal ganglion cell
RITC	rhodamine isothiocyanate
RPE	retinal pigment epithelium
RT	nucleus rotundus
SAC	starburst amacrine cell
SB	Shaver Black
SD	standard deviation
SE	standard error of the mean
SGC	stratum griseum centrale
SGFS	stratum griseum fibrosum et superficiale
SLu	nucleus semilunaris
SOP	stratum opticum
T(1-3)	tertiles
TBS	tris-buffered saline
TC	tectal commissure
T-C	treated minus control
TeO	optic tectum
TeO_v	visual layers of optic tectum
TeO_m	motor layers of optic tectum
TH	tyrosine hydroxylase
TNS	tris buffer, no salinity
TTX	tetrodotoxin
TXTBS	tris-buffered saline with Triton-X100
UV	ultraviolet
VCD	vitreous chamber depth
VW	visual wulst
V1	primary visual cortex
WGA	wheat-germ agglutinin
WL	White Leghorn

Chapter 01

Introduction to the visual system

1.0 Overview

In this, the first of two introductory chapters, the relevant components of the vertebrate visual system will be described in order to establish the anatomical and functional foundation for a review of the centrifugal visual system (CVS). The CVS is a highly organised (i.e. topographically and anatomically) visuomotor system centred on an excitatory projection to the retina, which exists in all vertebrate groups (Réperant et al., 2007), including humans (Honrubia and Elliott, 1968). Two avian animal models were used in the experiments described in Chapters **6** to **9**: The post-hatch chicken (*Gallus gallus*) was used for a series of studies into eye growth and the adult pigeon (*Columba livia*) was used for an investigation into the anatomical connectivity of the CVS. As such, a particular focus of the introductory information below is directed towards the avian visual system and the differences/analogies that exist between it and the mammalian visual system.

1.1 Gross ocular anatomy

The structure of the eye can be represented as a tri-laminar structure with: the outermost layer, the sclera, a tough outer shell of the eye; the middle layer, the uveal tract and the inner layer, the retina (Kolb, 1995). The posterior segment can be considered as a continuation of the meningeal layers of the CNS (Nolte and Angevine, 2000). The outer layer of the globe, the sclera, is an extension of the *dura mater* extending posteriorly from the eyeball as the sheath of the optic nerve. The anterior one sixth of the outer layer, the cornea, is specialised to allow the passage of light, with transition of the sclera to the transparent cornea occurring at the limbus. The middle layer, the uveal tract, contains the vascularised choroid and is equivalent to the arachnoid and pia mater. The uveal tract extends anteriorly to the ciliary body and the stroma of the iris, again at the level of the limbus. The ciliary body contains the ciliary muscle that is involved in modulation of the refractive properties of the crystalline lens, i.e. accommodation (Pocock and Richards, 2004). The inner-most layer, the retina and the optic

nerve to which it gives rise represent the grey and white matter of the brain, respectively (Nolte and Angevine, 2000).

1.1.2 Avian ocular specialisations

The eyes of birds (as a function of body weight), are on average 36% larger than other vertebrate groups (Howland, Merola and Basarab, 2004). The barn owl has an axial length (i.e. the distance from the anterior surface of the cornea to the anterior surface of the retina) that is almost twice the size as that predicted by body weight (Harmening and Wagner, 2011) (**Fig. 1.1 B**). Optically, axial length determines the area over which an image of an object is focused. An increased axial length enhances spatial resolution by increasing the area (and importantly the number of photoreceptors), over which an image is spread (Zeigler and Bischof, 1993). In birds, nocturnality is a strong predictor of both eye and brain size (Garamszegi, Moller and Erritzoe, 2002). In general nocturnal species have large eyes (relative to body weight), which are specialised for increased light sensitivity, i.e. capturing photons. Morphologically, increased light sensitivity is achieved in ocular design by an increased corneal diameter to axial length ratio (Fite, 1973; Hall and Ross, 2007). In contrast, diurnal birds tend to exhibit an attenuated corneal diameter to axial length ratio for enhanced spatial resolution (**Fig. 1.1 A**). Certain nocturnal birds, e.g. predatory species such as owls (*Strigiformes*), exhibit both increased corneal diameter *and* elongated axial lengths (Zeigler and Bischof, 1993) (**Fig. 1.1 B**), and thus, to a degree compromise image brightness for increased visual acuity. Such an optical design results in the distinct tubular ocular morphology shown in **Figure 1.1** (Walls, 1942; Fite, 1973; Harmening and Wagner, 2011). Notable exceptions to this relationship include flightless nocturnal species, e.g. Kiwis (*Apterydidae*), which exhibit a far smaller eye size than would be predicted by avian body weight, and instead show a greater dependence on olfactory and tactile modalities (Martin et al., 2007).

As well as gross ocular morphology, bird eyes exhibit a number of specific anatomical adaptations, e.g. avascular retinae. In the absence of retinal blood vessels, a specialised highly vascularised region of the posterior uveal tract, the pecten oculi, protrudes deep into the vitreous chamber (**Fig. 1.1 A**) and provides nutrition and oxygenation to neurons of the outer retina instead (Wingstrand and Munk, 1965). This particular example will be elaborated upon in **Section 1.6.2**.

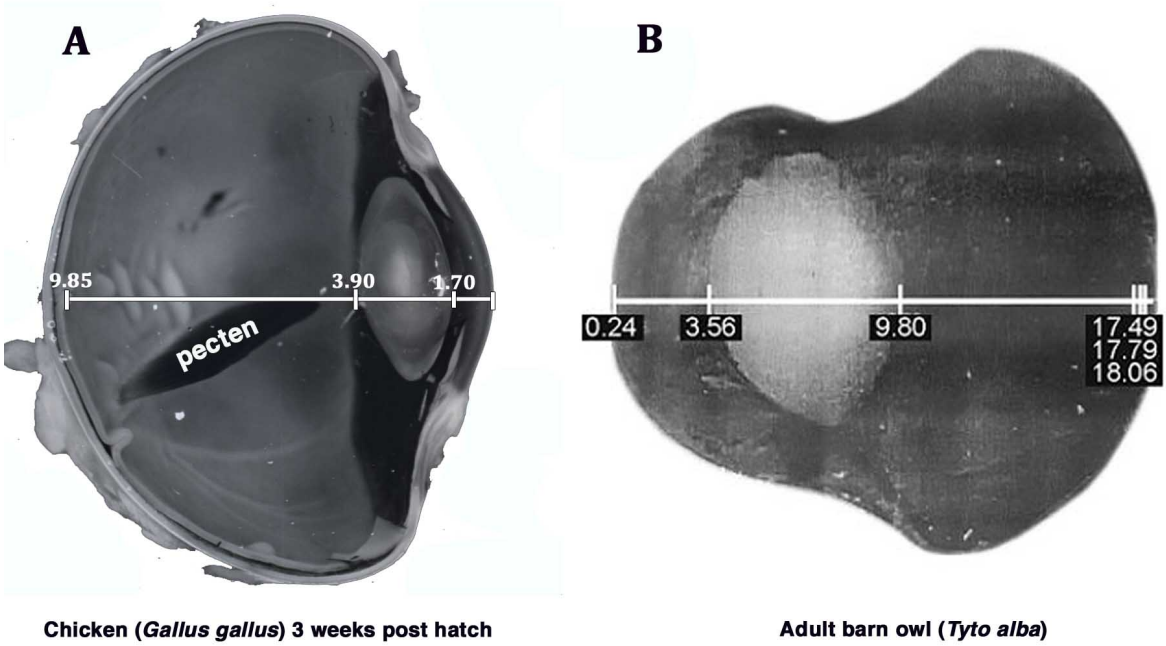

Fig. 1.1. **Ocular morphology of diurnal and nocturnal bird species. (A)** Ocular morphology of a diurnal bird species (chicken, *Gallus gallus*) and **(B)** a nocturnal species (barn owl, *Tyto alba*)**.** Note the extension of the pecten oculi into the vitreous chamber from the posterior uveal tract in **A.** Ocular dimensions are in millimetres. Image **A** is taken from Erichsen et al. (2002) and Image **B** is taken from Harmening and Wagner (2011).

A second example of avian ocular adaptation is in accommodation, i.e. the ability of an eye to vary its focal power in order that a retinal focal position be maintained for targets located at varying distances from the eye (Sivak, 1980). While accommodation in mammals is achieved by the action of the ciliary muscle upon the lens alone, in birds it has been shown that, in addition, ciliary muscle contraction exerts a backward force on the inner lamella of the cornea

via Crampton's muscle (**Fig. 1.2a**). This in turn acts to flatten the *peripheral* cornea and steepen the *central* cornea in a manner that can account for approximately a third of the accommodative power of the eye (Glasser, Troilo and Howland, 1994). Thus, in birds, accommodation is achieved through both changes in crystalline lens thickness and corneal curvature in contrast to mammals that use the lens alone (Gundlach, Chard and Skahen, 1945).

A number of eye adaptations serve to make avian accommodation particularly effective: **1**) An annular pad that surrounds the equator of the lens, **2**) a direct connection between the ciliary muscle and the lens annulus and **3**) the scleral ossicles that are situated around the cornea-sclera border (Zeigler and Bischof, 1993; Franz-Odendaal, 2006) (**Fig. 1.2b**). These components all act to provide effective transmission of ciliary muscle action directly onto the lens. In addition, it is thought (and seems logical), that the scleral ossicles are important in maintaining the aspherical shape of the eye (**Fig. 1.1**), and thus contribute to the optimum balance of high acuity and light sensitivity (Walls, 1942).

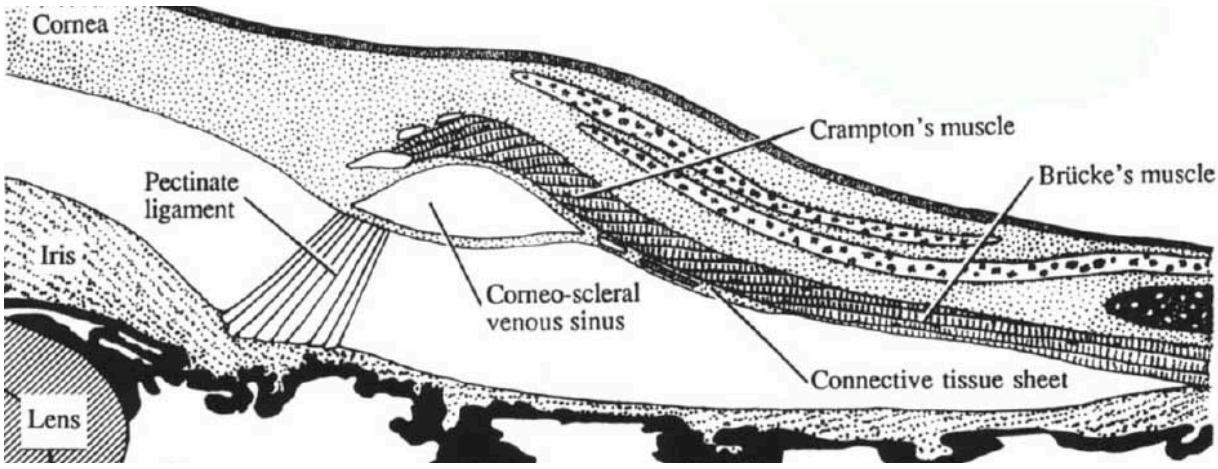

Fig. 1.2a. Anatomy of the avian corneo-scleral border. Site of action of corneal accommodation that occurs via contraction of the ciliary muscle upon Crampton's muscle, which exerts an inward force on the inner corneal lamella. Such an organisation in birds allows for greater accommodative power through associated changes in corneal radius of curvature. Taken from Glasser et al. (1994).

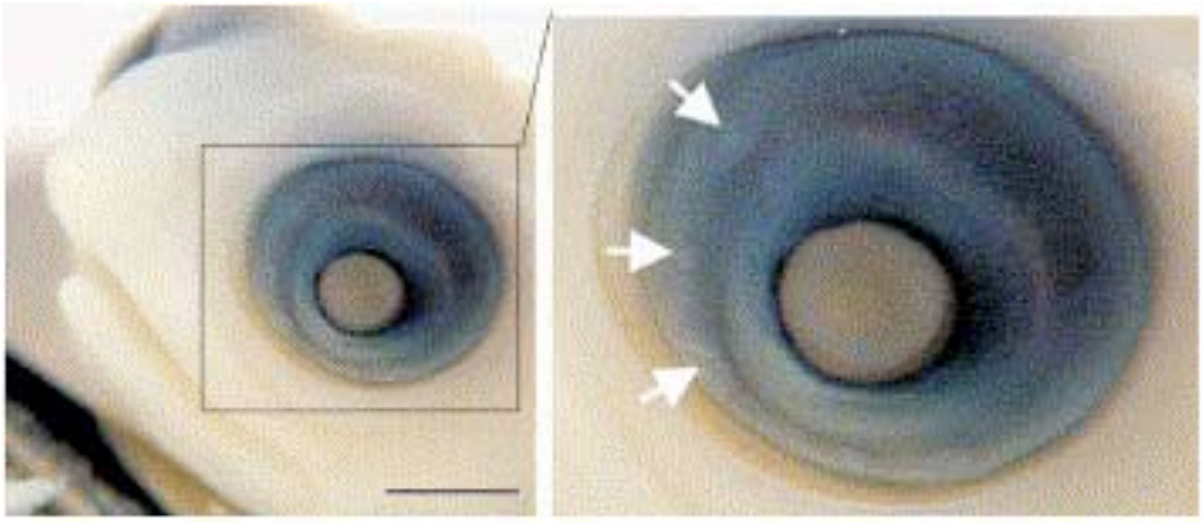

Fig. 1.2b. The developing scleral ossicles of the snapping turtle. (*Chelydra serpentina*). An adaptation common to sauropsids (i.e. a groups of amniotes including birds and reptiles), which is important for effective transmission of ciliary muscle action to the lens during accomodation. Taken from Franz-Odendaal (2006).

Walls (1942) showed that Crampton's muscle was reduced (or absent) in aquatic birds presumably as corneal accommodation would be negated in water (Levy and Sivak, 1980). Studies of the accommodative power of aquatic bird species have demonstrated the ability for large accommodative changes in the order of 50 Diopters (D) in order to compensate for the induced hyperopia (long-sightedness) that results from an air to water transition. Such aquatic bird species are able to remain 'emmetropic' in both conditions (Goodge, 1960; Levy and Sivak, 1980). To put these figures in context, a typical non-aquatic species, e.g. the pigeon, has an accommodative range of only ~17 D (Gundlach et al., 1945).

1.2 Organisation of the Retina

In all vertebrates, the innermost layer of the posterior eye is the retina, comprising the retinal pigment epithelium (RPE) and the neural retina. In mammals, the retina is developmentally derived from the presumptive diencephalic region of the embryonic prosencephalon. From a visual processing perspective, the diencephalon houses the 'relay neurons' of the thalamus

(dLGN) that transmit visual information to the visual cortex (V1) in a highly ordered, topographic manner (Jeffery, 1985; Huberman, Feller and Chapman, 2008). Two classes of photosensitive cell (rods and cones), adapted to absorb specific intensities and wavelengths of light, are present (Schultze, 1866; Müller, 1872). These contain photosensitive pigment within their outer segments, a region characterised by a stacked membranous disk arrangement. The retina is a highly organised, laminated structure contacted on its inner surface by the vitreous humor and by the choroid on its outer surface (Kolb, 1995). The outermost layers of the retina, i.e. those most proximal to the choroid, house the outer segments of the photoreceptors. Rods are highly sensitive to light whilst cones, named because of their progressive distal tapering of the membranous outer segment discs to a point, are less sensitive, while all rods are sensitive to the same range of wavelengths of light, different cone types contain photosensitive pigments with specific absorption spectra (Ahnelt and Kolb, 2000), a factor crucial in chromatic vision. The inner and outer segments of the photoreceptors are situated in the outer segment layer, subjacent to the RPE and their somata are situated in the overlying outer nuclear layer (ONL). The outer limiting membrane (OLM) defines the division between these two layers (Remington, 2005).

The RPE is a multifunctional, pigmented layer situated between the photosensitive outer segments of the photoreceptor layer in the neural retina above, and the choroid below, i.e. towards the sclera (Strauss, 1995b). The development and function of the RPE and photoreceptors are highly interdependent, with perhaps its main or most obvious function being the absorption of scattered light and thus improving the optical quality of the eye. The RPE has a second major metabolic role in the renewal of the photoreceptor outer segments (Strauss, 1995a). Phagocytosis of outer segments, as well as the subsequent homeostatic demands that are presented by the high rate of outer segment turnover, require effective protection against the effects of oxidative stress. This is in part achieved at the boundary of the RPE with the choroid, as defined by Bruch's membrane (Remington, 2005), which not only

provides for the high and specific metabolic demands of the outer retina but is also important in dissipating away from the retina the heat resulting from light absorption by melanosomes within the RPE (Strauss, 1995a). The soma of photoreceptors extend neuronal processes into the outer plexiform layer (OPL), within which dendrites of bipolar and horizontal cells also project, forming a complex connectivity for transmission of photoreceptor activity towards retinal ganglion cells (RGCs). The pattern of synapses formed between one or more photoreceptors with bipolar cells and horizontal cells (in the ONL) and, subsequently, the way in which bipolar cells and amacrine cells (which are situated within the inner nuclear layer (INL)), interact with retinal ganglion cell dendrites (within the inner plexiform layer (IPL)) is crucial in determining the receptive field properties of RGCs (Field and Chichilnisky, 2007) (**Fig. 1.5**).

1.2.1 Retinal interneurons

1.2.1.1 Bipolar cells

In the OPL, individual photoreceptor response signals are conveyed to numerous bipolar cells, which in turn contact RGCs in the IPL. At least ten types of bipolar cell are thought to exist (Boycott and Wassle, 1991; Euler and Wassle, 1995), nine of which are driven by cone input (Field and Chichilnisky, 2007). Furthermore, each cone is likely to drive one of each type of bipolar cell (Grunert, Martin and Wassle, 1994). Thus, the divergence of photoreceptor, predominantly cone, signals onto numerous distinct bipolar cell types forms the basis of numerous functionally distinct, parallel pathways, which are an important feature of visual information processing (Wassle, 2004).

1.2.1.2 Amacrine cells

'Axon-less' inhibitory retinal interneurons are situated in the INL, with processes extending into the IPL, i.e. amongst bipolar-RGC synapses. Over fifty distinct amacrine cell types exist

(MacNeil et al., 1999), with almost all types localising GABA or glycine but, in addition, co-localise a vast array of other neurotransmitters (Kolb, 1997), e.g. serotonin, dopamine and acetylcholine. For that reason, only a very broad description of their function can be given to amacrine cells as a group, i.e. modification of bipolar cell-RGC connectivity. Specific classes of amacrine cells will be discussed in depth in later sections (e.g. the target amacrine cells of centrifugal efferents in the retina) however, as a group, perhaps their most striking feature is their morphological diversity (Mariani, 1982; Kolb, 1997) (**Fig. 1.3**).

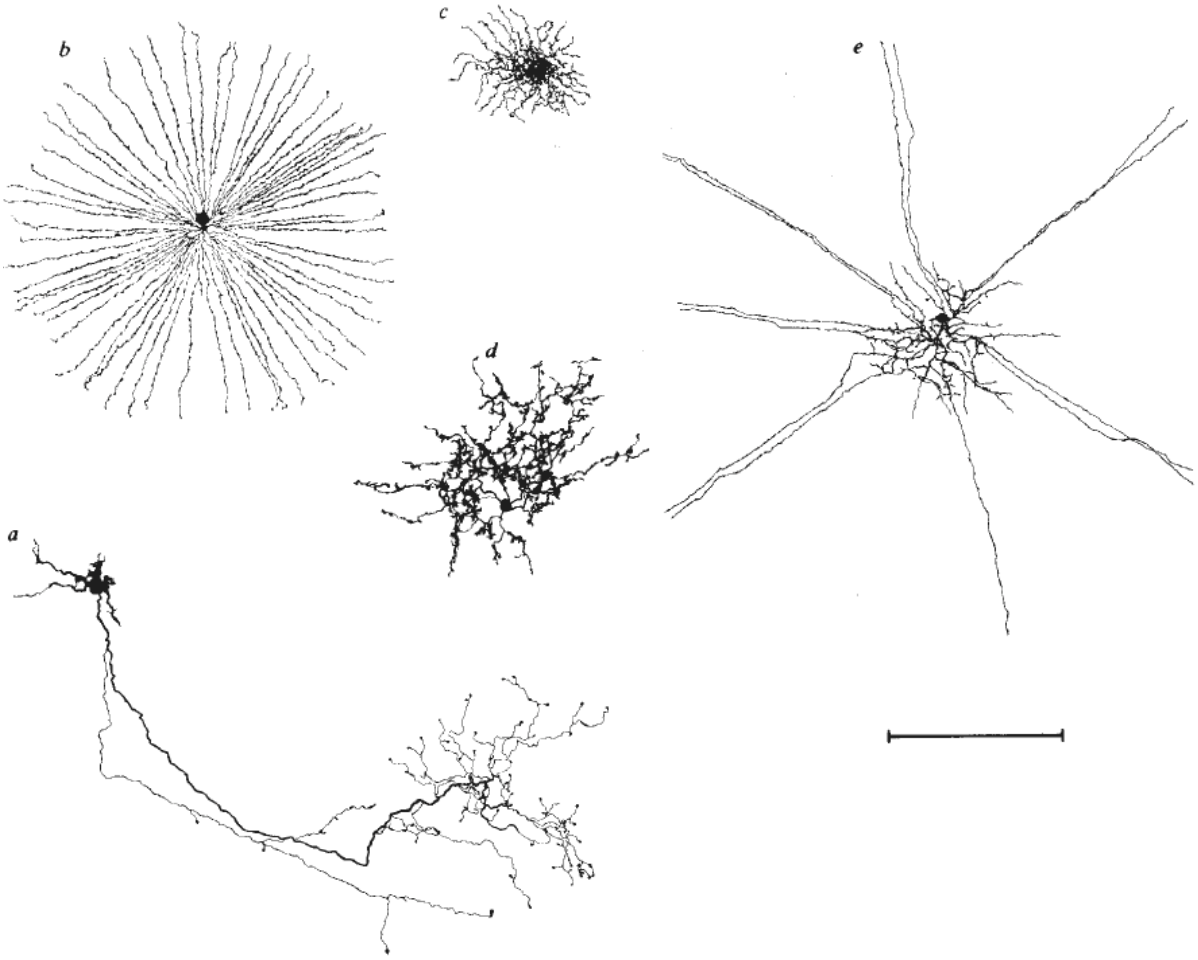

Fig. 1.3. Amacrine cell morphology. Drawings of Golgi-impregnated amacrine cells from the flat-mounted pigeon retina highlighting the diversity in morphology of amacrine cells. (**b-e**) 'Ordinary' amacrine cells that lack an axon and a exhibit radial symmetry; (**a**) an association amacrine cell showing morphological polarisation and a distinct intra-retinal axon. Taken from Mariani (1982). **Scale bar = 100 μm.**

Further, it may be the case that specific amacrine cell types target distinct RGC populations, suggesting that the amacrine cell 'design' is tailored towards determining the response properties of a given RGC, e.g. asymmetric inhibition of ganglion cells by starburst amacrine cells to produce direction selective responses within the retina in some 'lower' vertebrates, e.g. the pigeon (Maturana and Frenk, 1963) and rabbit (Barlow and Hill, 1963) (**Section 1.3.2**).

1.2.1.3 Horizontal cells

These are retinal interneurons with laterally directed processes that extend into the OPL where they contact the inner segments of numerous photoreceptors. Horizontal cells are thought to contribute to the formation of the inhibitory surround of the classical centre-surround receptive fields of bipolar cells and RGCs (Dacey, 1999), a mechanism believed to be based upon inhibitory GABAergic termination on the peripheral photoreceptors of a horizontal cell's receptive field, which thus reduces the ability of neighbouring photoreceptors to respond to light stimuli, i.e. lateral inhibition. However, more recently, this mechanism has been challenged. According to an alternative view, horizontal cells act to modulate, rather than inhibit, photoreceptor responses through glutamate release (Hirano et al., 2007). Three types of horizontal cell (HI, HII and HIII) have been identified. HI cells synapse with rods and cones, HII cells contact cones alone and HIII are specific to red and green cones (Kolb, Mariani and Gallego, 1980; Remington, 2005).

1.2.2 Retinal ganglion cells (RGCs)

Classically, three types of vertebrate RGC exist. The terminology for these subtypes varies across species, e.g. in monkeys they are labelled as midget, parasol and small bistratified types. In carnivores these subtypes are called X, Y and Z, (or beta, alpha and gamma, respectively) (Field and Chichilnisky, 2007). Historically, the distinction of RGC type was based upon both morphology and response characteristics. Since this initial classification, modern anatomical and genetic techniques have made it possible to identify at least 17 distinct RGC types

(Dacey, 2004; Coombs et al., 2006; Huberman and Niell, 2011). The intra-retinal circuitry that underlie 3 of the RGC types is shown in **Figure 1.4.**

So-called trigger cell characteristics determine the specific response properties of the centre-surround organisation common to all RGCs. Broadly, RGCs are divided into tonic and phasic types. Tonic RGCs, which correspond to midget, X, or beta cell types, are characterised by small centre receptive fields (as defined in part by the dendritic field spread of their dendrites into the inner plexiform layer), and respond with sustained excitatory responses to changes in light intensity. Tonic cell activity is processed via the parvocellular pathway, their axons terminating upon the parvocellular layers of the dLGN (Perry, Oehler and Cowey, 1984). Conduction of responses from tonic RGCs is slow and responsiveness is largest to high contrast stimuli. The phasic (or parasol) RGCs comprise roughly ten percent of the total population and form the basis of the magnocellular pathway, the axons of which terminate upon the magnocellular layers of the dLGN (Perry et al., 1984; Rodieck, Binmoeller and Dineen, 1985; Watanabe and Rodieck, 1989). Phasic RGCs have a faster response to larger, low contrast stimuli and comprise the principal pathways involved in dim, or 'mesotopic' light, i.e. scotopic vision. A third component, the small bistratified RGCs, were defined through their distinct dendritic morphology and trigger characteristics, which did not conform to the midget cell mould (Dacey and Lee, 1994). Small bistratified RGCs were found to convey a specific 'blue on/yellow off' signal to the koniocellular layers of the LGN that intersperse with the parvo- and magnocellular layers (Dacey and Lee, 1994; Martin et al., 1997; Field and Chichilnisky, 2007) (**Fig. 1.4**).

The term parallel processing is used to describe the manner in which the specific properties of visual input are conveyed to the brain, however the properties of these three types of RGC have in common a centre-surround receptive field arrangement. As has been alluded to, individual RGC receptive field properties are tuned to respond to the specific characteristics of

a given stimulus. For instance, an RGC that responds to movement of a stimulus in a given direction would be inhibited by movement in the opposite or null direction (**Fig. 1.6**).

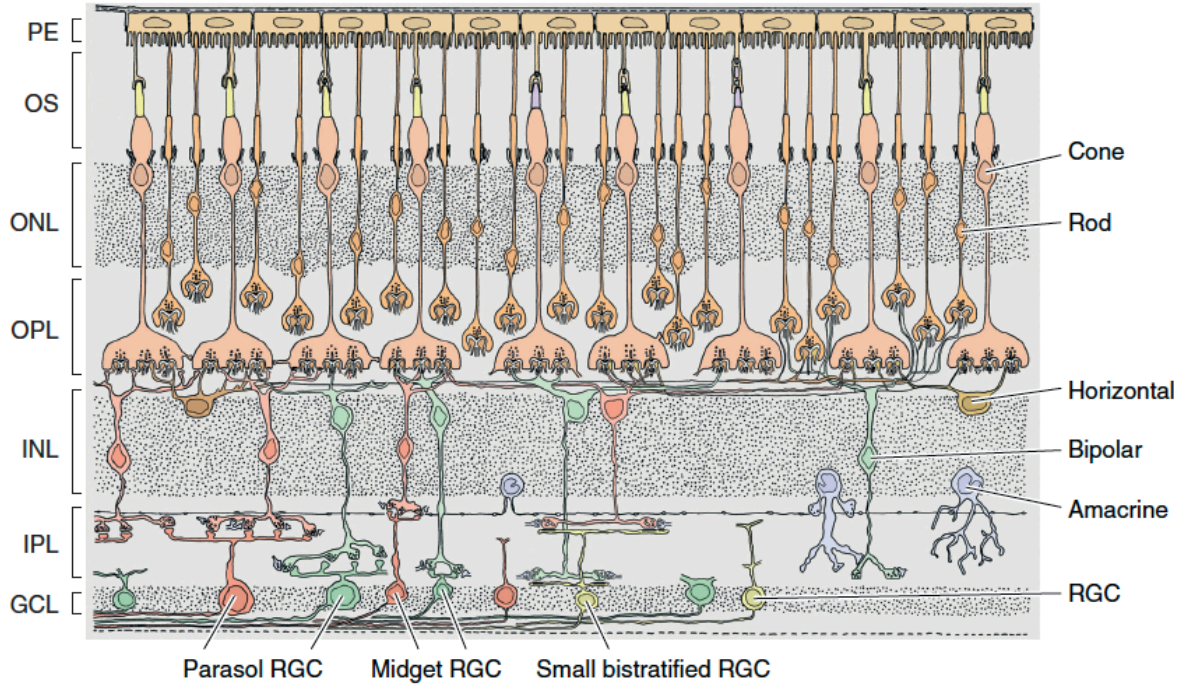

Fig. 1.4. Schematic of retinal architecture in cross-section. Five major cell classes exist in the retina, two of which, retinal ganglion cells and certain populations of amacrine cells, fire action potentials. Rod and cone photoreceptors transduce light into electrical signals, which are conveyed to retinal ganglion cells (RGCs) via 3 classes of retinal interneurons. Horizontal cells perform lateral processing through interactions with bipolar cells and photoreceptors, while amacrine cells similarly perform lateral processing, interacting with bipolar cells and RGCs. Bipolar cells integrate and convey photoreceptor signals to RGCs. Taken from Field and Chichilnisky (2007).

1.3 Receptive fields

1.3.1 'Simple' - So-called 'simple' receptive fields refer to the classic mutually antagonistic, concentric, 'on' or 'off' responses to light stimuli. Seminal work by Hartline and colleagues (Hartline, Wagner and Macnichol, 1952; Hartline, Wagner and Ratliff, 1956) (for which he was later awarded the Nobel prize) demonstrated that the principle of lateral inhibition is exhibited by neighboring ommatidia in the horseshoe crab (*Limulus polyphemus*).

Subsequently, Stephen Kuffler's work on both the frog and cat retinae [93] (Kuffler, 1953, 1973) led to the discovery of the on centre/off surround and off centre/on surround receptive fields of RGCs. On centre/off surround RGCs (or simply 'on-centre') are depolarised in response to illumination of the centre of their receptive field, while illumination of the peripheral receptive field would lead to hyperpolarisation and a decrease in firing response (**Fig. 1.5**).

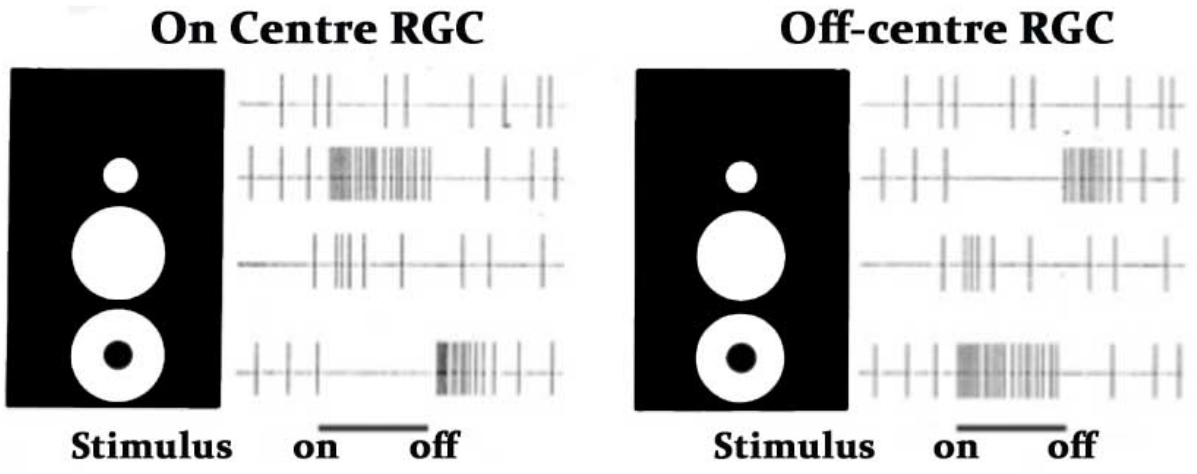

Fig. 1.5. Receptive field properties of on-centre and off-centre RGCs. On-center RGCs (**left**) respond maximally to a light stimulus (**white**) in the centre of the receptive field but are activity is inhibited in response to illumination of the receptive field surround. Off-centre RGCs (**right**) respond maximally to illumination of the receptive field surround but activity is inhibited by illumination of the receptive field centre. In both cases, if the receptive field centre, and surround are stimulated, a transient activity is induced (Kuffler, 1953).

Conversely, the response of the off centre/on surround RGCs to the same stimuli would be the opposite. Simultaneous stimulation of the centre and periphery of either on and off centre receptive fields causes equal inhibition and excitation inducing only a mild response (**Fig. 1.5**). The organisation of the centre-surround receptive field not only determines the response to a light stimulus but also visual acuity and contrast sensitivity. An RGC with a small on-centre field, e.g. a tonic or midget RGC (**Fig. 1.4**), would have a higher contrast sensitivity to a light spot on a dark background or white bars in a sine-wave grating than would an RGC type with

a larger dendritic tree area, e.g. phasic or parasol RGC. Thus, the relative space occupied by the centre and surround components in part defines the response properties of a cell.

1.3.2 'Complex' - 'Complex' receptive fields respond to specific components of a stimulus, e.g. its direction of motion or orientation. In this section, the direction selective ganglion cell (DSGC) is described as an example. In birds and amphibians, for example, the proportion of complex relative to simple receptive field RGCs is greater than that found in mammals such as cats and monkeys, owing to a higher relative density of amacrine cells to bipolar cells in the IPL (Dowling, 1968; Mariani, 1982). Of particular interest and relevance to this project, a study by Mariani (1982) proposed that a subtype of amacrine cell, i.e. Ramon y Cajal's association amacrine cells (AACs) that notably are the target cell of efferent centrifugal axons (Uchiyama and Stell, 2005) (**Section 1.5.2**), were a good candidate for providing the anatomical basis for direction selectivity. Because the response properties of DSGCs are tuned to both the direction of movement and velocity of a stimulus, a greater response may be elicited if the movement of a stimulus in a given direction is fast than if it is slow (Barlow and Hill, 1963).

On-off DSGCs do not distinguish their response to light or dark stimuli and thus receive both on and off bipolar input, while on-DSGCs receive only on-bipolar cell input and thus respond most vigorously to bright stimuli moving in the preferred direction. The interneuron connectivity that is able to generate the direction selective responses of DSGCs, in general, is dependent upon the type of bipolar cell type (ON or OFF) involved and a subtype of Class 1 (i.e. radially organised) amacrine cell (**Fig. 1.3**), the starbust amacrine cell (SAC) (Dong et al., 2004; Wei and Feller, 2011).

It is thought that the basis of directional preference in DSGCs is achieved through the pattern in distribution of excitatory (e.g. cholinergic/glutamergic) and inhibitory (GABAergic) synapses that SACs make with DSGCs (Briggman, Helmstaedter and Denk, 2011). While excitatory, cholinergic input from SACs to DSGCs is distributed more (but not entirely) evenly

across the dendritic field of a DSGC, the inhibitory, GABAergic terminal distribution upon the DSGC is biased towards a specific side or axis of its dendritic tree relative to the soma. The region of high GABAergic terminal distribution defines a null direction, i.e. stimulus motion into the receptive field of the DSGC from this direction would not elicit a response. So how is this achieved in terms of intra-retinal neural circuitry?

The current understanding is as follows. Importantly, SACs elicit a greater response to movement of a stimulus moving from the centre of its receptive field, outwards (centrifugal) as opposed to movement towards the centre of its receptive field (centripetal). Thus a centrifugal stimulus, i.e. moving in the preferred direction of an SAC, but in the 'null' direction of the DSGC would elicit a strong GABAergic response at SAC/DSGC terminals that would in turn induce a large dominant inhibitory response (cancelling out the concurrent excitatory cholinergic response). Therefore, there would be an overall suppression in the firing rate of the DSGC for movement in that direction. Conversely, stimulus movement in the preferred direction of an SAC and in the preferred direction of the DSGC would elicit a strong cholinergic response to the DSGC combined with a weak GABAergic response (owing to the reduced proportion of GABAergic terminals), the summation of which would induce a maximal rate of firing in the DSGC. The mechanisms by which glutamatergic and cholinergic input from bipolar cells and SACs, respectively, input to DSGC are direction selective (**Fig. 1.6**) are unknown, however, again, asymmetrical inhibition by SACs is proposed as one possibility (Wei and Feller, 2011).

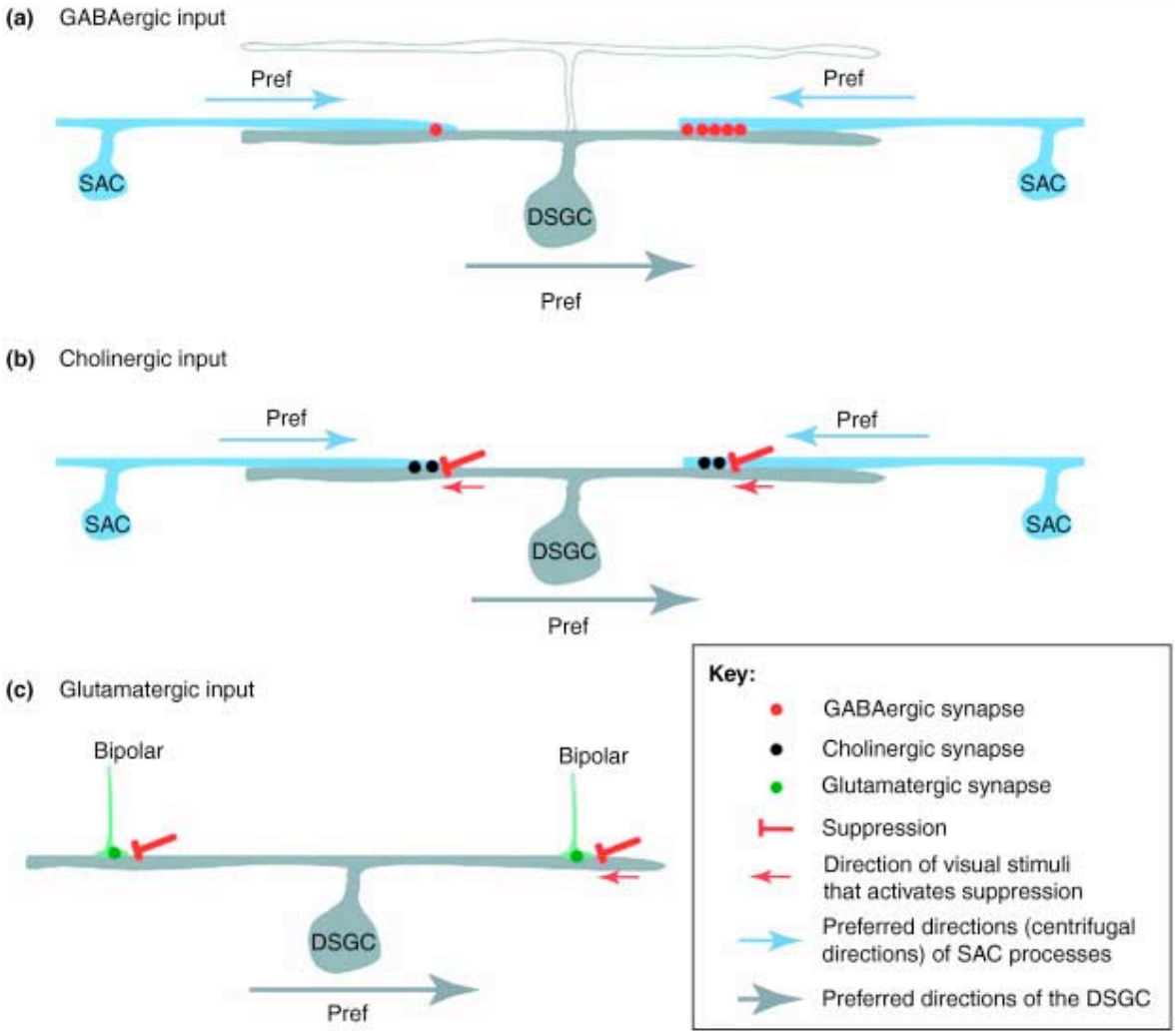

Fig. 1.6. The basis of direction-sensitive ganglion cells (DSGC) receptive fields. Directional preference in DSGCs is achieved through the pattern in distribution of excitatory (e.g. cholinergic/glutamergic) and inhibitory (GABAergic) synapses that starburst amacrine cells (SACs) make with DSGCs. Importantly**,** SACs elicit a greater response in response to centrifugal movement of stimuli (i.e. from the centre of the receptive field, outwards), than centripetal movement of stimuli, i.e. the opposite. Thus, the position of an SAC relative to the DSGC and the asymmetric distribution of excitatory and inhibitory terminals of SACs upon the DSGCs is crucial in determining the preferred directional specificity of the ganglion cell. GABAergic (**a**) and cholinergic interaction (**b**) of SACs, and glutamatergic interaction of bipolar cells (**c**) with DSGC dendrites to generate asymmetric responses to stimulus movement in preferred (**Pref**) and null directions. Taken from Wei and Feller (2011).

1.4 Visual pathways

Two parallel **retinofugal,** i.e. retinal efferent pathways, carrying visual information are common to the avian and mammalian visual systems. The **retino-tectal** pathway of non-mammalian amniotes is analogous to the mammalian superior colliculus-pulvinar-cortical projection while, similarly, the avian **retino-thalamic** pathway is homologous to the retino-geniculocortical pathway, (i.e. retina-dLGN-V1) in terms of function and connectivity (Karten, 1969; Shimizu and Bowers, 1999).

In mammals, the dominant visual pathway is the **retino-thalamic** pathway, while in birds this pathway is relatively underdeveloped and the **retino-tectal** pathway is perceptually dominant (Butler, 1994). Generally speaking, the **retino-tectal** pathway is directed towards the mediation of visuomotor behaviors, such as visual attention and orientation, while the **retino-thalamic** is involved in discrimination tasks such as fine detail, colour perception (Karten et al., 1973) and 'visual memory' (Shimizu and Hodos, 1989).

1.4.1 Retino-tectal pathway

In birds, the **retino-tectal** pathway is the dominant visual projection, with 90% of visual information being conveyed to retinorecipient layers 3, 4, 5 and 7 of the optic tectum (TeO) (Yamagata and Sanes, 1995), a structure analogous to the mammalian superior colliculus. A retinotopic map of the locations of salient stimuli exists within the superficial retinorecipient layers of the TeO (TeO_v). Deeper motor layers of TeO (TeO_m) receive other topographic sensory inputs, (e.g. somatosensory and auditory), as well as input from motor regions of the telencephalon, and are concerned with orienting movements in response to visually salient stimuli (Knudsen, 2011).

TeO_v and TeO_m overlap in layer 10 within which are situated tecto-isthmic neurons that project to the retinopetal neurons of the isthmo-optic nucleus (ION), i.e. the primary afferents

of centrifugal cells (**Section 1.5 onwards**). TeO_m neurons project to the nucleus rotundus (RT), which projects, in turn, to the entopallium of the telencephalon (Karten and Hodos, 1970) (**Fig. 1.7**). TeO_v layers project both to the ION and the nucleus principalis opticus thalami (OPT) (Remy and Gunturkun, 1991), the latter of which innervates the visual hyperpallium (an area specialised for analysis of visual features). Between the TeO_m and RT, a different organisation is established. Instead visual information is processed through at least five parallel channels of distinct visual 'attributes' (or response characteristics), in a manner analogous to the SC projection to the pulvinar nucleus in mammals. This reorganisation is maintained in the projection from RT to the entopallium, as has been shown electrophysiologically (Wang, Jiang and Frost, 1993), anatomically (Laverghetta and Shimizu, 2003) and behaviourally (Shimizu, Patton and Husband, 2010). For example, neurons of the anterior RT exhibit an increased response to colour and luminance features of a stimulus, while central and posterior areas are more responsive to moving stimuli (Wang et al., 1993; Shimizu et al., 2010). Anatomically, the parallel channels of the RT were mapped upon the entopallium in the anterior-posterior axis (**Fig. 1.7**). Moreover, the entopallium in turn projects to more anterior regions of the telencephalon, within which parallel channels are processed separately (Husband and Shimizu, 1999) (**Fig. 1.9**).

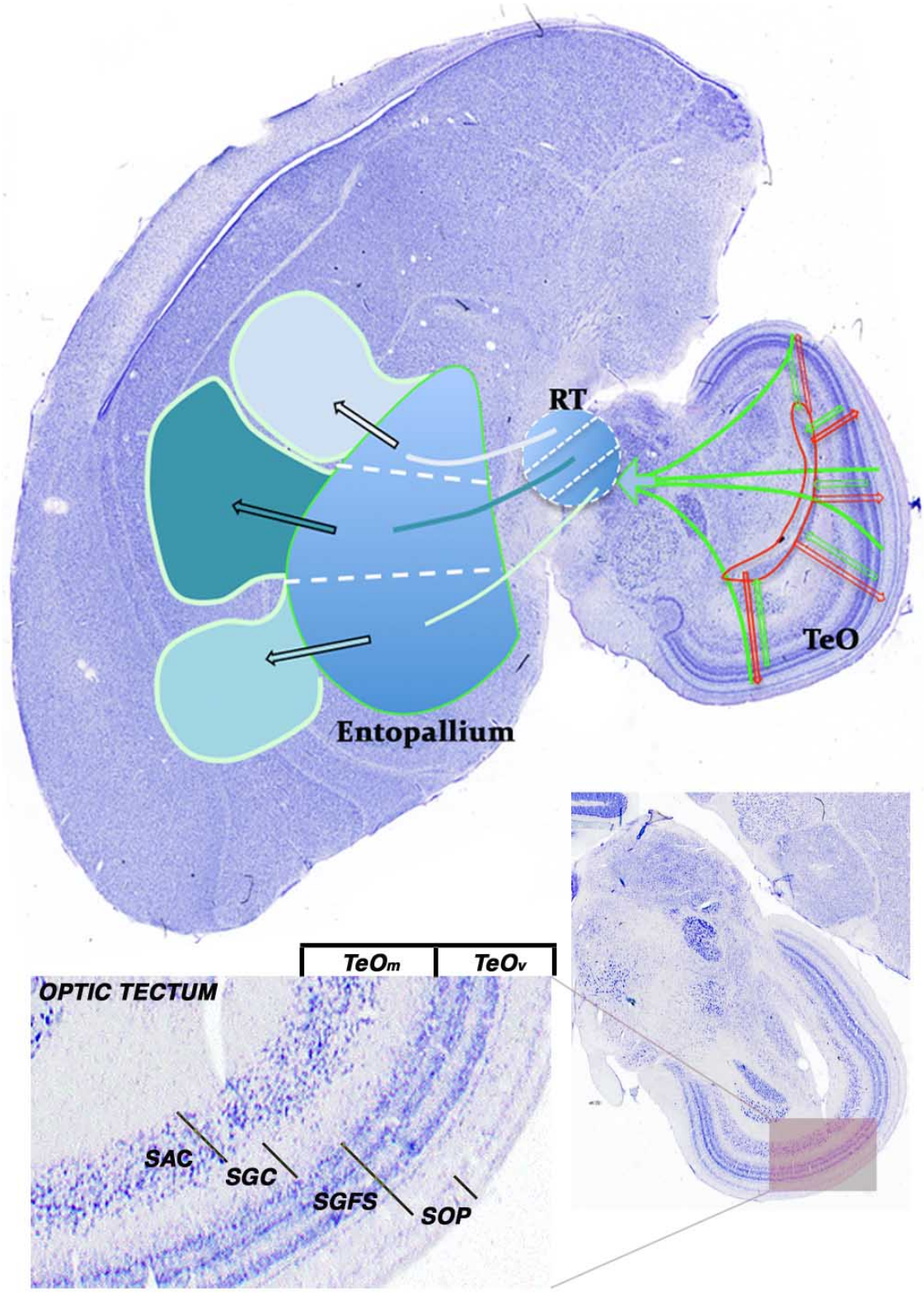

Fig. 1.7. (See overleaf for figure legend)

Fig. 1.7. Retino-tectal pathway organisation. Modulation of TeO efferent pathway to RT by the isthmic nuclei (**red and green arrows**, see **Section 1.4.1**) and the parallel processing of visual information in nucleus rotundus (RT) to subdivisions of the entopallium. RT receives tectal input via a subset of tectal 'ganglion' cells from the visual layers of the optic tectum (TeO_v). The cell to cell topography in the retino-tectal projection is reorganized at this juncture, and is replaced by distinct parallel channels that convey information relating to specific visual attributes of a given visual scene in a manner analogous to the mammalian pulvinar. The RT subsequently projects to the entopallium, withinin which the separation of the channeled information is maintained. In this figure, pathways are superimposed upon a sagittal section of the New Caledonian crow brain. SAC, stratum album centrale; SGC, stratum griseum centrale, SGFS, stratum griseum et fibrosum superficiale; SOP, stratum opticum; TeO, optic tectum. Based upon Shimizu et al. (2010).

Tectal activity is modulated by a complex interconnectivity that exists between the optic tectum and a group of nuclei that constitute the isthmic complex. Nucleus isthmi parvocellularis (Ipc) receives topographic input from layer 10 of the TeO (i.e. within the stratum griseum et fibrosum superficiale (SGFS) layers (**Fig 1.7**), which in turn projects reciprocally to retinorecipient layers 2-6 where it exerts an inhibitory GABAergic influence (Gunturkun and Remy, 1990). In contrast, nucleus isthmi magnocellularis (Imc) receives a more sparse and less organised tectal input and projects reciprocally to layers 12-14, exerting an excitatory cholinergic influence (Wang, Major and Karten, 2004). A third structure, nucleus semilunaris (SLu) also connects reciprocally with the TeO in a manner comparable to that of Ipc. The specific characteristics of the SLu interconnectivity with TeO and, subsequently, RT show distinct visual field specificity. For example, the dorsal SLu exhibits reciprocal interconnectivity with the dorsal TeO (upon which the ventral retina projects), which in turn projects to the caudal RT. Conversely, the ventral SLu has a reciprocal projection with the ventral TeO, corresponding to the region of inferior visual field afferents, which in turn

projects to the rostral RT (Hellmann, Manns and Gunturkun, 2001). Furthermore, Hellmann et al. (2001) showed that RT also receives direct afferent input from SLu and in turn, RT sends a substantial collateral pathway back to TeO. As well as the reciprocal tectal connections characteristic of the ishmic nuclei, SLu has also been shown to project to the lateral spiriform nucleus (SpL), which in turn relays basal ganglia input to the TeO_m (Reiner, Brecha and Karten, 1982).

1.4.2 Retino-thalamic pathway

In contrast to birds, **in mammals** [05] the majority of RGC axons target the dorsal lateral geniculate nucleus (dLGN). Within the dLGN, and subsequently through the geniculocortical projection, the segregation of the independent channels that transmit different attributes of visual information, i.e. parvo-, magno- and koniocellular components is maintained. Within the cerebral cortex, visual information is then transmitted to numerous extrastriate areas. This cortico-cortical projection is divided into the dorsal and ventral streams that transmit magnocellular and parvocellular channels, respectively. Unlike in birds, the retina-geniculocortical projection is the dominant visual pathway in mammals. As reflected by its dominance in visual processing in mammals, the retino-geniculocortical connectivity is predictably complex. Cats, monkeys and ferrets among others exhibit a highly degree of organisation within the dLGN (Briggs and Usrey, 2009) (**Fig. 1.8**). In these examples, the dLGN is separated into distinct layers, each receiving input from a common eye. In certain carnivorous and primate species [06], such an organisation is maintained through to V1 within which eye specific projections are represented as ocular dominance columns (Hubel and Wiesel, 1962; Wiesel and Hubel, 1974). The organisation of the layers is further split up based upon the physiological properties of the retinal input, i.e. parvo, magno or koniocellular layers (**Section 1.2.2**).

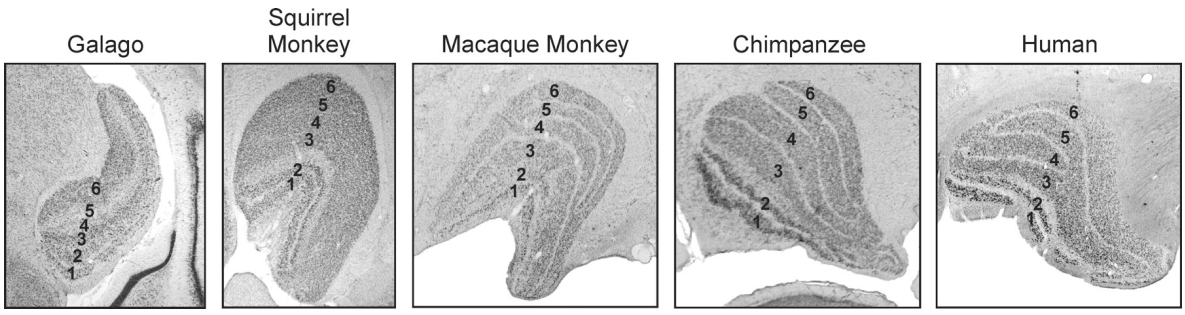

Fig. 1.8. Dorsal lateral geniculate nucleus organisation in mammals. The degree of anatomical complexity, i.e. lamination of the LGN, is varied across species'. In those species that do exhibit lamination, laminae are specific to one eye and further divided based upon the physiological properties of the retinal input, i.e. magno, parvo or koniocellular pathways. Taken from Briggs and Usrey (2011). (Briggs and Usrey, 2011)

An important factor in geniculocortical connectivity is the mode of firing. Tonic firing of thalamic relay neurons, i.e. those neurons that project to V1, is directly related to the magnitude of the action potential to which it responds. Conversely, in burst firing mode, thalamic relay neurons elicit an all or none response, the magnitude of which is not dependent on the degree of excitation evoked by the stimulus (Sherman, 2009). The response properties of these firing modes relate to distinct roles in visual perception. The benefit of a graded response, i.e. that of a thalamic neuron in tonic firing mode, is in the accurate reproduction of the attributes of a visual scene. On the other hand, the benefit of burst firing mode, characterised by an all or none response, comes from a higher signal to noise ratio. As a result, neurons in burst firing mode are associated with novel stimulus detection. It has been suggested that neurons outside of the area of visual attention at a given moment are often in burst mode such that they are more responsive to novel stimuli (Sherman, 2009).

The mechanism by which thalamic relay cell modes are changed is unknown but presumably it is the role of one of a number of feedback pathways. These pathways include a substantial feedback to dLGN that originates from the visual cortex (corticogeniculate pathways) (Briggs and Usrey, 2009), an inhibitory feedback projection from the thalamic reticular nucleus

(Crick, 1984), which surrounds the thalamus and receives direct thalamic and cortical input and finally an excitatory feedback pathway from the parabrachial region of the midbrain (Sherman, 2009).

Analogous to that described in mammals, the avian **retino-thalamic** pathway projects bilaterally (although predominantly ipsilaterally) from the nucleus principalis opticus thalami (OPT) (avian dLGN) to the intercalatus hyperstriatum accessorium and hyperstriatum dorsale of the visual wulst (VW), which in turn project to the hyperstriatum accessorium of the VW (Karten and Hodos, 1970; Karten et al., 1973) (**Fig. 1.9**).

As a reflection of the relative dominance of the **retino-tectal** pathway over the **retino-thalamic** pathway, injection of an anterograde pathway tracer into the VW labels RGCs (predominantly in the yellow field) at a mean density of 783 cells/mm^2 (Miceli et al., 2006), while injection of TeO leads to a density of labeled cells of up to 18000 cells/mm^2 (Remy and Gunturkun, 1991), representing ~96% dependence on **retino-tectal** visual processing in pigeons. While the physiological properties of which the avian **retino-tectal** pathway is known to play a role in are well established, the role of the **retino-thalamic** pathway in birds is less well understood. It has been suggested that the avian tectofugal pathway is predominantly involved in the processing of lateral, far-field information (Gunturkun and Remy, 1990; Remy and Gunturkun, 1991). While experimental disruption of telencephalic regions of the **retino-thalamic** pathway in pigeons were found to cause deficits in visual memory tasks (Shimizu and Hodos, 1989) as well as sun guided navigation tasks (Budzynski et al., 2002).

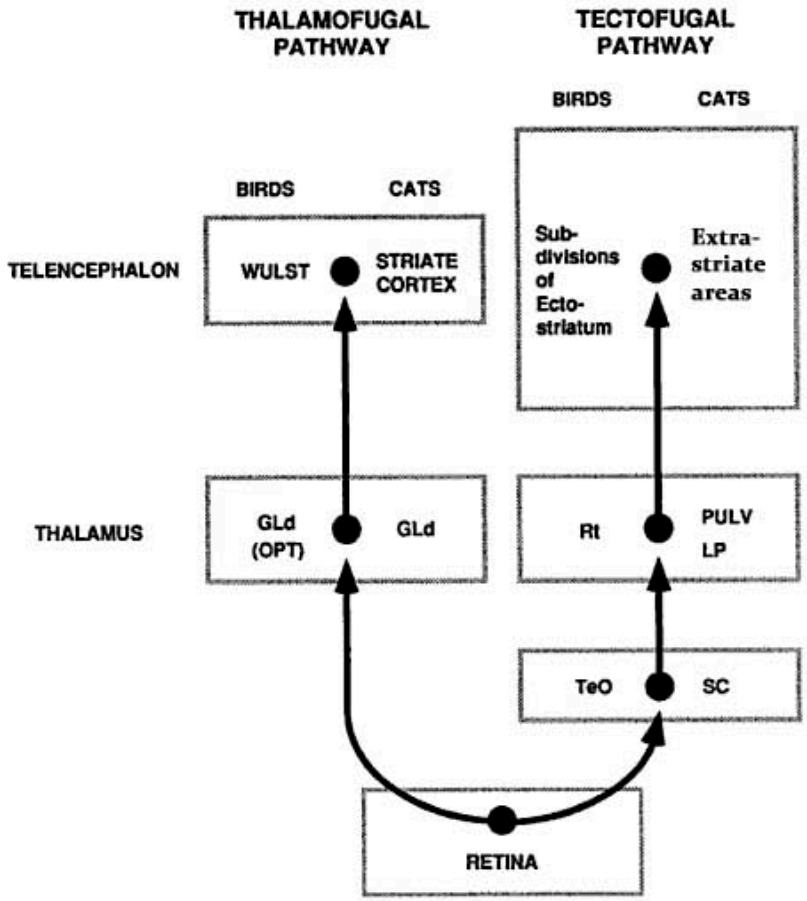

Fig. 1.9. Retina-tectofugal / retina-thalamofugal pathway organisation. Pathways of the **retino-thalamofugal** (**left**) and **retino-tectofugal** (**right**) pathways showing bilateral projections from both nucleus geniculatus lateralis pars dorsalis (GLd), (i.e. dLGN in mammals) and the optic tectum (TeO) to the visual wulst (VW) and nucleus rotundus (RT) respectively. OPT, nucleus principalis opticus thalami; PULV, pulvinar; SC, superior colliculus.Taken from Zeigler and Bischoff (1993).

1.5 Centrifugal visual system (CVS)

A highly topographic neural pathway projecting from the brain to the retina was first demonstrated in the Golgi-stained sparrow retina by Ramon y Cajal in the late nineteenth century. Such a centrifugal pathway has subsequently been shown to exist in all classes of vertebrate (Monakow, 1889; Cajal and Greeff, 1894; Zucker and Dowling, 1987; Derobert et al., 1999; Réperant et al., 2007), including primates (Gastinger et al., 2006). However, the existence of centrifugal efferents in so-called 'higher vertebrates' is still not widely

acknowledged among vision scientists, as has been alluded to by Gerald Wasserman in his paper '*No retinal efference in Humans: An urban legend*' presented to the International Society of Psychophysics in 2010. One reason for this is perhaps the fact that it is in birds (*Aves*), and in particular pigeons (e.g. Woodson et al., 1991), chickens (e.g. Cowan, 1971) and the Japanese quail (e.g. Uchiyama and Ito, 1993), that the vast majority of subsequent studies have been focused. In addition, inter-order variability in CVS organization, i.e. between birds and mammals could prohibit direct analogies as to the function of retinal efferents, a subject that is addressed in **Chapter 10**. However, clearly, an understanding of what is a highly topographic classic feedback system may be of great significance in understanding the role of feedback pathways in sensory systems on a more global level. Neuroanatomically, the avian CVS is particularly well suited to experimental investigation. A large, well delineated structure, the midbrain isthmo-optic nucleus (ION) houses between ten and twelve thousand retinopetal axons (projecting towards the retina), with each innervating a single isthmo-optic target cell (IOTC) within the retina. Although, in the case of the pigeon, axons can bifurcate to innervate up to 2-3 IOTCs). Furthermore, a morphologically diverse sub-population of surrounding neurons, unconstrained by a nuclear boundary, similarly project to the retina (Clarke and Cowan, 1975). However, in marked contrast to the ION, the retinal termination of these so-called ectopic *cells*, situated within the ectopic *area*, are not thought to demonstrate topography, with each terminating on numerous target cells within the retina (**Fig. 1.10**). With a few notable exceptions (Hayes and Webster, 1981; Weidner et al., 1987; Woodson et al., 1995; Medina et al., 1998), the majority of past studies that consider the ectopic cell population, do so as an extension of centrifugal neurons from isthmo-optic nucleus. Studies of the CVS can be broadly split into those elucidating its connectivity (**Section 1.5.1**) and neurochemical properties (**Section 1.5.2.1**) within the brain and the retina, those studying the electrophysiological properties of the neurons both projecting to- and within the retina

(**Section 1.5.7.1**), and/or those attempting to elucidate the functional significance of the system (**Section 1.5.7**).

1.5.1 Anatomy of the CVS

Broadly speaking, the CVS comprises a feedback loop, originating and terminating in the retina (**Section 1.5.2**). Visual information in the form of action potentials is transmitted via axons of RGCs to the avian homologue of the mammalian superior colliculus, the optic tectum (TeO). Long trans-laminar dendritic appendages from tecto-isthmic neurons within layers 9/10 of the TeO extend into retino-recipient layers (2-5) of the TeO and subsequently convey visual information via the tecto-isthmic tract to the ipsilateral isthmo-optic nucleus (Cowan and Clarke, 1976; Crossland and Hughes, 1978; Uchiyama, 1989; Woodson et al., 1991; Woodson et al., 1995; Uchiyama, Yamamoto and Ito, 1996). However, it is not known whether centrifugal neurons of the surrounding ectopic area receive tectal input or indeed whether they are a 'visually innervated' population at all (Uchiyama et al., 1996; Réperant et al., 2006), a point that is specifically addressed in the experimental results **Chapter 9**.

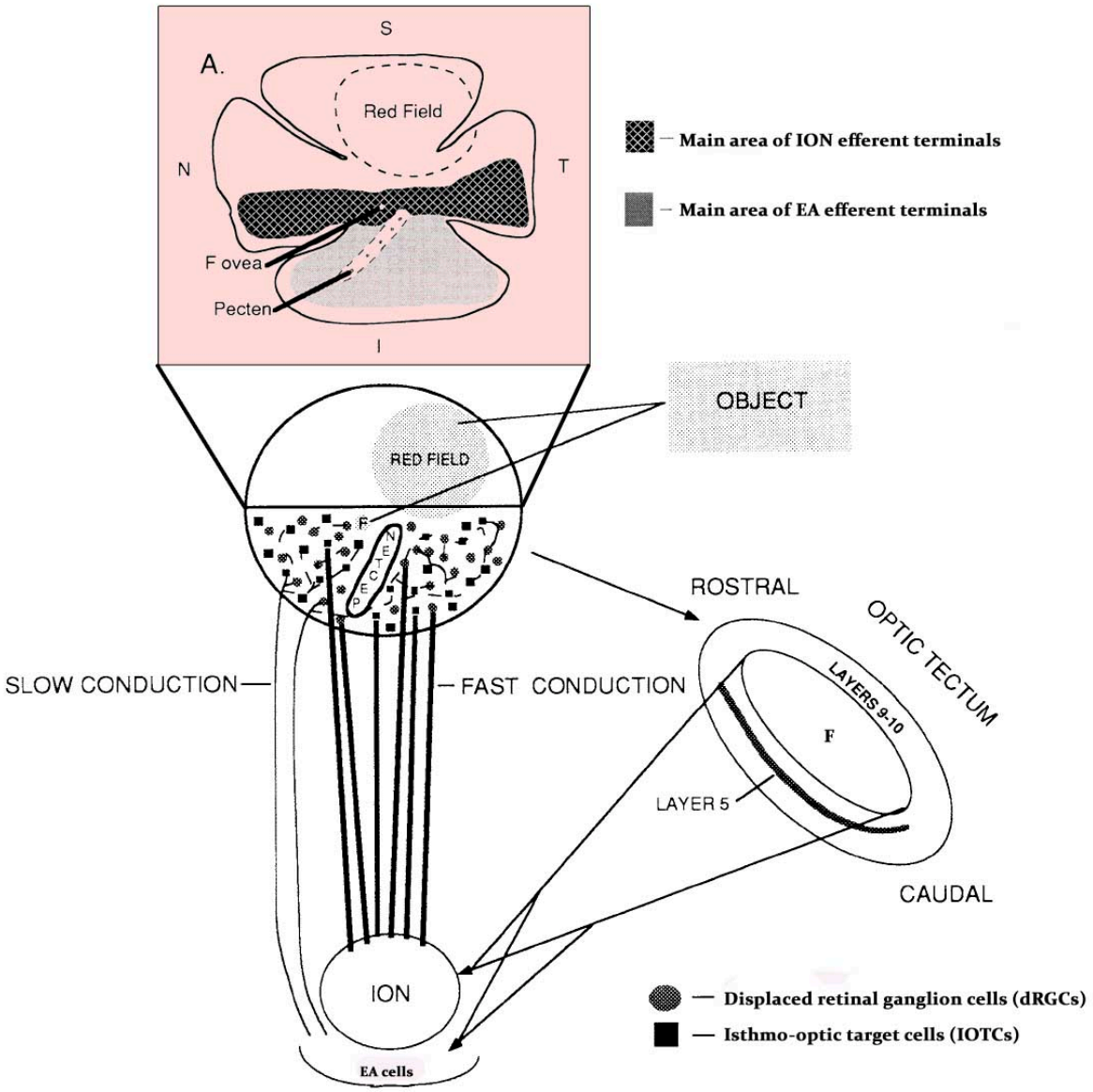

Fig. 1.10. Differences in ION and EA connectivity. Schematic of the CVS loop, highlighting the topography, conduction velocities and retinal target cells of ION and EA efferents in the ventral retina. Isthmo-optic neurons project axons to target cells in the ventral retina. Secondary axons from these target cells innervate retinal ganglion cells (RGCs) across the retina. The retinal projection to the optic tectum then feeds back upon the isthmo-optic nucleus, forming a closed-loop retinal feedback system. Inset **A** shows the pattern of termination of ION and EA cell efferents in the ventral retina. ION, isthmo-optic nucleus; EA, ectopic area; S, superior; I, inferior; N, nasal; T, temporal. Modified from Woodson et al. (1995)

Axons of the ION and presumably of the EA coalesce at the anterior aspect of the ION/EA complex, forming the isthmo-optic tract (IOTr) dorsolaterally (**Fig. 1.12**). They then extend rostrally within the midbrain at the dorso-medial aspect of the TeO before infiltrating the optic tract at the mesencephalic/diencephalic border juncture (Cowan and Powell, 1962; Galifret et al., 1971; Miceli et al., 1997). Finally, these axons decussate completely at the optic chiasm into the contralateral optic nerve where, interestingly, fibers in the pigeon have been shown in some cases to bifurcate before entering the retina (Woodson et al., 1995). A subpopulation of EA cells project to the ipsilateral retina (ipsilateral EA cells) (Clarke and Cowan, 1975). While the exact route that they take is unknown, it is assumed that they share a common pathway to the optic chiasm (i.e. via the IOTr), within which they remain uncrossed. The question of alternate routes for ipsilateral EA cells is addressed in **Chapter 9**. Tecto-isthmic neurons receive a highly topographic input from the retina and in turn project to the ION, within which, again, retinotopy is preserved (Woodson et al., 1991; Li et al., 1998; Li, Hu and Wang, 1999).

The organisation of the CVS 'loop' (**Fig. 1.12**) is especially complex. Efferent target cells of both ION (IOTCs) and EA are strictly confined to the ventral retina (Catsicas, Catsicas and Clarke, 1987; Lindstrom et al., 2009) and receive a highly topographic convergent input from ION centrifugal neurons (**Section 1.5.2**). Within the retina, axons of IOTCs project to amacrine cells (which in turn connect to RGCs) of the (predominantly) dorsal retina but in a seemingly random manner, i.e. two proximal IOTcs in the ventral retina may have terminations in the dorsal retina that are distant from one another (Lindstrom et al., 2009). Having said that, Catsicas et al., (1987) showed that the subsequent projection of IOTCs to the dorsal retina was somewhat topographic, i.e. ventro-nasal IOTCs project to the dorso-nasal retina. Furthermore, they noted that the more ventrally situated the IOTC, the more dorsal its termination.

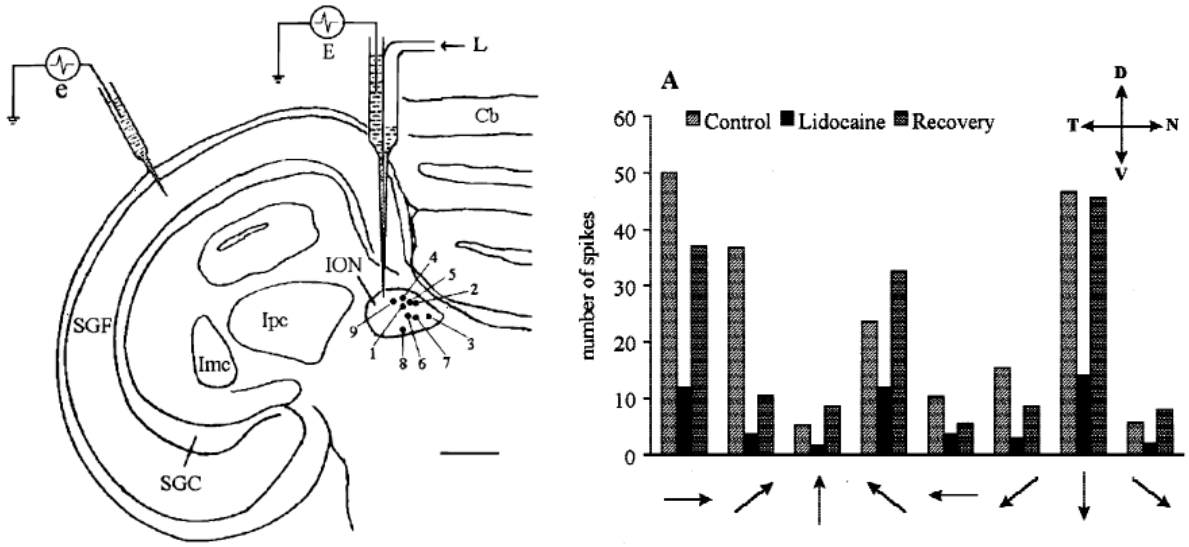

Fig. 1.11. Experimental demonstration that the CVS comprises a closed-loop. In this important study, recordings were made from ION and TeO neurons that responded to the same visual stimulus presentation. A double-barreled pipette in the ION, enabled lidocaine to be injected into the ION to suppress the activity of the ION recording site. It was found that suppression of the ION neuron with lidocaine strongly suppressed the responsiveness of the corresponding tectal neuron. Crucially, if the same procedure was performed on ION and tectal cells that didn't overlap, the responsiveness of the tectal neuron was not affected. These findings provide strong evidence that a given retinal ganglion cell in the retina that was projecting to the TeO, which in turn projected to ION was receiving feedback from the same ION cell via an isthmo-optic target cell in the ventral retina, I.e. a closed loop feedback system. Simultaneous recording from TeO (**e**) and ION cells (**E**). A double barreled pipette was used in the ION for injection of lidocaine (**L**) to reversibly block cell excitation. Cb, cerebellum; ION, isthmo-optic nucleus; Imc, nucleus isthmi magnocellularis, Ipc, nucleus isthmi parvocellularis; SGC, stratum griseum centrale, SGF, stratum griseum et fibrosum superficiale. **Scale bar = 500 *μ*m.** Taken from Li et al. (1998).

The contradiction in the literature regarding the intra-retinal connectivity prompted questions as to whether the CVS 'loop' was in fact 'closed', i.e. homotopic in spite of this apparent deviation in organisation. Li et al. (1998) answered the question with a particularly pertinent study in the pigeon. A double-barreled pipette, which enabled both recording of

ION units and subsequent suppression of activity through injection of lidocaine was used in combination with a recording electrode in the optic tectum (**Fig. 1.11**). Once the receptive fields of tectal and ION regions were found to overlap (to a light stimulus), injection of lidocaine into the recording site within ION was found to strongly reduce the responsiveness of the corresponding tectal neuron (**Fig. 1.11 right**). Importantly, when the receptive fields of ION and tectal recording sites did not overlap, injection of lidocaine had no effect on tectal neuron responsiveness. Crucially these findings showed that a given RGC in the dorsal retina that was projecting to the TeO and in turn innervated an ION cell was receiving feedback from the same ION cell via an IOTC in the ventral retina, i.e. 'a closed loop' organisation.

Fig. 1.12. **A schematic representation of the centrifugal visual system**. (**Red arrows: Afferent pathways**) Retinal efferents (i.e. RGC axons) project to the contralateral retino-recipient layers (2-6) of the optic tectum. Tecto-isthmic neurons in layers 9/10 project dendrites to retino-recipient regions (**C**) and project to the isthmo-optic nucleus (ION) (and potentially the ectopic area (EA)) via the tecto-isthmic tract. (**Green arrows: Efferent pathways**) Centrifugal efferents from ION and EA project to the contralateral retina via the isthmo-optic tract (IOTr) where axons terminate upon ishthmo-optic target cells (IOTCs). IOTCs in turn project to, and regulate the gain of, retinal ganglion cells across the retina. **(A)** proximal structures of the ION and EA; **(B)** anterior-posterior location of the ION (A1.75) and IOTr (A2.20-2.70); **(C)** location of a tecto-isthmic neuron; (**Far right**) rostral-caudal sections through the pigeon ION. EA, ectopic area; FLM, fasciculus longitudinalis medialis; GCT, substantia grisea centralis; ION, isthmo-optic nucleus; IOTr, isthmo-optic tract; Ipc, nucleus isthmi parvocellularis; LLd, nucleus lemnisci lateralis pars dorsalis; LoC, locus ceruleus; nIV, trochlear nerve.

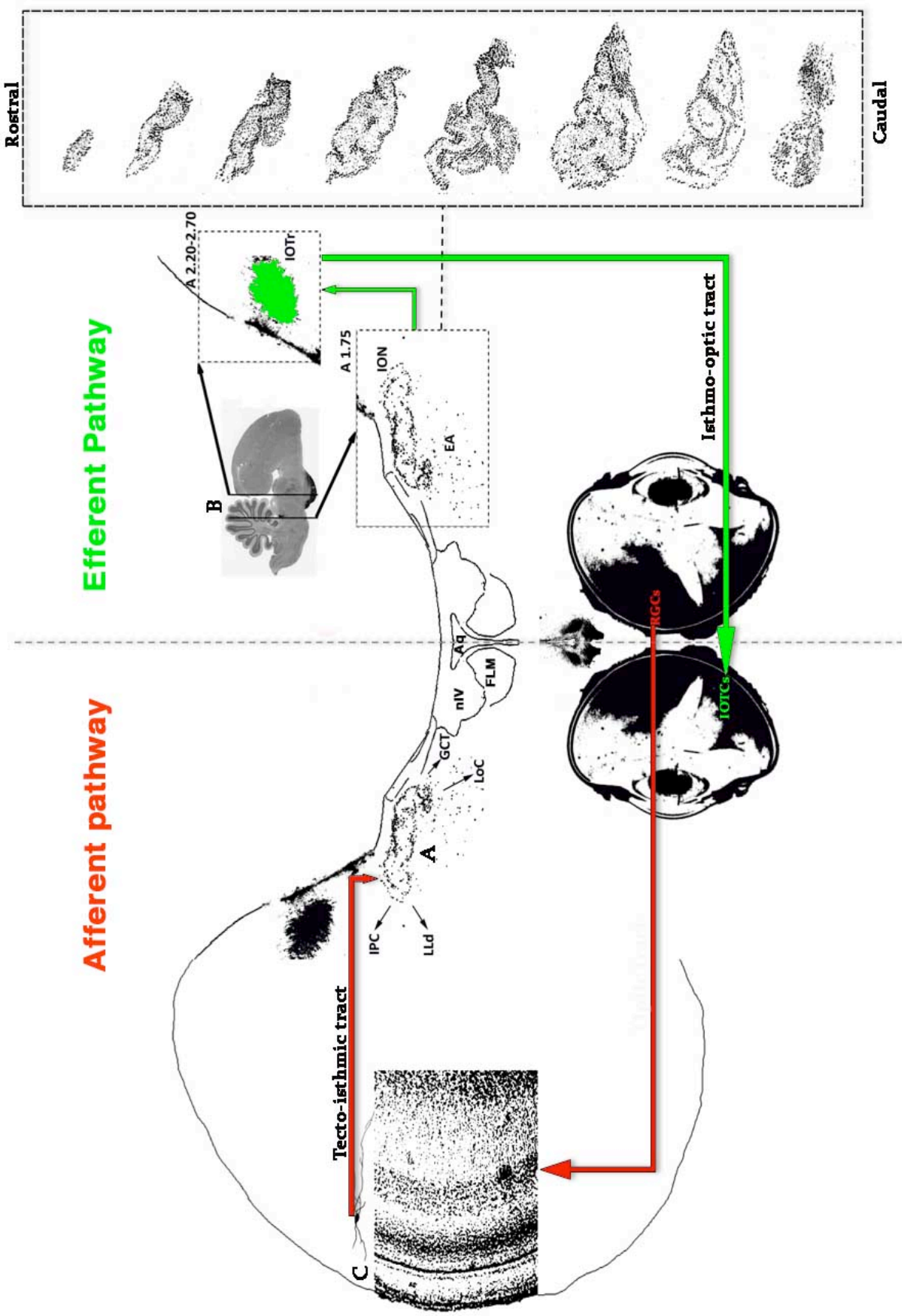

Fig. 1.12. *(See previous page for figure legend)*

1.5.2 Retinal termination

Within the retina, ION-derived centrifugal efferents disperse within the nerve fibre layer, cross the inner plexiform layer and synapse with IOTCs in the inner nuclear layer. As mentioned above, IOTCs, initially termed 'association amacrine cells' (AACs) by Ramon y Cajal (1893), and subsequently 'proprioretinal cells' by Catsicas (1987), are the retinal targets of ION cell efferents of the IOTr.

The term amacrine has a Greek etymology; '*a-makros inos',* literally translated as 'without long fibre'. However, Cajal's AACs actually have a horizontal axon that can extend across long distances within the retina and, as such, the terminology has recently been changed to the less ambiguous isthmo-optic target cell (IOTC). IOTCs possess a specialised dendritic organisation that acts to envelope presynaptic boutons of efferent fibres. Described as a pericellular nest by Cajal and as resembling a bunch of grapes by others (Lindstrom et al., 2009), the target cell termination, which bizarrely is confined to the inner nuclear layer rather than the inner plexiform layer, is characterised by numerous pre-synaptic boutons (between 5 and 20 per efferent fibre in chickens) adjoining the target cell soma, suggesting that input to the IOTCs is substantial (Lindstrom et al., 2009). One of the more provocative findings in the century of research that has characterised the CVS is that the 'convergent' termination of isthmo-optic axons is entirely confined to the ventral retina (Catsicas et al., 1987) (**Fig. 1.13 A**). Although several (probably spurious), theories of potential CVS functions (see **Section 1.5.7**), predominantly based upon predator detection and attention switching hypotheses followed this finding, the significance of this organisation is still unexplained. Such an organisation may simply be a developmental remnant as suggested by Uchiyama and Ito (1993). Given the extensive cell death that occurs during the embryological development of the CVS, it was suggested that the organisation of IOTCs within the ventral retina was due to the increased likelihood of an IOTC making a connection with an ION cell axon protruding through the

ventral orbital fissure during development, thus increasing the likelihood of survival into the post-embryological system [97].

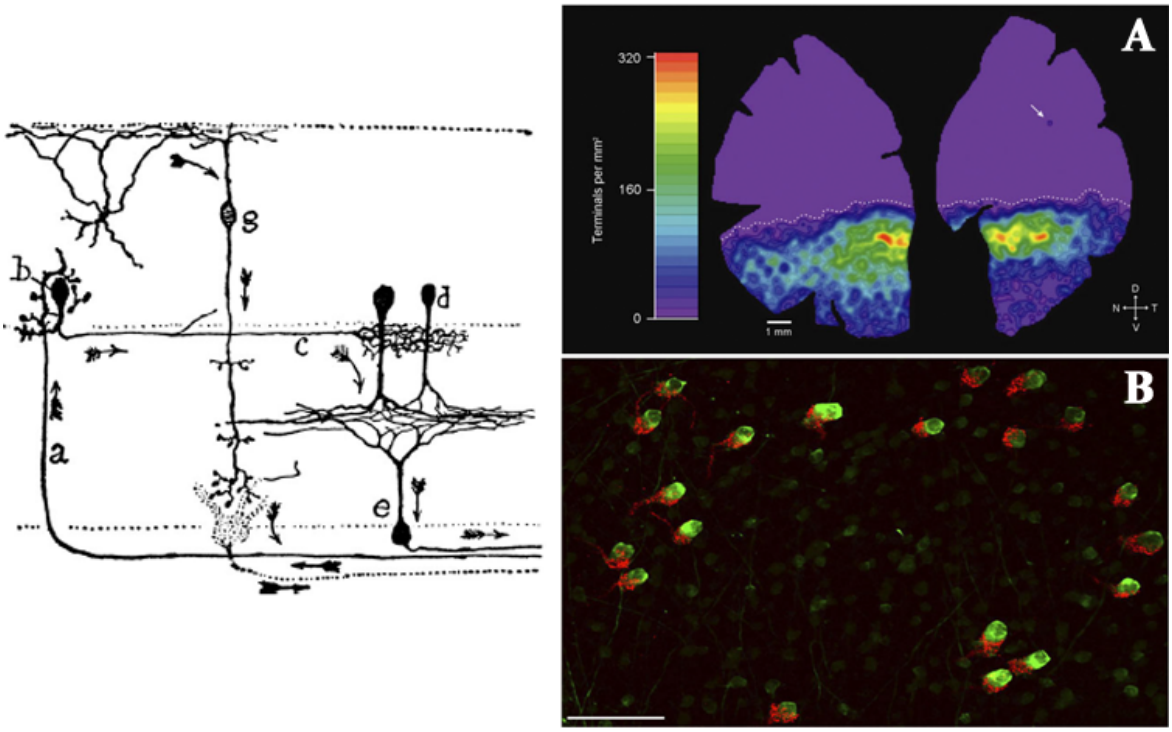

Fig. 1.13. Intra-retinal connectivity of centrifugal efferents. Left schematic shows the intra-retinal connectivity of centifugal efferents. Centrifugal axons enter the retina via the optic nerve head and terminate upon isthmo-optic target cells (IOTCs; **b**) in the inner nuclear/inner plexiform layer border. IOTCs project secondary axons to 'ordinary' amacrine cells (**c**), which, in turn, modulate the activity of retinal ganglion cells (**e**) Taken from Cajal (1972). **(A)** Termination of centrifugal efferents upon IOTCs in the chick retina. Colour scale represents density of efferent termination with brighter colours denoting higher density; **(B)** Fluoro-Ruby red labeled IOTCs (**red**) following intra-cranial injection of ION double labeled for parvalbumin. **A** & **B** Taken from Lindstrom et al. (2009). **(Cajal, 1972)**

EA cell efferents terminate within the retina as so-called divergent or widespread efferent fibres (Maturana and Frenk, 1965; Woodson et al., 1995), with each axon branching to contact numerous target cells. Similar to convergent efferent fibers, retinal termination is confined to the ventral retina but occupies a more inferior distribution than convergent terminals (Woodson et al., 1995). One of the more controversial areas of the literature concerns the

potential termination of centrifugal efferents upon displaced retinal ganglion cells (dRGCs), a subgroup of ganglion cells confined to the ventral retina that project to the nucleus of the basal optic root (nBOR) and nucleus lentiformis mesencephali, pars magnocellularis (LMmc), of the accessory optic system (AOS) (Britto et al., 1988). The nuclei of the AOS are involved in the processing of visual signals generated by self-motion and subsequently, the ability to distinguish object motion (Brecha and Karten, 1981). While the distribution of dRGCs within the retina corresponds to the region of termination of centrifugal efferents (Hayes and Holden, 1983b; Lindstrom et al., 2009) and 'close contact' has been observed between 2.7% of centrifugal terminal arborisations (Hayes and Holden, 1983a) subsequent studies have been unable to confirm such connectivity (e.g. Lindstrom et al., 2010).

The work of Woodson and colleagues (1995) in the pigeon addressed this controversy in a particularly clear and comprehensive anatomical study. Through the use of a combination of anterograde and retrograde pathway tracing techniques, they were able to clarify a number of anatomical unknowns concerning the CVS, as well as further characterising the ION/EA efferents classified through identification of the independent source of these two distinct groups, i.e. demonstrating that the ION gives rise to convergent (or restricted) efferent fibers (**Fig. 1.14**) and EA to divergent efferent fibers projections (Maturana and Frenk, 1965). Injections of the retrograde pathway tracer cholera toxin subunit B (CtB) into the medial ION/EA complex labeled convergent and divergent (or widespread) efferent fibers of the midtemporal and midnasal contralateral retina, respectively, while injections into the lateral complex labeled terminals within a radius of 1 mm around the area centralis (Weller et al., 2009).

Perhaps the most pertinent point of their work was the corroboration of the observations of Maturana and Frenk (1965), Brecha and Karten (1981) and Hayes and Holden (1983) that centrifugal efferents make 'presumptive contact' with somata and proximal dendrites of

dRGCs (citing unpublished double labeling studies of Woodson and Britto). However, they further clarify that it is in fact divergent (i.e. ectopic cell efferent projection) fibre terminals that are involved in this projection (**Fig. 1.14**).

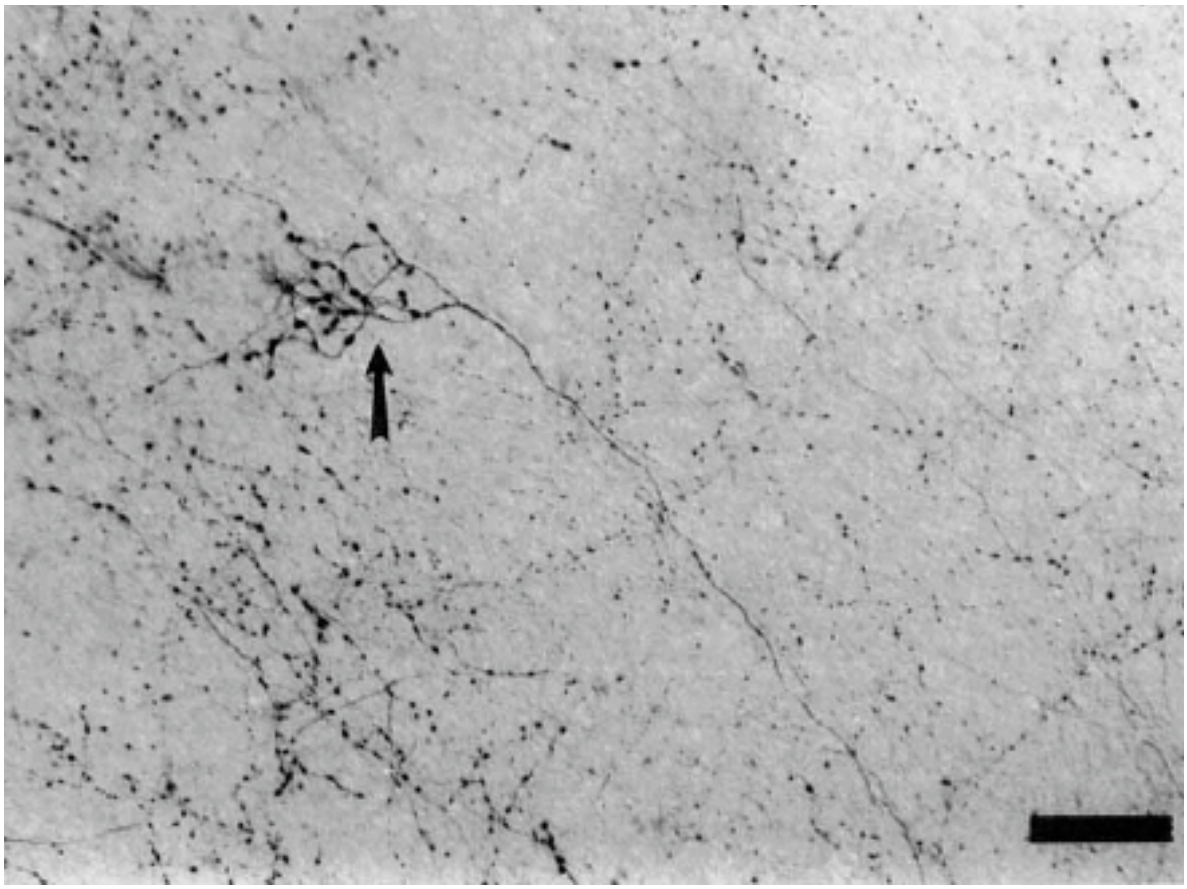

Fig. 1.14. Intra-retinal centrifugal efferent terminations. Anterogradely labeled Cholera toxin subunit b termination of a restricted efferent fiber on an IOTC (i.e. ION efferents) in the pigeon retina following intra-cranial injection of the isthmo-optic nucleus (**arrow**). Surrounding, less distinct terminals are of the widespread efferent fibers (i.e. EA cell efferents). Taken from Woodson et al. (1995). **Scale bar = 50 μm**.

A recent review by Wilson and Lindstrom (2011) dismisses the idea of a CVS-AOS link, pointing out that, while the distributions of centrifugal efferents and AOS afferent dRGCs are similar, they do not overlap. Although in support of this position they cite a number of papers involving the three main bird species normally used for such studies, in fact, the specific contradictory points that the listed papers are perceived to make are not stated. Furthermore,

apart from a lack of direct evidence for such connectivity, which in each case could be explained by methodological limitations, no compelling evidence *against* this connectivity exists. For example, Nickla et al. (1994) adopted cytochrome oxidase labeling as a marker for both IOTCs and three types of ganglion cell in the chick, including dRGCs (as confirmed by combination with the pathway tracer rhodamine β-isothiocyanate (RITC) labeling of dRGCs following intra-cranial injection of nBOR). Through lesions of the isthmo-optic tract, they ascertained that axotomising neurons of the ION/EA complex diminished cytochrome oxidase labeling in centrifugal efferent target cells, but did not affect labeling of dRGCs. However, as stated in their discussion of this finding, while it may well be the case that centrifugal efferent cytochrome oxidase labeling was diminished because of the disruption, the persistence of cytochrome oxidase labeling in dRGCs could be a result of the fact that *primary* afferentation of dRGCs is likely to be independent of centrifugal efferents, i.e. visual input via photoreceptors and retinal interneurons). Furthermore, a study by Lindstrom et al. (2009) was unable to confirm or refute that centrifugal efferents made contact with dRGCs, because of the inconsistency apparent in using NADPH-diaphorase (a nitric oxide synthase) immunoreactivity as a marker for both centrifugal efferents and dRGCs (which are more weakly stained).

As a side note, however, recent volumetric analysis of visual nuclei of over 70 species of birds across 17 orders (Gutierrez-Ibanez et al., 2011) found that while, predictably, ION volume is strongly correlated with TeO volume, the former is also strongly correlated with the volume of LMmc of the AOS. The relevance of such findings relates to the principle of proper mass (Jerison, 1973), that is the idea that the size of a neural structure is correlated with the importance of the behaviour it subserves. By extension, a correlation between the size of one structure within another across 70 species could be evidence for a common functional role involving these brain areas.

1.5.2.1 Neurochemical properties

In the chick, the efferent fibers of ION neurons contain NADPH-diaphorase immunoreactivity while the IOTCs themselves contain both NADPH-diaphorase (Morgan, Miethke and Li, 1994) and parvalbumin immunoreactivity (Fischer and Stell, 1999; Lindstrom et al., 2010). Parvalbumin is a protein commonly expressed by GABA-producing neurons however, IOTCs were not found to contain GABA immunoreactivity (Fischer and Stell, 1999). In addition, IOTCs were found to exhibit immunoreactivity to glutamate/AMPA receptor subunits (Fischer and Stell, 1999). An identified subpopulation of glucagon-expressing amacrine cells share a common distribution within the ventral retina as IOTCs however they are in fact a distinct amacrine cell type (Fischer et al., 2005), with glucagon amacrine cells occupying a more ventral position than IOTCs which are predominantly located along a midline streak (Lindstrom et al., 2009). That being said, these cells may be a target for the more ventral termination of EA centrifugal EA efferents (Woodson et al., 1995) (**Fig. 1.10**).

1.5.3 Isthmo-optic nucleus (ION)

In birds, the location of the source of restricted efferent fibers projecting to the retina is the isthmo-optic nucleus (ION). In the pigeon, the ION contains approximately 12,000 centrifugal neurons, with somewhat fewer (~ 10,000) in the chicken (Miceli et al., 1999). In both the pigeon (Karten and Hodos, 1967) and chicken (Kuenzel and Masson, 1988), structurally, it is ovoid in the coronal plane and elongated in the sagittal plane, with the ventral border tapered towards the dorsal roof of the midbrain at the dorso-medial aspect of the optic tectum (**Fig. 1.15**). It is bordered medially, rostrally and caudally by the substantia grisea centralis (GCt), ventro-medially by locus ceruleus (LoC), ventro-laterally by n. lemnisci lateralis pars dorsalis (LLd) and laterally by n. isthmi, pars parvocellularis (Ipc) (**Fig. 1.12**). The ION spans ~700 μm in the transverse and ~1000 μm in the axial plane, at the level of the trochlear nucleus (CNIV) (Karten and Hodos, 1967). A distinct peripheral bi-layer of morphologically homogeneous

neurons border the nucleus (Güntürkün, 1987) (**Fig. 1.16**), but far from being a simple oval border, in the transverse plane, numerous invaginations give a complex convoluted structure. The border cells are spherical with two or more dendritic processes protruding into the internal neuropil region (Cowan and Powell, 1962; Güntürkün, 1987).

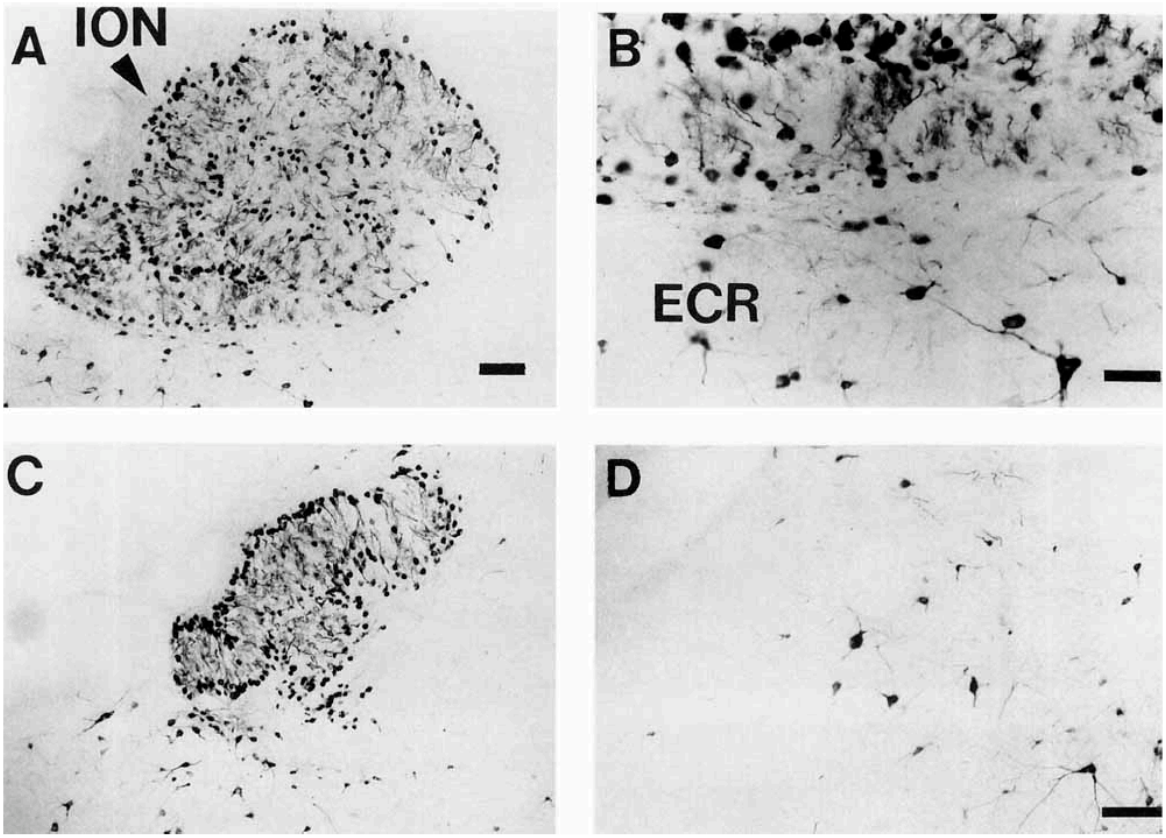

Fig. 1.15. ION and EA organisation. Retrogradely labelled cholera toxin subunit B isthmo-optic nucleus (ION) and neurons of the surrounding ectopic are (EA) following intra-vitreal injection in the pigeon. (**A)** Caudal ION. Note the dendrites of border cells projecting into the neuropil and the numerous invaginations. (**B)** High magnification inset of **A** showing the distinct morphology of proximal EA cells. (**C)** Rostral ION and surrounding EA cells. (**D)** EA rostral to ION. Taken from Woodson et al. (1995). **Scale bars = 100 *μ*m.**

Retrograde degeneration studies following suction removal of the TeO early in embryonic development of the chicken suggest that around 50% of afferent input to ION is indirect visual input from retinal ganglion cells via deep layers of the optic tectum (layers 9/10) (TeO)

(McGill, Powell and Cowan, 1966). Although the superficial retino-recipient layers 2-6 of TeO do not therefore project to ION, tecto-isthmo optic neurons in layers 9 and 10 of TeO show extensive dendritic arbors that extend into these layers (McGill, 1964; Woodson et al., 1991). In addition, a number of pretectal areas, including n. griseus tectalis, n. spiriformis lateralis and area pretectalis (AP), all have the potential to project upon the ION via tectal interneurons (Réperant, 1973; Uchiyama et al., 1996; Réperant et al., 2006). Functionally, both AP and n. griseus tectalis receive direct visual input and are thought to be involved in visuomotor performance, e.g. unilateral lesions of AP have been shown to abolish the pupillary light reflex in the contralateral eye via the Edinger-Westphal nucleus (nEW) (Gamlin et al., 1984; Gamlin and Cohen, 1988). Furthermore, bilateral lesions of nucleus spiriformis lateralis have led to impairment of visual tracking of a moving target (Réperant et al., 2007).

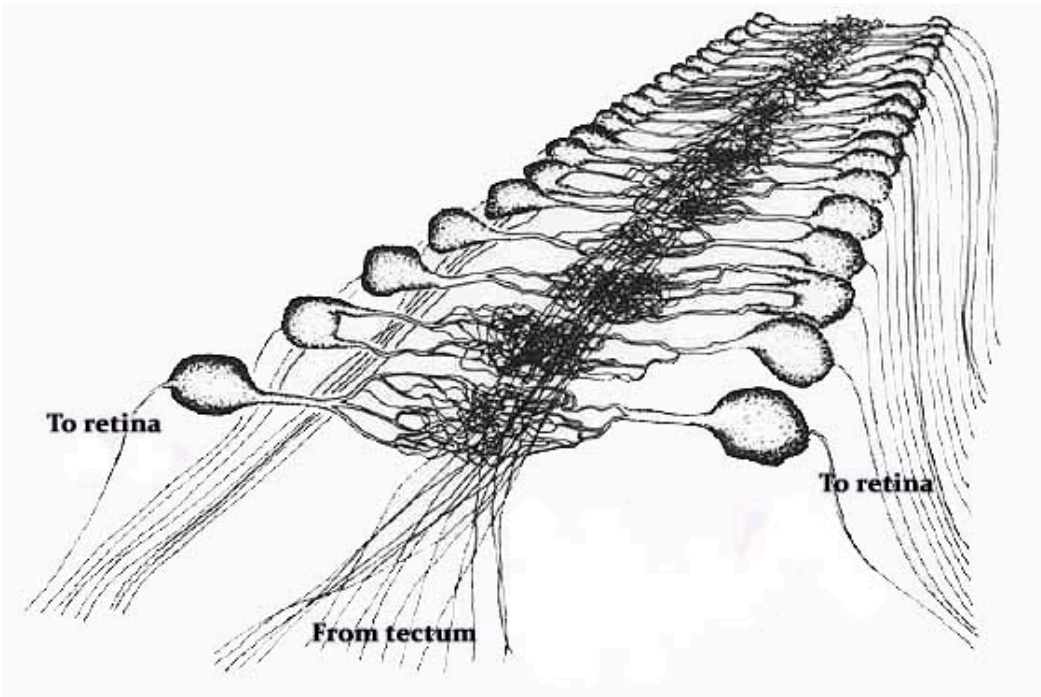

Fig. 1.16. Semi-schematic diagram of ION connectivity. Simplified demonstration of ION connectivity based upon a Golgi study in the Japanese quail. tectal input entering the central neuropil region where morphologically homogeneous border cells extend 1-3 primary dendrites. Each border cell sends a single axon to a target cell in the retina. Taken from Güntürkün (1987)

Crossland and Hughes (1978) used a combination of [^{3}H]proline and horseradish peroxidase (anterograde and retrograde pathway tracers, respectively) in order to define the tectal afferentation of ION. Following up on degeneration studies after lesions of the TeO McGill (1964), they were able to localise the tectal source of ION afferents to cells within layers 9 and 10, i.e. the deep sublaminae of the stratum griseum et fibrosum superficiale (SGFS) by using [^{3}H]proline injections at different depths of TeO. HRP was injected into the ION with the intention of identifying extra-tectal sources of afferent input, while [^{3}H] proline was again used to inject the ION in order to follow the course of the isthmo-optic tract. The literature is particularly inconclusive as regards the former, i.e. extratectal afferent inputs, predominantly because of the technical difficulties associated with containing intra-cranial injections within the boundaries of the ION. Miceli et al. (1997, 2002) sought to overcome such problems through the use of a trans-synaptic pathway tracer, RITC. Following intra-vitreal injection, RITC is transported to ION/EA, where it is then able to cross the junction between the centrifugal neuron and is transported farther to presumptive afferent centres. In this study, a group of serotonin (5-HT) immunoreactive neurons of nucleus linearis caudalis (LC) of the dorsal raphe complex (as well as the expected tectal afferentation in layers 9/10) were labeled. One obvious shortfall of this approach, however, is that afferents specific to ION or EA are not discernible. In order to characterise the source of 5-HT afferents to centrifugal neurons, RITC axonal tracing was then used in the same way but in combination with 5-HT immunohistochemistry. Interestingly, 5-HT immunoreactivity was not present in the border cells of the ION but only ventrally in the neuropillar region. Although a population of 5-HT-ir neurons in the EA region surrounding the ventral perimeter of ION were observed to project dendrites through the border and into the ventral neuropil of ION, these were not double labeled with RITC and as such were not 'true' ectopic neurons.

1.5.4 Ectopic area (EA)

Approximately 3000 centrifugal neurons of heterogeneous morphology (**Fig. 1.17**), both within the population and as distinct from the morphology of ION cells, surround ION in, on first assessment, a seemingly random, 'reticular' distribution (Miceli et al., 1999). EA cells are a heterogeneous population of neurons with a great diversity of size, orientation, shape and distribution. Somata range from round and multi-polar to pyramidal or flattened- 'squamous-like', while dendritic processes arborise to form dendritic trees that span up to 500 μm in diameter (Hayes and Webster, 1981; Medina et al., 1998). Synapses are often observed between EA cells as well as with other surrounding populations, presumably of the LoC, GCt, and Ipc and potentially with neurons of the medially proximal oculomotor nuclei.

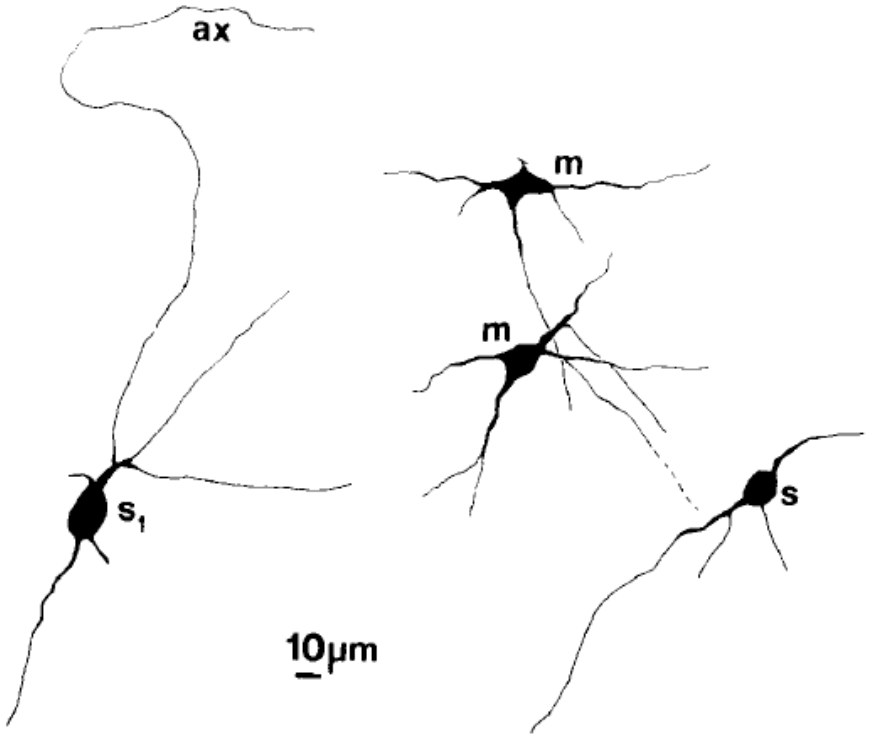

Fig. 1.17. **Morphology of HRP labeled EA cells.** Showing the morphological heterogeneity of ectopic area (EA) cells. Interestingly the soma of **S1** was observed to project an axon towards the contralateral ION, an interesting finding in the context of the pathway tracing studies described in **Chapter 9**, wherein a potentially crossed centrifugal cross-talk projection is reported. Taken from Hayes and Webster (1981).

The majority of EA cells project to the contralateral retina, however a small subpopulation project to the ipsilateral retina (**Section 1.5.5**). As I have alluded to in previous sections, the distribution of centrifugal EA cells in amongst non-centrifugal cells within the ectopic *area* prevents reliable interpretation of retrograde labeling following injection of pathway tracers into EA regions, and thus, identification of EA afferents. In addition, trans-neuronal labeling techniques following intra-vitreal injections do not allow ION and EA afferents to be discerned. As such, while the findings of studies that primarily investigate ION afferents may apply to EA cells as well, no conclusions for independent sources of EA afferents have been identified. In fact, it is not known whether, or not, EA cells receive afferent input from TeO (i.e. visual input). A major goal of the experiments described in the results **Chapter 9** was to overcome these methodological problems, first and foremost in order to elucidate whether or not centrifugal EA cells do receive tectal input.

1.5.5 Ipsilateral EA projection

Only a handful of studies have specifically investigated the population of EA cells that project to the ipsilateral eye (O'Leary and Cowan, 1982; O'Leary, Gerfen and Cowan, 1983; Weidner et al., 1985; Wolf-Oberhollenzer, 1987). The very existence of these cells (at least post-embryonic development) was a source of, albeit limited, controversy wherein they were referred to as 'wrong-half' cells (Pequignot and Clarke, 1992). However, advances in pathway tracing techniques provided confirmation that the pathway did, in fact, persist into adulthood (O'Leary et al., 1983; Weidner et al., 1985). The basis of Weidner's study into the projection was a multiple-technique approach that neatly demonstrated the basis of the past contradiction in findings, with retrograde degeneration studies shown to be particularly variable, while the more modern approaches, using WGA-HRP or RITC, labeled ipsilateral EA neurons much more consistently.

In a later study by Weidner (1987), perhaps the most interesting and provocative finding related to the EA. While the pigeon was found to have an EA cell number that corresponds to 22% of the ION cell number, the corresponding figure in the barn owl was found to be 29%. Moreover, pigeons had an ipsilateral EA cell number that amounted to 13% of the contralateral EA projections, while that of the barn owl is 27.5% of the contralateral EA cell number. The difference in proportion of contralateral EA relative to ION cell number could be explained, and to a degree would be expected, by the lack of definition in the nuclear border of the ION. However, an increase in the proportion of ipsilateral centrifugal neurons relative to the contralateral EA is particularly thought provoking when considered in the context of the large difference in visual field binocular overlap of these two species and also their diurnal vs. nocturnal habits.

Unlike the mammal, the avian optic nerve was found to undergo a complete decussation at the optic chiasm (Harris, 1904; Cowan, Adamson and Powell, 1961). A small number of ipsilateral fibers were not ruled out by Cowan (1961) (*'careful examination of all our tissue has failed to show any appreciable number of degenerating fibers on the ipsilateral side'*), but studies using more sensitive tracing techniques eventually demonstrated that, in the adult, there are some ipsilaterally projecting retinal axons, making up about 1% of the contralateral projection (O'Leary et al., 1983). The existence of ipsilaterally projecting fibers does not, however, confirm that this is the same pathway taken by centrifugal efferents of ipsilateral neurons. A number of potential alternative pathways exist whereby centrifugal efferents could reach and innervate the ipsilateral retina. In the mammal, the corpus callosum is the primary interhemispheric pathway, but in the avian brain, no such structure exists, and instead, a number of midbrain commissural tracts (i.e. the anterior commisure (AC), posterior commisure (PC) and the tectal commisure (TC)) subserve a comparable axonal route between the two sides of the brain. Inter-hemispheric connectivity is involved in lateralisation, such that a left-right hemisphere division of function may be established, e.g. ocular dominance.

Surgical transection of the TC (and therefore its rostral continuation, the PC) has been shown to reverse an innate right eye dominance (Güntürkün, 1985) during visual behavior in pigeons (Güntürkün and Bohringer, 1987). O'Leary and colleagues (1983) identified a separate component of the ipsilateral retinofugal pathway that decussates at the optic chiasm but then takes advantage of the commissural anatomy described above (in this case the TC) to re-cross the midline and 'come to lie close to the ipsilateral isthmo-optic tract' (wherein their pathway could not be followed any further). This double-decussation was not unique in their studies, with a second comparable pathway having been identified in the posterior commissure that went on to innervate pretectal structures. Both of these examples were from studies of embryonic chicks (embryonic day 12), but in fact, by embryonic day 17 the tract involving the pretectum was no longer present. It remains unclear whether this is also true of the tract near the IOTr. While it is highly plausible that the ipsilateral centrifugal efferents do merely project to the ipsilateral retina by remaining uncrossed at the optic chiasm, the intriguing possibility that these axons take an alternative route is one of the questions addressed by the anatomical experiments described in **Chapter 9**.

1.5.6 Development of the CVS

Numerous developmental studies in the chick have taken advantage of the pattern of the development of the CVS, not least because of the dramatic period of natural cell death (i.e. apoptosis) during which the majority of the EA_I neurons degenerate. Prior to the cell death phase of development, the ION alone consists of around 22,000 neurons (embryonic day 11) (Cowan and Clarke, 1976; O'Leary and Cowan, 1982). However, between embryonic days 13 and 17, 60% of ION neurons (Cowan and Clarke, 1976) and 53% of EA neurons degenerate (O'Leary and Cowan, 1982).

During the development of the chick, a number of transient tracts are present that, in part, presumably result from targeting error during development. For example, retinal efferents are

found to form a retino-retinal tract between days 7 and 9, whereby axons of the optic nerve enter the contralateral optic nerve at the optic chiasm and innervate the contralateral retina (O'Leary et al., 1983). Moreover, a numerically more prominent ipsilateral pathway from EA and an efferent projection from the ION to the ipsilateral tectum (Wizenmann and Thanos, 1990) are both present during embryonic development, but neither persists because of either the degeneration of the projecting cell itself degenerating, or its inappropriate connection (Cowan and Clarke, 1976; O'Leary et al., 1983).

1.5.7 Function of the CVS

In certain species, the function of centrifugal efferents to the retina has been well characterised. In the horseshoe crab, for example, the retinopetal projection has a role in the regulation of circadian rhythms (Powers and Barlow, 1985; Uchiyama, 1989). A functional role for centrifugal efferents in vertebrate species, however, has proven more elusive. In this section, clues to potential function from past experiments as well as various hypotheses that have been suggested during a century of research will be presented. Studies into the function of the CVS can be broadly divided into those relating to the response properties of CVS neurons through electrophysiological studies, the organisation of the CVS, including its afferent and efferent connectivity, as well as those suggested in the context of a comparative evolutionary approach.

1.5.7.1 CVS neuron response properties

Although there is no direct synaptic input to RGCs from ION neurons, centrifugal efferents are known to enhance the responsiveness of RGCs to visual stimuli, locally and transiently, through complex intraretinal connectivity (Miles, 1972a; Uchiyama and Ito, 1993). Importantly, however, their indirect input cannot elicit firing in an RGC without intraretinal phototransduction of light stimuli (Erchenkov, Gusel'nikov and Zaborskis, 1972; Miles, 1972b). In the pigeon, 72-86% of RGCs receive centrifugal efferent modulation (Miles, 1972b; Holden,

1978). A number of experiments have attempted to describe the response characteristics of these neurons. Holden and Powell (1972) measured the responses of ION neurons to different visual stimuli in the pigeon and identified 3 main types, all with restricted receptive fields of $<5^{o}$ and wide inhibitory surrounds of up to 100^{o}. Thirteen percent of recorded neurons were directionally selective with a preference to horizontal, anterior movement (in the lateral visual field), while 43% were responsive to motion but not to the direction of motion, and the third type that again made up 43%, were so-called 'posterior minimum' neurons, i.e. responsive to motion in all directions but with only a minimal response to posterior motion. Pearlman and Hughes (1976a) had comparable findings in their study of the response properties of RGCs in the pigeon retina. A second part to their study followed up on previously unsuccessful attempts by Miles (1972d) to reversibly block centrifugal innervation of the retina using a cooling probe, showed that all RGC types were affected comparably (Pearlman and Hughes, 1976b). Importantly, however, they showed that the inhibition caused by cryo-blocking did not alter the receptive field properties of the RGCs, dispelling previous assertions that centrifugal efferents enhanced RGC activity through disinhibition of their suppressive surrounds (Miles, 1972c).

The preference of DSGCs in the pigeon retina to anterior-ward motion motivated the first major behavioral approach to uncovering the function of the CVS (Rogers and Miles, 1972). Following lesion of the ION, a paradigm was devised to test responsiveness to the introduction of novel stimuli, in this case the introduction of a red bead into the posterior visual field during feeding. Lesioned chicks were shown to have a delayed recognition time when compared with sham-operated controls (**Fig. 1.18**).

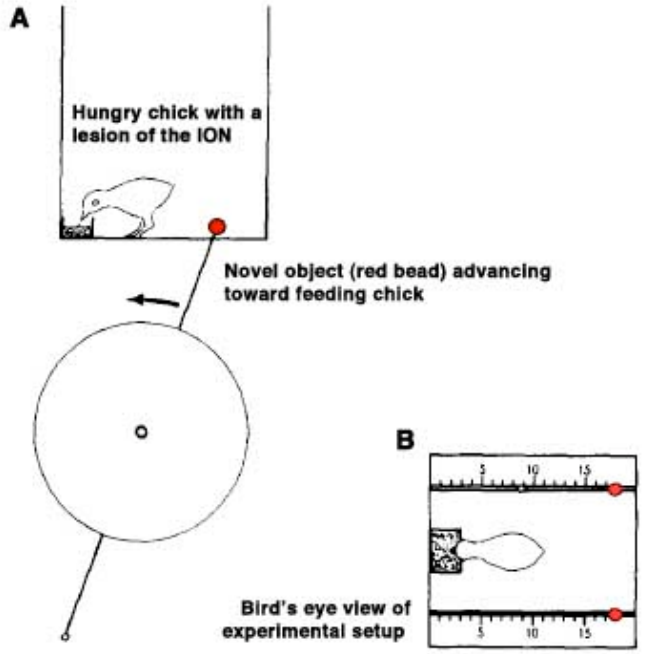

Fig. 1.18. CVS function: Novel object test. In this experiment, the ability of a chick to detect a novel object in the absence of centrifugal efferent input to the retina was assessed. Bilateral lesions of the ION were performed and the time taken for a feeding bird to detect a red bead moving into the peripheral, temporal visual field was assessed. It was found that lesions of the ION delayed the recognition time when compared to sham-operated controls. **(A)** Experimental paradigm used to investigate the role of the CVS in visual attention. Chicks with a lesion of the ION were found to have a delayed response to a novel red object approaching from behind during feeding. **B)** birds-eye-view of the setup used. Taken from Rogers and Miles (1962).

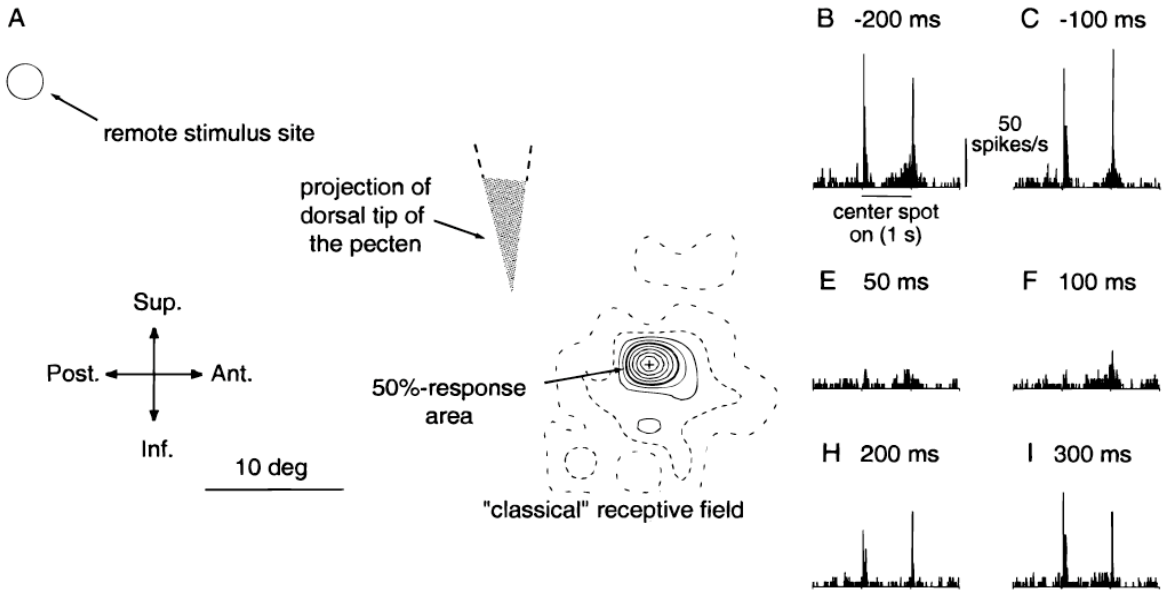

Fig. 1.19. Experimental demonstration of the extensive inhibitory receptive field properties of ION neurons. The extent of the inhibitory receptive field of ION neurons were characterized by recording from ION in response to a black spot stimulus. Subsequently, a second stimulus (**remote stimulus site**) was introduced at different time-points and positions in the visual field relative to the first stimulus. It was found that the extent of the inhibitory field of the ION neuron was widespread, encompassing up to two thirds of the visual field. In addition, the second stimulus was found to have an inhibitory effect upon the ION neuron when presented at the same time or up to 200 ms after the first stimulus (**E-H**). Taken from Uchiyama, Nakamura and Imazono (1998).

More recently, Uchiyama et al. (1998) further characterised the large suppressive surrounds of ION neurons in the context of an 'attentional object selection' hypothesis. While recording from the ION and stimulating isolated neurons with the onset of a black spot, a second stimulus was presented at different time-points before and after onset of the centre stimulus. The response to the centre stimulus was diminished when the surround stimulus was presented at the same time or up to 200 ms afterwards (**Fig. 1.19**). Furthermore, this surround inhibition was found to extend to encompass at least two thirds of the visual field. Thus, the centrifugal input to the retina not only facilitates or enhances RGC activity but also suppresses a large proportion of the surrounding visual field. Uchiyama presents a winner-takes-all

mechanism in the context of an intra-retinal scanning mechanism that leads to focal gain enhancement in the region of a salient stimulus. Such a mechanism was first suggested in a broad preliminary investigation into the CVS by Galifret (1971), which he described as a 'scanning mechanism acting without any movement of the eye'. (Ohno and Uchiyama, 2006)

Studies by Marin and colleagues (Marin, Letelier and Wallman, 1990) and more recently by Ohno et al. (2006) have demonstrated a relationship between ION neuron excitation with the onset of visual stimuli that induce saccades (in the chicken and quail, respectively). The former study found that local centrifugal excitation is suppressed immediately before, during and after onset of saccades, whilst the latter investigation demonstrates that there is an increase in retinopetal activity about 200 ms prior to onset of saccades, the intensity of which was shown to be directionally sensitive. Interestingly, the directional sensitivity shown by IOTCs in response to saccade onset corresponds to that seen in studies by Holden (1972) in which enhancement of RGC activity by centrifugal efferents was in part dependent on the direction in which a given visual stimulus was introduced into the visual field of a pigeon.

Finally, it is worth mentioning that centrifugal (ION) innervation of the retina is fast (**Fig. 1.11**). The conduction velocity of centrifugal axons is 11-24 m/s (Galifret et al., 1971), as expected from the myelination of the axon fibres of between 1-4 μm diameter (Cowan and Powell, 1963; Galifret et al., 1971). As Wilson and Lindstrom (2011) stated in a recent review, it seems obvious that the CVS must put a premium on speed. For example, if a predicted delay of 75 ms exists between the onset of a stimulus and subsequent centrifugal modulation of RGC gain, an object moving at 20°/s will only have moved 1-5°. While this is an abstract fact in the context of function, it does lend itself to the attention spotlight/attentional object selection theories described below (Holden, 1990). Given the high acuity of both the central and peripheral retina in birds, as compared with the distinct peripheral decrease in acuity in mammals (Zeigler and Bischof, 1993), it would make sense, particularly in prey species, to have

a specialised mechanism that is comparably effective at highlighting salient information anywhere in the visual field. However, such uniform high acuity across the retina would inevitably exert limitations on the capacity of higher visual areas to process such a large volume of information simultaneously (Koch and Davis, 1994). Thus, a system such as the CVS, which not only enhances RGC gain in a region of interest but also suppresses surrounding regions, would act to limit the inevitable overload. Such a system is perhaps analogous to the function of the thalamic reticular nucleus of the mammalian visual system, which acts similarly through selective inhibition of thalamocortical information transmission, or selective amplification of optimal signals from corticothalamic pathways (Guillery, Feig and Lozsádi, 1998). Furthermore, while it is known that RGC gain modulation by centrifugal efferents cannot alter receptive field properties of RGCs, it may be the case that the firing mode of the RGC can be altered by this input in a manner analogous to the tonic/burst mode changes described for dLGN neurons in **Section 1.4.2**.

1.5.7.2 Organisation and function

The CVS shows a great degree of variability in organisation between species (Réperant et al., 1981; Weidner et al., 1987; Réperant et al., 1989; Feyerabend, Malz and Meyer, 1994; Réperant et al., 2006; Réperant et al., 2007). It is potentially possible to elucidate function from this variation by identification of the relationship between specific adaptations in different animals with, for instance, corresponding differences in CVS organisation, or through identification of common ecological pressures that have led to similar anatomical organisation between species. A straightforward example of this concept is the observation that ground-feeding birds appear to have larger centrifugal projections than several raptor species (Shortess and Klose, 1975; Weidner et al., 1987) or those that 'feed on the wing' (Feyerabend et al., 1994) such as swallows (*Hirundo rustica*), thrushes (*Turdus merula*) and hawfinches (*Coccothraustes coccothraustes*). One could infer a number of ideas from this information (and indeed a

number of these studies have) based upon basic anatomy, predator/prey classification, etc. (Réperant et al., 1989)

An interesting aspect of the anatomy and organisation of the CVS is that the termination of the pathway on the retina has a distinct pattern, i.e. it is strictly confined to the ventral retina, corresponding to the superior visual field. Putting aside the specific connectivity and neurochemical properties of this particular example, it is interesting to bear in mind that such a division in the retina is not an uncommon occurrence, particularly in birds. Studies by Wortel and colleagues sought to investigate dorsal-ventral adaptation in the pigeon (1984) and chicken (1986), and specifically investigate a potential difference in spectral sensitivity. An increased sensitivity to UV light in the short wavelength range was identified in the chicken dorsal retina relative to the ventral retina of the same species, while pigeons were found to have an even greater near UV sensitivity in both the dorsal and ventral retina compared to the chicken. The basis for near UV sensitivity is due to the distribution and density of UV sensitive photoreceptor neutral UV transparent oil droplets. Wortel suggested that the pigeon's high, homogeneous distribution of near UV sensitivity across the retina might be an adaptation functionally relevant to its renowned navigational prowess. Furthermore, they suggest that the localised dorsal UV sensitivity in chickens may be directed towards a predator detection paradigm that takes advantage of the UV reflectance of shadows. The latter example is particularly relevant to the most recent functional theory relating to the CVS (Wilson and Lindstrom, 2011), which suggests that the ventral termination of centrifugal fibers, which in turn modulate RGC activity in predominantly the dorsal retina, are arranged such that 'moving shadows' of overhead predators fall upon this region and therefore would serve as an escape mechanism. Detection of the position of the shadow on the ground region scanned by the dorsal retina could then be translated to determine the position of the predator in the sky that in turn could be scanned/tracked and escaped from. Numerous other potential roles for the CVS are based upon the dorsal/ventral retinal termination asymmetry including a visual

attention switching mechanism that was proposed to be involved in predator detection (i.e. ventral retina) during feeding (i.e. dorsal retina), i.e. the searchlight hypothesis (Holden, 1990; Clarke, Gyger and Catsicas, 1996), which incidentally was proposed as a function of the thalamic reticular formation in the mammalian visual system (Crick, 1984).

A non-avian example of a dorsal-ventral retina specialisation, the South American opossum, has a distribution of oil droplets confined solely to the ventral retina, with a tapetum lucidum (a specialised layer superficial to the retina with specific reflective and absorptive properties) confined to the dorsal retina (Ahnelt, Hokoc and Rohlich, 1995; Temple, 2011). This is presumably as an adaption to a nocturnal (increased light sensitivity from the tapetum) and arboreal ecology (increased spectral sensitivity for foliage discrimination). Further dorsal-ventral differences in retinal organisation are found in the observed dominant distribution of S-cones in the ventral retina of various species, including, for example, the rabbit (*Oryctolagus cuniculus*) (Juliusson et al., 1994) and the house mouse (M*us musculus*) (Szel et al., 1992; Szel, van Veen and Rohlich, 1994; Szel et al., 1996). This arrangement led to the 'skylight hypothesis', which proposes that an increased preponderance of S-cones in this retinal region may provide increased contrast to facilitate the detection of predators against the background of a blue sky.

A number of hypotheses are based upon the atypical intra-retinal connectivity of the CVS, specifically the dorsal retina bias of RGC modulation by IOTCs. The preferential modulation of the dorsal retina, which corresponds to the inferior visual field, in combination with comparative studies that described a more 'organised' or complex CVS in ground-feeding birds, led to the proposal that the CVS may play a role in pecking accuracy. Hahmann and Gunturkun (1992) pursued this idea in the same study described above and, subsequently reported a deficiency in pecking accuracy. However, Wilson and Lindstrom (2011) argue that the 'pecking accuracy or success' hypothesis is neatly ruled out by a consideration of specific

details of pecking behaviour, e.g. the duration of a peck is too short to allow for any visually guided correction. Furthermore, as noted by Rogers and Miles (1972), a lesion of the ION would inevitably damage the mesencephalic branch of the trigeminal nerve and could thereby potentially explain a resulting motor deficit such as that seen in pecking accuracy (Zeigler and Miller, 1975). Further evidence to the contrary came from a recent study that showed that there is no link between ION volume and specific behaviors predicted by previous lesion studies (Gutierrez-Ibanez et al., 2011), e.g. pecking behavior (Hahmann and Gunturkun, 1992) and predator detection (Holden, 1990).

The majority of studies into the function of the CVS consider the ION and EA as a single entity. However, the suggestion that ION and EA may have independent functions was raised by Hahmann and Gunturkun (1992). Following lesion of the ION, EA, or both, it was reported that deficits in visual discrimination, visual acuity and detection of moving targets were all apparent and, furthermore, that such deficits were apparent with lesions of the ION but not with lesions of the EA. Other studies, however, have not been able to reproduce this deficit (Shortess and Klose, 1975; Knipling, 1978b). Indeed, crucially, in the study by Knipling (1978) the IOTr rather than the ION itself was lesioned, thus ruling out the possibility of trigeminal nerve damage, which as mentioned previously could explain Hahmann and Güntürkün findings. The sole hypothesis for an independent EA function is derived from the contentious possibility, as previously mentioned, that divergent EA efferents terminate upon dRGCs of the inferior retina. The potential involvement of the EA in modulation of the accessory optic system led Woodson et al. (1995) to propose a role in the enhancement of retinal stabilisation of gaze and potentially in the control of the optokinetic response (Fite et al., 1981).

1.6 Adaptations: An evolutionary perspective on CVS function

Evolution has led to a great diversity of organisms in the natural world. The individual requirements of an individual or a species are shaped by its ecology leading to specialisations

or adaptations driven by selective pressures. Although there is great scope for variation between species, a common specialised region of the retina among vertebrates is the area centralis, a region defined by a relatively high proportion and density of cones that may or may not contain a depression in the centre (the fovea). The area centralis and fovea are anatomical adaptations that enable enhanced visual acuity (or resolving ability) along the optical axis. In certain species, such as the chicken or mouse, the area centralis does not contain a fovea, while in others, e.g. the pigeon and primates, both an area centralis and a fovea are present (Walls, 1942). Indeed, in the pigeon a second specialised region of high acuity is present in the dorsotemporal retina, i.e. the red field or area dorsalis (Galifret, 1968; Hayes, 1982); a uniform thickened region, comparable to the parafoveal region of the area centralis, although the red field does not have a depression (Hayes, 1982). While the central and nasal retina of the pigeon retina are laterally directed, in an arrangement that lends itself to high acuity distant vision, the location of red field corresponds to the inferior nasal visual field, providing high acuity for near and binocular vision (Bloch and Martinoya, 1982). The terminology of red field and the yellow field (the latter, thus far undefined, refers to the remainder of the retina, including the area centralis and the fovea) arises from the presence of oil droplets and microdroplets with individual colour properties situated on the distal cone photoreceptor inner segments (Pedler and Boyle, 1969). Leure-duPree (1978) identified five types of oil droplets. While these are distributed in different proportions within the yellow field, the area dorsalis, although still containing all five types, has a high proportion of red droplets. Functionally, oil droplets are photopigment specific and are thought to enhance the spectral sensitivity and colour discrimination of cones (Bowmaker, 1977).

1.6.1 Eye orientation

Animal species that have their eyes positioned frontally within the skull, a common feature of carnivore predators in particular, often have a comparable degree of binocular overlap and

usually, but with exceptions, not least in all bird species, a partially crossed optic chiasm. Eyes positioned laterally within the skull (e.g. as in rabbits, pigeons, etc.), i.e. species often preyed upon, sacrifice a degree of depth perception through stereopsis for an increased panoramic visual field, presumably for an enhanced ability to detect approaching predators.

As well as relating to feeding behaviour, the degree to which the organisation of the ION varies within different avian species, and more broadly, orders, may have implications with regards to potential function. For example, it is possible that the level of lamination and size/volume of the ION relates to varying eye orientation in different species. A survey of over forty avian species was carried out by Iwaniuk and colleagues (2008) in which measurements were taken for orbital convergence, binocular visual field, axial length, brain volume, TeO volume, VW volume and telencephalon volume, with the intention of establishing whether there was any correlation between orbit orientation, eye size and VW volume. A significant correlation between orbital convergence and increasing VW volume was found. These results, specifically those for optic convergence, combined with the relationship identified between ION organisation and species with different feeding behaviours (Weidner et al., 1987; Feyerabend et al., 1994), present the starting blocks for an investigation into a possible correlation between ION organisation and orbit orientation. According to one hypothesis, a negative correlation might be expected between the angle of orbital convergence and ION cell number, degree of nuclear lamination and organisation. Should the ION have a role in providing visual continuity in a panoramic field as suggested by Cajal, in species with laterally orientated orbits, it may also conceivably be involved in disparity sensitivity and stereopsis. En route to the dLGN, optic nerve fibers partially decussate at the optic chiasm such that each cerebral hemisphere receives a retinotopic representation that comprises nasal and temporal hemi-retinal projections from contralateral and ipsilateral eyes, respectively. Such an arrangement is the basis for binocular vision and in part, stereopsis, i.e. the ability to perceive depth (Harris, 1904). Strictly speaking, stereoscopic vision is not solely dependent upon the

relative degree of binocular overlap but also upon specialised binocular receptive fields within the visual cortex. The retinal disparity that emanates from the separation of the two eyes within the skull, such that a comparison between the marginally different points of perception are 'compared', allows for perception of visual field depth (Iwaniuk and Wylie, 2006).

1.6.2 Retinal vasculature

Reptiles and birds, unlike mammals, including humans, have an entirely avascular retina that allows for greater visual acuity as compared to that seen in 'higher' vertebrates such as mammals. In the latter, the retinal blood vessels present in the inner layers of the retina inevitably degrade the resolution of the 'formed image'. The human area centralis, which contains the fovea, is an avascular region within an otherwise vascular retina. Given that the fovea is specialised for high-resolution vision, this adaptation is not unexpected.

How then are species with avasuclar retinas adapted to meet these same high metabolic demands? In birds, the oxygenation and nutrient requirements of the retina are provided for by diffusion from the choroidal vasculature into the retina as well as a specialised region of the choroid, the pecten oculi (**Fig. 1.20**). This vascular, pigmented structure extends from a base in the uveal tract at the optic disk, deep into the ciliary region of the vitreous chamber. It has been shown that through specialised, regular, high frequency cyclotorsional eye movements combined with a 'drag effect' within the viscous vitreous humor facilitate diffusion of nutrients across the barrier of the pecten oculi, into the vitreous humor, providing nutrition and oxygenation to retinal neurons (Wingstrand and Munk, 1965; Pettigrew, Wallman and Wildsoet, 1990; Zeigler and Bischof, 1993). Given the benefits of this organisation, the evolutionary basis for an apparent 'backwards step' in higher vertebrates to a vascular retina, and therefore reduced acuity, is an intriguing one. Pettigrew and colleagues (1990) proposed that cyclotorsional eye movements co-evolved with the pecten in order to optimise the perfusion of oxygen and nutrients to the inner retina and that, in turn, allowed specialised

ocular adaptations that were not available to the mammal. Conversely, as discussed in the next section, it is possible that adaptations such as this may have been selected against, in favour of a vascular retina that compromised increased acuity (other than in the area centralis) so that the metabolic demands of the retina were not 'on a knife-edge'. Briefly, extending the previous example of the pecten oculi, a correlation between nocturnal/diurnal nature and pecten oculi, complexity is apparent. Nocturnal species such as the great horned owl possess a less 'pleated' (7-8 pleats) pecten than diurnal raptors such as the red-tailed hawk (17-18 pleats). It has been suggested that this variability may be due to the role of the pigmentation of the pecten oculi potentially acting to protect against ultra-violet damage to blood vessels (Gultiken et al., 2011). Alternatively, it may act as an intra-ocular 'hood' to block excessive glare from sunlight (Barlow and Ostwald, 1972), i.e. factors that would only present ecological pressures for diurnal species.

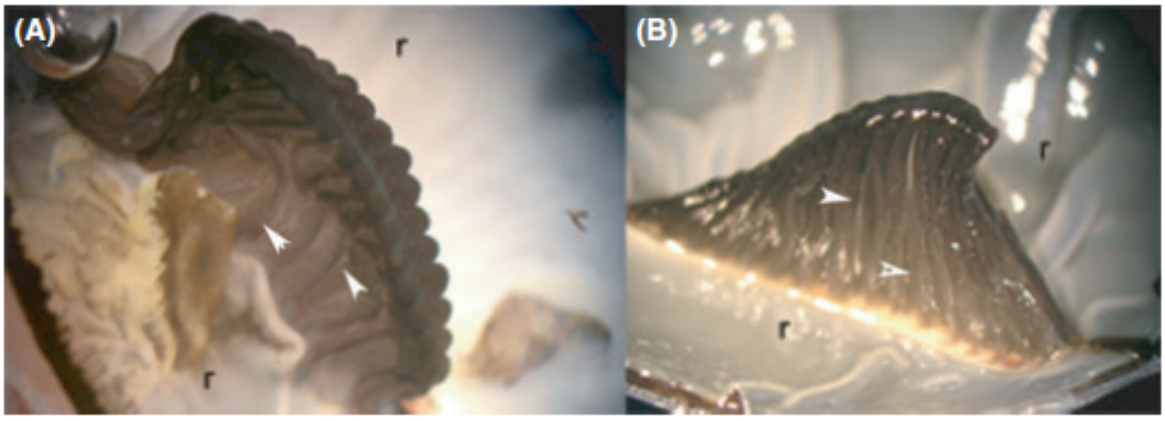

Fig. 1.20. The appearance of the pecten oculi in the common buzzard (*Buteo buteo*) Note the large base and pigmentation that results in the darkened appearance. The large number of pleats of the buzzard pecten (17-18) is typical of a diurnal bird species, with nocturnal species usually having fewer. Imaged **(A)** before **(B)** and after removal of the vitreous body. Taken from Gultiken et al., 2011.

It is thought that early primates were probably nocturnal (Martin and Martin, 1990), which, in the context of colour vision, may have led to selective loss of photopigment diversity. Broadly speaking, birds have tetrachromatic vision, while nocturnal primates are dichromatic (lacking

S-cones) and diurnal primates are (trichromatic). This nocturnal lifestyle may also have led to selective pressures favouring more light sensitive vision, i.e. a rod dominated, vascularised retina, as opposed to sharp, high acuity vision provided by an avascular retina and cone dominant tetrachromatic vision. Adaptation of the eye to nocturnal conditions seems to follow one of two paths. The first scenario is the development of smaller eyes, with a corresponding reduction in the size/volume of visual brain structures. The basis of this shift is a decreased reliance on visual senses and an enlargement of another sensory system or systems that are more suited to a given nocturnal lifestyle or perhaps even a subterranean environment. Alternatively, and conversely, a species could evolve from a diurnal towards a nocturnal lifestyle by adapting the visual system to meet different requirements. Examples of this would be greater eye size in order to increase the chance of capturing photons through so-called binocular summation, by increasing the proportion of sensitive photoreceptors, i.e. rods, to spectrally sensitive cones, and to increase the density of rod photoreceptors in order to improve visual acuity in dim light. A typical and well-studied example of these adaptations is the strigiform order (i.e. owls). The barn owl (*Tyto alba*) is highly adapted to a nocturnal, predatory lifestyle and as discussed in **Section 1.5.5**, were found to have a significantly greater proportion of ipsilateral EA cells relative to their total as a fraction of their total centrifugal cell number than the more commonly studied species, e.g. pigeons. In fact Weidner et al. (1987) studied the centrifugal visual system in twelve species of strigiforms and raptors, however, due to animal protection laws, the majority were studied using Nissl-stained tissue from collections, i.e. not specifically labeled for centrifugal neurons. Therefore, for the most part, only conclusions relating to ION organisation, (and not EA) could be made. In general it was established that species within strigiform and raptor orders had a relatively poorly organised (in this case, far fewer cells and a less delineated boundary) CVS when compared with ground feeding bird species. On average, these species only had around a tenth the number of centrifugal neurons found in the pigeon.

1.7 Summary

Over a century of research on the CVS has focused almost exclusively on that of birds, particularly the pigeon (*Columba livia*), chicken (*Gallus gallus*) and Japanese quail (*Coturnix coturnix japonica*) (**Section 1.5**), in large part because, in these species, the CVS is relatively large and more clearly delineated as compared to other vertebrate groups (Réperant et al., 2007). For example, mammals, including primates have a far less organised example of the system, with the axons of only a few tens of neurons terminating in the retina (Gastinger et al., 2006). In itself, this variability in organisation may be crucial to identifying the function of the system, i.e. numerous co-incidental species differences may correlate with the degree of CVS organisation. For instance, it may be the case that the CVS is only a major component in non-mammalian species with a prominent tectofugal visual system, e.g. reptiles, amphibians, birds etc. In fact, such a division is too simplistic as a great deal of variation in organisation exists between closely related species (Shortess and Klose, 1975; Weidner et al., 1987; Feyerabend et al., 1994). In this chapter, I have given an overview of the major components of the visual system that are relevant to CVS organisation and function. An understanding of the latter is the main goal of current research into the CVS but fitting physiological, anatomical and behavioural findings into a ecological context has thus far been a stumbling block.

1.8 Aims

Local ocular mechanisms are critical in the post-natal development of the eye (emmetropisation) although modulation of such mechanisms by higher brain processing is also necessary in at least some instances. A feedback projection to the retina that is involved in modulation of retinal activity, such as the CVS, would be a possible candidate for such a function.

The first specific aim of this work was to establish whether the CVS was involved in the regulation of post-natal eye growth in the chick. High contrast vision is dependent upon

refracted light being precisely focused at the level of the retina (i.e. photoreceptors). In order for this to happen, ocular growth must be tightly coupled to the combined refractive power of the optical components of the eye, e.g. the cornea and lens. **Chapter 2** will give an overview of emmetropisation, the process by which ocular component growth is controlled. In order to investigate the role of the CVS in the development of emmetropia, centrifugal efferents to the retina were disrupted through an electrolytic lesion of the isthmo-optic tract. Subsequently, the refractive state, corneal radius of curvature and ocular component dimensions were measured over the course of three weeks post surgery under 4 seperate developmental conditions:

1. Normal visual development (**Chapter 6**)
2. Constant light rearing (**Chapter 7**)
3. Minus lens treatment (**Chapter 8**)
4. Plus lens treatment (**Chapter 8**)

The second aim was to investigate the midbrain connectivity of the CVS. While a good deal of recent work has been directed towards the target(s), connectivity and neurochemical properties of centrifugal efferents within the retina (Lindstrom et al., 2009; Lindstrom et al., 2010), the potential for elucidating the function of the system, may rest on an identification of the source of afferent connections to centrifugal neurons in the brain. The literature is particularly inconclusive as regards the so-called ectopic neurons that surround the main source of centrifugal efferents, the isthmo-optic nucleus. As such, the main focus was on identifying sources of afferent input to this area. In order to investigate sources of afferent input to the ION/EA, intra-cranial injections of retrograde pathway tracers were made into the ION/EA (**Chapter 9**).

Chapter 02

An introduction to emmetropisation

2.0 Overview

The aim of this chapter is to provide background information into the optical, clinical and molecular basis of emmetropisation, the term given to the process by which visual experience guides ocular growth to provide high contrast vision. A great amount of research is focused towards the identification of the factors involved in the driving and regulation of this process and a number of animal models, including the chicken (Wallman and Adams, 1987; Schaeffel and Howland, 1991), the tree shrew (McBrien and Norton, 1992; Siegwart and Norton, 1998) and the monkey (Troilo and Judge, 1993; Smith et al., 1999; Smith et al., 2002) have been used. Emmetropisation is a predominantly visually-guided process with the visual cues being decoded by intra-retinal mechanisms (Troilo and Wallman, 1991; Wildsoet and Wallman, 1995). However, it is generally accepted that without a brain-retina connection, which can be achieved experimentally through sectioning of the optic nerve for example, the accuracy of this process is impaired (Troilo, Gottlieb and Wallman, 1987; Wildsoet, 2003) (**Section 2.6**).

2.1 Introduction

An understanding of the mechanisms involved in the regulation of eye growth is important for identifying the aetiology and epidemiology of refractive errors. The principal optical components of the eye, the cornea and the lens, form the anterior and posterior boundary of the anterior chamber, respectively. The posterior surface of the lens is in contact with the vitreous humour, a transparent gel, which fills the vitreous chamber of the globe, contacting the retina that lines the inner posterior surface of the globe. The optical power of the cornea accounts for around two thirds of the total power of the human eye while the lens provides the balance for adjusting the eye's refractive power (Bennett and Rabbetts, 1998), enabling focusing on objects at different distances, i.e. accommodation (**Section 1.1.2**). In the unaccommodated eye, if a distant object is in focus it said to be emmetropic, i.e. the

combined optical power of anterior chamber components act to focus the image of an object on the retina.

2.2 Refractive state

2.2.1 Ametropia

Ametropia is the term given to a refractive condition that is not emmetropic, i.e. an image is focused behind (hyperopia) or in front of (myopia) the retina. Ametropias can be classified as spherical or astigmatic. Spherical ametropias form a symmetrical sharp image around the optical axis, but not in the focal plane of the retina. An astigmatic ametropia results from the two principal meridians of the eye having differing power. Astigmatism is expressed as the difference in optical power of the two meridians (Bennett and Rabbetts, 1998).

2.2.2 Myopia/hyperopia

When an image is formed in front of the retina, the resulting refractive error is termed myopia, i.e. the optical components of the eye are too powerful for its axial length (or conversely, the axial length is too long for the combined power of the optic components of the eye). A myope is unable to focus on objects that are beyond the far point of the eye, which is defined as the point conjugate with the fovea of the unaccommodated eye. Through accommodation, a myope is able to focus on objects within the far point, and to that end, are able to focus on objects nearer to him/her than if they were emmetropic (Bennett and Rabbetts, 1998).

The prevalence of myopia has reached epidemic proportions in some populations, with a particularly high incidence in East Asia, for example. The result of this is an increasing trend in its prevalence worldwide. Moreover, the phenotype of myopia, i.e. an enlarged eye, increases the susceptibility to a range of ocular pathologies, including glaucoma, cataract and retinal detachment (Rabin, Van Sluyters and Malach, 1981).

Conversely, hyperopia is characterised by a reduced vitreous chamber depth, such that the focal plane of an image is in front of the retina. A hyperope is able to focus on objects beyond the far point (Bennett and Rabbetts, 1998). As a result, the ability to focus on objects is dependent upon the eye's accommodative power. Accommodative capability declines with age until a point, i.e. presbyopia, at which stage, the ability to accommodate is lost. Subsequently, spectacle lens correction is necessary for activities that require near vision, e.g. reading.

2.3 Emmetropisation

During post-natal/hatch development, visual experience acts, in part, to guide ocular growth through predominantly intra-retinal mechanisms, to reduce neo-natal refractive error towards zero (or a slight hyperopia), in a process termed *emmetropisation*. Newly born or hatched animals are typically hyperopic, i.e. the focal plane of the image is behind the position of retina. The initial growth rate of the eye, to a degree, passively acts to compensate for the imposed refractive error (Wallman, Adams and Trachtman, 1981; Wildsoet, 1997). However, visually-driven active modulation, or fine-tuning (in the case of neo-natal hyperopes), of this developmental correction is critical for the development of emmetropia (Troilo and Wallman, 1991), i.e. the point at which the refractive error is reduced to zero or low ametropia. The chick has been the most widely used model for investigations into the mechanisms of emmetropisation (**Section 2.1**). The consensus of numerous studies is that emmetropisation is an active, visually guided process, which is in turn aided by passive, non-visually guided ocular growth .

Although the effects of visually guided growth, i.e. emmetropisation, are observed principally during early development, i.e. the critical phase of development, the capability to compensate to visual cues with age is maintained, albeit reduced in maturity. A sharp drop off in this response is apparent in chicks (Papastergiou et al., 1998).

2.4 Form deprivation

A widely used experimental model for myopia is form deprivation. Form deprivation induced myopia (FDM) can be achieved experimentally by lid suture (Yinon, Rose and Shapiro, 1980; McBrien and Norton, 1992; Smith et al., 1999) or through occluder wear (Wallman et al., 1981; Gottlieb, Fugate-Wentzek and Wallman, 1987; Wallman et al., 1987) (**Fig. 2.3**). The ocular phenotype induced by form deprivation in chicks is characterised by an elongated axial length (Hodos and Kuenzel, 1984), an increased equatorial diameter and increased anterior chamber depth (the distance from the anterior cornea to anterior lens surface (**Chapter 3**)) (Gottlieb et al., 1987). Form deprivation induced changes in axial length are greatest during the critical phase of development (Irving, Sivak and Callender, 1992; Siegwart and Norton, 1998). For example, in one year old chicks, the axial length of form deprived, chicks increased by ~160 μm over 5 *weeks* relative to untreated eyes, compared with approximately a 100 μm increase in axial length *per day* in form deprived chicks during the critical phase (Papastergiou et al., 1998). Furthermore, significant axial elongation following form deprivation or corneal opacification is also reported in adult monkeys (Wiesel and Raviola, 1979; Smith et al., 1999; Troilo and Nickla, 2005) and humans (Rabin et al., 1981; Gee and Tabbara, 1988; McBrien and Adams, 1997).

2.5 Optical manipulation

Optical defocus, be it experimentally induced through the use of spectacle lenses or innate as is observed in numerous neo-natal vertebrate species, including humans (Cook and Glasscock, 1951; Brown, Koretz and Bron, 1999) [10], that are born with relative hyperopia (e.g. +3 to +5 Dioptres (D) in the chick) (Wallman et al., 1981), has been shown to induce changes in the growth rate of ocular components, such that the defocus is corrected, or at least reduced.

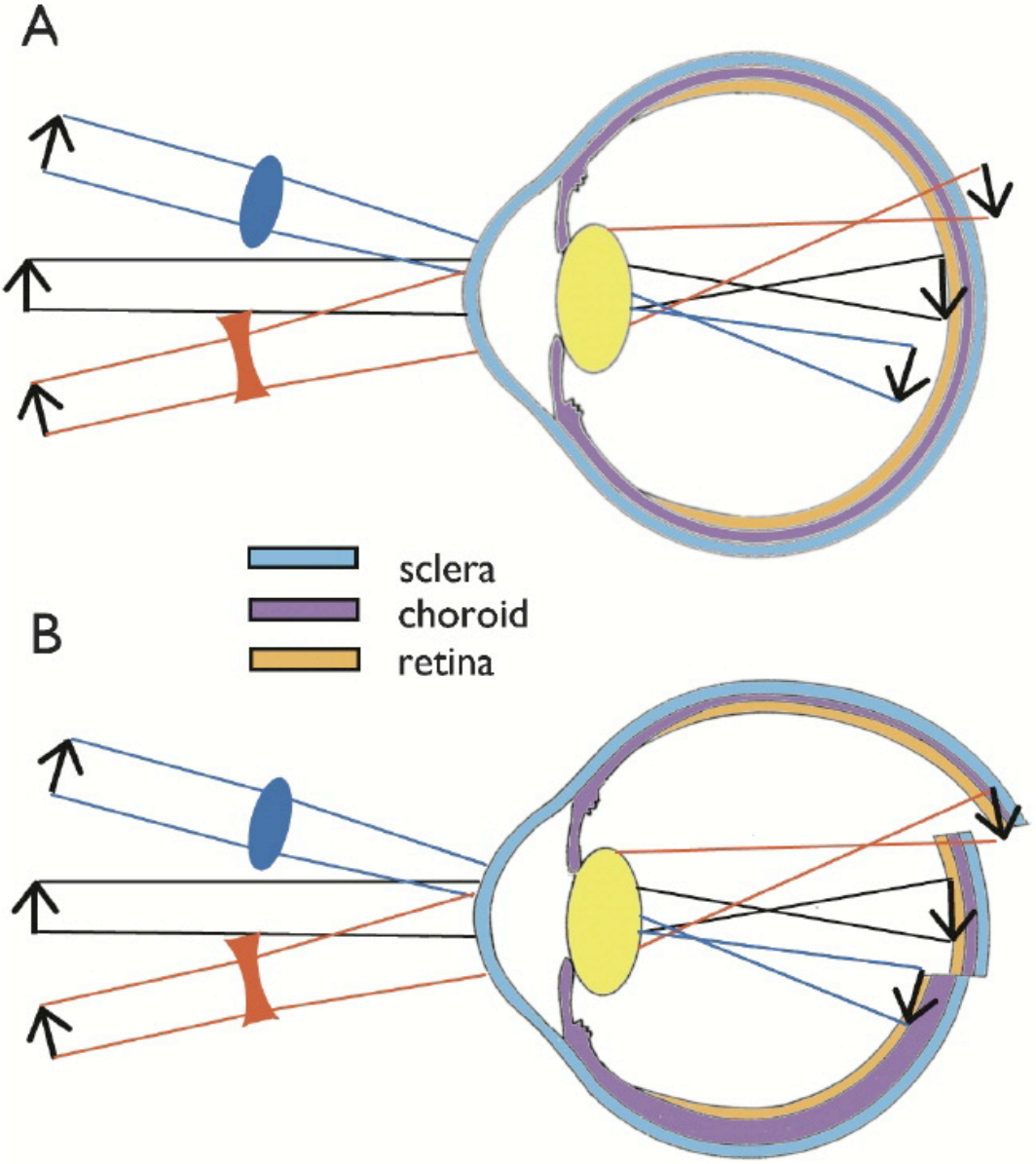

Fig. 2.1. Axial compensation to lens defocus. Schematic representation of the scleral, choroidal and retinal responses to plus and minus powered lens manipulation in emmetropization. **(A)** The effect of plus (**blue**) and minus (**red**) lens wear on the focal plane of an image relative to the retina (**orange**), choroid (**purple**) and sclera (**blue**). Plus lens manipulation changes the focal plane of an image in front of the retina while minus lens manipulation has the opposite effect. **(B)** Shows the scleral, choroidal and retinal response to plus and minus lens manipulation. Plus lens wear induces an reduced rate of scleral elongation pre-empted by choroidal thickening in response. Minus lens wear induces an increased rate of scleral elongation pre-empted by choroidal thinning. In both cases, the plane of the photoreceptors are repositioned in line with the modified focal plane of an image. Taken from Wallman and Winawer (2004).

A spectacle lens fitted in front of a chick's eye induces changes in the rate of scleral elongation to accurately negate or compensate for the power of the lens (Troilo and Wallman, 1991). Thus, a positive lens would cue a reduction in the normal rate of globe elongation in combination with a thickening of the choroid, until the combined optical power of the spectacle lens and anterior segment matched the focal plane, corresponding to the position of the retina (**Fig. 2.1**). If normal visual experience is resumed, i.e. by removing of the lens, remarkably, in chicks the affected eye is able to recover, correcting for the induced myopic defocus by slowing eye growth (Wallman and Adams, 1987). This recovery can only be achieved fully if the chick is still in the critical phase of development, which is characterised by increased growth rate and high neuronal plasticity (Wallman et al., 1981; Irving et al., 1992). Non-human primates are also able to respond to imposed defocus in the correct direction, to an albeit reduced degree. However, in comparison with chicks, recovery from deprivation myopia is generally limited if the occluder is removed (Troilo and Judge, 1993; Troilo and Nickla, 2005).

The response to imposed myopic (plus lens)/hyperopic (minus lens) defocus or form deprivation can be considered to have two phases. The first phase takes place in a matter of minutes. A change in choroidal thickness in the appropriate direction guides the underlying retina towards the plane of focal convergence of an image (Zhu et al., 2005) (**Fig. 2.1**). Conversely, an increase or decrease in the rate of ocular (scleral) elongation in response to hyperopic and myopic defocus respectively and takes a matter of days to be induced in chicks (Kee, Marzani and Wallman, 2001). Moreover, the individual time-course of this response combination is different for myopic defocus, hyperopic defocus and form deprivation as found by studies employing short-term treatment time courses for lens wear (Zhu et al., 2005) and form deprivation (Kee et al., 2001). Zhu and colleagues (2005) conclude that the choroidal response to myopic defocus occurs within 10 minutes and takes about 1-2 hours to reach its full effect. The apparently increased 'potency' of hyperopic

defocus to induce changes in choroidal thickness is in concordance with the finding that the sum growth of chick eyes exposed to short periods of myopic and hyperopic defocus interchangeably is in the direction cued by myopic defocus, i.e. a thickening of the choroid, pushing the retina towards the image whose focal plane is in front of the retina (Winawer et al., 2005). Kee and colleagues (2001) investigated the characteristics of the early response of the chick eye to hyperopic defocus in comparison with form deprivation. They found that while the onset of choroidal thinning was comparable, i.e. after 1 hour, the rate of scleral expansion was greater in response to lens wear than occluder wear. The sclera exhibited an initial slowing of scleral proteoglycan synthesis relative to the control eye following a 3 hour occluder wearing period. Following the same treatment, lens wearing chicks showed a significant increase in scleral elongation within 8 hours while form deprived eyes took 24 hours. These results present evidence towards at least partially independent mechanisms in the response to lens and diffuser wear.

It is important to note the complementary role of the choroid and the mechanisms of scleral expansion (Mertz and Wallman, 2000). For example, given the latency of the 'start' and 'stop' signals to increase or decrease the rate of scleral expansion, in a hypothetical eye that lacked a choroid, not only would the response be delayed but once compensation to defocus was achieved, the delay in response to revert the rate of expansion back to normal would result in an overshot of the initial refractive error (Zhu, Winawer and Wallman, 2003; Wallman and Winawer, 2004) (**Fig. 2.2**). Thus, as the sclera is not directly innervated, molecular cues that modulate its rate of elongation must either be generated in, or pass through the choroid (Wallman and Winawer, 2004; Nickla and Wallman, 2010). The source of these molecular signals and their role in the interaction of scleral and choroidal mechanisms are discussed further in **Section 2.7.**

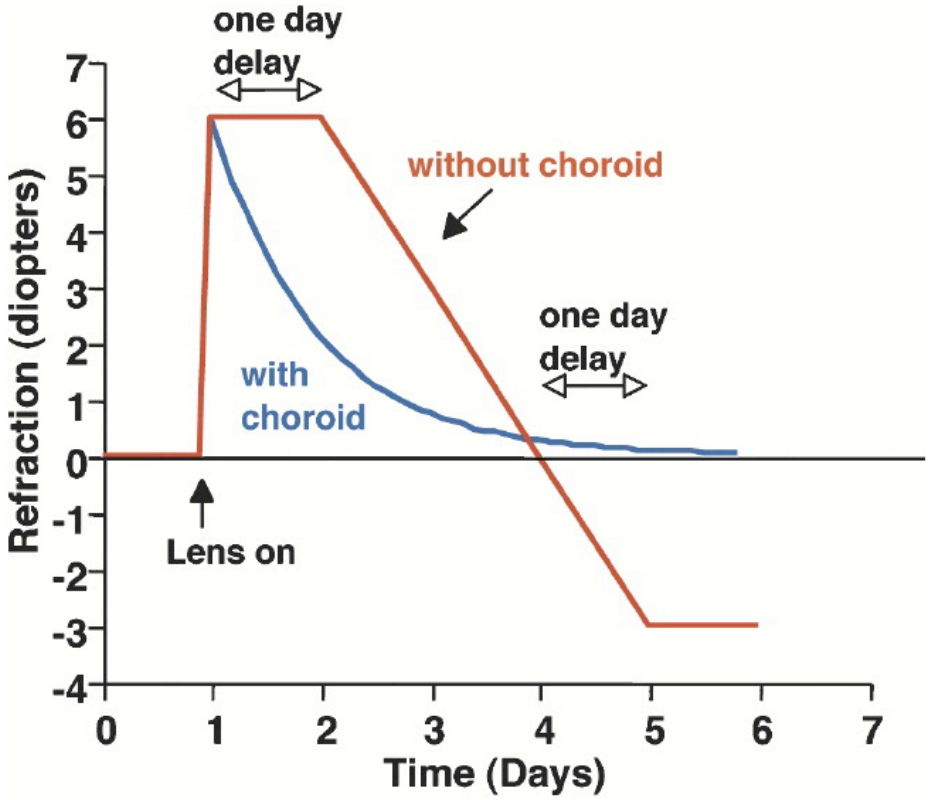

Fig. 2.2. The relationship between choroidal and scleral responses to lens wear. In this hypothetical model, in the absence of a choroid, the initial response to lens wear, i.e. choroidal thickening (plus) or thinning (minus) subsequent, slower changes in the rate of scleral growth are delayed resulting in a delayed rate of compensation. In addition, following compensation, the delay in reestablishing a stabilising rate of growth would lead to an over-compensation to the imposed defocus. With the choroid intact, the response to defocus is virtually immediate and no overshoot in compensation would occur. Thus the early response of the choroid to defocus is crucial in buffering the subsequent scleral growth rate. Taken from Wallman and Winawer (2004).

2.6 Surgical manipulation

Brain centre influences upon emmetropisation are not essential for the ability to respond to defocus cues, as has been shown in studies that achieve retinal disconnectivity from the brain through optic nerve section (ONS) (Troilo et al., 1987; Wildsoet, 2003), or through exposure of retinal ganglion cells (RGCs) to colchicine (Morgan, 1981) or tetrodotoxin (TTX) (McBrien et al., 1995), which act to destroy RGCs and block RGC action potentials,

respectively. However, in the absence of the normal communication between the retina in the brain, certain resulting impairments are evident.

Under normal visual conditions, eyes that have undergone ciliary nerve section (CNS) show an anterior chamber anomaly, specifically a thinning of the lens. However, vitreous chamber depth and refractive state remain unaffected. Furthermore, chicks treated regularly throughout development with the RGC toxin, colchicine, still respond to myopic defocus induced by positive lens wear, but not to hyperopic defocus imparted by negative lens wear (Choh et al., 2008). A combination of CNS and ONS induces inter-ocular asymmetry with vitreous chamber dependent axial elongation in the affected eye. However this asymmetry is not coupled with predicted refractive state changes, presumably due to CNS induced anterior chamber effects. Furthermore, these subjects show an exaggerated response to both form deprivation and spectacle lens-induced defocus (Wildsoet, 2003). In addition, otherwise untreated chicks raised in constant light develop a relative hyperopia characterised by a flattened cornea and an enlarged vitreous chamber (Li et al., 1995a). While lens-induced effects are not affected by changes in diurnal rhythms, chicks raised in constant light have a reduced response to FDM (Bartmann et al., 1994). Importantly, the severe effects of constant light, which are the focus of **Chapter 7**, have not been found to be affected by brain-retina disconnectivity following ONS surgery (Li and Howland, 2000).

On the basis of the observed effects of the surgical manipulations described above, it is apparent that emmetropisation is a process guided predominantly by local (intra-ocular) mechanisms independent of the brain. One of the more intriguing examples of this comes from the ability of local regions of the chick (e.g. Wallman et al., 1987) and monkey (Smith et al., 2009) eye to respond to localised defocus imposed by lens wear (Miles and Wallman, 1990; Diether and Schaeffel, 1997) and occluder wear (Wallman et al., 1987) (**Fig. 2.3**). Strong evidence for local intra-retinal mechanisms being the driving force behind emmetropisation

comes from the finding that such complex responses persist following optic nerve section (Troilo et al., 1987).

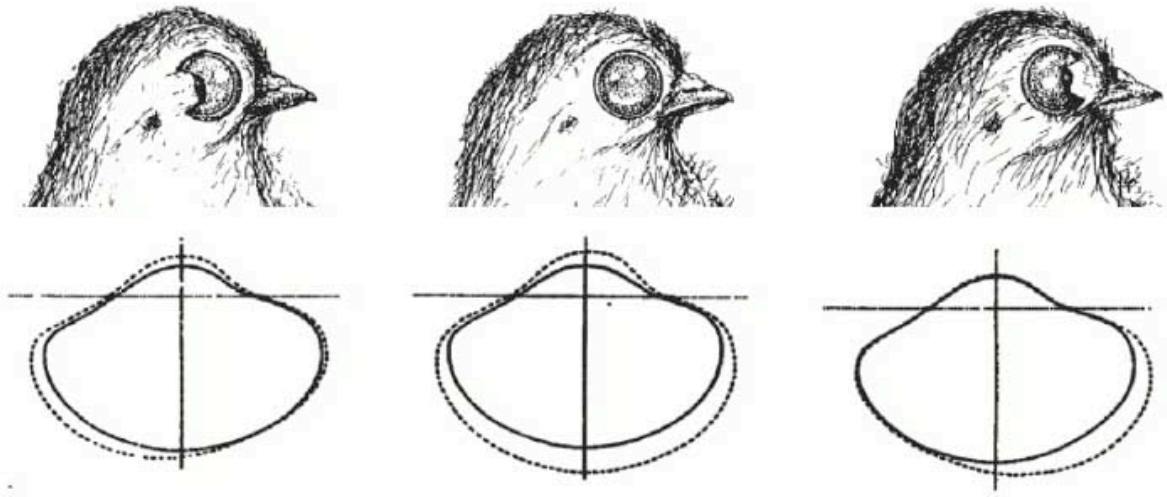

Fig. 2.3. Local ocular compensation to form deprivation. When an occluder is placed over the eye of a chick in the critical phase of development, choroidal thinning and axial elongation result, f.e. form deprivation. Localised form deprivation of the temporal (**left**) or nasal (**right**) retina alone induces local choroidal thinning and scleral elongation responses in the deprived part of the eye only (i.e. temporal sclera elongation following deprivation of the nasal visual field (**left example**), while the region of the eye that is subject to normal visual experience is unaffected. Complete form deprivation through occluder-wear induces symmetrical axial elongation (**centre example**). Importantly, a local ocular response to form deprivation still occurs following optic nerve section. The fact that such a complex response is possible without brain-retina connectivity is strong evidence that emmetropization is modulated, predominantly by intra-retinal mechanisms. Taken from Wallman et al. (1987).

2.7 Intra-retinal mechanisms of emmetropisation

A number of molecular candidates have been implicated in such mechanisms through experimental manipulations, e.g. using specific neurotransmitter receptor antagonists and assessing the subsequent capability of the treated eyes of treated animals to compensate for lens wear. The findings of such studies have been particularly useful in confronting the

questions regarding common and distinct mechanisms for the different visual manipulations described above.

2.7.1 Dopamine – The dopamine antagonist, apomorphine, prevents axial elongation following both hyperopic defocus and FDM (Stone et al., 1989; Iuvone et al., 1991; Schmid and Wildsoet, 2004), while the response to myopic defocus following apomorphine treatment is exaggerated (Schmid and Wildsoet, 2004). In addition, it is perhaps significant that atropine, a cholinergic pathway inhibitor had the same effect as apomorphine on axial elongation in response to both FDM and hyperopic defocus. Moreover, the pooled inhibitory effect of atropine and apomorphine on development of FDM was no greater than that of atropine alone (Schmid and Wildsoet, 2004), suggesting that dopaminergic and cholinergic effects may act via a common pathway.

In vitro studies showed that scleral chondrocytes had an increased mitotic rate in the presence of RPE cells (Seko, Tanaka and Tokoro, 1994). Furthermore, apomorphine had little effect on the rate of mitosis of chondrocytes by themselves, but when added to the culture in the presence of RPE cells, significantly decreased the mitotic rate, suggesting that dopamine indirectly increases the rate of scleral growth via interaction with the RPE (Seko, Tanaka and Tokoro, 1997; Witkovsky, 2004). Contradictory in vivo findings have been reported following measurement of retinal dopamine levels after lens wear. For example, Bartmann et al. (1994) found no significant difference in retinal dopamine levels following myopic or hyperopic defocus, while elsewhere reduced intra-retinal dopamine levels were reported following hyperopic defocus and increased levels following myopic defocus (Guo et al., 1995). Consistent with findings that dopamine antagonists prevent FDM, chicks raised in constant light (i.e. 24 hour/day light) show a dramatic reduction in intra-retinal dopamine levels accompanied by reduced axial elongation response following form deprivation while showing normal responses to lens wear (Stone et al., 1989; Bartmann et al., 1994). In support

of these findings, when the RPE is chemically destroyed, as one would expect given the apparent interdependence of dopamine and the RPE, axial elongation in response to FDM is inhibited (Oishi and Lauber, 1988). However, following RPE removal, axial elongation in response to constant light is *not* affected (Oishi and Lauber, 1988). Axial elongation induced by constant light rearing (i.e. raised in 24 hour/day light) is likely therefore to be an optical defocus driven mechanism, presumably induced by the severe corneal flattening that accompanies this treatment. Importantly, while it appears that responses to FDM and lens induced myopia have different mechanisms (Schaeffel and Howland, 1991; Schaeffel et al., 1992), dopamine pathways are likely to be involved in both.

2.7.2 Glucagon – Wallman (1993) suggested that local mechanisms of ocular growth are under the control of amacrine cells. Experimental destruction of around half of all amacrine cells in the chick did not prevent deprivation myopia or lens induced hyperopia thus implicating surviving populations as having a role (Fischer, Morgan and Stell, 1999b). Glucagon-expressing amacrine cells were one of the surviving populations and it has subsequently been shown that expression of ZENK (an early onset genes known as erg-1 in mammals) by these cells is correlated with the sign of imposed defocus (Fischer et al., 1999a). Specifically, ZENK expression is increased during myopic defocus and has thus been implicated as a stop sign for ocular growth (Fischer et al., 1999). Inhibition of glucagon expression by treatment with des-His^{1}-Glu^{9}-glucagon amide reduced the response to plus lenses while the glucagon agonist Lys^{17,18} Glu^{21}-glucagon-amide prevented FDM and the normal response to minus lenses (Feldkaemper and Schaeffel, 2002). ZENK expression in glucagon amacrine cells is exclusive to defocus sign and not to other basic visual cues such as spatial frequency or retinal image contrast (Bitzer and Schaeffel, 2002). Interestingly, in the same study, unilateral plus or minus lens treatment in chicks, led to up regulation of ZENK expression in glucagon-expressing amacrine cells in both treated *and* control eyes (Bitzer and Schaeffel, 2002).

The role of glucagon has been reported modulate equatorial expansion of the eye and also in ACD growth through the action of a subpopulation of glucagon containing retinal cells called bullwhip cells (Fischer et al., 2008). Colchicine, as mentioned, acts to chemically destroy RGCs and intravitreal treatment has been reported to induce ACD shortening and equatorial expansion (Fischer et al., 1999b). Bullwhip cells, are situated around the circumference of the retina and are destroyed following colchicine treatment, however, intravitreal injection of glucagon following colchicine treatment has been shown to prevent the ACD shortening and equatorial expansion normally observed (Fischer et al., 2008).

2.7.3 Nitric oxide – The NOS inhibitor L-NAME reduces the effect of form deprivation in chicks (Fujikado et al., 1997). Specifically, inhibition of nNOS (the neuronal isoform), with $N^{(\omega)}$-propyl-L-arginine, inhibits the choroidal response to myopic defocus while inducing, i.e. disinhibiting, axial elongation. This effect coincides with a decrease in the levels of retinoic acid (Nickla, Damyanova and Lytle, 2009) whose expression is known to suppress scleral expansion (Mertz and Wallman, 2000) thus demonstrating a crucial link between the early choroidal response and gradual scleral changes.

NOS containing tissues exist in the chick, including subpopulations of amacrine cells, ganglion cells, photoreceptors, stromal and endothelial cells of the choroid and the RPE, as well as efferent isthmo-optic axons and IOTCs (Morgan et al., 1994). In order to ascertain the specific population(s) that were involved in emmetropisation (or at least narrow down the 'search area'), once again the surviving cell populations were investigated following treatment with a neurotoxin, in this case quisqualate, which is known to destroy numerous populations of retinal cells but without interfering with emmetropisation mechanisms. Following treatment, labeling of NADPH persisted in isthmo-optic efferents and IOTCs, photoreceptors and displaced ganglion cells as well as Müller cells. Labeling for NOS

remained in amacrine cells resembling glucagon-expressing amacrine cells and IOTCs (Fischer and Stell, 1999).

2.8 Summary: CVS and emmetropisation

As has been alluded to, it is generally accepted that while a brain-retina connection is not *necessary* for emmetropisation, however, in its absence, i.e. following optic nerve section, the 'set-point' of emmetropia is changed and under normal developmental conditions, eyes develop moderate to severe hyperopia (Troilo et al., 1987; Wildsoet and Schmid, 2000). Importantly some of the more complex emmetropisation mechanisms, such as those that regulate how local retinal regions compensate for form deprivation, persist in the absence of a brain-retina connection. The CVS has been proposed as a candidate for brain-retina modulation of emmetropisation (Fischer and Stell, 1999), as a result of the nitric oxide immunoreactive cells that centrifugal efferents target within the retina (Morgan et al., 1994). However, the potential role of the CVS has, until now (**Chapters 6** to **8**), not been investigated.

As a side note, one that is not followed up in the experimental chapters of this project, there are a number of examples of unilateral treatment influencing both treated and control eyes (Bradley, Fernandes and Boothe, 1999). As discussed in **Section 2.7.2** above, unilateral lens treatment induces up regulation of ZENK in glucagon amacrine cells in *both* eyes. Furthermore, while monocular form-deprivation induces relative myopia in the treated eye, Schaeffel and Howland (1991) note that binocular form deprivation over a small experimental time period (7 days) induced 'form-deprivation *hyperopia*' in both eyes. These examples, are evidence for inter-ocular communication and, while no pathway has been proposed for this effect, the centrifugal pathway, of which there is a minor ipsilateral projection, is one potential candidate for involvement in binocular growth symmetry. The midbrain connectivity of centrifugal neurons and the potential existence of inter-

hemispheric cross talk that may regulate this symmetry is addressed in the results **Chapter 8**.

Chapter 3

Methods 01: CVS and eye growth

3.0 Overview

The aim of the present study was to elucidate whether unilateral disconnection of the ION and surrounding EA from the retina had an effect on the capability for, or accuracy of, emmetropisation under the following conditions:

- **'Normal' conditions,** i.e. 14 hours light, 10 hours dark
- **Constant light,** i.e. 24 hours light
- **Myopic defocus**
- **Hyperopic defocus.**

In each instance, a tungsten electrode (AM systems, UK), insulated except for the tip was used to make an electrolytic lesion (i.e. current generated by a stimulus isolator was passed through the electrode) of the isthmo-optic tract [13]. Subsequently, over the course of a three week survival period ocular phenotyping was performed in order to assess any potential effect of centrifugal efferent disruption on post-natal ocular growth. In addition, a pathway tracing paradigm was used to allow accurate determination of lesion success. In this chapter, primary methods, i.e. those common to the above four above subdivisions of the experiment designed to investigate the potential role of the CVS in the regulation of the development of emmetropia, will be described. In the subsequent results chapters, specific changes and additions to these experimental templates will be addressed in context.

3.1 Animal husbandry

Chicks were obtained as eggs from a hatchery specialised for biomedical research (Henry Stewart Ltd. UK) and were incubated at 37.4°C and 40% humidity for 18 days, at which point they were transferred to a temperature controlled hatching chamber for the remainder of the 21-day gestation period [12]. Once hatched, the chicks were transferred to a custom made, temperature controlled (25-27°C) brooding pen for the first week, before being transferred

to a larger pen heated by an overhead lamp for the remaining duration of the study. Food and water were available *ad libitum*, with the exception of 1-2 hours prior to induction of general anaesthesia. During this time, chicks were food deprived but still had unlimited access to water. Unless otherwise stated, chicks were kept on a 14 hours on/10 hours off lighting schedule with the illumination in the brooder and floor pen at 250 to 300 lux.

3.2 Stereotaxic technique

A stereotaxic frame, consisting of a frame assembly (model 1730; Kopf, USA), a bird adaptor (model 915; Kopf, USA), and 45° non-rupture tip ear bars designed for bird use (model 1755; Kopf, USA), was used for all chick surgeries. Prior to anaesthesia of the chick, an electrode was positioned in a micromanipulator (model 1760-61; Kopf, USA). Ear bars were positioned such that where they met corresponded to the middle point of the frame, i.e. coordinates; 0.00, 0.00, 0.00). One ear bar was removed and the tip of the electrode was then lowered to the tapered end of the remaining ear bar. The position of the electrode tip was carefully guided until it was aligned in the anterior-posterior (AP), medial-lateral (ML) and dorso-ventral (DV) planes with the ear bar centre. Subsequently, co-ordinates were recorded for each axis with the electrode in place. Additionally, the electrode was lowered beyond the ear bar position and raised in order to determine whether the electrode axis was correctly aligned within the micro manipulator. This process was repeated 3 times and the mean of each axis was used as the final ear-bar zero from which co-ordinates for specific brain regions were derived.

Once the chick was anaesthetised, the feathers around the external auditory canal were cut, and the animal was placed in the frame, making sure that the ear bars were engaged within the internal auditory canal. Confirmation of the correct positioning of the ear bars was possible by noting the consistent between animal distance between the ear bars with the chick in place. Anterior-posterior rotation of the head in the frame was prevented by the use

of the bird adaptor, which consisted of a tooth bar that was positioned at the base of the beak and a curved beak bar that rested around the upper beak (Kuenzel and Masson, 1988). Following surgery, the ear, tooth and beak bars were removed, and the chick was removed from the frame and allowed to recover under close observation.

3.3 Determination of ION/IOTr co-ordinates

In order to ascertain accurate and consistent co-ordinates for the isthmo-optic nucleus and the isthmo-optic tract of the 4/5-day-old shaver black chick, the method of Kuenzel and Masson (1988) was used. In total five 4-5 days old chicks were given an overdose of sodium pentobarbital (Euthatal) and perfused intra-cardially with 100 ml of 0.1 M phosphate buffered saline (PBS) followed by 250 ml of 2.5% paraformaldehyde in 0.1 M PBS. The dorsal cranium was then carefully incised to ensure fixative access to the brain. The skull, with brain and eyes intact was post-fixed in the same solution for at least a further 72 hours. The skull was then set up in the stereotaxic frame, making sure that the ear bars were seated correctly in the inner auditory canal and the dorsal cranium and underlying meninges were carefully removed to expose the brain.

A #10 scalpel blade mounted to an electrode carrier and zeroed with respect to ear bar zero in the AP and ML planes (a priori), was used to remove the majority of the telencephalon in the coronal plane at an AP level estimated to be approximately 2 mm rostral to the optic chiasm (**Fig. 3.1**). In the caudal direction, progressive 200 μm slices were taken in the same way until familiar landmarks in the midbrain were visible. In this case, the anterior commissure and the anatomy of the ventricle of the TeO were used to determine the distance to the IOTr and ION. When proximity was judged to be ~0.5 mm, the approach of progressive, thinner (100 μm) slices were taken until the position of the IOTr could be visualised using a surgical microscope. At this stage a second carrier holding an electrode was introduced and the tip of the previously 'zeroed' electrode was guided to the position of

the IOTr. The AP, ML and DV coordinates were then recorded. The electrode was subsequently removed and guided back three times to obtain repeated measures. For each subsequent 100 µm slice, the same procedure was followed until the IOTr was no longer present, at which point, the same process was continued for the determination of ION coordinates.

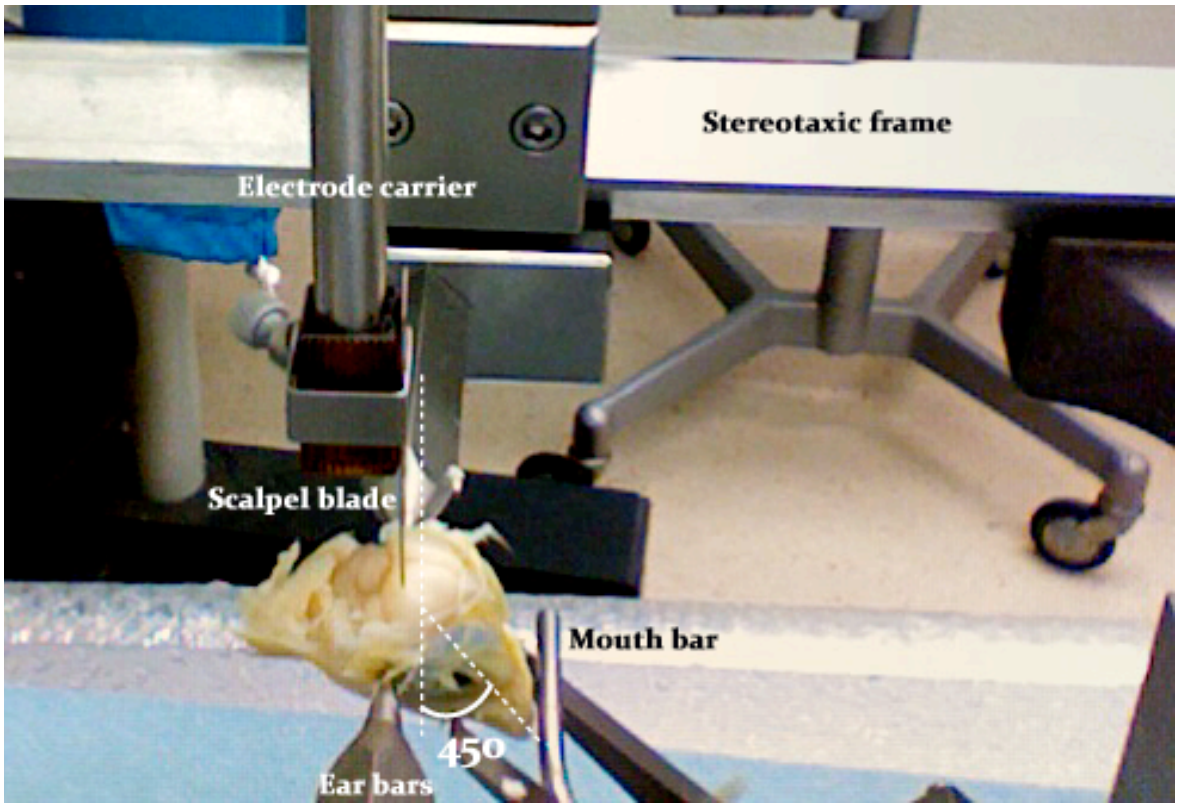

Fig. 3.1. Determination of ION/EA and IOTr stereotaxic coordinates using the method of Kuenzel and Masson (1988). A formaldehyde fixed intact chick skull is placed in the stereotaxic frame (i.e. ear bars and mouth bar) before careful dissection of the dorsal cranium. A scalpel blade placed in an electrode carrier is used to cut progressive coronal brain slices in the rostral-caudal direction until such a time that the target region is visible (or associated landmarks are apparent). At this stage, an electrode carrier with an electrode is introduced and lowered to the target region. Repeated co-ordinates can then be taken and used as preliminary stereotaxic co-ordinates for surgery. Note that fine-tuning is required in order to account for tissue shrinkage associated with fixation.

Fine-tuning of the coordinates obtained using this method was necessary. Initially, a stereotaxic injection of a dye (trypan blue) was made into an intact, fixed brain, using the pre-determined coordinates above (according to the protocol for intracranial injections found in **Chapter 4**). Microtome sectioning and histological analysis of the injected brain sections allowed initial adjustments to the coordinates if required. Because fixation causes shrinkage of tissue, the next stage of co-ordinate determination required lesions of the ION or IOTr to be performed on chicks under terminal anaesthesia. Once surgeries were complete, chicks were perfused and sectioned brain tissue was processed in order to assess the accuracy of the coordinates used (according to the protocol in **Section 3.9** and **3.10**).

3.4 Electrolytic lesion of the IOTr

Four to five days post-hatch (corresponding to a body weight of between 37 g and 45 g in healthy chicks), general anaesthesia was induced (and maintained as necessary) in chicks by intra-muscular injection of a ketamine hydrochloride (50mg/kg) and xylazine (3.5 mg/kg) solution (prepared from stock 100 mg/ml solutions in filter sterilised dH_2O), combined with a pre-operative intra-muscular injection of analgesic (ketoprofen 0.1 mg/kg). Once deeply anaesthetised (as determined primarily by a lowered respiratory rate and an absent toe-pinch reflex), subjects were placed in a stereotaxic frame (Kopf, USA) as described earlier. Initially, the scalp was incised to reveal the dorso-caudal cranium. A craniotomy was performed using a dental drill, revealing the dura mater. A small cut was made in the dura using a micro-scalpel and a tungsten electrode, insulated except for the tip, was lowered to predetermined coordinates (**Section 3.3**), corresponding either to the ION or the IOTr:

- **Co-ordinates for the ION: AP: +2.00; ML: -1.75; DV: +4.50**
- **Coordinates for the IOTr: AP: +2.30-2.70; ML: -2.00; DV: 5.15**

The electrode was then lowered a further 200 μm for three to four minutes in order to penetrate the pia mater overlying the dorsal midbrain. The electrode was then raised back

to the previous dorso-ventral position. An electrolytic lesion was made, passing 0.90 mA DC current for between 15-25 seconds. The electrode was left in place for a further 15 seconds before being disconnected from the stimulus isolator and raised out of the brain. Instead of receiving an ION or IOTr lesion, a proportion of subjects underwent a sham procedure whereby lesions were placed in superficial intra-cranial space or nearby brain regions, (e.g. in the TeO lateral to the IOTr/ION) that were not intended to disrupt isthmo-optic efferents. In some cases, the electrode was lowered to the co-ordinates of the isthmo-optic tract, but no current was passed. The craniotomy was filled using bone-wax (if required) and the scalp incision sutured. A custom made hard-plastic concave disc was super glued to feathers surrounding the wound in order that unwanted pecking from siblings did not compromise the healing process.

3.5 Corneal radius of curvature

The radius of corneal curvature (CR) was measured on awake chicks using a modified videokeratometer, based on the design of Schaeffel and Howland (1987). The videokeratometer consisted of a 520 mm diameter ring of 6 IR LEDs (5 mm diameter, wavelength: 875 nm; code #497-0486, RS Components Ltd, UK) attached to a monochrome 640 x 480 pixel Firewire camera (model DMK 21F04, The Imaging Source Ltd. GmbH) fitted with a 40 mm extension tube, 2x extender, a lens (f = 50 mm, model #B5014A-KA, The Imaging Source Ltd. GmbH) and an IR filter (code #092-58x0.75, The imaging Source Ltd. GmbH).

Measurements were taken in awake chicks that were gently restrained such that each eye, in turn, was positioned at the focal plane of the camera (~520 mm). The ring of reflected LED point sources was centered with respect to the cornea (**Fig. 3.2**). Images of the LED point sources reflected by the cornea were sampled in real-time and used to calculate corneal curvature in the 2 principal meridians using custom written software (**Fig. 3.2 A**). Six

readings were taken for each eye, and for each reading obtained, the measurements for the two orthogonal meridians were averaged. Means of the six repeated readings were then averaged. Right eyes were consistently measured first, and all measurements were taken in the dark.

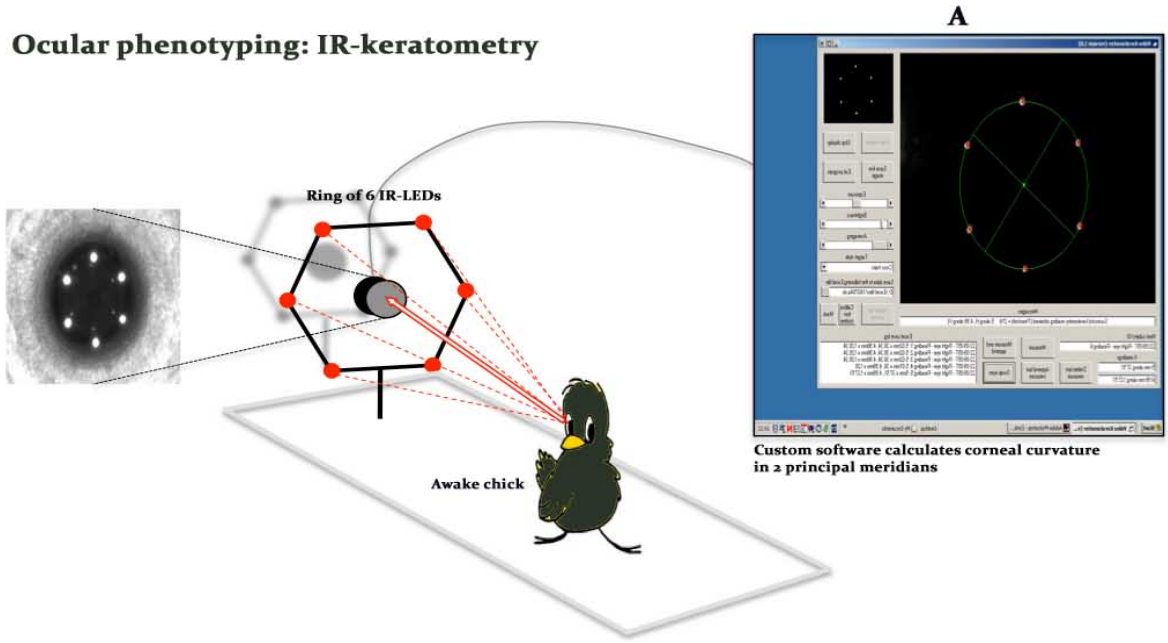

Fig. 3.2. Infra-red keratometry. Schematic of the apparatus used to measure corneal radius of curvature using infra-red video-keratometry. The radius of corneal curvature (CR) was measured on awake chicks using a modified videokeratometer. Awake chicks were held such that the eye to be measured was positioned at the focal plane of the camera. Images of the LED point sources reflected by the cornea were sampled in real-time and used to calculate corneal curvature in the 2 principal meridians using custom written software (**A**).

3.6 Refractive state

Streak retinoscopy was used to measure the refractive state (REF) of both eyes of all chicks to prescreen for ametropia prior to surgery and during post-treatment phenotyping. Measurements were carried out on non-cyclopleged, awake chicks in dim light and were not corrected for the small eye artifact of retinoscopy (Glickstein and Millodot, 1970). Refractive

state is determined in this way by passing a collimated streak of light from a retinoscope across the pupil and observing the direction of the response of the retinal reflex, that is depending on whether a 'with' (the reflex is in the same direction as the motion of the retinoscope) or an 'against' (the opposite) response is observed. By holding plus or minus powered lenses in front of the eye, the far point is shifted until it coincides with the working distance, i.e. the constant distance between the retinoscope and the subject (i.e. 0.4 m). At this point a 'neutralisation' reflex is observed (i.e. a static 'flash' reflex), whereby the entire retina is luminous and no 'with' or 'against' response is present. For each eye, the refractive state of the 2 principal orthogonal meridians was averaged and corrected for the working distance of 0.4 m.

3.7 Ocular component dimensions

Following measurement of CR and REF, general anaesthesia was induced (and maintained as necessary) by intra-muscular injection of a ketamine hydrochloride (50mg/kg) and xylazine (3.5 mg/kg) solution (prepared from stock 100 mg/ml solutions in filter sterilised dH_2O). Chicks were set up in a custom-made head-stabilisation apparatus. Eyelids were opened using custom lid retractors. A 20 MHz transducer (f = 25 mm) connected in series with a Panametrics pulser-receiver (model 5073PR, USA) and a personal computer fitted with a digitising card (model DP110, Acqiris, Switzerland) was mounted on a goniometer and encased within a perspex adaptor that allowed a continuous flow of isotonic saline, thus creating a saline stand-off between the transducer and the cornea of 15 mm (**Fig. 3.3 i**). Once positioned proximal to the subject's cornea, a saline bridge formed and was maintained by a low-pressure (0.05 ml/min) perfusion pump. The angle of the transducer relative to the eye was adjusted in the medial-lateral, dorso-ventral and circumferential planes until it was judged to be optimally aligned with the optical axis of the eye.

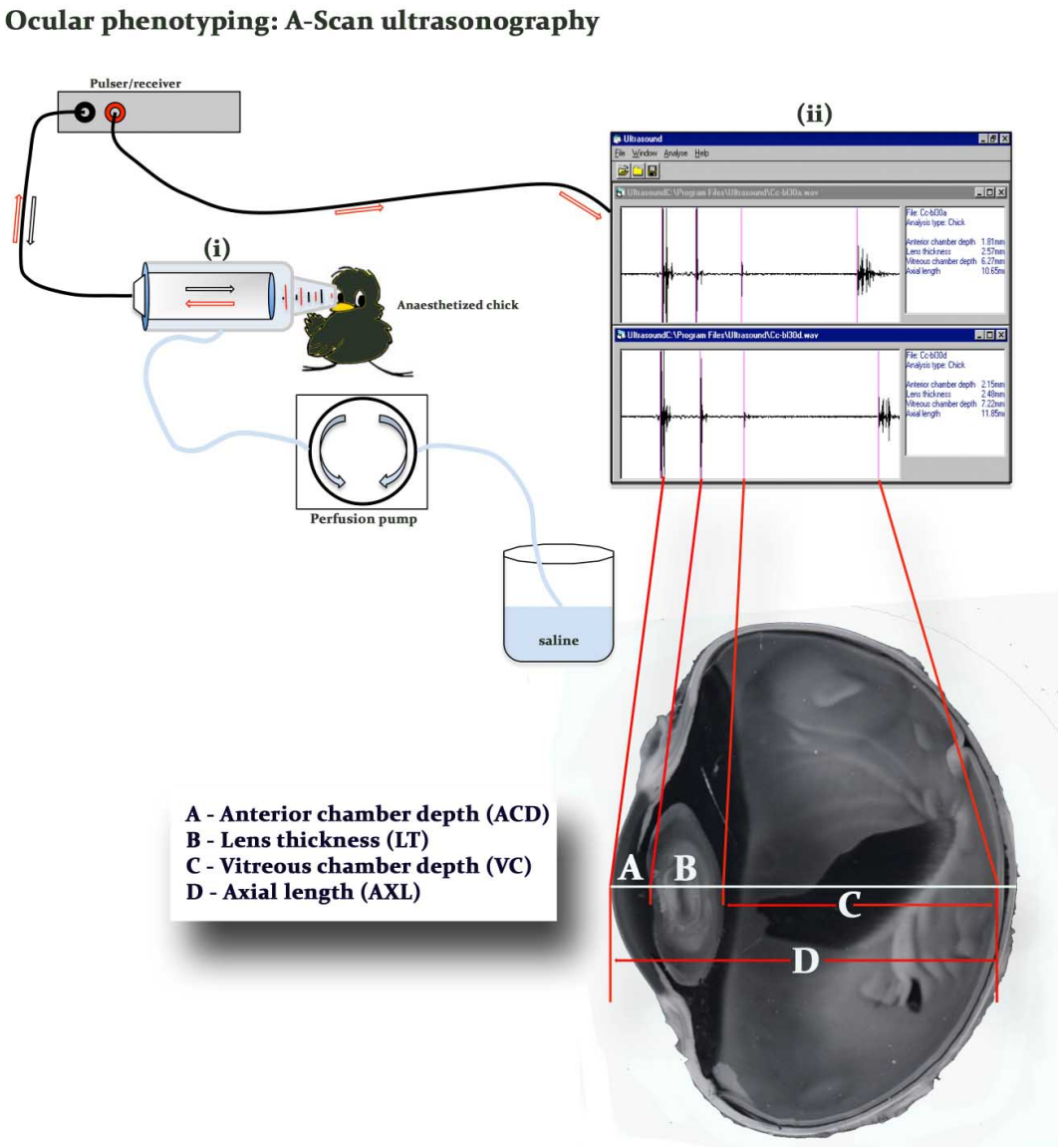

Fig. 3.3. A-scan ultrasonography. Schematic of the apparatus used to measure ocular component dimensions using A-scan ultrasonography. Anaesthetized chicks were positioned on a heating pad with their heads stabilized via a custom made beak adaptor. A pulser/receiver encased within a Perspex adaptor and mounted on a goniometer was positioned close to the anterior corneal surface of the eye. Low pressure flow of isotonic saline through the Perspex adaptor, maintained by a low pressure perfusion pump created a saline bridge with the cornea. (**i**) Transducer with perspex adaptor through which saline was perfused. (not to scale with chick). (**ii**) Typical waveforms for the four principal ocular component boundaries shown as A-D on the hemisected eye inset.

Waveforms were sampled at 100 MHz, and averages of 50 waveforms analysed automatically using custom-written Visual Basic software (**Fig. 3.3 ii**), assuming ultrasound velocities of 1.608 mm/μs in the lens and 1.534 mm/μs in the other ocular media (Wallman and Adams, 1987). Data were saved to a spreadsheet, as they were acquired. The instrument was calibrated daily using a dH_2O filled cuvette of known internal dimensions. Accuracy of the instrument was ± 20 μm over the range of 1-12 mm. The average of six readings were obtained for each eye with a realignment of the instrument after every two readings.

3.8 Intra-vitreal injection of WGA

Following ultrasonography 21-days post-treatment, whilst still under anaesthesia, unconjugated-WGA (Vector Labs, UK) was injected into the vitreous chamber of the eye contralateral to the hemisphere in which the IOTr lesion had been made. WGA was used in this case over the perhaps more obvious choice of cholera toxin B subunit (CtB) for two main reasons. CtB is widely acknowledged to be the most sensitive retrograde pathway tracer available and in addition, unlike WGA is transported monosynaptically, which, in this instance would be most suitable for consistent determination of remaining centrifugal cell number. However, in this case, WGA was used primarily for two main reasons: Firstly, unlike CtB, retrograde labeling is typically confined to the cell somata. The dense overlapping retrograde labeling typical of CtB would have potentially caused difficulties in discerning individual cell somata and would therefore compromise accurate stereological analysis. Secondly, although trans-synaptic transport, a feature of WGA, was not a necessary feature for the analysis in this instance, it provided an extra facet to the parallel investigations into sources of afferent input to centrifugal cells that are reported in **Chapter 9**. The potential inconsistency in retrograde labeling intensity in the primary neurons, i.e. in this case centrifugal neurons, that can be a feature of trans-synaptic transport were minimized through a comprehensive optimisation study into injection volume and survival time (**Section 5.6.1**). The eyelid was opened using custom-made lid retractors, and a pilot hole was

made into the dorso-nasal sclera, proximal to the limbus, using a 25-gauge needle. A 50 μl Hamilton syringe was used to inject 30 μl of 1% WGA close to, but without damaging, the retina. The syringe was held in place for 30 seconds, in order to allow dispersion of WGA within the globe before being withdrawn. The eyelid was allowed to close naturally and the animal recovered from the anesthetic in a temperature controlled chamber. Once animals had regained balance and the ability to perch (usually 45 – 60 minutes), they were returned to their pen.

3.9 Perfusion/fixation

After a survival time of 48 hours (**Section 5.6.1**) post-injection, subjects were given an overdose of sodium pentabarbital (Euthatal) and perfused intra-cardially with 300 ml of 0.1 M phosphate buffered saline (PBS) followed by 500 ml of 2.5% paraformaldehyde in 0.1 M PBS. Brains were then excised and post-fixed in the same solution for 48 hours and subsequently cryoprotected in a 20% sucrose/0.1 M phosphate buffer (PB) solution for a further 48 hours.

3.10 Histology

Brains were sectioned on a frozen-stage microtome (model HM 440 E, Microm International, GmbH) at a thickness of 50 μm in the coronal plane. Three 1:3 series were collected, with one series mounted directly onto double gelatin-subbed slides for Cresyl-violet staining. The remaining series, one for immunohistochemistry and the other as a backup, were collected in reaction pots containing 0.1 M TBS with 0.04% sodium azide, and stored at 4^{o}C. Mounted tissue was air-dried at room temperature for at least 48 hours and subsequently for 30 minutes in a 50^{o}C oven before Cresyl violet staining (**Section 3.12**).

3.11 Immunohistochemistry

One of the other sets was subsequently processed for α-WGA immunohistochemistry. After pretreatment with 0.3% H_2O_2, 10% methanol 'quench' solution to remove endogenous

peroxidases, free-floating sections were incubated at room temperature, in a 3% 'blocking' solution of normal horse serum (NHS) diluted in 0.1 M Tris-buffered saline containing 0.005% Triton X-100 (TXTBS). Sections were then directly transferred to a solution containing a 1:1000 dilution of biotinylated αWGA (BA-0024, Vector Labs, UK) in TXTBS with 1% NHS where they were incubated for 24 hours at room temperature under continuous agitation. With intervening washes in TBS, sections were then incubated under the same conditions in a 1:500 solution of biotinylated rabbit-anti goat IgG (PK-6105, Vector Labs, UK) in TBS with 1% NHS. Again, with intervening washes in TBS, the sections were incubated in peroxidase ABC Elite complex (1:100 dilution in TBS with 1% NHS) for 2 hours under the same conditions. Further washes in TBS preceded overnight acclimatisation to 0.05 M Tris buffer (TNS) at 4°C. The peroxidase activity was visualised by placing the sections in a 0.5% DAB solution diluted in TNS with 0.09% H_2O_2 until the colour had developed sufficiently. After washes in TNS, sections were mounted on double gelatin-subbed slides, air-dried for 48 hours, dehydrated in ascending alcohols, cleared in xylene and coverslipped in DPX mountant.

3.12 Cresyl violet staining

Cresyl violet solution was prepared by dissolving 5 g of sodium acetate in 600 ml of deionised water (dH_2O) and stirring 7.04 g of Cresyl violet fast acetate (Sigma, UK) in the resulting solution overnight. The pH of the solution was adjusted to 3.5 with glacial acetic acid and made up to a final volume of 1.0 L with dH_2O.

For staining, mounted sections were dehydrated in ascending alcohol concentrations (70%, 95% and 100%) at 5 minute intervals before being transferred to a 50% alcohol/50% chloroform solution for 20 minutes, to increase the porosity of the tissue to the stain. The tissue was then hydrated in descending alcohol solutions (95%, 70%, dH_2O), again at 5 minute intervals before being transferred to the Cresyl violet stain for 10-20 minutes. When

staining had become denser than optimum, (i.e. to compensate for destaining that occurs during the final dehydration stage), the tissue was then washed in dH_2o for 5 minutes and dehydrated in ascending alcohol solutions and finally into xylene to clear. Sections were then coverslipped in DPX mountant.

3.13 Stereological analysis

One 1:3 series of WGA labeled sections was traced and neuronal counts made using a Leica microscope (model DM 6000 B) in conjunction with MBF Biosciences' Stereo Investigator software [Version 8] (**Fig. 3.4**). Cell counts for contralaterally projecting ION and EA as well as ipsilaterally projecting EA neurons were made separately and subsequently combined to give the total remaining number of neurons (i.e. ION + EA), subtracted from the mean cell count in sham-operated control cases (mean count = 4000, **Fig. 5.7**), and expressed as a percentage of CVS disruption:

% Lesion success = [(Sham cell count – Lesion cell count) / Sham cell count] x 100

3.14 Data analysis

In analysing the effects of IOTr lesions, subjects were rank ordered and split into quartiles (Q1-4) (**Chapter 6**) or tertiles (T1-T3) (**Chapters 7** and **8**) based upon the total percentage lesion success. Q1 or T1 contained the lowest percentage lesion success and Q4/T3 the highest. A number of past lesion studies have provided examples of structures, in which, to cause a functional deficit it was necessary to achieve a high lesion (i.e. >90%) success. As such, in order that any potential effect could be clearly observed, in each experiment, chicks were divided across the range of lesion success, such that a trade off between the number of subjects in each group and the range of lesion success over which they spanned were comparable across experiments. As a result, while tertile groups were used in **Chapter 7**

(constant light (n=17) and **Chapter 8** (minus (n=20) and plus (n=21) lens wear), in **Chapter 6** (normal visual experience, n=54), quartile groups were used.

All statistical analysis was carried out in SPSS 16.0. Within-animal (fellow eye) comparisons were performed using paired-sample t-tests while across lesion group (quartile/tertile) comparisons were tested with one-way ANOVAs at each measurement time point. The Games-Howell post-hoc test was used to account for uneven distribution of variance. Individual sample correlations were analysed with a linear regression model and expressed as Pearson correlation coefficients within plots and ANOVAs in the text. Parametric tests were used in this case as, although the assumption for even distribution of variance was not met, as shown by a significant levene's test, the assumption for normal distribution of the raw data was met. A separate analysis was carried out using non-parametric tests, i.e. Wilcoxon T-tests as a substitute for paired t-tests, which generated a comparable output. In the case of ANOVAs, a post-hoc test that accounted for uneven distribution of variance was used and the assumption for the normal distribution of the residuals was met. Unless otherwise stated (e.g. box and whisker plots), error bars on graphs denote standard error of the mean (SEM) [18].

Fig. 3.4. Stereological analysis of percentage lesion success. Shown are typical examples of EA neuron distribution in a chick with a isthmo-optic tract lesion (IOTr) success of >90% (**left**) and a sham operated control (**right**). Unstacked tracings of 1:3 series' of 50 μm sections are shown beneath the stacks with black dots representing EA neuron location. Note the paucity of EA cell density in the >90% lesion case. Centrifugal neurons were labeled following intra-vitreal injection of wheat-germ agglutinin (WGA) of the eye contralateral to the lesion of the IOTr 3 weeks post surgery (i.e. once ocular phenotyping was completed). For details of survival time and injection volume optimization see **Section 5.6.1**.

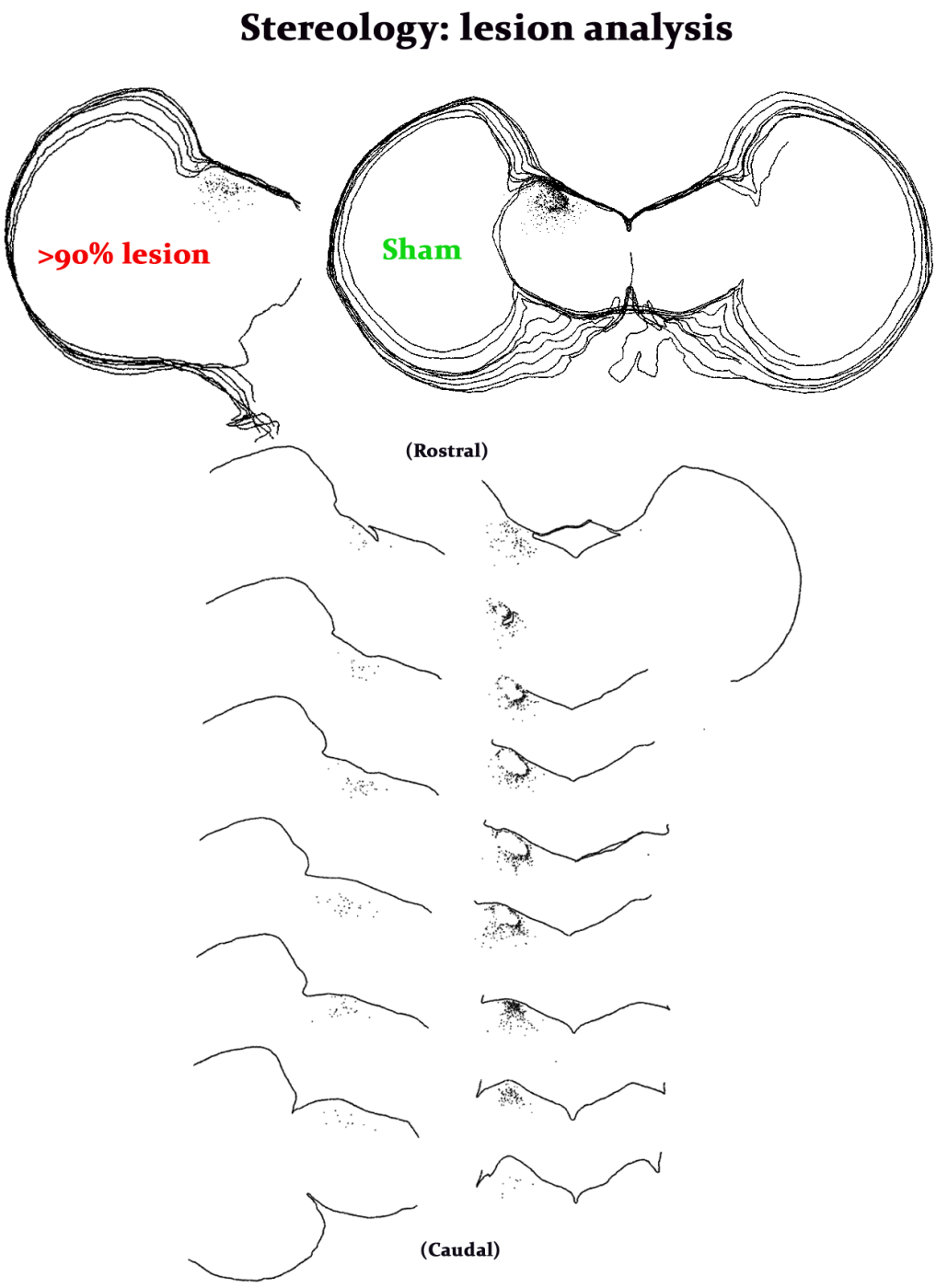

Fig. 3.4. (See previous page for figure legend)

Chapter 4

Methods 02: neuroanatomy of the CVS

4.0 Overview

The materials and methods described in this chapter relate to experiments carried out to investigate the anatomical organisation of the CVS. The purpose of this series of experiments was to investigate the midbrain connectivity of the ION and EA.

4.1 Animal husbandry

Adult homing pigeons were obtained from a local breeder (or when available, as re-use subjects from a different research group within Cardiff University) and housed in pairs. Food and water were available *ad libitum*, with the exception of 1-2 hours prior to induction of general anaesthesia. During this time, pigeons were food deprived but still had unlimited access to water. Pigeons were kept on a 14 hours on/10 hours off lighting schedule with the illumination at 250 to 300 lux.

4.2 Intra-vitreal injection

General anaesthesia was induced (and maintained as necessary) by intra-muscular injection of a ketamine hydrochloride (50mg/kg) and xylazine (3.5 mg/kg) solution (in filter sterilised dH_2O), combined with a pre-operative intra-muscular injection of analgesic (ketoprofen 0.1 mg/kg). The eyelid was opened using custom-made lid retractors and a pilot hole was made into the dorso-nasal sclera, proximal to the limbus, using a 25-gauge needle. A 50 μl Hamilton syringe was used to inject 10-30 μl of tracer close to, but without damaging, the retina. The syringe was held in place for 30 seconds, in order to allow dispersion of tracer within the globe before being withdrawn. The eyelid was allowed to close naturally, and the animal was allowed to recover from the anaesthetic in a temperature controlled recovery chamber. Once animals had regained balance and the ability to perch (usually 1-2 hours), they were returned to their pen.

4.3 Stereotaxic technique

The technique used for surgeries involving pigeons was largely comparable to that of chicks (**Section 3.2**), however custom adaptations were required according to the method described by Karten and Hodos (1967). A stereotaxic setup, consisting of a frame assembly (model 1730; Kopf, USA), a custom made pigeon adaptor, i.e. ear bars which were 3 mm in diameter by 6 mm in tip length with a full radius on the end (model 1756; Kopf, USA), was used for all surgeries. For all surgeries, a 1 μl Hamilton syringe, secured in a micromanipulator (model 1772; Kopf, USA) was used. The ear bar zero for the needle tip was determined in the same way as described in **Section 3.2**.

Once anaesthetised, the feathers around the external auditory canal of the pigeon were cut and the animal was placed in the frame, making sure that the ear bars were engaged within the internal auditory canal. AP rotation in the frame was prevented by the use of a pigeon adaptor (model 1246; Kopf, USA) that rested on the pleural operculum. Following surgery, the pigeon was gently removed from the apparatus and allowed to recover under close monitoring. Once animals had regained their balance and the ability to perch, (usually 1-2 hours) they were returned to their pen.

4.4 Intra-cranial injection

General anaesthesia was induced (and maintained as necessary) by intra-muscular injection of a ketamine hydrochloride (50mg/kg) and xylazine (3.5 mg/kg) solution (in filter sterilised dH_2O), combined with a pre-operative intra-muscular injection of analgesic (ketoprofen 0.1 mg/kg). Once deeply anaesthetised (as determined primarily by a lowered respiratory rate and an absent toe-pinch reflex), subjects were placed in a stereotaxic frame. Initially, the scalp was incised to reveal the dorso-caudal cranium. A craniotomy was performed using a dental drill, revealing the dura mater. A small cut was made in the dura using a micro-scalpel and a 1 μl Hamilton syringe was lowered to coordinates corresponding to the isthmo-

optic nucleus. The electrode was then lowered a further 200 μm for three to four minutes in order to penetrate the pia mater overlying the dorsal midbrain. The electrode was then raised back to the previous dorso-ventral position. A pressure injection of between 0.4 – 0.9 μl (tracer dependant) was made over the course of 5-10 minutes. The craniotomy was then filled using bone-wax and the scalp incision sutured. Once removed from the stereotaxic frame, the animal was allowed to recover from the anaesthetic in a temperature controlled recovery chamber. Once animals had regained their balance and the ability to perch, (usually 1-2 hours) they were returned to their pen.

4.5 Perfusion/fixation

After a tracer-dependent survival time, e.g. 6 days for cholera toxin subunit B, subjects were given an overdose of sodium pentobarbital (Euthatal) and perfused intra-cardially with 500 ml of 0.1 M phosphate buffered saline (PBS) followed by 500 ml of 2.5% paraformaldehyde in 0.1 M PBS. Brains were then excised and post-fixed in the same solution for 24 hours and subsequently cryoprotected in a 20% sucrose/0.1 M phosphate buffer (PB) for between 24 and 48 hours.

4.6 Histology

Brains were sectioned on a frozen-stage microtome (model HM440E, MICROM, USA) at a thickness of 50 μm in the coronal plane. Three 1:3 series were collected.

If a fluorescent pathway tracer was used, two series were mounted directly onto double gelatin-subbed slides, one for visualisation and one for Cresyl violet staining. Sectioning was carried out in dim light to prevent bleaching of the fluorescence. The remaining series was collected in a reaction pot containing 0.1 M TBS and stored in the dark at 4°C as a backup.

For non-fluorescent tracers, which were to be visualised using immunohistochemistry, e.g. WGA, one series was mounted directly onto double gelatin-subbed slides for Cresyl violet

staining and the two remaining series were immersed in separate reaction pots containing 0.1 M TBS for subsequent immunohistochemistry.

Mounted tissue was air-dried at room temperature for at least 48 hours and subsequently for 30 minutes in a 50°C oven. Mounted sections were then dehydrated in ascending alcohol solutions (70%, 95%, 100%), cleared in xylene and coverslipped with DPX mountant.

4.7 Immunohistochemistry/cresyl violet staining

Protocols for immunohistochemical labeling and counterstaining with Cresyl violet solution were followed as described in **Sections 3.11** and **3.12**, respectively.

4.8 Imaging

Visualisation of tissue was carried out using a Leica DM 6000 B connected to a monochrome camera (model). Images were captured using Leica Application Software (LAS, Version) on a PC. For cases that involved a single fluorescent tracer, images were captured as monochrome images and inverted. For cases in which 2 tracers were used, images were captured in 8 bit/channel RGB coloured format and if necessary, the channels of the 2 tracers were then separated (channel mixer function) such that one tracer was black and the other white. This adjustment allowed improved visualisation of fine morphological details as a result of the higher contrast with the background. All adjustments were made using Adobe Photoshop (Version CS2) on an iMac computer.

4.9 Materials

The pathway tracers used in the study are described below. The selection of tracer(s) to meet specific experimental requirements was based upon the following properties:

1. **Direction of transport**
2. **Delivery method**
3. **Optimum survival time**

4. Method of visualisation

4.9.1 Wheat germ agglutinin (WGA)

- WGA is a trans-synaptic retrograde pathway tracer.
- Used for labeling of centrifugal neurons following intra-ocular injection
- 30 µl of 1% WGA (in 0.1 M PB, pH 7.35); survival time: 48 hours
- Visualisation through immunohistochemistry (**Section 3.10**)
- Vector Labs, UK

4.9.2 Fast blue (FB)

- Fast blue is a monosynaptic retrograde pathway tracer.
- Used to identify afferent input to centrifugal neurons following ION/EA pressure injection.
- 0.04-0.09 µl of 2.5% FB (in 0.01 M PB, pH 7.35); survival time: 3-9 days
- Visualisation through florescence (emission λ 420 nm)
- Polysciences Inc. UK

4.9.3 Cholera toxin subunit B conjugated to Alexa Fluor 488 (CtB-488)

- CtB-488 is a monosynaptic retrograde pathway tracer.
- Used for labeling of centrifugal neurons following intra-ocular injection
- 15 µl of 1% CtB-488 (in 0.1 M PB, pH 7.35); survival time: 6 days
- Visualisation through florescence (emission λ 519 nm)
- Invitrogen, UK

Chapter 05

Optimisation of experimental design

5.0 Overview

This chapter presents the results of preliminary experiments that were carried out to fine tune the experimental parameters used to carry out the experiments described in **Chapters 6-8**:

- Chicken strain selection (**Section 5.4**).
- Choice of lesion target, i.e. isthmo-optic nucleus (ION) or isthmo-optic tract (IOTr) (**Section 5.5**).
- Determination of lesion success (**Section 5.6**).

5.1 Experimental design

5.2 Ocular phenotyping

Prior to surgery, chicks were pre-screened for existing ametropia and weighed in order to assess general health. Streak retinoscopy was performed to measure refractive error and IR keratometry to measure corneal radius of curvature. Following surgery, depending upon the experimental design, these techniques were combined with A-scan ultrasonography, used to measure ocular component dimensions along the optical axis. The time-points at which post-treatment ocular measurements were taken varied between experiments and as such will be outlined at the beginning of the relevant results sections, however the time points below show the structure common to all three experiments:

1. Prescreen for ametropias (3 days post hatch)
2. Electrolytic lesion of the isthmo-optic tract (4/5 days post hatch) (**Section 3.4**).
3. Ocular phenotyping techniques:
    - Infra-red keratometry (**Section 3.5**).
    - Streak retinoscopy (**Section 3.6**).
    - A-scan ultrasonography (**Section 3.7**).

4. Pathway-tracing for analysis of lesion success. (day 25/26) (**Section 3.8**).
5. Perfusion/fixation (day 27/28) (**Section 3.9**).

In subsequent variations of this general experimental paradigm, a lesion of the IOTr or ION was combined with a manipulation of visual experience, including:

- Constant light (**Chapter 7**)
- Hyperopic defocus (**Chapter 9**)
- Myopic defocus (**Chapter 9**)

5.3 Animal model

The neonatal chick is a well regarded and widely used model for studies of eye growth and emmetropisation (**Section 2.1**). Studies have shown that perturbations in early visual experience disrupt emmetropisation, producing refractive errors that share characteristic features with those naturally occurring in humans. For example, myopia induced in the chick through form deprivation is characterised by an increase in the axial length of the eye, which is principally due to an elongation of the vitreous chamber, and this is also observed in naturally occurring myopia in humans.

5.4 Strain selection

In order to ensure that any potential effect of the disruption induced by a lesion of the IOTr could be determined, it was imperative that a strain of chicken was used that provided a consistent and reliable baseline for post-natal ocular growth. Typically, chicken strains can be divided into those bred for egg-laying and those for meat consumption (broilers). The attributes that are selected for in broiler chicken strains, i.e. fast growth rate, were preferable for this study. However, no broiler strains were available locally at the time, and as a result, a layer strain, white leghorn (WL), was initially chosen. In preliminary measurements following the 21-day post hatch period, it became evident that the amount of

variability in refractive state both between animals and between the eyes of the same animal (i.e. anisometropia) was unusually high in this strain. In order to maximise the possibility of finding a more suitable experimental strain, two alternative strains, Dekalb White (DW) and Shaver Black (SB), were obtained as eggs and once hatched, were compared to the WL chicks. Measurements for refractive state using streak retinoscopy (**Section 3.6**), and ocular component dimensions using A-scan ultrasonography (**Section 3.7**) were performed on chicks of SB and DW strains after 7, 14 and 21 days post hatch in order to assess their suitability.

5.4.1 Refractive state

Twenty-one days post-hatch, there was no significant difference between the means of absolute refractive error between the 3 strains ($F_{2,24}$ = 0.469, p=0.631). However, WL chicks showed a greater variance in refractive error (7.058 D^2) compared with SB (0.072 D^2) and DW (1.566 D^2) strains (**Fig 5.1**). Anisometropia was not significantly different between the three strains ($F_{2,24}$ = 0.328, p=0.723), but the WL strain showed higher variance in mean anisometropia (0.525 D^2) than that found in the DW (2.127 D^2) strain, suggesting that both progression towards emmetropia and development of refractive state symmetry between the eyes of an individual chick in the WL strain were both impaired (**Fig. 5.2** and **Table 5.1**).

Interestingly, 7 days post hatch SB chicks showed a significantly greater amount of anisometropia (t_{15} = -2.053, p=0.024) when compared to the DW strain (**Table 5.1**). However, after 14 and 21 days post surgery, no significant difference in the mean anisometropia of the two strains was observed (all p>0.295).

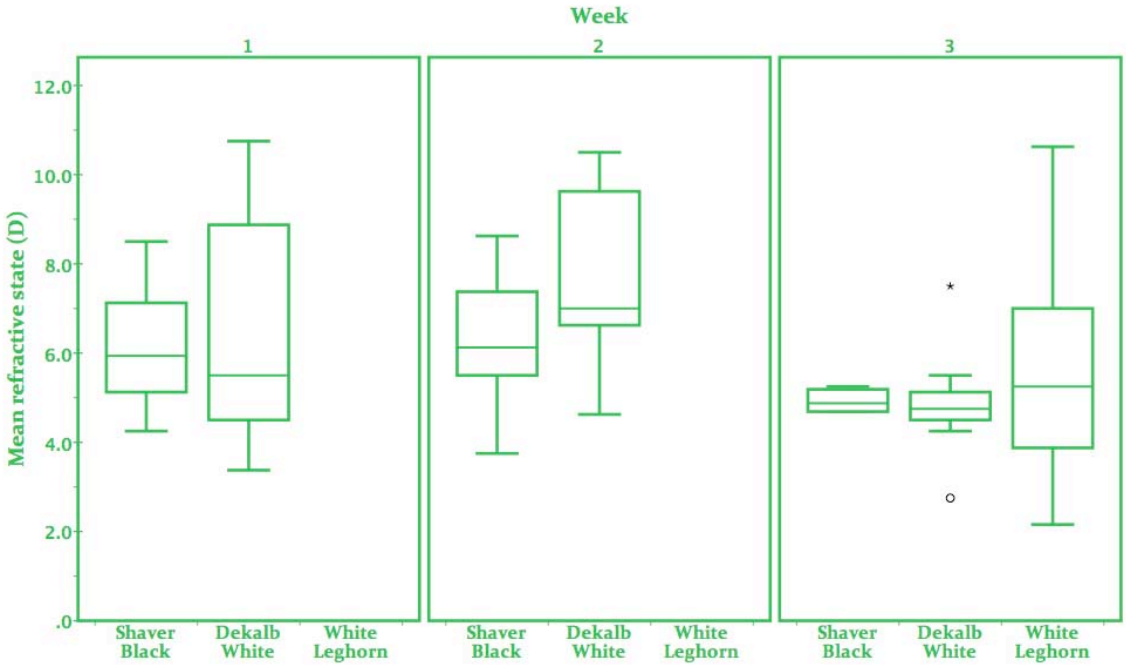

Fig. 5.1. Strain comparison: Absolute refractive state. Mean refractive state across three strains of chicken, 1, 2 and 3 weeks post-hatch. White leghorn (WL) measurements were taken after 3 weeks only. Three weeks post-hatch, the WL strain showed a great degree of variability in absolute refractive state, while Shaver Black (SB) and Dekalb White (DW) strains were found to exhibit a more stable baseline. This greater within-strain variability in the WL chicks reduced the likelihood that, what would potentially be a small lesion effect, would be detected. As such the WL strain was excluded as a possible model. In the above graph, refractive state measurements are not corrected for working distance. Error bars represent upper and lower 25% of the sample, the box length represents the interquartile range of the sample, while the line across the box represents the median value of the sample. Circles represent outlier values greater than one and a half box lengths from the boundary of the box, while asterisks represent outlier values greater than 3 box lengths away from the upper or lower boundary of the box.

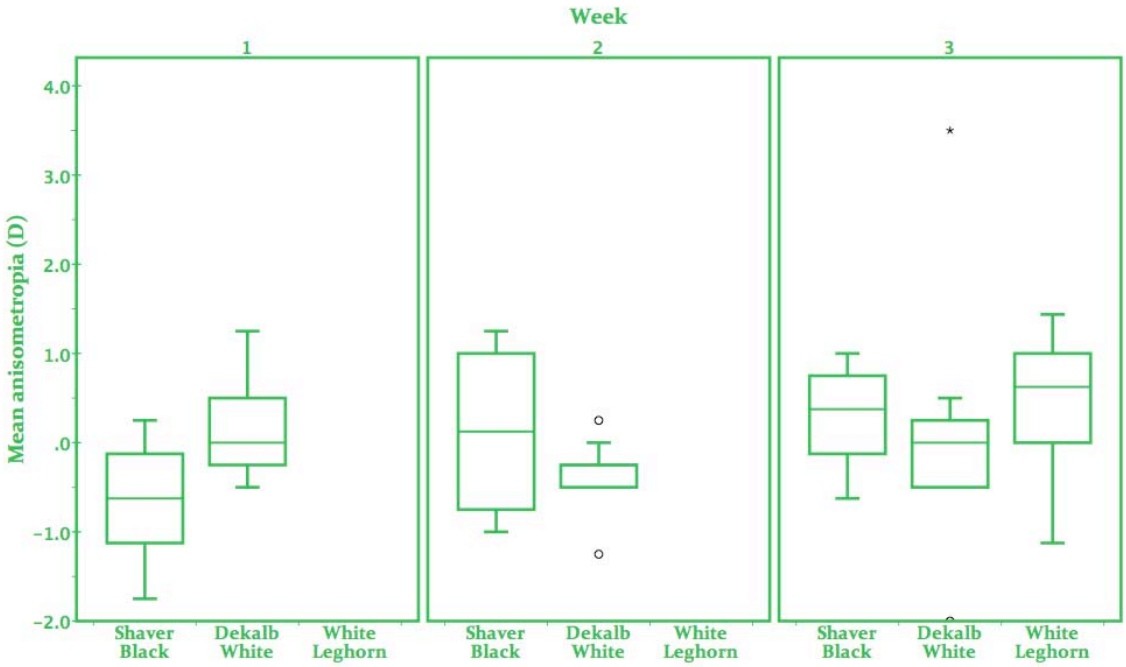

Fig. 5.2. Strain comparison: Anisometropia. Mean anisometropia across three strains of chicken, 1, 2 and 3 weeks post-hatch. White leghorn measurements were taken after 3 weeks only. At the 3 week post hatch time point, the inter quartile range of anisometropia in the 3 strains of chick were comparable, however, the White Leghorn strain showed an overall wider range in anisometropia. Error bars represent upper and lower 25% of the sample, the box length represents the interquartile range of the sample, while the line across the box represents the median value of the sample. Circles represent outlier values greater than one and a half box lengths from the boundary of the box, while asterisks represent outlier values greater than 3 box lengths away from the upper or lower boundary of the box.

5.4.2 Ocular component dimensions

The vitreous chamber depth (VCD) of the WL strain showed greater variance (0.211 mm^2) when compared to SB (0.060 mm^2) and DW (0.084 mm^2) strains after 21 days post-hatch, however, there was no significant difference between their values ($F_{2,23}$ = 2.662, p=0.091) (**Fig. 5.3**). Furthermore, no significant difference in VCD asymmetry was found between groups at this time point ($F_{2,23}$ = 0.204, p=0.817) (**Fig. 5.4**). No significant differences in the

amount of VCD asymmetry between SB and DW strains was found at 7 or 14 days post hatch time points (all p>0.147) (**Fig. 5.4**).

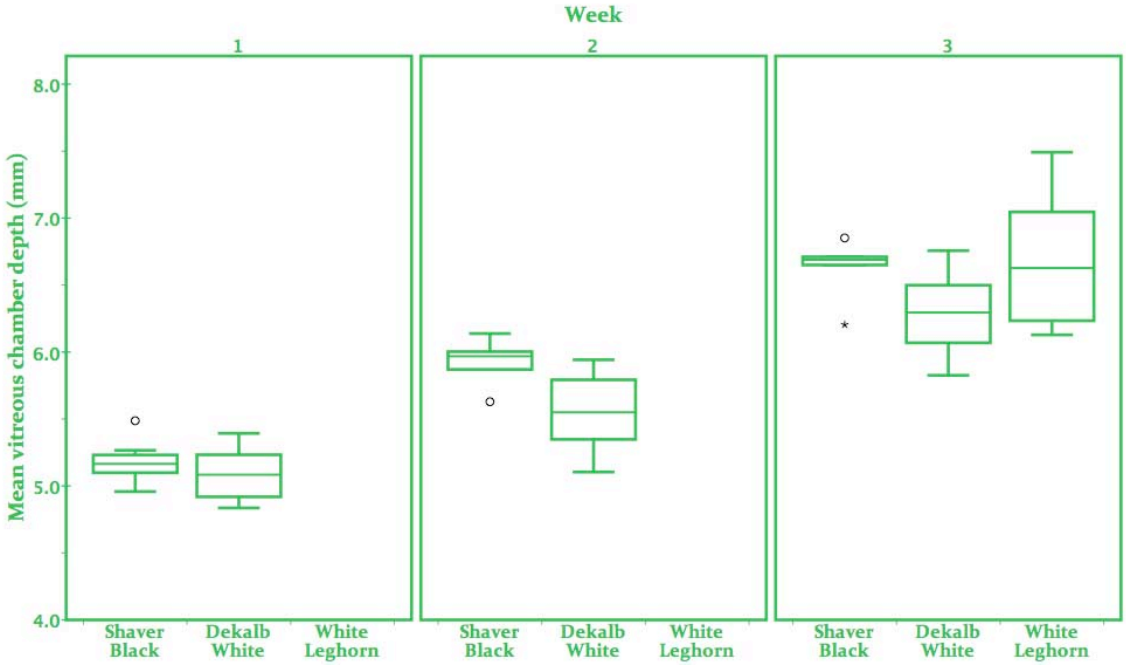

Fig. 5.3. Strain comparison: Absolute vitreous chamber depth (VCD). Mean VCD measurements across three strains of chicken, 1, 2 and 3 weeks post-hatch (WL measurements were taken after 3 weeks only). White leghorn (WL) chicks showed greater within-strain variability in VCD measurements than Shaver Black (SB) or Dekalb White (DW) strains at the 3 weeks post-hatch time point. At 1 and 2 weeks post hatch, SB and DW strains showed similar within-strain variability. Error bars represent upper and lower 25% of the sample, the box length represents the interquartile range of the sample, while the line across the box represents the median value of the sample. Circles represent outlier values greater than one and a half box lengths from the boundary of the box, while asterisks represent outlier values greater than 3 box lengths away from the upper or lower boundary of the box. Corresponding data can be found in Table 5.1.

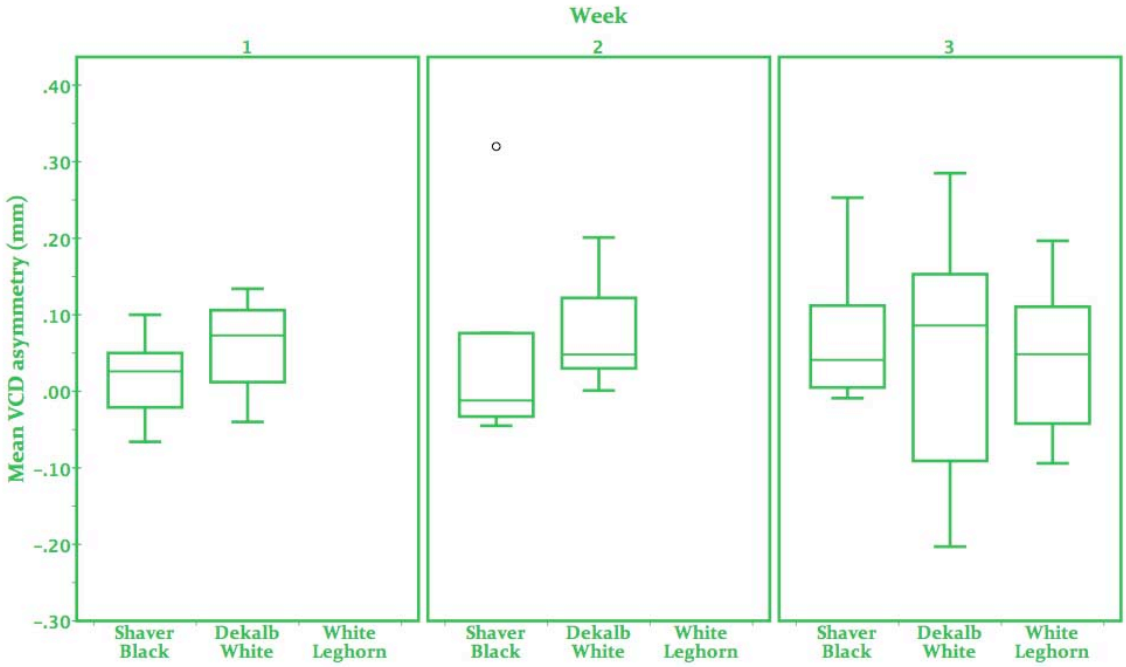

Fig. 5.4. Strain comparison: Vitreous chamber depth asymmetry. Mean vitreous chamber depth asymmetry (R-L) across three strains of chicken, 1, 2 and 3 weeks post-hatch. White leghorn measurements were taken after 3 weeks only. At 1 and 2 weeks post-hatch, Shaver Black (SB) and Dekalb White (DW) exhibited a similar degree of within-strain variability, although the VCD asymmetry in the SB strain was closer to zero at both time points. Three weeks post-hatch, the DW strain showed the greatest amount of within-strain variability in VCD asymmetry, while the inter quartile range of the SB strain was narrower than that of both the WL and DW strains. Error bars represent upper and lower 25% of the sample, the box length represents the interquartile range of the sample, while the line across the box represents the median value of the sample. Circles represent outlier values greater than one and a half box lengths from the boundary of the box.

Table 5.1. Strain comparison: Anisometropia and vitreous chamber depth (VCD) asymmetry. Anisometropia and vitreous chamber depth asymmetry (±SD) across three strains of chicken over a period of 3 weeks post-hatch. While the mean anisometropia and VCD asymmetry of the 3 strains of chicks shown below provide a stable baseline from which a potential lesion effect could be gauged, the variability in the mean absolute refractive state of the White Leghorn strain suggested that these chicks had an impaired ability to emmetropise (**Fig. 5.1**).

Anisometropia	Chicken strain		
Days post-hatch	**Shaver Black** (n=8)	**Dekalb White** (n=9)	**White Leghorn** (n=13)
7 days (D)	-0.66±0.67	0.17±0.68	Not measured
14 days (D)	0.13±0.98	-0.36±0.42	Not measured
21 days (D)	0.28±0.66	0.14±1.46	0.53±0.72
VCD asymmetry			
7 days (mm)	0.018±0.054	0.060±0.059	Not measured
14 days (mm)	0.049±0.140	0.084±0.071	Not measured
21 days (mm)	0.080±0.107	0.038±0.156	0.045±0.099

5.4.3 Strain selection summary

The WL strain was found to exhibit higher variance in both absolute refractive state and anisometropia, showing an impaired ability to emmetropise. Importantly, the baseline inter-quartile range of anisometropia in the WL strain was unexpectedly wide (**Fig. 5.1**), thus confirming the decision that it was an unsuitable strain. SB and DW strains both demonstrated comparable progression in refractive state towards emmetropia with time. Moreover, neither SB or DW strains were found to have a high amount of anisometropia or VCD asymmetry. Having said that, the amount of variability shown by the DW strain in VCD asymmetry was much greater than both the SB and DW strains. In addition, throughout the 3 week measurement period, the mean VCD asymmetry in the SB strain was consistently closer to zero than that of the DW strain (**Fig. 5.4**) and therefore provided a

preferable baseline to which a lesion effect could be measured. As such, the SB strain was considered to be more suitable than either the DW or WL strains.

5.5 Lesion target

In order to disrupt or eliminate centrifugal efferent fibers from the ION/EA, one can either destroy the soma of the efferent projection, i.e. the ION and surrounding EA, or disrupt the axons themselves, i.e. the IOTr. A number of factors are important when considering the lesion target and the subsequent interpretation of data obtained in such a study.

5.5.1 Size of lesion

ION/EA - While the ION is a small, confined structure, around 1000 μm in its longest axis (Cowan and Powell, 1963), the EA is sparsely distributed, extending a further 1000 μm rostrally and caudally from the ION as well as comparable distances ventrally and medially (Miceli et al., 1999).

IOTr - The IOTr forms a tight bundle of fibres at the roof of the midbrain and therefore represents a smaller lesion target (~400 μm in cross section).

5.5.2 Collateral damage to nearby regions

ION/EA - A lesion of a large region such as that which the EA occupies would inevitably lead to damage of proximal structures (**Fig. 5.5**). Lateral to the ION/EA is nucleus isthmus parvocellularis (Ipc), part of the isthmic nuclei complex that exhibits a highly topographic reciprocal inhibitory influence upon retinorecipient layers of the optic tectum (TeO). Ventro-laterally is the nucleus lemnisci lateralis, pars dorsalis, an auditory nucleus. Ventro-medially is Locus ceruleus (LoC), a region involved in regulation of arousal and that is densely interspersed with ectopic centrifugal neurons. Medially, is the substantia grisea centralis (GCT) (or periaqueductal grey), a nociceptive centre of the midbrain which, again, is interspersed with ectopic neurons.

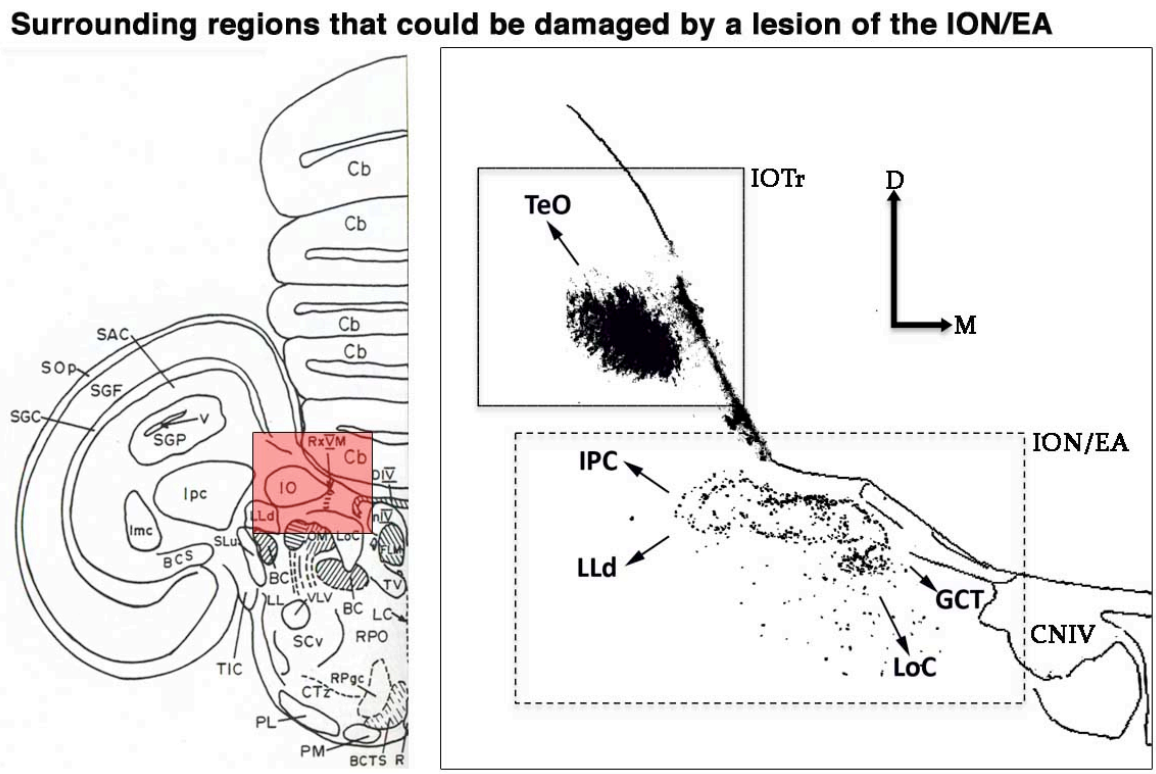

Fig. 5.5. Lesion target selection: Surrounding regions. The highlighted region of the midbrain placed in context by the red box in the accompanying brain map shows the position of regions and structures surrounding the ION/EA. The ION/EA complex is proximal to 4 important regions, nucleus isthmi parvocellularis (IPC) of the isthmic complex, nucleus lemnisci lateralis pars dorsalis (LLD), locus ceruleus (LoC) and substantia grisea centralis (GCT) while the isthmo-optic tract is nestled within the dorsal apex of the optic tectum, a region that, if targeted with a lesion is unlikely to cause damage to unintended structures. CNIV, trochlear nerve; EA, ectopic area; TeO, optic tectum; ION, isthmo-optic nucleus; IOTr, isthmo-optic tract; nIV, trochlear nucleus.

IOTr - Fibers of the IOTr course caudo-rostrally within the dorso-medial aspect of the SGF layers of the TeO. Medial to the IOTr, the tectal commissure extends as a flat sheet across the midline, forming the dorsal roof of the cerebral aqueduct. The TeO extends laterally, while ventrally to the IOTr are the dorso-medial apex of deep layers of the TeO.

5.5.3 Damage to nerve tracts

ION/EA - The mesencephalic branch of the trigeminal nerve passes through the medial aspect of ION. Disruption of this tract in the pigeon has been shown to severely impair the process by which grain is grasped by the tip of the beak and moved to the back of the mouth (Zeigler and Miller, 1975).

5.5.4 Damage to blood vessels

The ION and proximal EA are situated in amongst a dense vasculature (**Fig. 5.6**). Any damage to such blood vessels has the potential to affect regions that such blood vessels supply. Diaschisis (i.e. subdued neural activity), could result in affected regions (Schoenfeld and Hamilton, 1977) (**Section 6.3**).

5.5.5 Lesion target summary

Given the factors described above, compared with that of the ION, a lesion of the IOTr would be less likely to cause damage to surrounding proximal structures, predominantly due to the smaller lesion required and the minimal damage to vasculature and/or unintended neural pathways.

Under the assumption that ipsilateral EA efferents remain uncrossed at the optic chiasm, following a lesion of the ION/IOTr the contralateral 'treated' eye would continue to receive ipsilateral centrifugal input. Furthermore, the ipsilateral 'control' eye would still receive its normal contralateral input but not ipsilateral EA efferents. Thus, the CVS connectivity, such that it is, does not allow a strict 'treated' and 'control' eye division.

For the purposes of the experiments reported in **Chapters 6** to **8**, the eye contralateral to the lesion will be referred to as the 'treated eye' and the eye ipsilateral to the lesion will be referred to as the 'control' eye (**Fig. 5.7**). In all cases, the lesion was in the left midbrain

hemisphere. Therefore, the right eye was the treated eye and the left eye was the control eye.

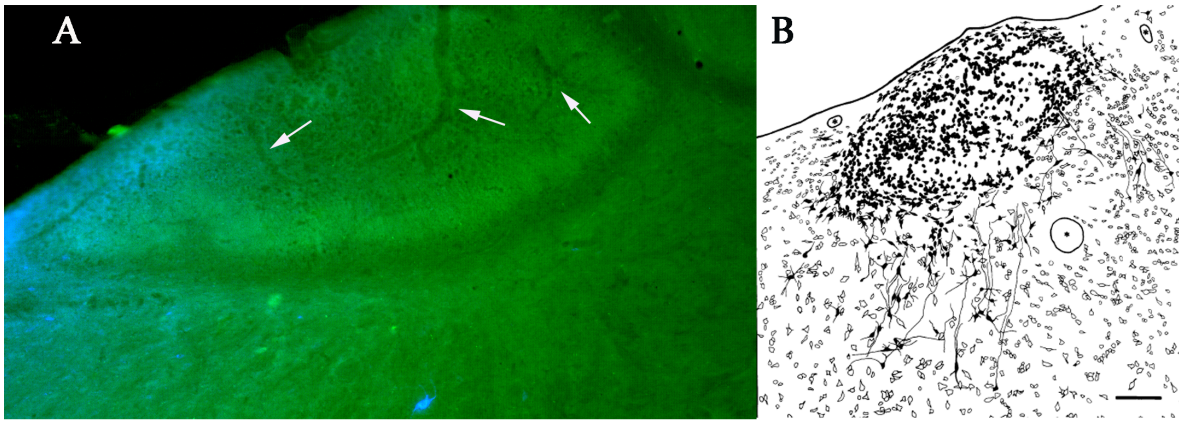

Fig. 5.6. Lesion target: Vasculature of the ION/EA complex to emphasize the likelihood of ischemia or diaschisis to unintended targets. Lesioned induced damage to vasculature has the potential to induce changes in the neuronal activity of other regions that share a common blood supply, thus potentially complicating the behavioral or physiological interpretation of the surgery. The florescent micrograph of a 50 μm coronal section of the pigeon midbrain in (**A**) clearly shows the dense vasculature within the isthmo-optic nucleus (ION) (Taken from experiments in **Chapter 9**). In addition, (**B**) shows a tracing of the ION and surrounding ectopic area (EA) with the blood vessels that pass through the EA, proximal to the ION denoted by circled asterisks (taken from O'Leary et al. (1982). **Scale bar = 100 μm**

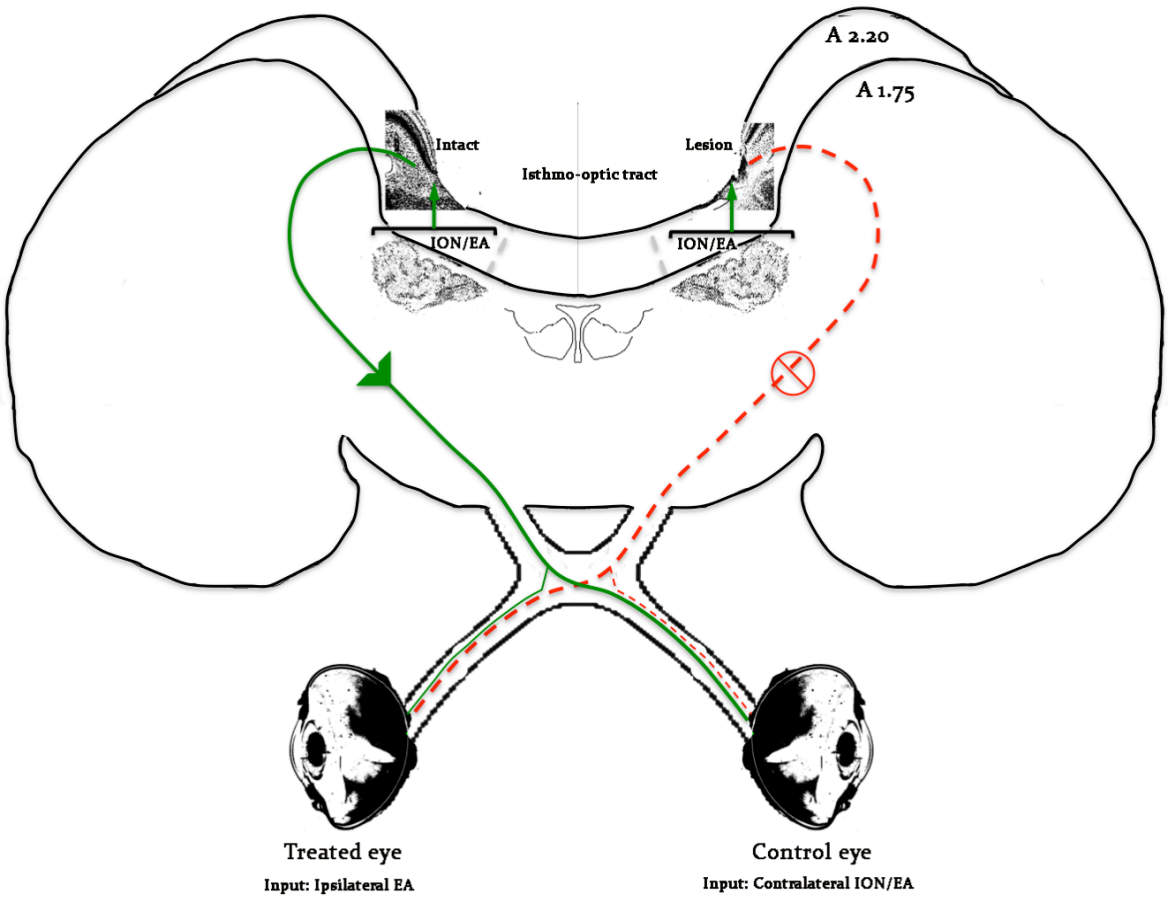

Fig. 5.7. Semi-schematic representation of the effect on retinal innervation of a lesion of the isthmo-optic tract (IOTr). The isthmo-optic nucleus (ION) projects via the isthmo-optic tract (IOTr) to the contralateral retina via the optic tract and optic nerve, respectively. In addition, small numbers of centrifugal fibers innervate the ipsilateral retina. In the above schematic, showing a coronal slice through relevant components of the centrifugal visual system, a unilateral lesion of the IOTr (**Lesion**) disrupts the path of centrifugal efferents (**red dashed line**), leaving the ION intact, but limiting the retina contralateral to the lesion to ipsilateral centrifugal input (**narrow solid green line**) (from the intact IOTr). Conversely, the eye ipsilateral to the lesion has the major contralateral centrifugal input intact (**solid green line**) but the ipsilateral centrifugal input is disrupted (**narrow dashed red line**). It is important to note that the presence of the ipsilateral centrifugal pathway precludes a straightforward treated eye/control eye division. **A1.75** - the anterior-posterior (AP) location of the ION/ectopic area (EA). **A2.20** – the AP position of the region of the IOTr targeted by the electrolytic lesion. The co-ordinates used are based upon those of Masson and Kuenzel (1968).

5.6 Determination of lesion success

Damage to the IOTr or ION caused by the electrolytic lesion was intended to disrupt the centrifugal efferents to the contralateral retina. An intra-vitreal injection of a trans-synaptically transported retrograde pathway tracer (wheat-germ agglutinin (WGA)) was administered into the treated eye 48 hours prior to perfusion (**Section 5.6.1**), in order to label residual ION and EA neurons in their entirety. As such, the degree of induced disruption could be assessed quantitatively through a comparison of the number of remaining CVS neurons in lesioned animals with the mean number of neurons labeled in the intact CVS of sham-operated subjects (**Fig. 5.8**). Using this method, the degree of success of each lesion was expressed as the percentage of centrifugal neurons destroyed.

5.6.1 Wheat germ agglutinin (WGA) optimisation

In these experiments the lectin, wheat-germ agglutinin (WGA), was used as a retrograde pathway tracer, i.e. the direction of axonal transport is opposite to the direction of action potential conductance to label the soma of efferent projecting axons may be labeled by WGA. However, unlike monosynaptic tracers, e.g. cholera toxin subunit B (CtB), WGA does not remain confined to the soma and once it reaches the efferent projecting cell body, it may be transported retrogradely and trans-synaptically along target cell soma afferent input towards a secondary soma. For this reason, it was necessary to determine the optimum injection volume and survival time parameters for labeling the primary target soma. Eight Shaver Black chicks were used for this study. Initially, the injection volume was optimised. Intra-vitreal injections of 1% WGA were performed using a volume of 10, 20, 30 or 40 µl and an arbitrarily chosen survival time of 72 hours. Following tissue processing and immunohistochemistry for WGA visualisation (for methods see **Section 3.11**), histological and stereological analysis showed that the greatest number of centrifugal neurons labeled was present following a 30 µl injection (**Fig. 5.9**). The decrease in labeling following 40 µl

compared with 30 µl injections was unexpected but could have been a result of neural damage caused by the increased injection volume and subsequent increase in intra-ocular pressure.

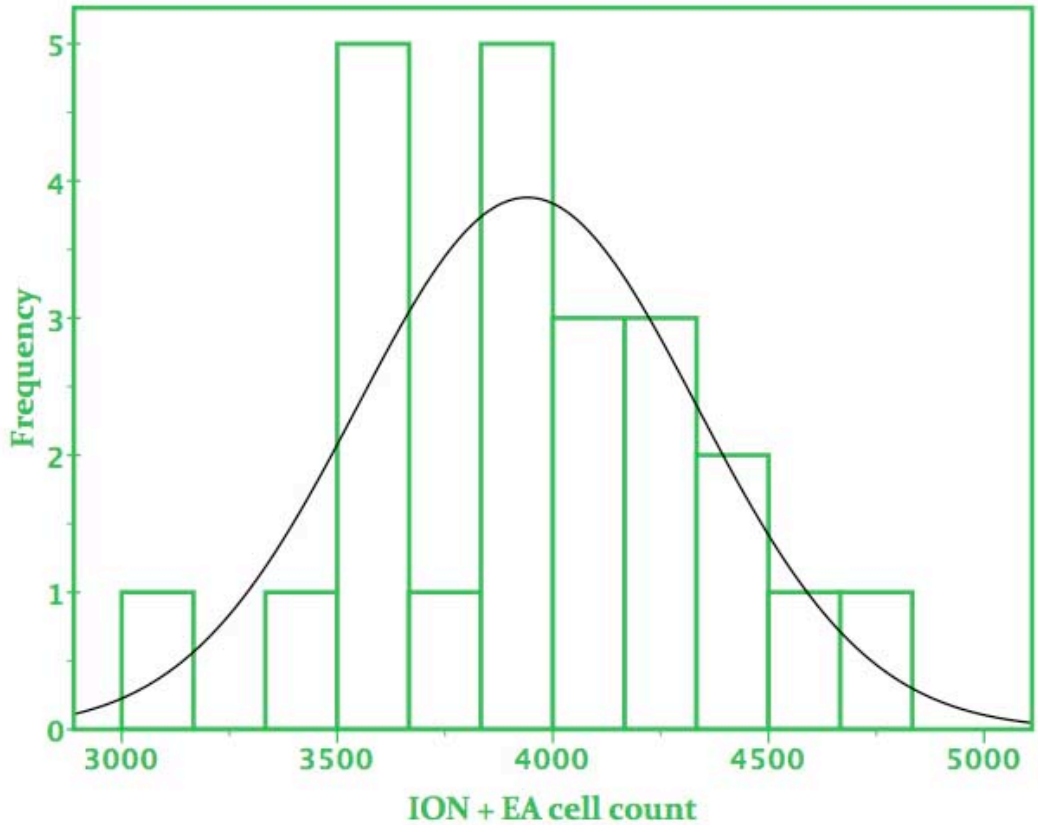

Fig. 5.8. Distribution of centrifugal cell number in sham-operated control cases. Percentage isthmo-optic tract lesion success was determined through comparison of the combined remaining wheat-germ agglutinin labeled isthmo-optic nucleus (ION) neuron and ectopic neuron cell count with the mean combined cell counts of sham-operated subjects from each of the emmetropization studies (i.e. lesion only, constant light and lens manipulation studies). The above histogram shows the distribution of total combined centrifugal cells in sham-operated controls. The mean to which lesion subjects were compared was 3940 ± 394 across 23 sham-operated control cases. Note that cell counts were taken from 1:3 series' of brain sections and have not been adjusted. As such, they represent roughly a third of the total number of centrifugal cells in the Shaver Black strain of chick.

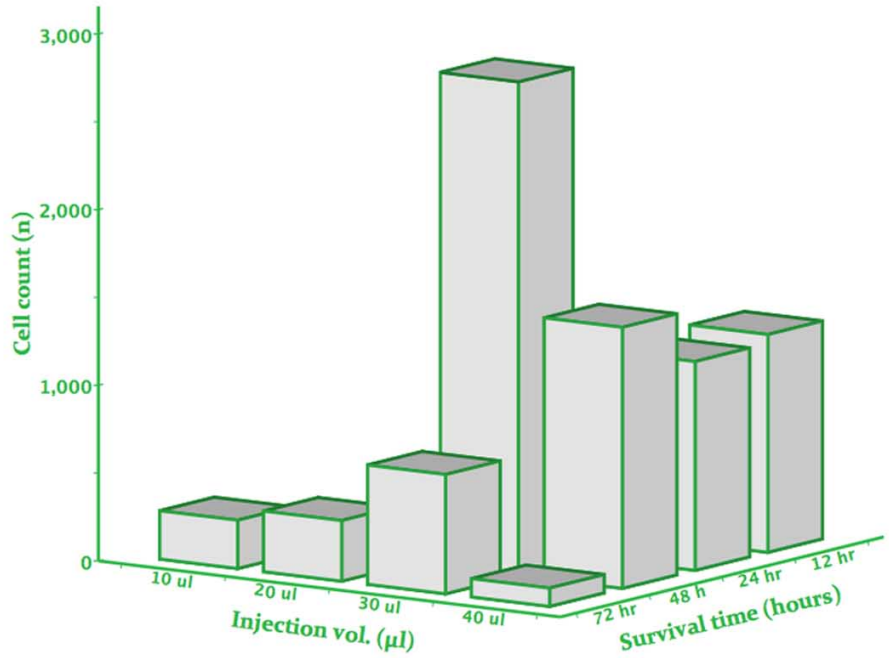

Optimum conditions: 30 µl injection volume & 48 hour survival time

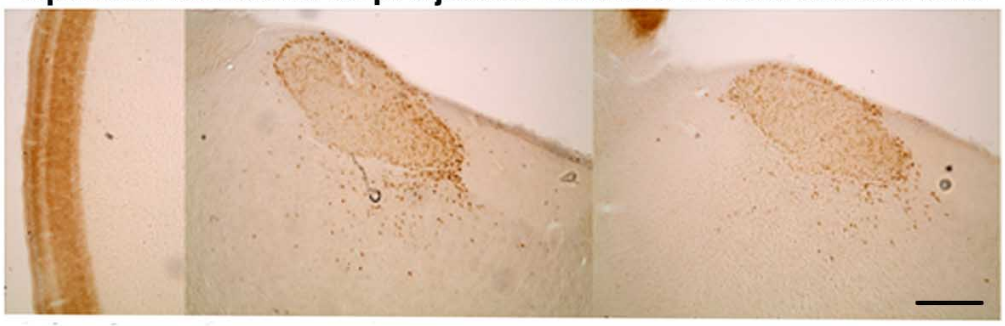

Fig. 5.9. Optimisation of injection volume and survival time parameters for intravitreal injection of wheat-germ agglutinin (WGA). The above figure shows the results of the optimisation of injection volume and survival time parameters for retrograde labeling of ION/EA using wheat-germ agglutinin (WGA). The bar chart above shows the number of centrifugal neurons labeled following an intra-vitreal injection volume of 10-40 µl WGA and survival time of 12-72 hours. The highest bar corresponds to the established optimum conditions (30 µl injection volume and 48 hour survival time). The retrograde labeling of centrifugal neurons resulting from this combination is shown in the photomicrographs below. Cell counts are taken from 1:3 series of brain sections and thus represent roughly a third of the total cell counts. **Scale bar = 250 *µ*m.**

Having established the most suitable injection volume, the optimum survival time was investigated. Following injection of 40 µl of WGA and survival times of 12, 24 or 48 hours, histological and stereological analysis of brain sections showed that the optimum survival time was 48 hours (**Fig. 5.9**). Subsequently, optimised conditions were combined in a single subject that showed a considerably higher number of centrifugal neurons labeled than other parameter combinations (**Fig. 5.9**).

5.6.2 Effect of IOTr lesion

Following seemingly successful lesions (as determined histologically), a remaining neuronal population frequently persisted, commonly distributed as a 'shrunken' ION with a diffuse population of ventromedially distributed EA neurons. Partial lesions of the IOTr again contributed to shrinkage of the ION and a reduction in labeled cell density both the nucleus and within the surrounding EA (**Fig. 5.10**).

Fig. 5.10. The effect of IOTr lesions on the number and distribution of centrifugal neurons. Photomicrographs taken from the red region of the corresponding schematic show labeled centrifugal cells following intravitreal injection of wheat-germ agglutinin (WGA) in chicks with of varying degrees of IOTr lesion success (0%, 60% and >90%). In control sham animals, the ION and surrounding EA region shows typical dense labeling while histology from a chick with a partial lesion (60%) had a shrunken nucleus with regions of decreased labeled cell density. The decreased size of the nucleus in the partial and the >90% lesion success cases is presumably due to retrograde degeneration following lesion of the isthmo-optic tract. **Scale bar (applies to all photomicrographs) = 250 *µ*m.**

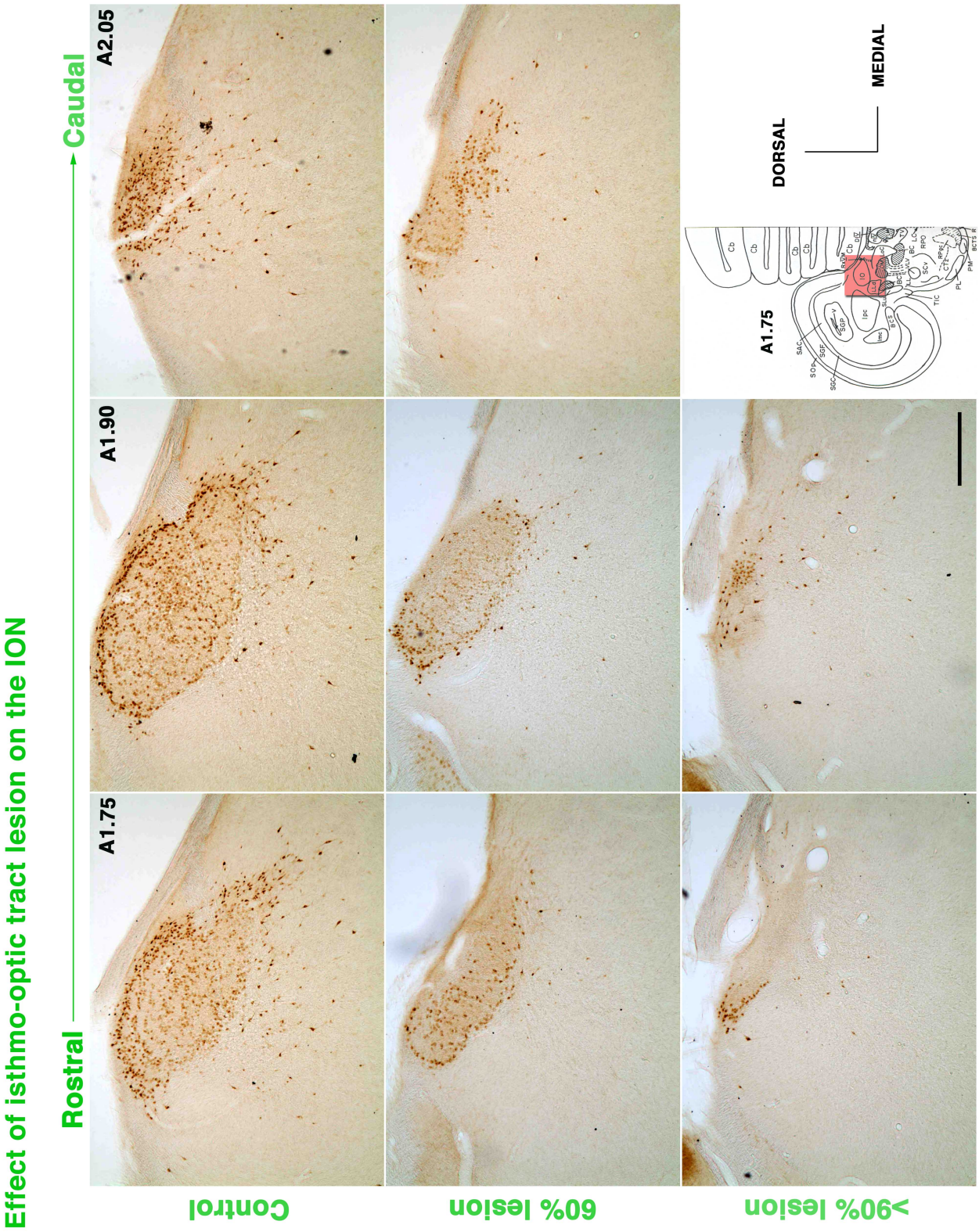

Fig. 5.10. *(see previous page for figure legend)*

5.7 Summary

A number of factors are crucial in the interpretation of a lesion study. In order to identify a lesion effect, it is important that the measured variable has a stable baseline. In this case, it was necessary that the chick strain that was used exhibited symmetrical eye growth that progressed towards emmetropia. As discussed in **Chapter 2**, the mechanisms that regulate eye growth are predominantly intra-retinal, i.e. when the eye is disconnected from the brain, it retains the ability to respond to growth cues with relatively minor perturbation. Thus, as it was likely that any effect of CVS disruption would be subtle, identifying an effect was dependent on choosing a suitable strain.

Although chicks are well regarded as models for studies on emmetropisation, different strains have been reported to show variability in both normal eye development (towards emmetropia) as well as in response to experimental manipulations, e.g. FDM (Troilo et al., 1995). Having initially identified a strain that was unsuitable due to excessive ocular asymmetry and impaired emmetropisation (WL) (**Section 5.4.3**), an alternative strain, Shaver Black, a cross between Rhode Island Red and Barrack Rock strains was found to be most suitable.

In some instances, interpretation of lesion success can be based upon resulting behavioral or physiological impairments, e.g. loss of vision following ONS. Alternatively, the success of a more discrete lesion of a neural structure, e.g. the Edinger-Westphal nucleus, can be determined both histologically and by the absence of accommodation. However, in the case of the CVS, no behavioral or physiological effects are known to result from destruction of either ION or IOTr, with past studies relying upon histological determination from Nissl stained tissue (Knipling, 1978a; Hahmann and Gunturkun, 1992; Nickla et al., 1994). The choice of lesion target and method of success determination are intertwined. With a lesion of the ION itself, quantification of lesion success can be relatively accurate, however, a large

lesion is required. Therefore, the likelihood of collateral damage and subsequent unrelated effects is great. Conversely, a lesion of the IOTr is not accurately quantifiable, but collateral damage is less likely. Here, we take advantage of the unique direct ION-retina connection in order to accurately quantify lesion success following IOTr lesion using a pathway tracing paradigm (**Section 5.6**).

In the next three chapters, I report the effects of disrupting centrifugal efferents to the retina in chicks on eye growth in chicks: **1)** raised with normal visual experience (**Chapter 6**); **2)** raised under constant 24 hour/day light (**Chapter 7**); **3)** when subject to plus or minus lens-induced defocus (**Chapter 8**).

Chapter 06

The effect of IOTr lesion on chicks with normal visual experience

6.0 Introduction

The chick has been the most widely used model for investigations into the mechanisms of emmetropisation (**Section 2.1**). The consensus of numerous studies is that emmetropisation is an active, visually guided process, which is in turn aided by passive non-visually guided ocular growth (**Section 2.3**).

Studies in the chick have suggested that isolation of the retina from the brain may alter the 'set-point' of emmetropisation (**Section 2.6**). When the retina is disconnected from the brain experimentally, through optic nerve section (ONS), eyes retain the ability to respond to visual cues, e.g. lens manipulation. However, without the influence of the higher brain centres, the accuracy of recovery after removal of such optical manipulation is, in some cases, impaired. Under normal visual conditions, ONS eyes develop moderate hyperopia (**Section 2.6**). While such studies argue that brain-eye connectivity is necessary for at least fine-tuning emmetropisation, the central pathways involved have yet to be elucidated.

The centrifugal visual system (CVS) is defined by its efferent projection from the brain to the retina, one that is particularly enlarged and well defined in the bird model (**Section 1.5**). In the chicken, about ten thousand neurons project in a highly topographic manner from the TeO, (a structure analogous to the mammalian superior colliculus) to the ipsilateral isthmo-optic nucleus (ION) in the midbrain and possibly neurons of the surrounding ectopic area (EA) (the latter is addressed in **Chapter 9**). This pathway transmits predominantly, but not exclusively, visual information. In turn, these CVS brain centres have major projections to the contralateral retina, while a numerically minor sub-population of ectopic neurons project to the ipsilateral retina (Clarke and Cowan, 1975). Within the retina, centrifugal axons terminate upon amacrine-like cells (IOTCs) in a distribution strictly restricted to the ventral retina (Catsicas et al., 1987; Lindstrom et al., 2009), while avoiding the central fovea (in pigeons (Woodson et al., 1995) but not in

chickens (Lindstrom et al., 2009)) and red field (Weller et al., 2009). Secondary axons arising from IOTCs innervate RGCs in a seemingly random distribution that covers the entire retina. Neurochemical studies of IOTCs have revealed nitric oxide synthase (NOS) activity (Morgan et al., 1994); a finding of potential significance because treatment of the retina with the NOS-inhibitor, L-NAME, prevents form deprivation induced myopia (FDM) (**Section 2.6.3**). Furthermore, the localised distribution of IOTCs and the complex intra-retinal connectivity of these cells (**Section 1.5.2**) makes the CVS an interesting candidate for the effects upon eye growth observed when the retina is isolated from the brain (**Section 2.6**).

6.1 Methods and experimental design

Fifty four Shaver Black chicks were used in this experiment. Prior to surgery, chicks were pre-screened for existing ametropia (3 days post hatch) and weighed in order to assess general health. Streak retinoscopy was performed to measure refractive error (**Section 3.6**) and IR-keratometry to measure corneal radius of curvature (CR) (**Section 3.5**). Seven and 21 days post surgery, IR-keratometry, streak retinoscopy and A-scan ultrasonography (**Section 3.7**) were performed. Percentage IOTr lesion success was determined by pathway tracing (**Section 3.8**). Following stereological determination of lesion success (**Section 3.13**), subjects were split up into rank ordered quartile groups (Q_1 to Q_4) with Q_1 corresponding to those chicks with the lowest lesion success (and sham operated controls (**Section 5.6**) and Q_4 those chicks with the highest (**Fig. 6.1**).

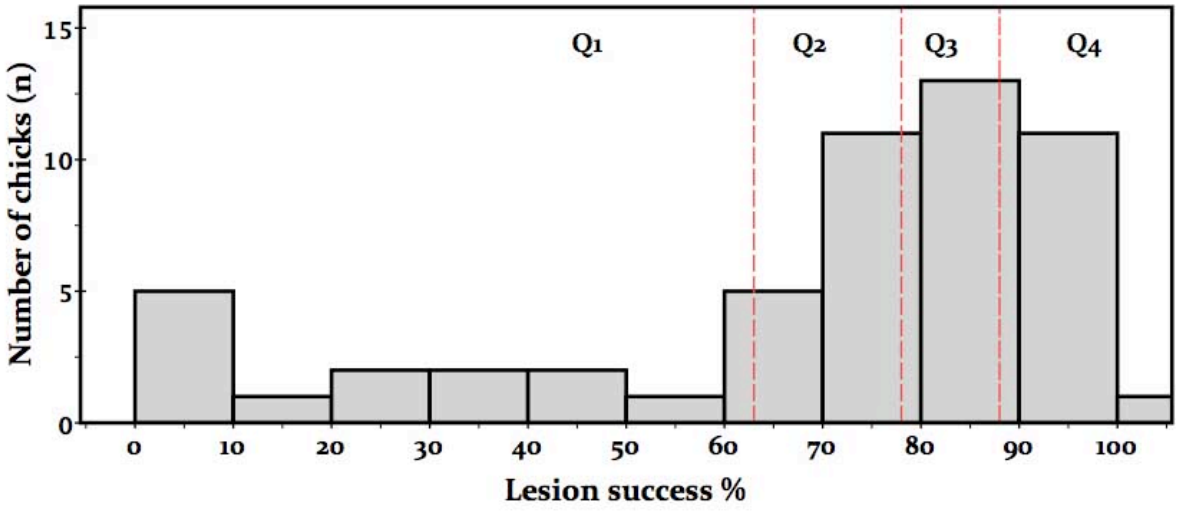

Fig. 6.1. Lesion success: normal visual experience. Histogram showing the distribution of percentage lesion success of individual subjects (n=54) and subsequent division into quartile groups of lesion success (Q1-4) (**vertical red dashed lines**). Examples of IOTr lesions from the above distribution are shown in **Figure 6.2**.

6.2 Results

6.2.1 Refractive state changes

An overall lesion effect on anisometropia was found 7 days post surgery ($F_{3,50}$ = 7.104, p<0.001). After 7 days post surgery, treated eyes (i.e. contralateral to the lesion) of subjects in the Q4 group of chicks showed a mean hyperopic shift relative to control (ipsilateral) eyes (2.31 D ± 2.46, p<0.005). Q1 to Q3 groups of chicks were not significantly anisometropic (all p>0.568). Furthermore, anisometropia in the Q4 group of chicks was significantly greater than that in the Q1 and Q2 quartile groups of chicks (Q4-Q1: 2.26 D ± 0.66, Q4-Q2: 2.11 D ± 0.71, both p<0.05) (**Fig. 6.2** and **Table 6.1**). However, when compared with the Q3 group of chicks, the difference did not reach significance, (1.89 D ± 0.74, p=0.081) (overall across quartile group effect: $F_{3,50}$ = 7.104, p>0.001).

At 21 days post-surgery, no overall across-group lesion effect was found, ($F_{3,50}$ = 2.340, p=0.085). The initially observed anisometropia in the Q4 group of chicks was

no longer apparent (-0.17 D ± 0.48, p=0.214), while Q2 and Q3 groups of chicks similarly showed no significant anisometropia (both p>0.520). Q1 treated eyes showed a small but statistically significant hyperopia relative to fellow control eyes (0.17 D ± 0.27, p<0.05), however, as stated this difference was not reflected by a significant effect between quartile groups of chicks (**Fig. 6.2** and **Table 6.1**).

Fig. 6.2. Examples of IOTr lesions: Normal visual development. The isthmo-optic tract (IOTr) courses anteriorly at the dorso-medial aspect of the optic tectum before merging with the optic tract. In these coronal sections of the chick midbrain, electrolytic lesions of the IOTr were made unilaterally, consistently on the left side of the midbrain (**A-F**). The right side of the midbrain was left untreated (**G-H**). In the bottom left hand corner of each example are details of the case from which the photomicrographs were taken, along with the corresponding lesion success percentage as determined by retrograde WGA labeling following intra-vitreal injections in the eye contralateral to the lesion prior to sacrifice. **Scale bar = 250 μm**

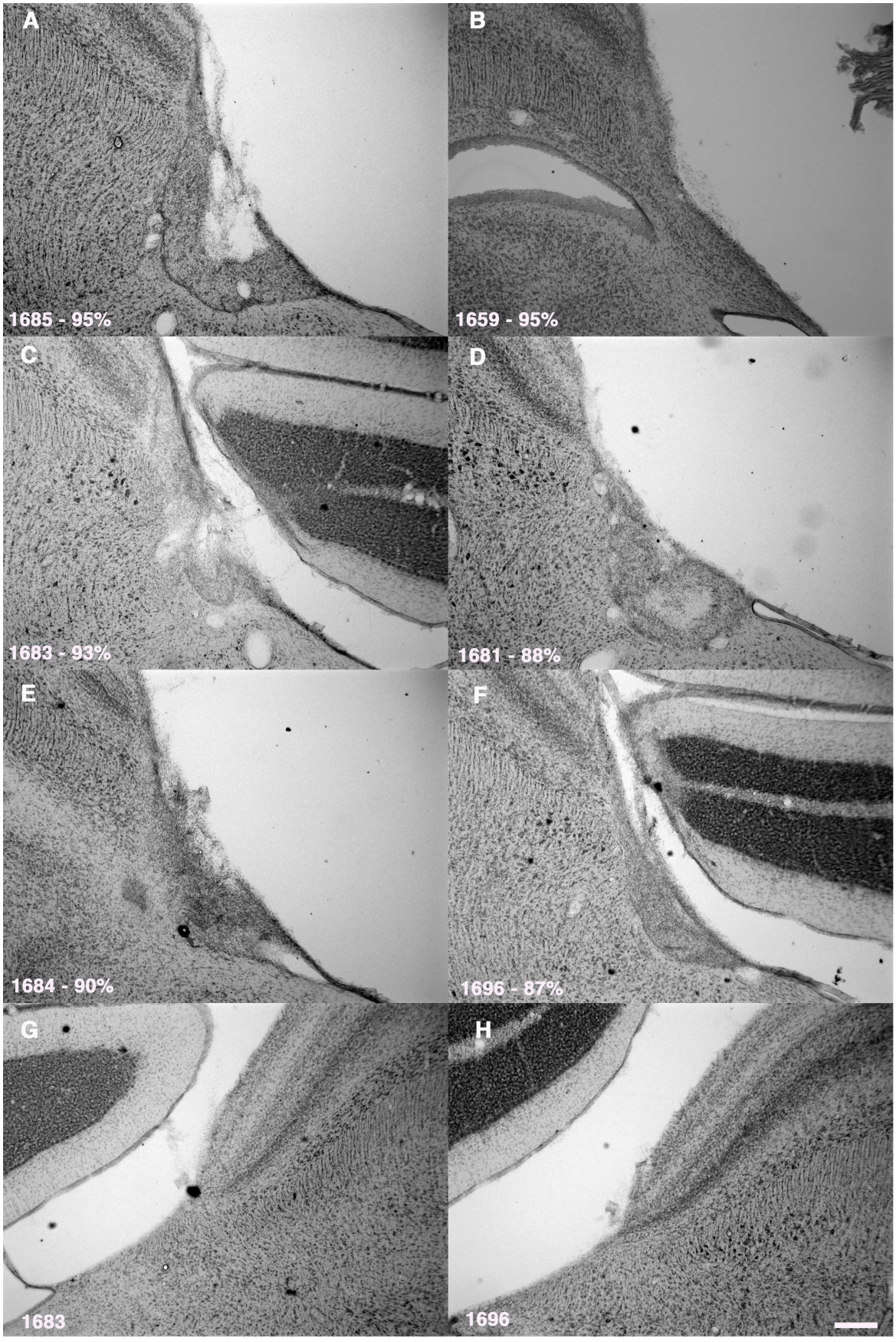

Fig. 6.2. (See previous page for figure legend)

Table 6.1. **Anisometropia across quartile groups of lesion success.** Anisometropia (T-C) (±SD) in groups of differing IOTr lesion success.

	Anisometropia (T-C) (D)			
	Q1 (n=14)	**Q2** (n=13)	**Q3** (n=13)	**Q4** (n=14)
At 7 days post surgery	0.05±0.36	0.20±0.96	0.42±1.21	**2.31±2.46*****
At 21 days post-surgery	0.17±0.27*	0.03±0.24	-0.05±0.34	-0.17±0.48

Statistical test results relate to within group analyses (i.e. Treated eye vs. control eye differences). Between quartile group comparisons are shown in **Fig. 6.2**. *p<0.05, **p<0.01, ***p<0.005** (paired t-tests).

6.2.2 Ocular component dimension changes

After 7 days post surgery, the treated eyes of the Q4 group of chicks had significantly shorter VCD and AXL components than fellow control eyes (both p<0.01) (**Table 6.2**). VCD and AXL within-animal asymmetry also reached significance in the Q1 group of chicks. Comparison of ocular component dimension asymmetry between lesion success quartile groups showed an overall statistical effect in both the VCD ($F_{3,50}$ = 8.149, *p<0.001*) and AXL ($F_{3,50}$ = 8.432, *p<0.001*) components, while ACD and LT dimensions did not (both p>0.533). The observed Q1 treated vs. fellow eye VCD and AXL asymmetry was not found to be significantly different from that observed in the Q2 or Q3 groups (all p>0.095). However, significant differences across quartile groups were found in VCD ($F_{3,50}$ = 8.149, p<0.001) and AXL ($F_{3,50}$ = 8.432, p<0.001) asymmetries. In the case of both VCD and AXL asymmetry, the Q4 group were significantly different from those seen in both Q1 (both p<0.01) and Q2 (both p<0.05*)*, but did not reach significance when compared with the Q3 group of chicks (VCD, p=0.060; AXL, p=0.084) (**Fig. 6.2**). A highly significant negative relationship was found between anisometropia and VCD asymmetry ($F_{1,52}$ = 238.163, p<0.001), strongly suggesting that the observed lesion-induced anisometropia was vitreous chamber depth-dependent (**Fig. 6.3**). Twenty-one days post-surgery, no significant difference was found between treated and fellow control eyes in either ACD or LT components. Treated eyes in

the Q2 to Q4 groups of chicks had significantly longer VCD and AXL components when compared to fellow control eyes (all p<0.05) (**Table 6.2**). There was no significant difference in the amount of asymmetry exhibited in any of the measured ocular components (all p>0.299*)* (**Fig. 6.4** and **Table 6.2**).

6.2.3 Corneal radius of curvature changes

No clear treatment effect was evident for CR. While comparison of CR data between fellow eyes (T-C) showed significant flattening of treated eyes in both the Q3 (0.035 mm ± 0.057, *p*<0.05) and the Q4 (0.045 mm ± 0.065, *p*<0.05) groups at day-21 post-lesion, these differences were not found to be significant when compared across groups at 7 days post surgery ($F_{3,49}$ = 1.690 , p=0.181) or 21 days post surgery ($F_{3,50}$ = 0.139, p=0.936). *(***Fig. 6.4**).

Table 6.2. Ocular component dimension asymmetry across tertile groups of lesion success

Ocular component asymmetry (T-C) (±SD), 7 days and 21 days post surgery.

	Ocular component asymmetry (T-C) (mm)			
7 days post-surgery	**Q1** (n=14)	**Q2** (n=13)	**Q3** (n=13)	**Q4** (n=14)
Anterior chamber depth	0.003±0.014	0.002±0.016	0.000±0.017	0.005±0.024
Lens thickness	0.006±0.022	-0.003±0.023	-0.005±0.022	-0.003±0.018
Vitreous chamber depth	0.024±0.031*	0.007±0.070	-0.010±0.061	**-0.123±0.142****
Axial length	**0.033±0.026*****	0.006±0.070	-0.015±0.063	**-0.121±0.141****
Corneal radius of curvature	0.004±0.049	-0.007±0.050	-0.010±0.039	0.029±0.061
21 days post-surgery				
Anterior chamber depth	-0.000±0.017	-0.001±0.015	0.001±0.022	-0.012±0.025
Lens thickness	0.010±0.023	0.006±0.019	0.007±0.026	0.008±0.023
Vitreous chamber depth	0.012±0.050	0.029±0.043*	0.029±0.035*	0.038±0.059*
Axial length	0.022±0.048	0.034±0.047*	0.036±0.034***	0.033±0.062
Corneal radius of curvature	0.031±0.058	0.034±0.071	0.035±0.057*	0.045±0.065*

Statistical test results relate to within group analyses (i.e. Is treated eye different to control eye). Between group comparisons are shown in **Fig. 6.4**. *p<0.05, **p<0.01, ***p<0.005 (paired t-tests).

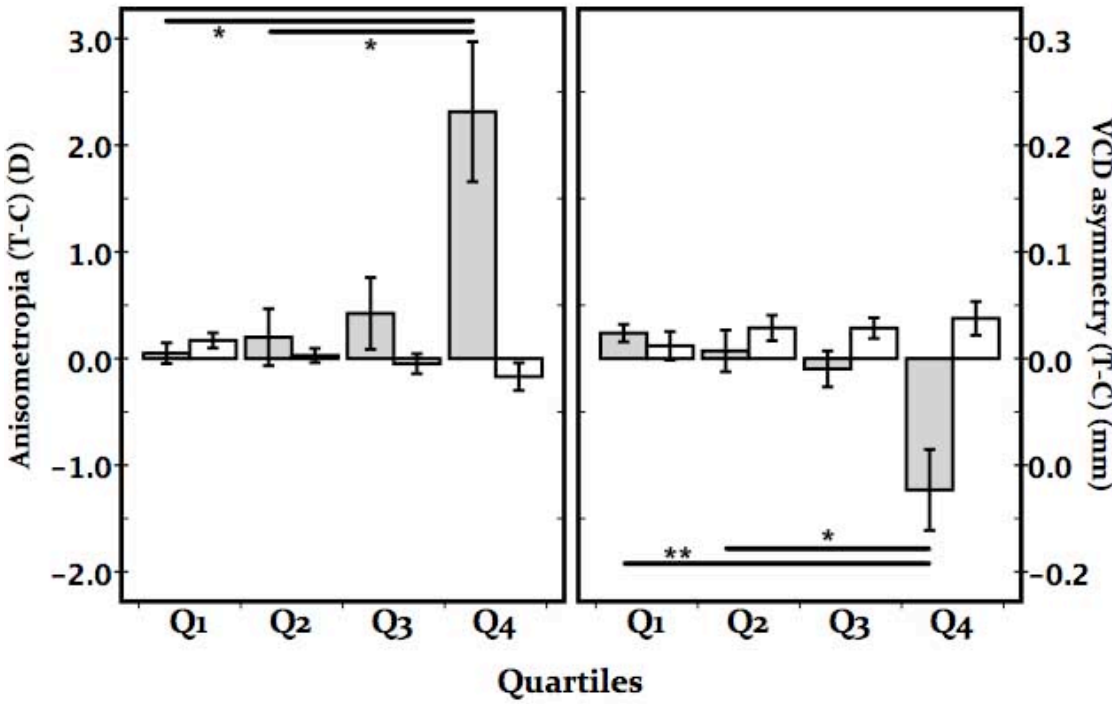

Fig. 6.3. Anisometropia and vitreous chamber depth in quartile groups. Anisometropia (**right**) and vitreous chamber depth asymmetry (**left**) 7 days (**grey**), and 21 days post-surgery (**white**). At 7 days post surgery, the amount of anisometropia (treated minus control eye) in the Q4 group of chicks was significantly greater than those in Q1 and Q2, i.e. Treated eyes of chicks in the Q4 group were significantly more hyperopic than those in Q1 and Q2. This difference was reflected in the results of the A-scan ultrasonography, which showed that chicks in the Q4 group of chicks had significantly more VCD asymmetry (treated minus control eye) when compared to chicks in the Q1 and Q2 groups of lesion success. Thus treated eyes of chicks in the Q4 group were significantly shorter than those in the Q1 and Q2 groups of chicks. 21 days post surgery, the initial asymmetry in both refractive state and VCD asymmetry were no longer evident. *Error bars denote SEs.* *p<0.05, **p<0.01, ***p<0.005 (One-way ANOVA with Games Howell post-hoc test).

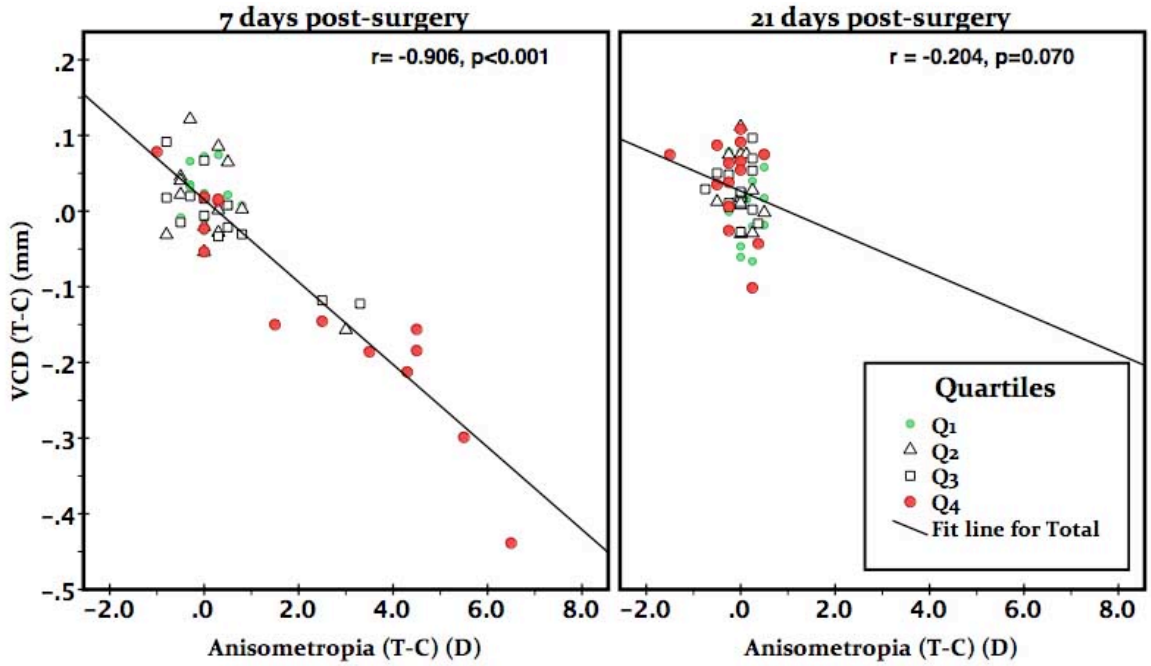

Fig. 6.4. Anisometropia vs. vitreous chamber asymmetry. Seven days post surgery, a strong correlation existed between anisometropia and VCD asymmetry, a trend that suggests the hyperopia exhibited by treated eyes of chicks in the Q4 group of lesion success was the result of a relative shortening of the VCD. Twenty-one days post surgery, the lesion induced anisometropia and VCD asymmetry observed after 7 days post surgery was no longer apparent and this was mirrored in the non-significant relationship observed in the right facet above.

Fig. 6.5. Ocular dimension asymmetry in quartile groups (T-C) 7 days and 21 days post-surgery. No significant asymmetry was evident in ACD, LT and CR components after 7 or 21 days post surgery however chicks of the Q4 group of lesion success exhibited significant VCD asymmetry relative to Q1 and Q2 groups as characterised by a relative shortening of the treated eye. Similarly this trend in VCD asymmetry is reflected in the significant AXL asymmetry in the Q4 group of chicks when compared with Q1 and Q2 groups of chicks. At 21 days post surgery, no significant asymmetry in any of the ocular component dimensions between quartile groups of lesion success. *Error bars denote SEs.* *p<0.05, **p<0.01, ***p<0.005 (One-way ANOVA with Games Howell post-hoc test).

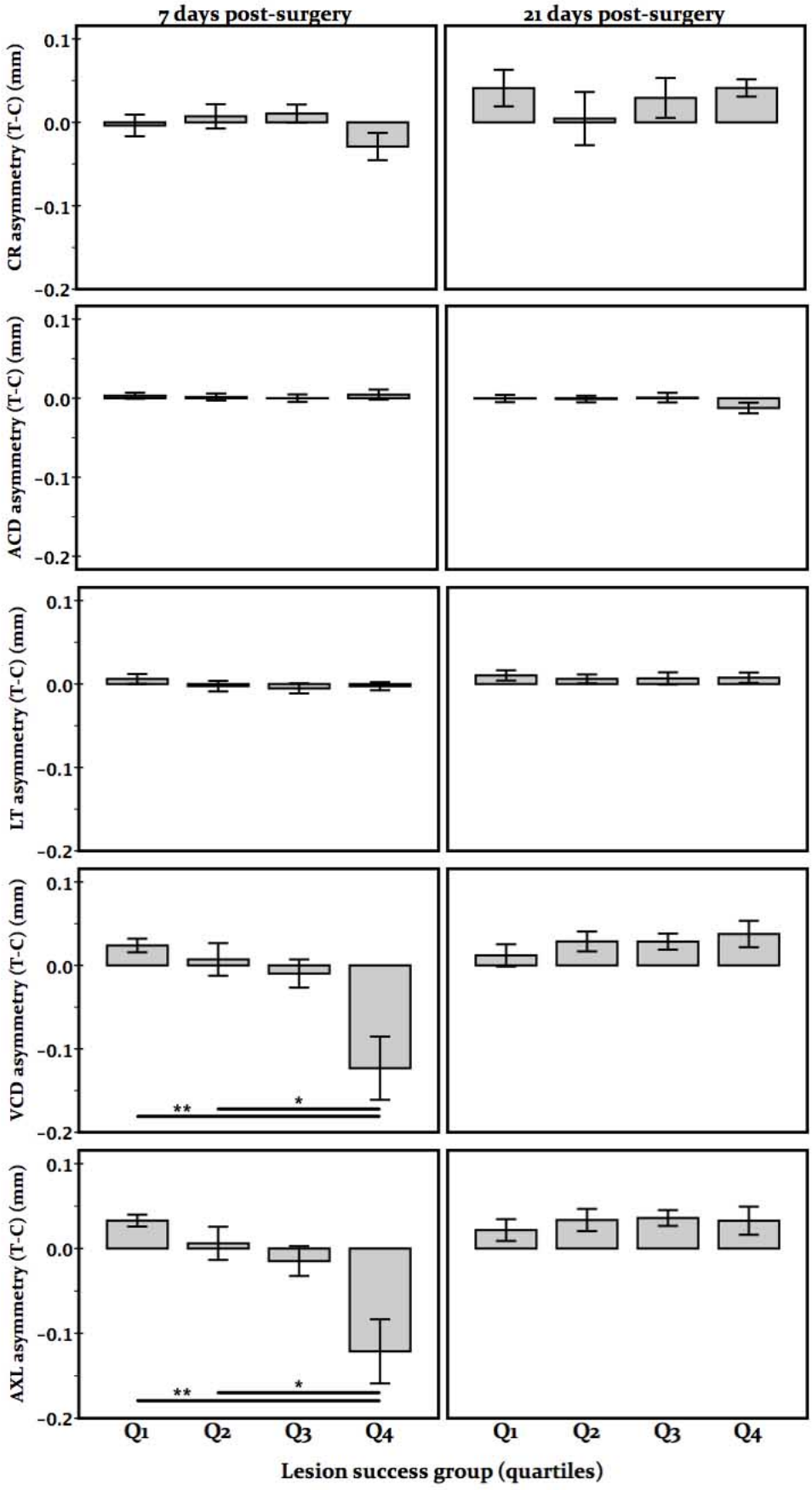

Fig. 6.5. (see previous page for figure legend)

6.3 Discussion

These results indicate that unilateral disruption of centrifugal ION and EA efferents to the retina of the contralateral eye initially induced a moderate hyperopia at 7 days post-surgery via reduced vitreous chamber depth in the treated, contralateral eye relative to that of the control, ipsilateral eye. After 21 days post-surgery, the observed optical and physical asymmetry was resolved. This suggests that the diminished 'accuracy' of emmetropisation seen in previous work, e.g. through ONS studies, was at least in part due to the severing of centrifugal axons.

An electrolytic lesion of the ION or IOTr both elicit the same end result, i.e. that centrifugal input to the retina is blocked, either through destruction of ION and EA somata or severance of the axon bundle (that in itself would most likely cause retrograde somata degeneration within the time-course of the experiment). However, when one considers the ipsilateral EA projection, complexities arise. The numerically minor ipsilateral EA tract has been assumed to reach its destination by remaining uncrossed at the optic chiasm. If true, a lesion of either the ION or the IOTr would not only disrupt contralateral efferents to the treated eye but also the ipsilateral efferents to the control eye. Furthermore, the contralateral treated eye would still be receiving its normal ipsilateral EA innervation (**Fig. 5.7**). As a result of this ambiguity in the distinction between 'treated' and 'control' eyes, it is first important to address the question of whether the induced relative hyperopia in the treated eye was due to the treated eye becoming relatively shorter or the control eye becoming longer than normal. There was a highly significant overall treated eye effect ($F_{3,50} = 5.929$, $p=0.002$) while the control eye effect was not significant ($F_{3,50} = 0.622$, $p=0.604$). This suggests that it was in large part a treated eye effect (**Fig. 6.5**)

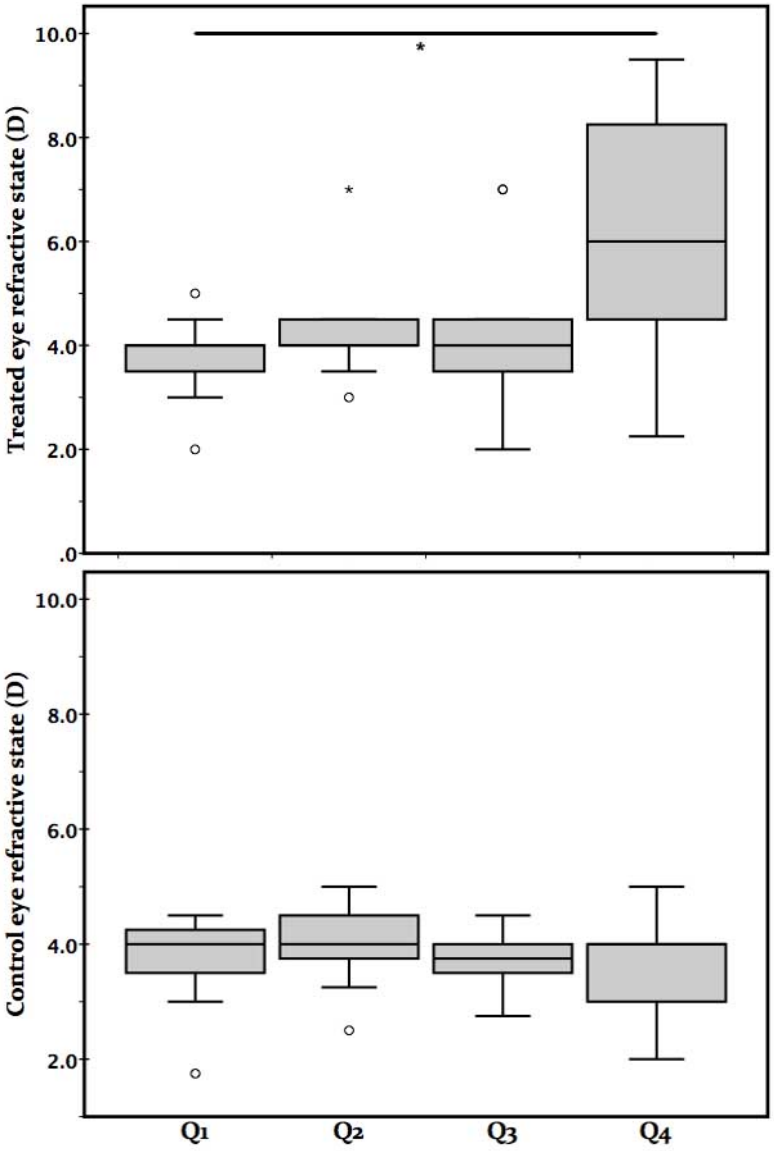

Fig. 6.6. Absolute refractive state in quartile groups of treated (**top**) and control (**bottom**) eyes after 7 days post surgery. Crucially, these data show that the asymmetry in refractive state (anisometropia) evident 7 days following lesion of the isthmo-optic tract was due to relative treated eye hyperopia, while the control eye refractive state was not significantly different to those of the Q1-Q3 groups of chicks. *p<0.05, **p<0.01, ***p<0.005 (One-way ANOVA with Games Howell post-hoc test). Error bars represent upper and lower 25% of the sample, the box length represents the interquartile range of the sample, while the line across the box represents the median value of the sample. Circles represent outlier values greater than one and a half box lengths from the boundary of the box, while asterisks represent outlier values greater than 3 box lengths away from the upper or lower boundary of the box [15].

Studies have suggested that isolation of the retina from the brain may alter the set-point of emmetropia (Wildsoet, 2003; Tepelus and Schaeffel, 2010). Under otherwise normal conditions, as already mentioned, ONS eyes develop moderate to severe hyperopia (Troilo et al., 1987). When ONS eyes are form deprived through the use of occluders, some studies suggest that, compared to eyes with an intact optic nerve, subsequent recovery (from an otherwise normal treatment response) leads to an axial hyperopic overshoot, i.e. an overcorrection of the induced refractive error (Wildsoet, 2003). It is therefore important to note that, at the end of the 21-day lesion-treated period, not only had the axial anisometropia been resolved, but also that the absolute refractive state and ocular component dimensions of subjects that had developed axial hyperopia within the first 7 days of treatment, were not significantly different to those in subjects that had not, i.e. there was no myopic overshoot after IOTr lesion.

Typically, lesion success is quantified through volumetric estimations from Nissl stained tissue (e.g. Knipling, 1978), or from a co-incidental behavioral deficit that results from a given lesion site, e.g. the absence of pupillary constriction response following lesion of the optic nerve (e.g. Li and Howland, 2000). However, our paradigm, i.e. using an intra-vitreal injection of WGA in the eye contralateral to the lesioned hemisphere (**Chapter 5**), allowed for a greater accuracy in determining both the number and location of remaining intact centrifugal connections. A lesion of the IOTr would, in theory, prevent retrograde transmission of WGA to the ION/EA. Our finding was that even an apparently complete lesion of the IOTr (as assessed by Nissl staining) rarely completely abolished WGA retrograde labeling within the ION/EA complex. The reasons behind this are unknown, however several possibilities exist:

1. Not all efferent axons take the same route to the retina.

2. The position of a given lesion was caudal to where the axons of the intact connections joined the fiber bundle.

3. As a result of the lesion technique, a portion of the myelinated axons were spared.

4. Given the age of the chicks used, and therefore the high degree of neuronal plasticity, recovery mechanisms, e.g. regenerative growth or compensatory branching of intact fibers may have occurred during the experimental time frame (Raisman, 1969; O'Keefe and Nadel, 1979).

A novel feature of our findings is that, while initial vitreous-chamber dependent hyperopia is readily comparable with that seen in chicks in ONS experiments, this effect has been shown to persist and, to a degree, progress for the duration of the experimental time frame (at least 28 days post-surgery) (Troilo, Gottlieb and Wallman, 1987). In contrast, our results clearly show that the anisometropia and VCD asymmetry measured after 7 days post-surgery had been corrected in the period between 7 and 21 days post-surgery. It has been suggested that the effect observed in ONS studies could be the result of retinal ganglion cell (RGC) death, however Troilo et al. (1987) noted that by the onset of RGC degeneration, i.e. 7 days post-surgery (Muchnick and Hibbard, 1980), significant hyperopia was already apparent. Furthermore, if the moderate hyperopia observed in these results was due to *degeneration* of centrifugal target cells, recovery from the initial ametropia presumably would not take place.

An alternative view is that rather than the target cells of centrifugal efferents becoming functionally quiescent, denervation may have induced a short period (i.e. 5 days to a week), of *hyperactivity*, which induced the ocular growth changes that were observed, i.e. an epileptogenic cell response (Morrell, 1961; Goddard, McIntyre and Leech, 1969; O'Keefe and Nadel, 1979). However, once centrifugal target cell degeneration had taken place, this active deregulation of intra-retinal mechanisms would no longer occur, thus corresponding with

the beginning of the recovery period observed here. Indeed, the activity/behavior of neurons following partial or full deafferentation is not fully understood. Von Monakow (1889) proposed that, while the local effect of a lesion is straightforward, i.e. removal of neural elements, the effect of a lesion at a distance on neurons to which the area of damage was connected, is more complex, inducing 'diaschisis' (Schoenfeld and Hamilton, 1977). Partially deafferented neurons can initially lose all responsiveness to any intact input for a given period, but subsequently re-establish function after the initial 'shock'. Moreover, diaschisis may be followed by 'denervation supersensitivity', a phenomenon described in the peripheral nervous system, whereby deafferentation of neurons induces a heightened state of reactivity to subsequent experimentally induced input (Stavraky, 1961; Sharpless, 1964; O'Keefe and Nadel, 1979). In the case of partial deafferentiation, the affected neuron would become more responsive to the summation of remaining input from intact afferents.

In a study aimed at elucidating retinal connectivity of centrifugal efferents, Nickla et al. (1994) found that cytochrome oxidase labeling of IOTCs was severely diminished (~97%) as a result of IOTr lesion. Survival times used in the study were between 9 and 36 days post-lesion and it was noted that the severity of the reduction in cytochrome oxidase labeling increased with the length of survival time, thus suggesting that the process of deafferentation-induced quiescence in IOTCs was progressive over a duration comparable to that used in this study. Unfortunately, the earliest time point of 9 days is outside the period of time in which a potential atypical cellular response would have been observed. Therefore, in the absence of pharmacological or immunohistochemical data, we can only speculate as to the effect (and its timescale) of the lesion on cells in the retina. Interestingly, however, the suggested time frames during which one would expect to observe the behavioral side-effects of diaschisis (one week or less) and subsequent denervation supersensitivity (1 to 4 weeks) are well matched to the pattern of ocular growth affects reported here.

Several approaches could be adopted to investigate the retinal response to an IOTr lesion. In a manner analogous to that employed by Nickla et al (1994) (above), the intra-retinal nitric oxide (or nitric oxide synthase (NOS)) levels within the retina could be measured at various time points following surgery. It has been noted in rats that following ONS surgery, RGC death takes place via a mechanism of nitric oxide mediated excitotoxicity (Lee et al., 2003) within a comparable time frame to that which requires explanation in these results. Expression of NOS within RGCs peaked at 5 days post surgery and had decreased to near normal levels by 28 days post surgery. If this is also the case in the chick, such a response could in part explain the temporally distinct nature of refractive error changes in response to ONS and IOTr lesion surgeries. Alternatively, the so-called 'recovery of function' phenomenon (Stein et al., 1969) could explain the transient nature of the lesion affect described above. In order to address this possibility, a multiple stage lesion treatment could be adopted (e.g. Stein, 1969, 1974), such that recovery of function at the lesion site is disrupted sequentially. Presumably, if recovery of function was the result of neuronal regeneration, e.g. collateral sprouting, etc., this approach would augment the observed lesion effect, and in the context of this study, prevent recovery from vitreous chamber dependent hyperopia.

Interestingly, it is worth noting that a systematic error was evident in our measurements of ocular component dimensions whereby right eye measurements were found to be consistently, albeit marginally, longer (e.g. AXL; right – left: 0.035 mm). We attribute this to an apparatus-based measurement error, as it has occurred in studies involving a different strain of chick (Chen et al., 2011b) (**Table 6.3**). In any event, this small artifact, in the context of this work, would actually serve to give a conservative account of our findings, since the error acts to bias towards an *elongated* right eye, whereas here we report a *shorter* right eye. It may, however, account for the small but statistically significant axial length and vitreous chamber depth elongation present in the Q1 group of

chicks after 7 days post-surgery and also in the Q2, Q3 and Q4 group asymmetry after 21 days post surgery, that all fall within or around the bounds of the bias described (**Table 6.3**).

Table 6.3. A-scan ultrasonography measurement error. Evidence based upon past experimentation using the same ultrasonography equipment that an apparatus based measurement error was present. Mean inter-ocular differences (right – left) in untreated White leghorn chicks (Chen et al., 2011b) and the asymmetry found in Q1 (sham control and low lesion success group of this study) measured using the same apparatus.

Ocular component dimension (mm)	Species/strain	
Asymmetry (Right-Left)	**White leghorn (n>1000)**	**Shaver black** (n=8)
Anterior chamber depth (mm)	0.003	0.003
Lens thickness	-0.002	0.006
Vitreous chamber depth (mm)	0.034	0.024
Axial length	0.035	0.033

6.4 Conclusion

In conclusion, our findings show that in the absence of centrifugal innervation of the retina, early refractive and ocular development of the chick is transiently disrupted. Although it has been shown conclusively that an intact brain-retina connection is *not* required for active compensation to imposed defocus, development of hyperopia has been reported in its absence (e.g. ONS studies). In this work, I report a comparable initial response after electrolytic lesion of the IOTr, which is consistent with the ONS response, and propose that ONS induced hyperopia is, at least in part, due to the severing of centrifugal efferents that make up around 1% of the optic nerve fibers.

Chapter 07

Effect of IOTr lesion on chicks raised in constant light

7.0 Introduction

Severe effects upon avian optical and ocular morphology from constant light (CL) rearing have been reported. Flattening of the cornea accompanied by lens thinning result in a relatively shallow anterior chamber. Such anterior segment effects develop in conjunction with abnormal vitreous chamber elongation, producing severe progressive hyperopia (constant light: 18.2 D; normal light: 2.8 D, after 11 weeks of treatment) (Li et al., 1995a). Interestingly, Li et al. (1995) found that chicks, when raised in CL, did not have a larger axial length compared to chicks raised in normal light due to the cancelling effect of the anterior chamber/vitreous chamber effects.

Chemically induced damage to photoreceptors of chicks raised in CL, was found to prevent the expected vitreous chamber elongation but not corneal flattening (Lauber and Oishi, 1990). Thus, one explanation for these findings is that, while corneal flattening is the result of the lack of a normal circadian rhythm, the axial elongation observed is the result of active emmetropisation to compensate for the anterior chamber effect. However, as Li et al. (1995) point out in their discussion of the effects of CL, chicks raised in constant dark conditions *also* develop flatter corneas and axial elongation (Gottlieb et al., 1987). Thus, in the dark, axial elongation cannot be the consequence of visually guided emmetropisation.

Constant light has been shown to prevent diurnal ocular growth rhythms (Weiss and Schaeffel, 1993) and fluctuations in intra-retinal dopamine levels (Bartmann et al., 1994). Under normal conditions, dopamine levels are highest during the day. Furthermore, eye elongation in the developing chick has been shown to take place *only* during the day, with a degree of shrinkage, if anything, during the night. Therefore, in order to further elucidate the influence of the CVS on emmetropisation, the aim of this part of the study was to investigate the effect of unilateral disruption of the CVS feedback to the retina on emmetropisation

when intra-retinal mechanisms guided by diurnal rhythms were removed, i.e. under CL conditions.

7.1 Methods and experimental design

A total of 25 Shaver Black (SB) chicks were used in this part of the study. All subjects were raised from hatch in constant light (24 hour/day). The illumination in the brooder and floor pen was 250 to 300 lux.

One group of age matched control chicks (n=8) were used to assess the normal, species specific baseline ocular growth pattern under constant light conditions (n=8), for comparison with the ocular growth pattern of subjects raised under normal diurnal light (NL) conditions (n=14) (Q1 chicks from the **Chapter 6**). A second group (n=17) either underwent IOTr lesion to disrupt centrifugal efferents to the retina unilaterally (n=12) or a sham procedure (n=5) (**Section 3.4**, **Fig. 7.1**). Streak retinoscopy (**Section 3.6**) was performed 7 and 21 days post-surgery, while A-scan ultrasonography (**Section 3.7**) measurements were taken at 21 days post surgery.

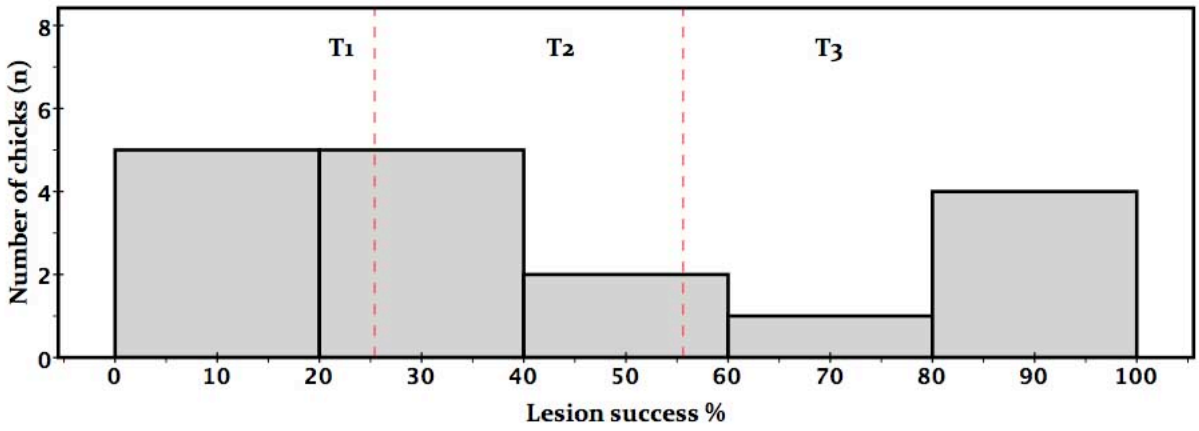

Fig. 7.1. Lesion success: Constant light. Histogram showing the distribution of percentage lesion success of individual subjects (n=17) into ranked tertile groups (T1-3). Red dashed Dotted lines tertile group boundaries. See **Fig. 7.2**. for histological examples of IOTr lesions.

Percentage lesion success was determined by pathway tracing (**Section 3.8**). Following stereological determination of lesion success, subjects were split up into tertile groups (T1-T3), with T1 corresponding to those with the lowest lesion success (as well as sham-operated controls) and T3 the highest.

Fig. 7.2. Examples of IOTr lesions: Constant light. The isthmo-optic tract (IOTr) courses anteriorly at the dorso-medial aspect of the optic tectum before merging with the optic tract. Tn these coronal sections of the chick midbrain, electrolytic lesions of the IOTr were made unilaterally, consistently on the left side of the midbrain (**A-F**). The right side of the midbrain was left untreated (**G-H**). In the bottom left hand corner of each example are details of the case from which the photomicrographs were taken, along with the corresponding lesion success percentage as determined by retrograde WGA labeling following intra-vitreal injections in the eye contralateral to the lesion prior to sacrifice. **Scale bar = 250 μm**

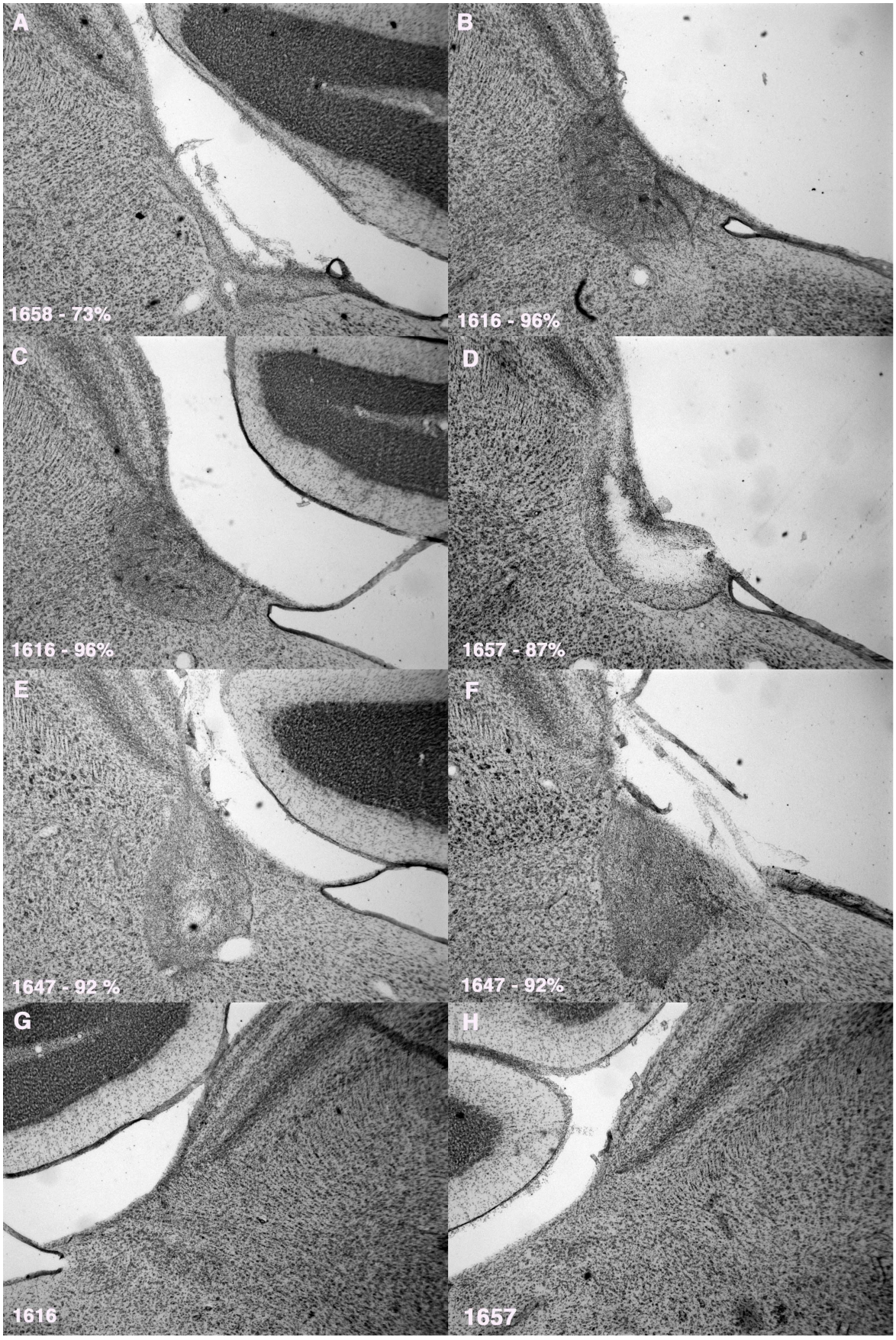

Fig. 7.2. (See previous page for figure legend)

7.2 Results

7.2.1 Constant light effect on non-lesioned chicks

Sham-operated SB chicks (as verified histologically) that had been raised in CL were significantly more myopic (t_{20} = 2.321, p<0.05) than chicks raised in NL 21 days following sham surgery. CL chicks developed a significantly shorter anterior chamber (t_{42} = 35.712, p<0.001) with a longer vitreous chamber (t_{42} = 13.840, p<0.001) and axial length (t_{42} = 4.305, p<0.001) compared to sham-operated SB chicks raised under normal 14 hours on/10 hours off light conditions (Q1 chicks from the previous experiment). However, unexpectedly, lens thickness was not significantly different between the two groups (**Table 7.1**).

Table 7.1. Normal light vs. constant light effect on ocular phenotype. Mean absolute ocular measurements for sham-operated chicks, comparing those raised under normal diurnal conditions (NL) and those in constant light (CL).

Absolute phenotyping measurements	**Diurnal light** (NL) (± *SD*) (n=14)	**Constant light** (CL) (± *SD*) (n=8)	**NL-CL** (± *SE*)
Refractive state (D)	3.77 ± 0.71	2.93 ± 1.36	0.85 ± 0.37*
Anterior chamber depth (mm)	1.716 ± 0.060	1.10 ±0.045	0.615 ± 0.017***
Lens thickness (mm)	2.475 ± 0.058	2.45 ± 0.026	0.025 ± 0.013
Vitreous chamber depth (mm)	5.987 ± 0.207	6.970 ± 0.259	-0.983 ± 0.071***
Axial length (mm)	10.178 ± 0.270	10.521 ± 0.223	-0.344 ± 0.080***

Statistical test results relate to within group analyses (i.e. Is treated eye different to control eye) *p<0.05, **p<0.01, ***p<0.005 (independent sample t-tests).

7.2.2 Refractive state changes in CL chicks with IOTr lesion

Seven days post-surgery, no significant difference was found in the mean absolute refractive state of the treated eyes across tertile groups of lesion success ($F_{2,14}$ = 1.063, p=0.372). The same was true for the refractive state of control ($F_{2,14}$ = 0.138, p=0.872). Furthermore, no significant anisometropia (i.e. within-animal difference) existed across tertile groups of chicks ($F_{2,14}$ = 1.926, p=0.182).

Twenty-one days post surgery, again, no significant difference in the mean (absolute) refractive state of either eye or anisometropia was evident (all p>0.095) (**See Table 7.1** and **Fig. 7.2**).

Table 7.2. Constant light: Refractive error and anisometropia following IOTr lesion. Mean absolute refractive state of the treated (T) and control (C) eyes and anisometropia in the tertile groups of different lesion success (T1-3). For reference, data are presented for sham-operated chicks raised in normal diurnal lighting at corresponding time-points.

	Absolute refractive error (D)			
	T1 (n=6)	**T2** (n=5)	**T3** (n=6)	**Q1** (NL) (n=14)
At 7 days – Control eye	4.33 ± 1.51	4.81 ± 3.00	5.13 ± 3.13	3.75 ± 0.73
At 7 days – Treated eye	3.46 ± 1.52	4.80 ± 3.31	5.75 ±3.25	3.80 ± 0.72
At 21 days – Control eye	2.54 ± 0.62	4.13 ± 3.56	5.50 ± 3.22	2.18 ± 0.46
At 21 days – Treated eye	2.65 ± 0.53	4.05 ± 3.86	4.42 ± 3.59	2.35 ± 0.65
	Anisometropia (T-C) (D)			
At 7 days post surgery	-0.88 ± 0.61*	-0.01 ± 0.58	0.67 ± 2.14	0.05 ± 0.36
At 21 days post surgery	0.10 ± 0.72	-0.08 ± 0.39	-1.08 ± 1.33	0.17 ± 0.27

Statistical test results relate to within group analyses (i.e. Is treated eye different to control eye). Between group comparisons are shown in **Fig. 7.2**. *p<0.05, **p<0.01, ***p<0.005 (paired t-tests)

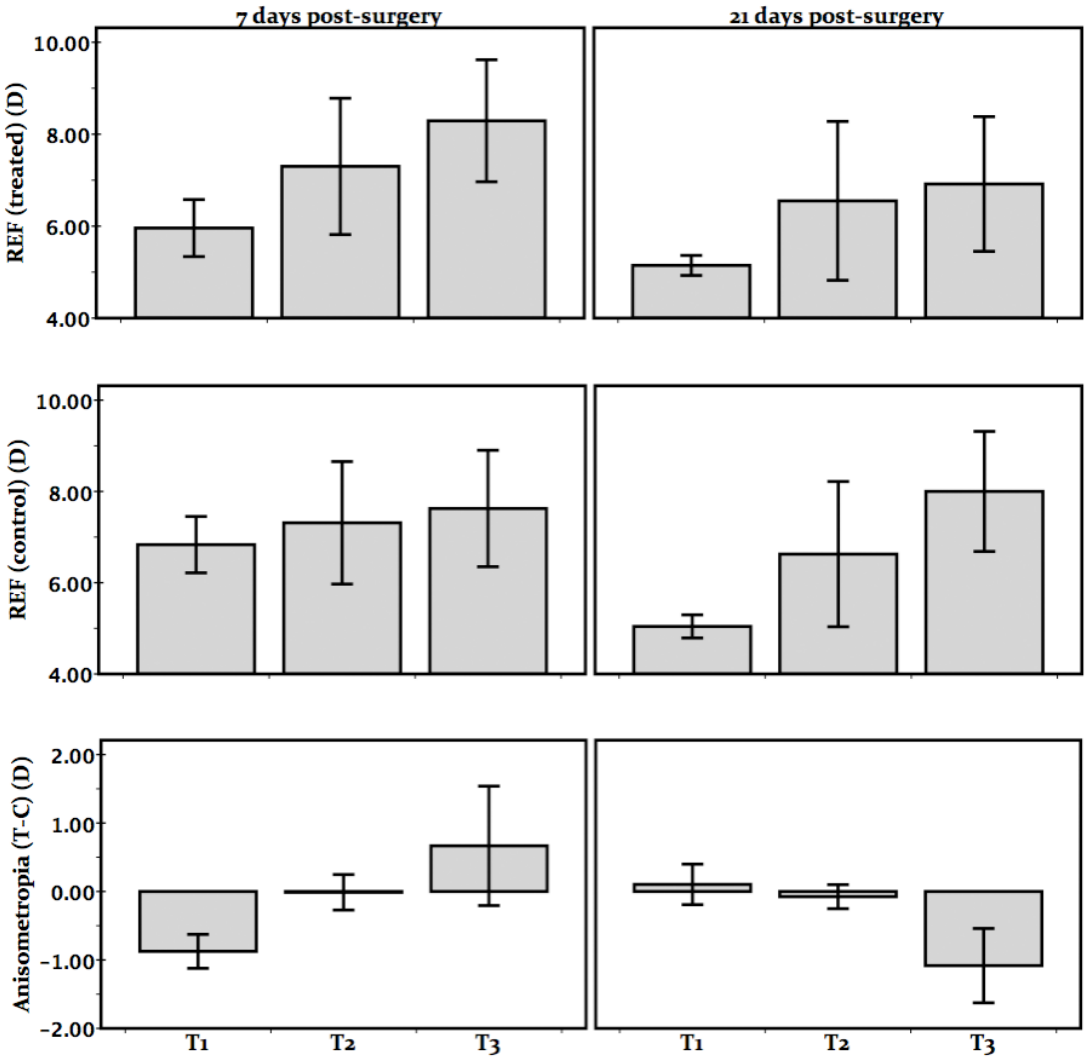

Fig. 7.3. Refractive state and anisometropia in tertile groups of chicks raised in constant light. Mean refractive state and anisometropia (T-C) of chicks (raised in constant light) in different tertile groups of lesion success, 7 (left) and 21 days (right) post surgery. No significant difference was apparent in either the absolute refractive state (top 2 panels) or anisometropia (bottom panel) in chicks compared between tertile groups of lesion success. Treated eyes of chicks in the T3 group showed a trend towards increased amount of hyperopia after 7 days, while control eyes showed a trend towards an increased amount of hyperopia after 21 days post surgery. However, as stated, these trends were not statistically significant (**Table 7.2**). *Error bars denote SEs.*

7.2.3 Ocular component dimensions changes in CL chicks with IOTr lesion

Twenty-one days post-surgery, no significant within-animal difference was found in anterior chamber components, i.e. anterior chamber depth (ACD) and lens thickness (LT) (both p>0.643). Moreover, no significant difference in ACD or LT component asymmetry (T-C) was evident between groups (both p>0.603) (**Fig. 7.4a**).

While there was no significant difference in the VCD component of *treated* (contralateral) eyes across tertile groups ($F_{2,14}$ = 1.258, p=0.315), a significant between-group difference in *control,* ipsilateral eye VCD was apparent ($F_{2,14}$ = 3.873, p=0.046). The mean VCD of the control eyes in the T3 group was significantly shorter than that of T1 (-0.398 mm ± 0.128, p=0.028) (**Fig. 7.3** and **7.4b**).

This reduction in the VCD of the control eye was reflected by the significant difference in VCD asymmetry ($F_{2,14}$ = 6.893, p = 0.008) and AXL asymmetry ($F_{2,14}$ = 7.806, p=0.005) that was found between groups. In the case of VCD asymmetry, the T3 group was significantly longer than that of the T2 group (0.267 mm ± 0.078, p=0.034) but did not reach significance when compared to T1 (p=0.102). Similarly, AXL asymmetry in T3 was significantly greater than that of T2 (0.282 mm ± 0.079, p=0.031) but not when compared to T1 (0.223 mm ± 0.086, p=0.078) (**Fig. 7.4b**).

Table 7.3. Constant light: Ocular component dimension asymmetry following lOTr lesion. Mean ocular component dimension asymmetry (T-C) in tertile groups of different lesion success (T1-3). For reference, data for sham-operated chicks raised in normal diurnal lighting at 21 days post-surgery.

21 days post-surgery	Ocular component dimension asymmetry (T-C) (mm)			
	T1 (n=6)	**T2** (n=5)	**T3** (n=6)	**Q1** (NL) (n=14)
Anterior chamber depth	-0.008 ± 0.008	-0.013 ± 0.019	0.001 ± 0.032	0.000 ± 0.017
Lens thickness	0.008 ± 0.008	0.018 ± 0.028	0.019 ± 0.025	0.010 ± 0.023
Vitreous chamber depth	0.087 ± 0.097	0.022 ± 0.046	0.290 ± 0.184*	0.012 ± 0.050
Axial length	0.087 ± 0.092	0.028 ± 0.037	0.309 ± 0.189*	0.022 ± 0.058

Statistical test results relate to within group analyses (i.e. Is treated eye different to control eye). Between group comparisons are shown in **Fig. 7.4a** and **7.4b**. *p<0.05, **p<0.01, ***p<0.005 (paired t-tests).

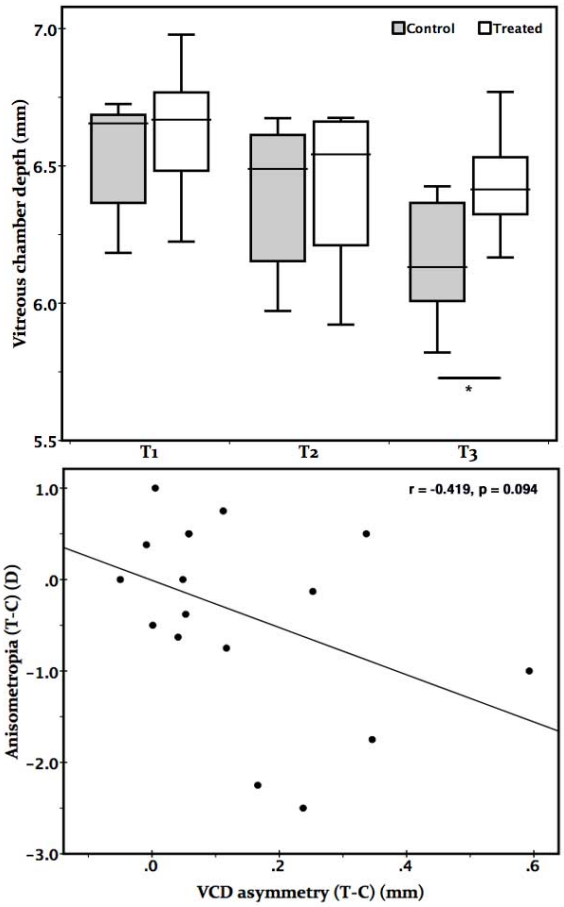

Fig. 7.4. Absolute vitreous chamber depth (VCD) in tertile groups and the relationship between VCD and anisometropia. (Top) Absolute vitreous chamber depth (VCD) of treated (**white bars**) and control eyes (**grey bars**) as a function of isthmo-optic tract disruption 21 days post-surgery. **(Bottom)** Anisometropia (T-C) plotted against VCD asymmetry (T-C). The graphs above convey two major points; firstly, the vitreous chamber depth that was evident in the T3 group of chicks was a product of a shorter vitreous chamber in the control eye, not, as one would expect the treated eye. Secondly, in contrast to the results of Chapter 6, the observed VCD asymmetry was not strongly correlated with anisometropia (**scatter plot**), which is likely to be a reflection of the corneal flattening that results from constant light rearing. One explanation is that disruption of centrifugal efferents inhibited VCD compensation (i.e. elongation) to constant light induced corneal flattening in the control eye. *p<0.05, **p<0.01, ***p<0.005 (one-way ANOVA with Games Howell post-hoc test). Error bars represent upper and lower 25% of the sample, the box length represents the interquartile range of the sample, while the line across the box represents the median value of the sample.

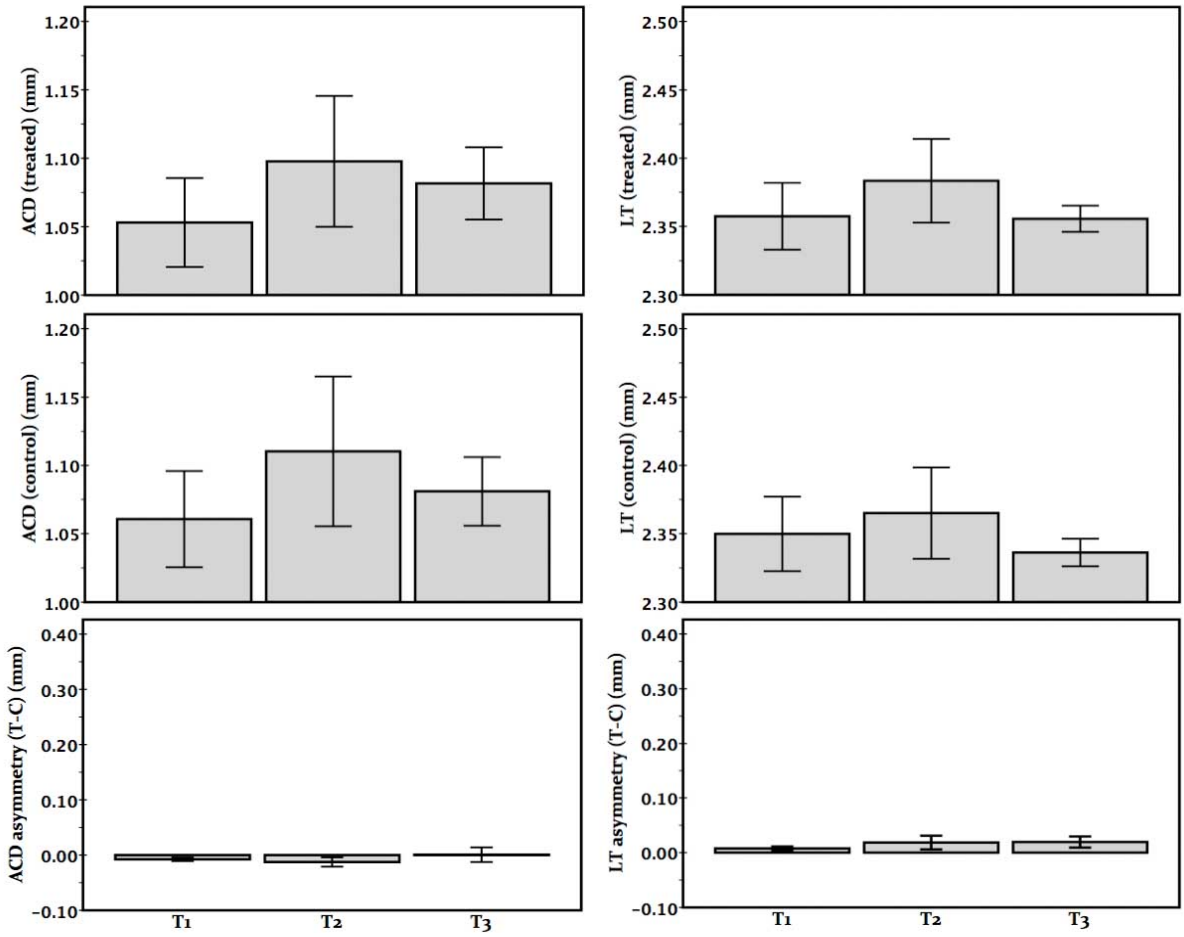

Fig. 7.5a. Anterior chamber depth (ACD) and lens thickness (LT) in tertile groups. Absolute ACD and LT dimensions and asymmetry between fellow eyes (T-C) of chicks (raised in constant light) in different tertile groups of lesion success, 21 days post surgery. No significant difference in ACD or LT components was evident between tertile groups of lesion success. *Error bars denote SEs.*

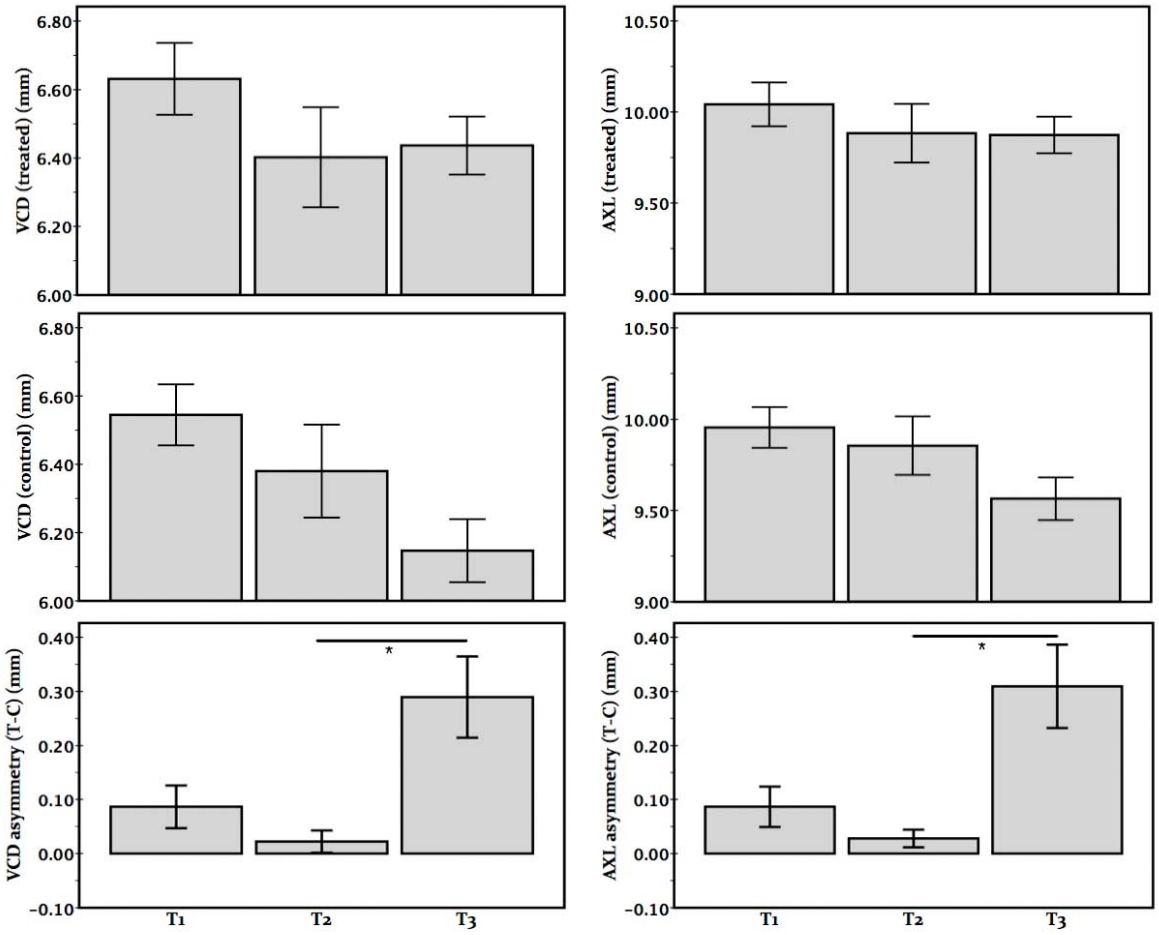

Fig. 7.5b. Vitreous chamber depth (VCD) and axial length (AXL) in tertile groups. Absolute VCD and AXL dimensions and asymmetry between fellow eyes (T-C) of chicks (raised in constant light) in different tertile groups of lesion success 21 days post surgery. Significant VCD and AXL asymmetry was apparent in the T3 group of chicks when compared with the T2 group. The absolute mean VCD or AXL of the treated eyes of T3 chicks showed no apparent elongation relative to T1 and T2 groups and instead this significant VCD and AXL asymmetry was in fact due to a relative shortening of the VCD and AXL of the control eye. *Error bars denote SEs.* *$p<0.05$ (one-way ANOVA with Games Howell post-hoc test).

7.3 Discussion

These results indicate that unilateral disruption of centrifugal efferents induces a relative vitreous chamber depth shortening in the *control*, ipsilateral eye under constant light conditions. The major findings of this study were as follows:

1. While the treated eyes, i.e. contralateral to the lesion of T3 chicks exhibited an ocular phenotype typical of CL treatment, control, ipsilateral eyes had a mean vitreous chamber depth that was significantly shorter.
2. In contrast to the findings from the first experiment (IOTr lesion in normal diurnal lighting), where induced contralateral hyperopia was *transient* (**Chapter 6**), the effect in CL persisted throughout the experimental time frame.
3. In contrast to findings of Li et al. (1995), CL-induced hyperopia was not apparent in the SB strain. While individual subjects within T2 and T3 developed the expected degree of hyperopia, i.e. 8 D and 10 D after 7 and 21 days, respectively (Li et al., 1995a), the remaining chicks were either equal to or more myopic than age-matched NL chicks (**Tables 6.1** and **6.2**).

7.3.1 Circadian rhythms regulate ocular growth

Disruption of circadian rhythms in the chick can be achieved by maintaining 24 hour/day light conditions or by form deprivation (Weiss and Schaeffel, 1993; Bartmann et al., 1994). The expression of a number of catecholaminergic and indoleaminergic proteins that have been implicated as having a role in ocular growth mechanisms are modified under the influence of CL, e.g. dopamine (Bartmann et al., 1994), serotonin (Bartmann et al., 1994; Schaeffel et al., 1994) and melatonin (Rada and Wiechmann, 2006). Intraperitoneal injection of melatonin in chicks on a normal 12h light/12 hour dark rhythms has been shown to lead to anterior chamber and vitreous chamber elongation in untreated chicks, However in form

deprived chicks, the anterior chamber depth is shorter (Rada and Wiechmann, 2006). Moreover, melatonin, which is synthesised ubiquitously in ocular tissues (Wiechmann and Summers, 2008), has been implicated as having un upstream role in the regulation of dopamine synthesis (Dubocovich, 1983).

7.3.2 *Why would centrifugal disruption cause reduced axial growth?*

The presence of nitric oxide in neural tissue is in 'anti-phase' with melatonin synthesis, i.e. high levels of NO and low levels of melatonin are present during the light and the opposite situation occurs in the dark. In the absence of diurnal rhythms, e.g. during CL, melatonin inhibits the activation of excitatory pathways by NO. Thus, in CL conditions, low melatonin levels lead to high levels of NO in neural tissues (Guerrero et al., 1996). As centrifugal efferents are known to synthesise NO, one potential explanation for these findings is that a constant light induced reduction of melatonin synthesis may have led to the *disinhibition* of NO synthesis. *Via* this mechanism, an IOTr lesion induced increase in NO synthesis could, in turn, have induced choroidal thickening (Nickla et al., 2009) and resulted in a reduction in the rate of ocular elongation. Having said that, the above explanation does not explain the curious asymmetry characterised by a relative shortening of the ipsilateral control eye.

7.3.3 Control eye effect: *Inter-ocular communication?*

The most unexpected finding of this experiment was that, while ocular growth in the *treated* eye resulted in a phenotype that was not significantly different to age matched control animals, the *control* eyes of T3 chicks had significantly shorter vitreous chambers when compared across tertile groups of chicks ($F_{2,14} = 3.873$, p=0.046). In this case, control eyes of the T3 group were significantly shorter than control eyes of T1 (-0.398 ± 0.128, p=0.028), while the VCD of treated eyes were not significantly different when compared across groups ($F_{2,14} = 1.258$, p=0.315) (**Fig. 7.3**).

Further evidence for a control eye effect is found from the highly significant negative relationship that existed between the control eye VCD with percentage lesion success for individual subjects ($F_{1,15}$ = 12.720, p=0.003) while only a much weaker (non-significant) negative correlation existed between the absolute VCD of the treated eye and percentage lesion success ($F_{1,15}$ = 2.203, p=0.158), which again was consistent with a control eye effect (**Fig. 7.5**).

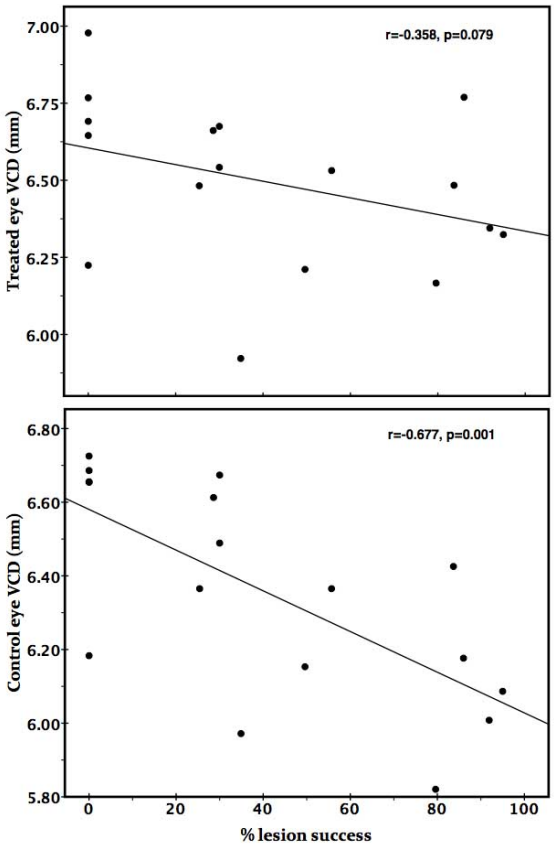

Fig. 7.6. Treated and control eye vitreous chamber depth vs. lesion success. Absolute vitreous chamber depth values plotted against percentage lesion success for control (**left**) and treated eyes (**right**). Twenty-one days post surgery, chicks in the T3 group of chicks exhibited significant VCD asymmetry when compared to chicks of the T2 group. A highly significant negative correlation between the control eye absolute VCD and percentage lesion success (**bottom**) suggests that this asymmetry was due to a relative shortening of the control eye and not as would be expected, the treated eye which did not show a significant relationship between absolute VCD and percentage lesion success (**top**).

These results, together with those in **Chapter 6**, suggest that the contralateral and ipsilateral centrifugal pathways both act to regulate emmetropisation, perhaps via separate pathways. When considered in the context of previous studies, which found that the growth of the two eyes is not entirely independent (Schaeffel and Howland, 1991; Weiss and Schaeffel, 1993), it raises the possibility that the parallel pathways of centrifugal efferents are involved (**Section 2.7**). This intriguing possibility will be discussed further in **Chapters 9** and **10**.

Having established in the previous experiment (**Chapter 6**) that centrifugal efferent disruption induces a transient hyperopia in the contralateral eye (7 days post surgery) that resolves by 21 days post-surgery, it is worthy of note that disruption in diurnal rhythms (as described here) prevents the above effect. In fact, when one considers the eyes in isolation, the refractive state of the *treated* eyes showed a significant positive relationship with percentage lesion success after 7 days ($F_{1,15}$ = 4.635, p=0.048) which, although still positive, was no longer significant after 21 days post surgery ($F_{1,15}$ = 2.569, p=0.130). Conversely, 7 days post surgery, the refractive state of *control* eyes was not significantly correlated with percentage lesion success ($F_{1,15}$ = 0.792, p=0.387), however a significant positive relationship with percentage lesion success was found after 21 days post surgery ($F_{1,15}$ = 6.650, p=0.021) (**Fig. 7.6**).

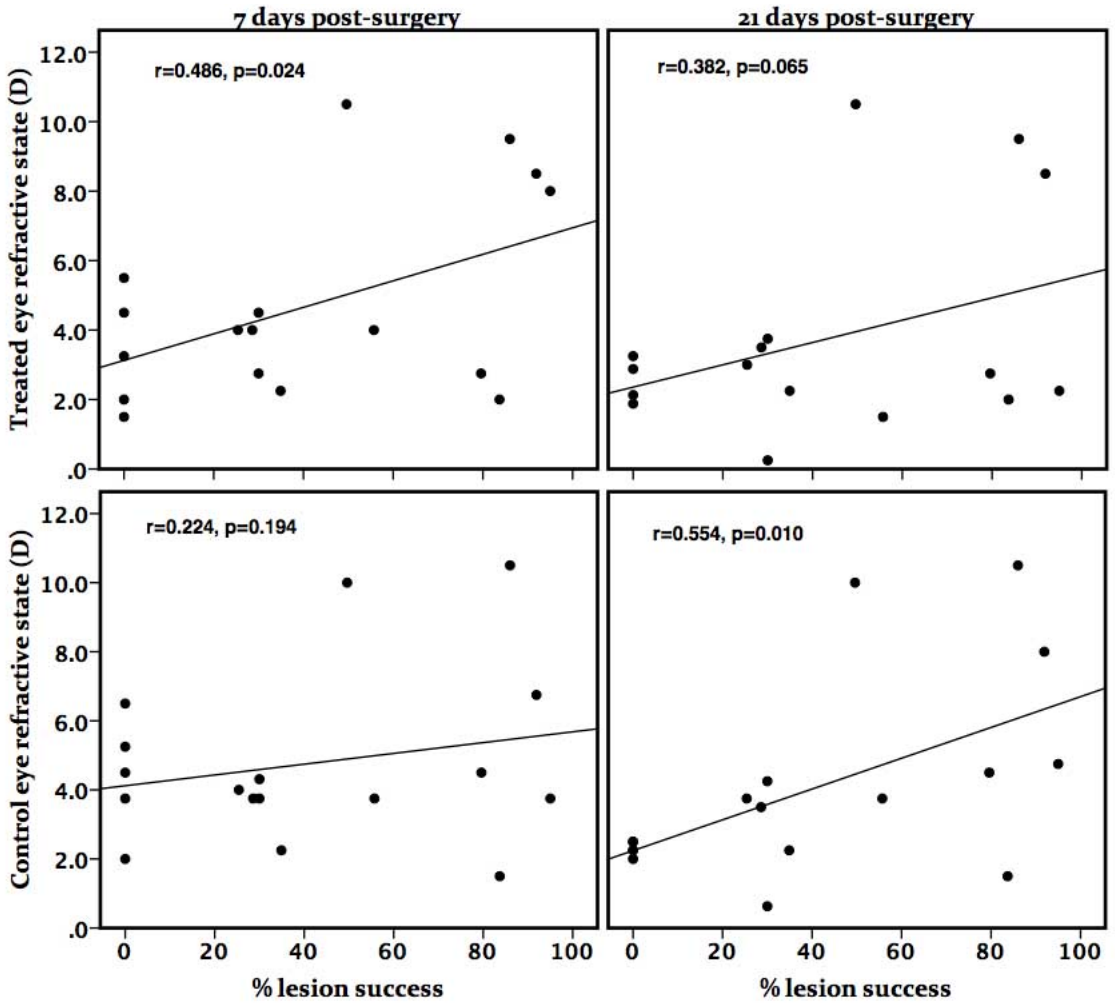

Fig. 7.7. Treated and control eye refractive state vs. lesion success. Absolute refractive state values plotted against percentage lesion success for treated (**top**) and control eyes (**bottom**) at 2 time points, 7 days (**left**) and 21 days (**right**) post surgery. At 7 days post surgery, the refractive state of treated eyes exhibited a strong positive correlation with percentage lesion success, suggesting that, similar to the findings of Chapter 6, lesion of the IOTr induces an initial hyperopic shift and the parallels with the previous experiment continue to 21 days post surgery where the positive correlation no longer reached significance. However, in contrast to **Chapter 6**, at 21 days post surgery, the control eye exhibited a significant positive correlation with percentage lesion success suggesting that disruption of centrifugal efferents led to a switch from an initial treated eye hyperopic shift after 7 days to a control eye hyperopic shift after 21 days.

7.3.4 Strain differences and CL induced hyperopia

The role of melatonin is also potentially a significant factor in the reduced response of the SB strain to CL induced hyperopia. Li and Howland (2006) studied the role of the pineal gland, a midline structure that regulates systemic melatonin expression, on the effects of CL. Importantly, they found that by covering the portion of the head overlying the pineal gland in a diurnal rhythm, protected chicks from the effects of CL.

The SB strain is a predominantly black feathered strain with a high between-animal variability in the degree of yellow or white feather patchiness. Thus, those chicks with dark feathers overlying the pineal gland may have offered greater protection to the effects of constant light than a white strain or SB chicks with white feather patches on top of their heads. That being said, as discussed in **Section 5.7**, different strains of chicks have been shown to demonstrate significant variability in both normal development and in response to experimental manipulations (Troilo et al., 1995). It is likely that inter-strain variability is important in this instance. For example, while Li et al. (1995) found that CL conditions induced severe hyperopia in chicks, they did not find an overall significant axial length elongation as a result of the combined effect of a shortened ACD and an elongated VCD. In these results, significant AXL elongation *was* observed, suggesting that, unlike in the case of the chick strain used by Li et al. (1995), the rate of VCD elongation in SB chicks was, to a degree, sufficient to counter CL-induced hyperopia. In addition, while Li et al. (1995) reported lens thinning in response to CL conditions, this effect was not observed in SB chicks.

7.4 Conclusion

In conclusion, under constant light conditions, unilateral disruption of centrifugal ION and EA efferents to the retina of the contralateral eye induced a vitreous chamber depth

asymmetry characterised by an apparent shortening of the *control* eye, i.e. the eye ipsilateral to the lesion, relative to both contralateral, *treated* eyes and sham operated controls (raised under the same conditions).

Chapter 08

Effect of IOTr lesion on compensation to lens defocus in chicks

8.0 Introduction

When spectacle lenses are placed in front of the eyes of chicks, tree shrews, monkeys and cats (among others) (**Chapter 2**), the sign of the refractive error induced by the lens is quickly recognised by intra-retinal mechanisms (Zhu et al., 2005) and subsequent changes, first in choroidal thickness and then in scleral growth rate, act to neutralise the defocus by bringing the retina in line with the focal plane of an image (when the eye is in an accommodated state).

In ONS chicks, compensation to minus lens wear was normal, but recovery following removal of the minus lens was deficient (Wildsoet, 2003). Furthermore, chicks treated regularly throughout development with the RGC toxin, colchicine, which causes excessive ocular growth with normal visual experience (Fischer et al., 1999b), are able to compensate for defocus induced by plus lens wear, but not for minus lens wear (Choh et al., 2008). Having established that (with normal visual experience), unilateral disruption of an efferent projection to the retina from ION and EA induced a moderate, transient axial hyperopia in the eye contralateral to the lesioned hemisphere of the midbrain (**Chapter 6**), this experiment sought to test first the capability of chicks with unilateral disruption of centrifugal efferents following IOTr lesion to first compensate for either plus or minus lens induced defocus and, subsequently, their ability to recover following removal of the lens.

The terminology in lens manipulation studies can often be confusing. For example, by fitting a minus powered lens in front of an eye, one has *imposed* hyperopic defocus and by fitting a plus lens, one has *imposed* myopic defocus. Moreover, following compensation to a minus lens over a period of days and its subsequent removal one has *induced myopia*. Similarly, upon removal of a plus lens, one has *induced hyperopia*. For simplicity, the more intuitive terminology, that is 'plus or minus lens *wearing*' (i.e. treatment) or 'plus or minus lens *treated*' (the latter for description following lens removal) will be used here throughout.

In addition, the acronym 'DPT' is used to describe the number of days post treatment (i.e. initial lens fitting), and is continuous irrespective of lens removal.

8.1 Methods and experimental design

Following electrolytic lesion of the left IOTr on day 4/5 post hatch, chicks were fitted with lens holders (**Section 8.1.1**). Plus, minus or sham lenses were fitted after 24-48 hours recovery time. Lens powers (-15 D and +10 D) were selected based on previous experience as being just beyond the level to which chicks can emmetropise in 1 week (Chen et al., 2011a).

IR-keratometry (**Section 3.5**) and streak retinoscopy (**Section 3.6**) measurements were taken 3, 7, 10, 14, and 21 days post lens treatment (DPT) and A-scan ultrasonography (**Section 3.7**) measurements were made on days 7, 14 and 21 DPT.

Percentage lesion success was determined by pathway tracing (**Section 3.8**). Following stereological determination of lesion success (**Section 3.13**), subjects were split up into tertile groups (T1-T3) with T1 corresponding to those chicks with the lowest lesion success (and sham-operated controls) and T3 those chicks with the highest.

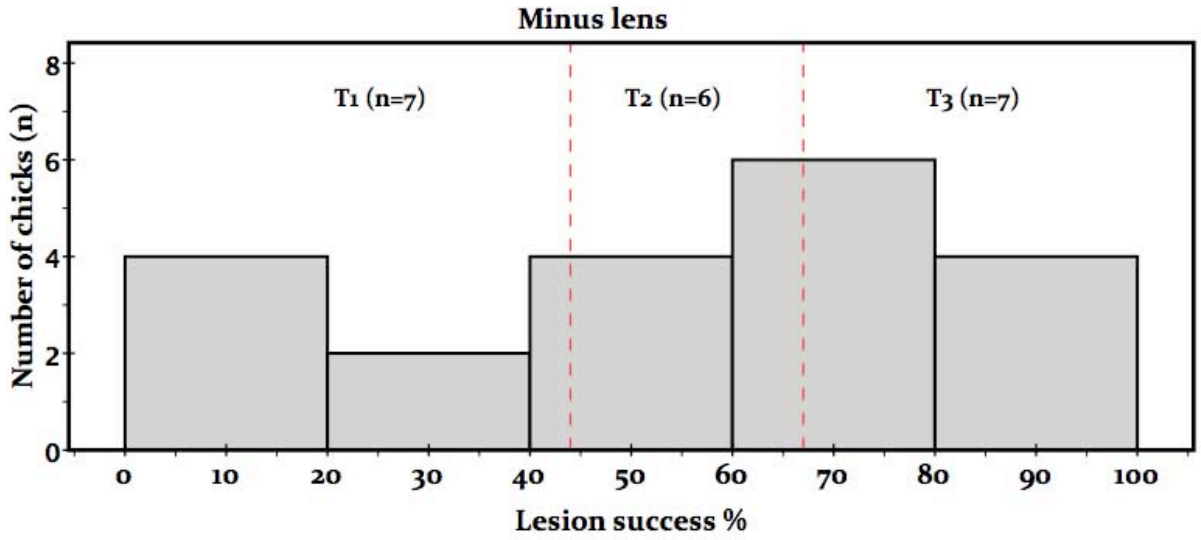

Fig. 8.1. Lesion success: Minus lens treatment. Histogram showing the distribution of percentage lesion success of individual subjects (n=20) into ranked tertile groups (T1-3). Dashed red lines show the division of subjects into tertile groups of lesion success. See **Fig. 8.3** for histological examples of IOTr lesions.

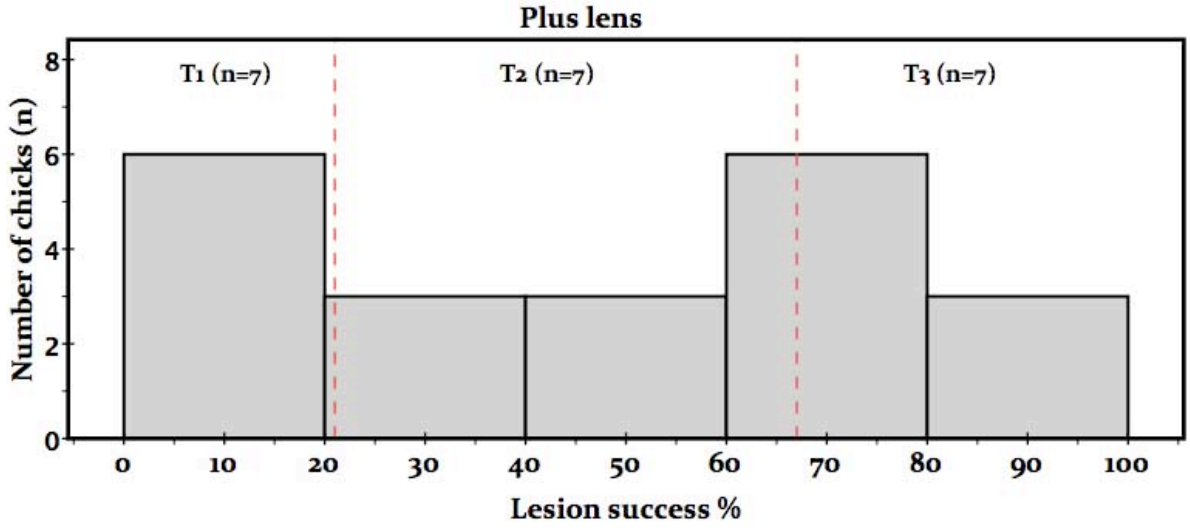

Fig. 8.2. Lesion success: Plus lens treatment. Histogram showing the distribution of percentage lesion success of individual subjects (n=21) into ranked tertile groups (T1-3). Dashed red lines show the division of subjects into tertile groups of lesion success. See **Fig. 8.3** for histological examples of IOTr lesions.

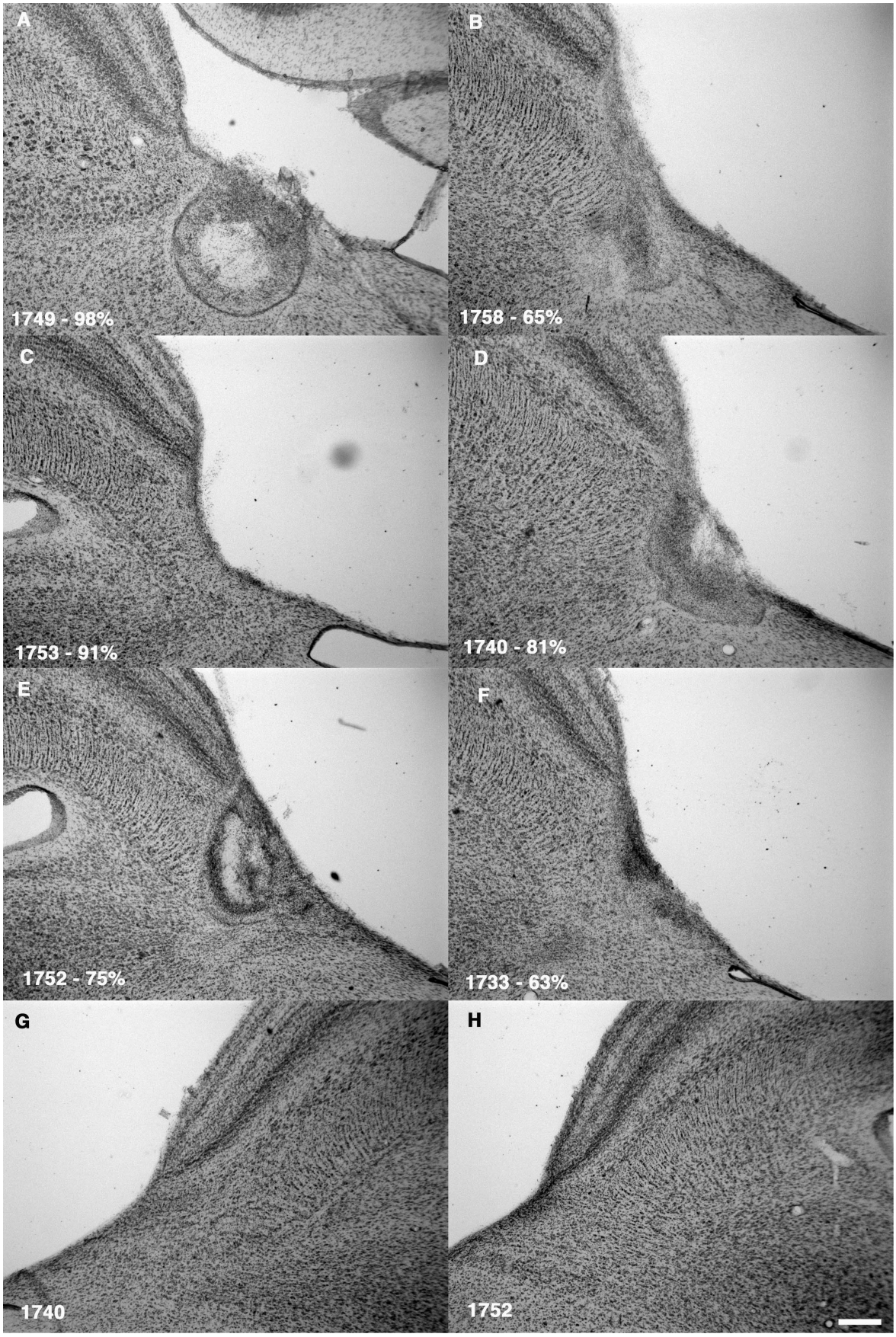

Fig. 8.3. (See overleaf for figure legend)

Fig. 8.3. Examples of IOTr lesions: Lens manipulation. The isthmo-optic tract (IOTr) courses anteriorly at the dorso-medial aspect of the optic tectum before merging with the optic tract. In these coronal sections of the chick midbrain, electrolytic lesions of the IOTr were made unilaterally, consistently on the left side of the midbrain (**A-F**). The right side of the midbrain was left untreated (**G-H**). In the bottom left hand corner of each example are details of the case from which the photomicrographs were taken, along with the corresponding lesion success percentage as determined by retrograde WGA labeling following intra-vitreal injections in the eye contralateral to the lesion prior to sacrifice. **Scale bar = 250 μm**

8.1.1 Lens holder fitting

Immediately following surgery to lesion the IOTr but while the bird was still under anaesthesia, a custom made lens holder was fitted over the eye contralateral to the lesion. Lens holders consisted of a 6-10 mm long section of 12 mm internal diameter rubber tubing glued to a 2-3 mm wide annulus made from rigid plastic. Pilot holes were made at regular intervals around the ridge so as to allow freedom in suture placement. Three notches cut into the base of the rubber tubing to allow for twice-daily removal and cleaning of the lens. In addition, the notches allowed air circulation. Nylon sutures (4-0, Ethilon, UK) were used to secure the lens holder in position, supplemented by cyanoacrylate adhesive (if required). Animals were allowed to recover from general anaesthesia in a temperature controlled recovery chamber, and once they had regained alertness, balance and the ability to perch (usually 60-90 minutes), they were returned to their pen. Chicks showed no ill effects from wearing the lens holder, eating and drinking as normal. Forty-eight hours post-surgery, a plus (+10 D, n=21), minus (-15 D, n=20) or plano lens (n=13) (**Table 8.1** and **8.3**) was fitted in the lens holder. Chicks were assigned a lens type at random. Lenses were removed (for less than a minute) twice daily to allow for cleaning. During this time, every effort was made to block visual experience. After 3 and 7 days lens wear, i.e. the midpoint and final day of lens

wear, measurements of refractive state and corneal radius of curvature (CR) were performed, requiring removal of the lens; however, both techniques were performed in the dark and usually took less than 15 minutes to complete. Lenses and lens holders were removed after 7 days of lens wear under general anaesthesia.

Fig. 8.4. Lens holder design. A Shaver Black chick during the lens-wearing phase of the experiment. Note the custom-made lens holder and disc used to protect the scalp incision site once the wound had been sutured closed. Notches at the base of the lens holder allowed for easy removal of the lens for twice-daily cleaning of the lenses and for measuring refraction and corneal curvature.

8.2 Results

8.2.1 Minus lens wearing phase

8.2.1.1 Refractive state changes

At both 3 and 7 DPT, minus lens treated eyes of each tertile group of chicks showed a significant myopic shift relative to control (fellow) eyes (**Fig. 8.4** and **Table 8.1**). However, the amount of anisometropia present after both 3 and 7 DPT was not significantly different across tertile groups of chicks (all $p>0.669$). The amount of anisometropia in minus lens wearing subjects was significantly greater in all tertile groups of chicks when compared with sham-operated, plano lens wearing chicks (all $p<0.014$).

8.2.1.2 Ocular component dimension changes

Changes in refractive state were mirrored by vitreous chamber elongation after 7DPT. Treated eyes had significantly longer VCD and AXL components when compared to fellow eyes and to plano lens wearing subjects (both p<0.001*)* (**Table 8.2**). However, no significant difference in any of the ocular components measured was found across tertile groups of chicks (all p>0.475) (**Fig. 8.4**).

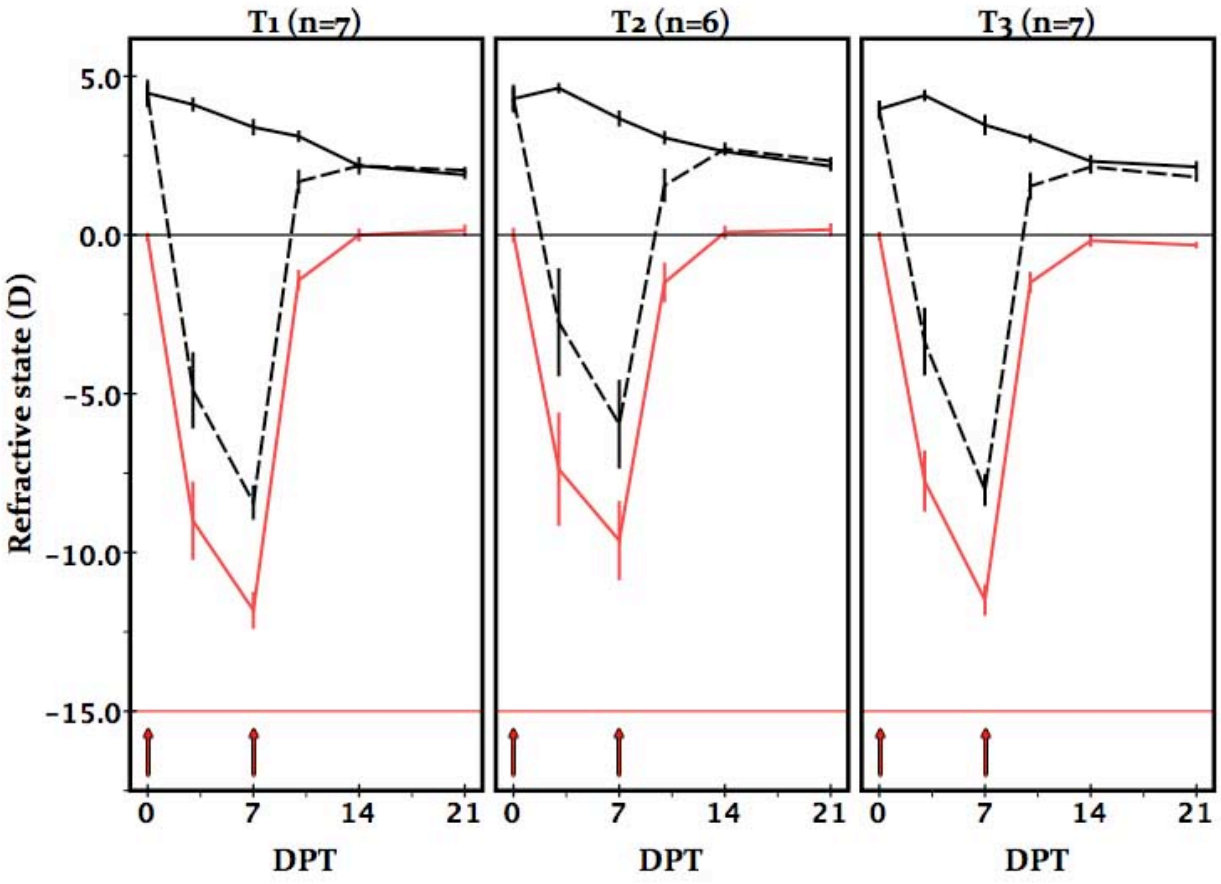

Fig. 8.5. Minus lens: Change in refractive state over time in tertile groups. Absolute refractive error (D) of the treated (**dashed black**) and fellow control (**solid black**) eyes of subjects over the 21-days following lens treatment (DPT). Anisometropia (T-C) (D) is represented by the **solid red trace**. Arrows denote lens wearing phase, i.e. day 0-7. The three main points to note from these data are firstly, that compensation to the power of the minus lens (-15 D), as represented by the horizontal red line was partial in all groups. Secondly, there was no difference in the amount of compensation to the lens across any of the tertile groups of lesion success. Thirdly, upon removal of the lens, recovery from the induced functional myopia was not affected by disruption of centrifugal efferents to the retina. *Error bars represent SE.*

8.2.1.3 Corneal radius of curvature changes

After 3 and 7 DPT, no significant difference in absolute CR was found between treated and control eyes (all $p>0.067$). Furthermore, there was no significant difference in the amount of CR asymmetry when compared between tertile groups: 3 DPT ($F_{2,10} = 2.115$, $p=0.171$) and 7 DPT ($F_{2,10} = 0.407$, $p=0.676$) (**Fig. 8.7**).

8.2.2 Minus lens recovery phase

8.2.2.1 Refractive state changes

By three days after minus lens removal, the refractive states of the treated eyes had largely recovered from the induced myopia. While the anisometropia of chicks in groups T1 and T3 groups remained significant (**Table 8.1**), the amount of anisometropia compared between groups of percentage lesion success was not significantly different ($F_{2,15} = 0.012$, $p= 0.988$). The amount of anisometropia in minus lens-treated chicks in all tertile groups vs. plano lens treated sham-operated control chicks remained significant ($t_{37} = 5.696$, $p<0.001$).

By 7 and 14 days after minus lens removal, the refractive states of treated eyes were no longer statistically different from fellow control eyes (**Table 8.1**). Furthermore, there was no

difference in the amount of anisometropia across tertile groups of lesion success (all p>0.101), or when compared to plano lens-treated sham-operated controls (**Table 8.1**).

8.2.2.2 Ocular component dimension changes

Seven days following minus lens removal, there was no significant difference in ocular component asymmetry across tertile groups of chicks (p>0.674), although at this stage significant within-animal (fellow control eye) differences were still apparent (**Table 8.2**). Moreover, no difference in ocular component asymmetry was evident between minus lens wearing and plano lens wearing sham-operated control birds (all p>0.343).

Fourteen days following minus lens removal, significant fellow eye differences remained (**Table 8.2**). However, only differences in ACD asymmetry across tertile groups of chicks were found to be significant ($F_{2,17}$ = 5.270, p=0.017) (**Table 8.2**). ACD asymmetry in T2 (t_{12} = -3.148, p=0.008) and T3 groups (t_{13} = 2.442, p=0.030) were statistically different from plano lens-treated, sham-operated controls. However, asymmetry in the remaining ocular component dimensions (i.e. LT, VCD and AXL) showed no such difference (all p>0.097) (**Table 8.2**).

8.2.2.3 Corneal radius of curvature changes

By 14 days following lens removal, the CR of treated eyes of the T3 group of chicks were significantly flatter than fellow control eye (t_4 = 3.260, p=0.031). No significant treated vs. control eye differences were significant in any groups at any other time points. Furthermore, there was no significant difference in the amount of CR asymmetry when compared across tertile groups of chicks at any time-point following lens removal (**Fig. 8.7**).

Fig. 8.6. Minus lens: Ocular component dimension asymmetry in tertile groups and sham operated plano lens wearing chicks (T-C) shown for 7, 14 and 21 DPT time-points. Consistent ACD elongation resulted from lens wear across tertile groups and sham operated plano wearing control chicks. In addition, vitreous chamber-dependent axial elongation was evident from minus lens wear after 7 DPT however there was no difference in the amount of elongation between tertile groups of lesion success. Upon removal of the minus lens after 7 DPT, the VCD and AXL asymmetry was reduced such that, again, no significant difference in asymmetry between tertile groups at either 14 or 21 DPT. *Error bars represent SE.*

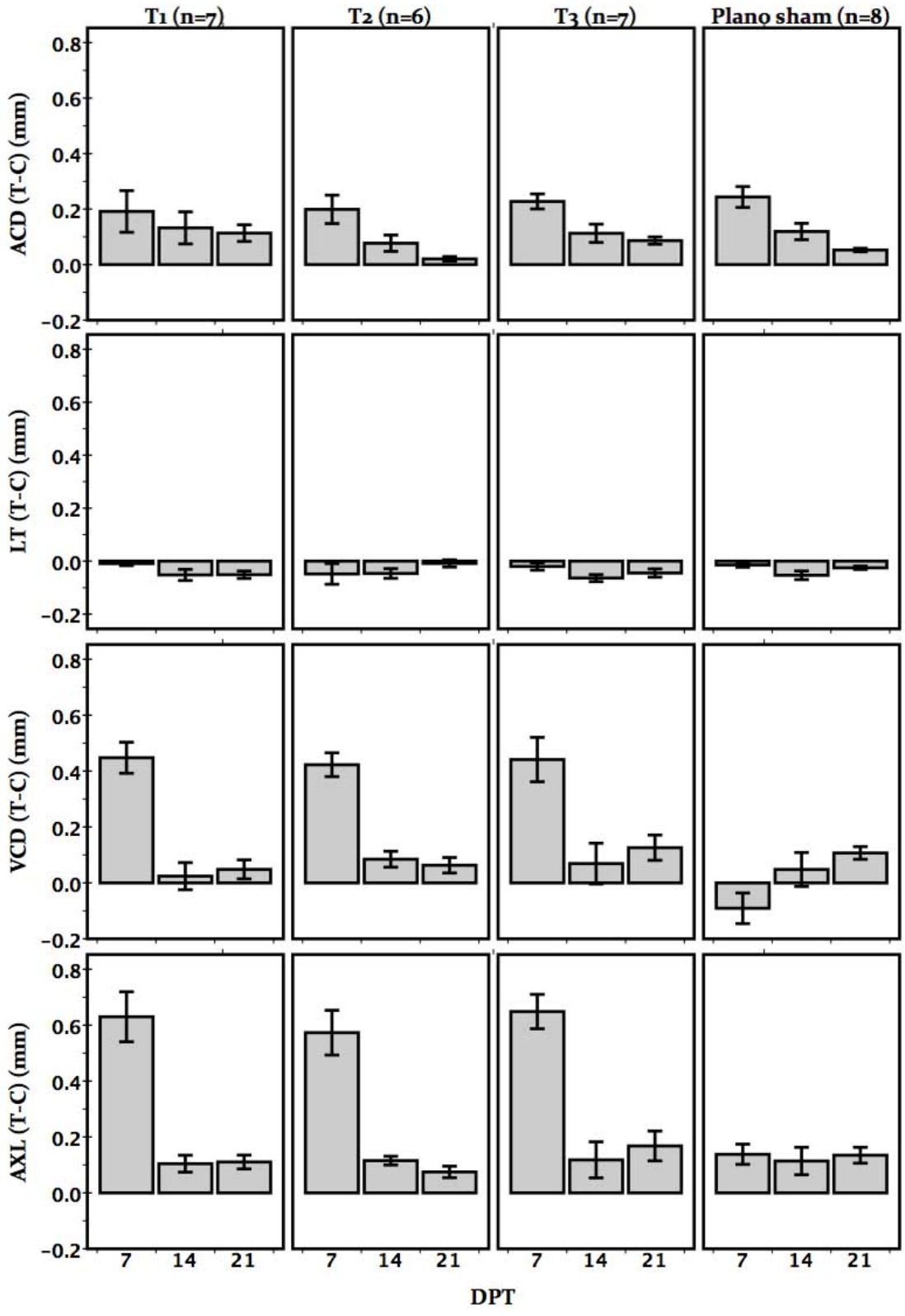

Fig. 8.6. (See previous page for figure legend)

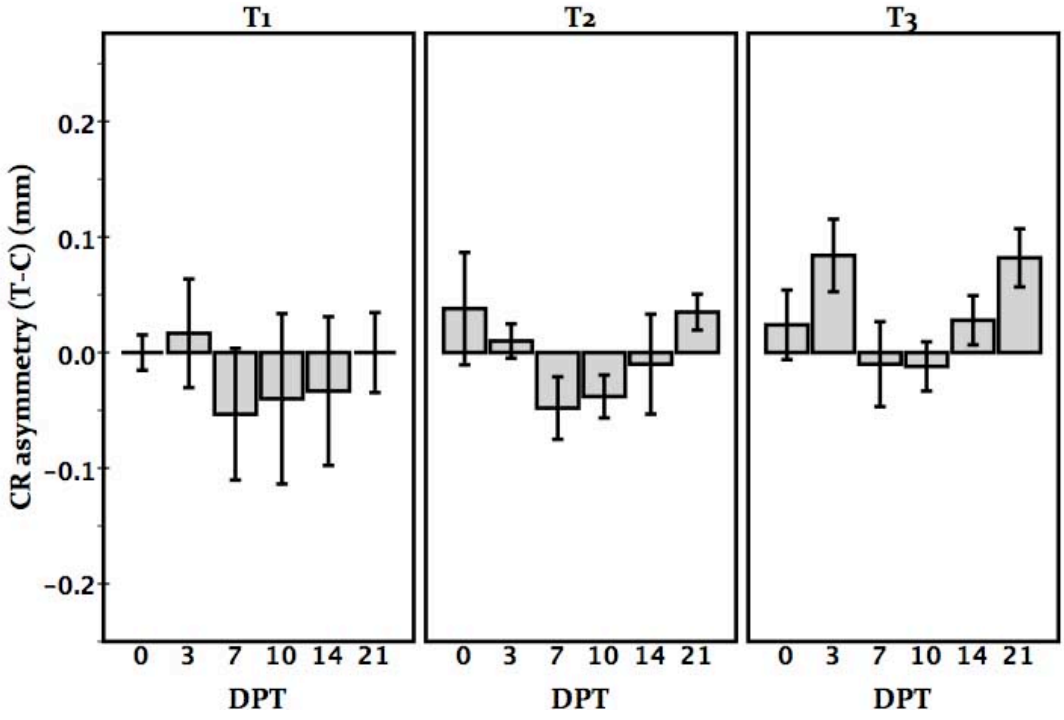

Fig. 8.7. Minus lens: Corneal radius of curvature (CR) asymmetry in tertile groups. No obvious or statistically significant lesion effect was apparent between tertile groups of lesion success**.** CR asymmetry (T-C) shown for minus lens-treated chicks at 0, 3, 7, 10, 14 and 21 DPT time-points. *Error bars represent SE.*

Table 8.1. Minus lens: Refractive state and anisometropia across tertile groups of lesion success. Absolute refractive state and anisometropia (T-C), (D±SD), for both minus lens wearing chick groups of differing ION/IOTr lesion success (%) and plano lens treated sham-operated controls.

	Refractive state (D)			
Pre-screen	**T1** (n=7)	**T2** (n=6)	**T3** (n=7)	**Plano sham**
Treated eye	4.39±0.98	4.29±0.93	3.93±0.79	4.22±0.87
Control eye	4.46±1.14	4.29±1.09	3.96±0.68	4.38±0.58
Anisometropia (T-C)	-0.71±0.37	0.00±0.57	-0.04±0.37	-0.17±0.48
3 days post- initial lens fitting (3 DPT)				
Treated eye	-4.89±3.18	-2.75±4.18	-3.36±2.83	3.53±0.21
Control eye	4.11±0.59	4.63±0.41	4.39±0.48	4.10±0.33
Anisometropia (T-C)	-9.00±3.27***	-7.38±4.38**	-7.75±2.55***	-0.60±0.33***
7 days post- initial lens fitting (7 DPT)				
Treated eye	-8.43±1.43	-5.96±3.43	-8.04±1.33	1.82±1.32
Control eye	3.39±0.69	3.67±0.63	3.46±0.86	2.90±0.62
Anisometropia (T-C)	-11.82±1.55***	-9.63±3.06***	-11.50±1.30***	-1.10±1.14
End of lens wearing phase				
3 days post- lens removal (10 DPT)				
Treated eye	1.68±1.01	1.56±1.07	1.54±1.14	3.02±0.75
Control eye	3.11±0.50	3.06±0.43	3.04±0.37	2.85±0.62
Anisometropia (T-C)	-1.43±0.87**	-1.50±1.26	-1.50±0.89***	0.17±0.81
7 days post- lens removal (14 DPT)				
Treated eye	2.18±0.73	2.71±0.51	2.14±0.57	2.10±0.48
Control eye	2.18±0.28	2.63±0.21	2.32±0.53	2.05±0.74
Anisometropia (T-C)	0.00±0.54	0.08±0.52	-0.18±0.51	0.05±0.32
14 days post- lens removal (21 DPT)				
Treated eye	2.04±0.30	2.33±0.30	1.82±0.40	1.80±0.48
Control eye	1.89±0.38	2.17±0.41	2.14±0.50	2.10±0.33
Anisometropia (T-C)	0.14±0.50	0.17±0.49	-0.32±0.28*	-0.32±0.17

Statistical test results relate to within group analyses (i.e. Is treated eye different to control eye). Between group comparisons are shown in **Fig. 8.4**. *p<0.05, **p<0.01, ***p<0.005 (paired t-tests).

Table 8.2. Minus lens: Ocular component dimension asymmetry across tertile groups of lesion success. The mean inter-ocular differences in ocular component dimensions (T-C) (±SD) for both minus lens wearing chick groups of differing ION/IOTr lesion success (%) and plano lens treated sham-operated controls.

7 days post- initial lens fitting (7 DPT)	Ocular component dimension asymmetry (T-C) (mm)			
	T1 (n=7)	**T2** (n=6)	**T3** (n=7)	**Plano sham**
Anterior chamber depth	0.192±0.198*	0.199±0.125*	0.228±0.071***	0.244±0.106***
Lens thickness	-0.009±0.020	-0.048±0.096	-0.020±0.037	-0.015±0.024
Vitreous chamber depth	0.448±0.147***	0.423±0.104***	0.441±0.210***	-0.091±0.155
Axial length	0.630±0.236***	0.573±0.196***	0.649±0.163***	0.138±0.102**
End of lens wearing phase				
7 days post- lens removal (14 DPT)				
Anterior chamber depth	0.132±0.153	0.077±0.072*	0.113±0.087*	0.119±0.083**
Lens thickness	-0.052±0.056*	-0.047±0.045	-0.064±0.035***	-0.053±0.046*
Vitreous chamber depth	0.024±0.128	0.085±0.070*	0.069±0.193	0.048±0.172
Axial length	0.104±0.080*	0.116±0.038***	0.118±0.170	0.114±0.139
14 days post- lens removal (21 DPT)				
Anterior chamber depth	0.114±0.079**	0.021±0.021	0.087±0.035***	0.053±0.018***
Lens thickness	-0.051±0.037*	-0.009±0.033	-0.045±0.041*	-0.025±0.018**
Vitreous chamber depth	0.048±0.090	0.063±0.068	0.126±0.120*	0.107±0.064***
Axial length	0.111±0.065***	0.075±0.050*	0.168±0.141*	0.135±0.080***

Statistical test results relate to within group analyses (i.e. Is treated eye different to control eye). Between group comparisons are shown in **Fig. 8.5**. *p<0.05, **p<0.01, ***p<0.005 (paired t-tests).

8.2.3 Plus lens wearing phase

8.2.3.1 Refractive state changes

At both time-points (3 and 7 DPT) during the plus lens treatment phase, treated eyes of chicks in each tertile group showed a significant hyperopic shift relative to control eyes (**Fig. 8.8 and Table 8.3**). However there was no significant difference in the amount of anisometropia between tertile groups of chicks at the 3 DPT ($F_{2,18}$ = 0.649, p=0.534) or 7 DPT ($F_{2,18}$ = 1.607, p=0.228) time points. Furthermore, the amount of anisometropia in plus lens wearing chicks was significantly greater in all tertile groups of chicks than that observed in sham-operated, plano lens wearing chicks both 3 DPT (t_{43} = 24.175, p<0.001) and 7 DPT (t_{40} = 13.275, p<0.001) (**Table 8.3**).

8.2.3.2 Ocular component dimension changes

At 7 DPT, the VCD and AXL of treated eyes were significantly shorter than fellow control eyes in T2 and T3 groups of chicks but not in T1 (**Table 8.4).** Similarly, the VCD and AXL components of plus lens treated eyes were significantly shorter than plano lens wearing, sham-operated control eyes in T2 and T3 groups (all p<0.045) of chicks but not in T1 (p>0.114) (**Fig. 8.9**). No significant difference in VCD ($F_{2,18}$ = 0.666, p=0.526) or AXL asymmetry ($F_{2,18}$ = 0.643, p=0.537) was found across the tertile groups of chicks.

8.2.3.3 Corneal radius of curvature changes

At 3 and 7 DPT, no significant difference in absolute CR was found between treated and control eyes (all p>0.360). Furthermore, there was no significant difference in the amount of CR asymmetry when compared across tertile groups of chicks either prior to surgery, at 3 DPT ($F_{2,6}$ = 0.135, p=0.876) or at 7 DPT ($F_{2,7}$ = 0.316, p=0.739) (**Fig. 8.10**).

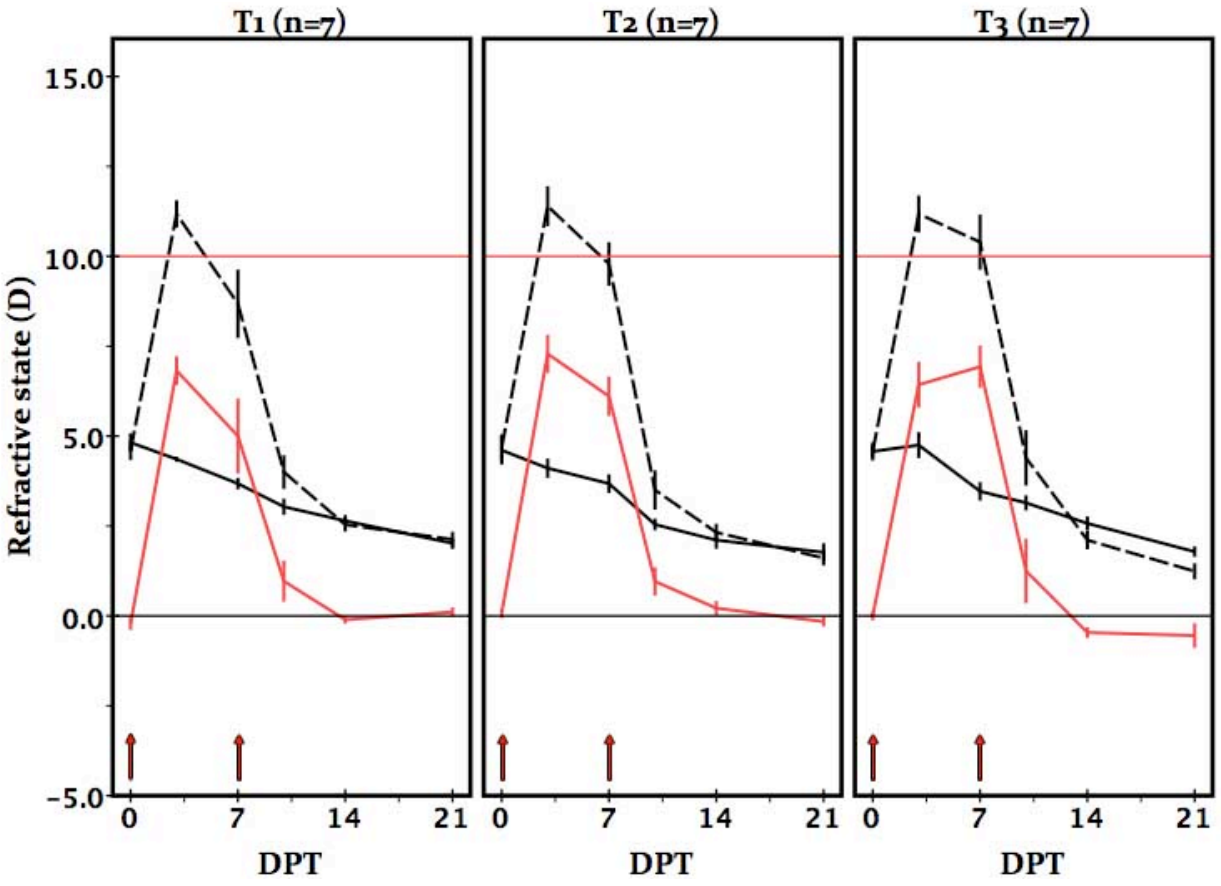

Fig. 8.8. Plus lens: Change in refractive state over time in tertile groups. Absolute refractive state of the treated (dashed black), untreated control (solid black) eyes of subjects over the 21-day experiment duration. Anisometropia (T-C) is represented by the solid red trace. Arrows denote lens wearing phase. As with the results of minus lens treatment, the three main points to note from these data are firstly, that compensation to the power of the plus lens (+10 D), as represented by the horizontal red line was partial in all groups. Secondly, there was no difference in the amount of compensation to the lens across any of the tertile groups of lesion success. Thirdly, in contrast to the recovery from minus lens wear, recovery from plus lens wear resulted in an overshoot of the induced functional hyperopia to relative significant myopia. *Error bars represent SE.*

8.2.4 Plus lens recovery phase

8.2.4.1 Refractive state changes

Three days following plus lens removal, treated eyes had recovered from the induced hyperopia, and no significant anisometropia remained (**Table 8.3**). Similarly, there was no

significant difference in the amount of anisometropia in plus lens-treated chicks across tertile groups ($F_{2,17}$ = 0.062, p=0.940) or when tertile groups were compared with plano lens wearing, sham-operated control chicks (all p>0.101).

Seven days following lens removal, anisometropia in the T3 group of chicks showed a numerically small but statistically significant overshoot in recovery when compared to both fellow untreated eyes (-0.46 D ± 0.39, p=<0.050) (**Fig. 8.8**) and plano lens treated, sham-operated controls (-0.60 D ± 0.19, *p<0.01*). The anisometropia in T3 was significantly different when compared to the T2 group of chicks (-0.68 D ± 0.22, *p<0.020*) but not when compared to T1 (-0.36 D ± 0.22, p=0.373).

Fourteen days following lens removal, this apparent overshoot in refractive state persisted in the T3 group (-0.65 D ± 1.07), however it was no longer statistically significant when compared with (**a**) fellow control eyes (-0.55 D ± 0.91, *p=0.162*), (**b**) plano lens treated, sham-operated controls (-0.35 D ± 0.34, *p=0.320*) or (**c**) other tertile groups of chicks ($F_{2,18}$ = 2.119, *p=0.149*) (**Fig. 8.8**).

8.2.4.2 Ocular component dimension changes

Seven days following plus lens removal, significant within-animal (fellow eye) differences in ACD (T1 and T3) , VCD (T3) and AXL (T3) were apparent (**Table 8.4**). However, there was no difference in ocular component asymmetry across tertile groups (VCD; $F_{2,18}$ = 2.092, p=0.152; AXL; $F_{2,18}$ = 1.721, p=0.207). Both ACD ($t_{8.143}$ = -3.146, p=0.013) and LT asymmetry (t_{13} = 2.969, p=0.011) in the T3 group of chicks were significantly different from plano lens treated, sham-operated controls (**Fig. 8.9**). However, the differences involved were, again, very small.

Comparison of treated eyes with fellow control eyes 7 days following lens removal showed a significantly longer VCD (0.134 mm ± 0.089, p<0.01) and AXL (0.159 mm ± 0.101, p<0.01) in

the treated eyes of T3 group only. Fourteen days following lens removal, the apparent overshoot in correction from the initial lens effect persisted in the T3 group of chicks (VCD; 0.108 mm ± 0.060, AXL; 0.141 mm ± 0.066, both $p<0.005$) (**Table 8.4**). However, no significant differences in VCD or AXL asymmetry were found across tertile groups (VCD; $F_{2,17} = 1.997$, $p=0.166$; AXL; $F_{2,17} = 2.751$, $p=0.092$) (**Fig. 8.9**).

8.2.4.3 Corneal radius of curvature changes

No significant treated vs. control eye differences in CR were found in any groups at any time points. Furthermore, there was no significant difference in the amount of CR asymmetry compared across tertile groups at any time point following lens removal (all $p>0.145$) (**Fig. 8.10**).

Fig. 8.9. Plus lens: Ocular component dimension asymmetry in tertile groups and sham operated plano lens wearing chicks (T-C) shown for 7, 14 and 21 DPT time-points. A lower amount of ACD elongation was evident in plus lens treated chicks than was observed in chicks treated with minus lenses. Vitreous chamber-dependent axial shortening was evident from plus lens wear after 7 DPT however there was no significant difference in the amount of VCD compensation between tertile groups of lesion success. Upon removal of the plus lens after 7 DPT, the VCD and AXL asymmetry was reduced such that, again, no significant difference in asymmetry between tertile groups at either 14 or 21 DPT, however there was a trend towards an overcorrection in the T3 group of chicks. *Error bars represent SE.*

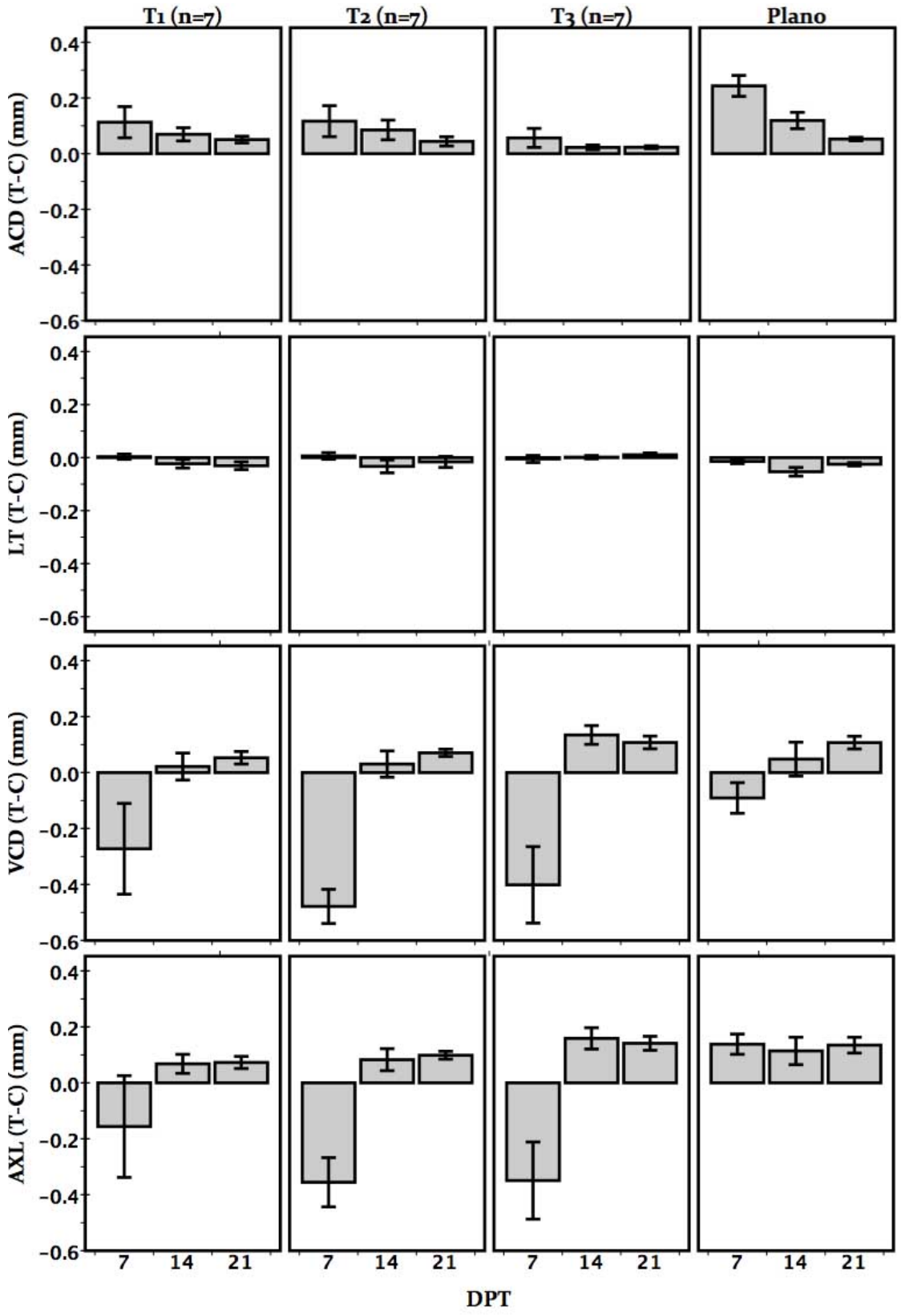

Fig. 8.9. (See overleaf for figure legend)

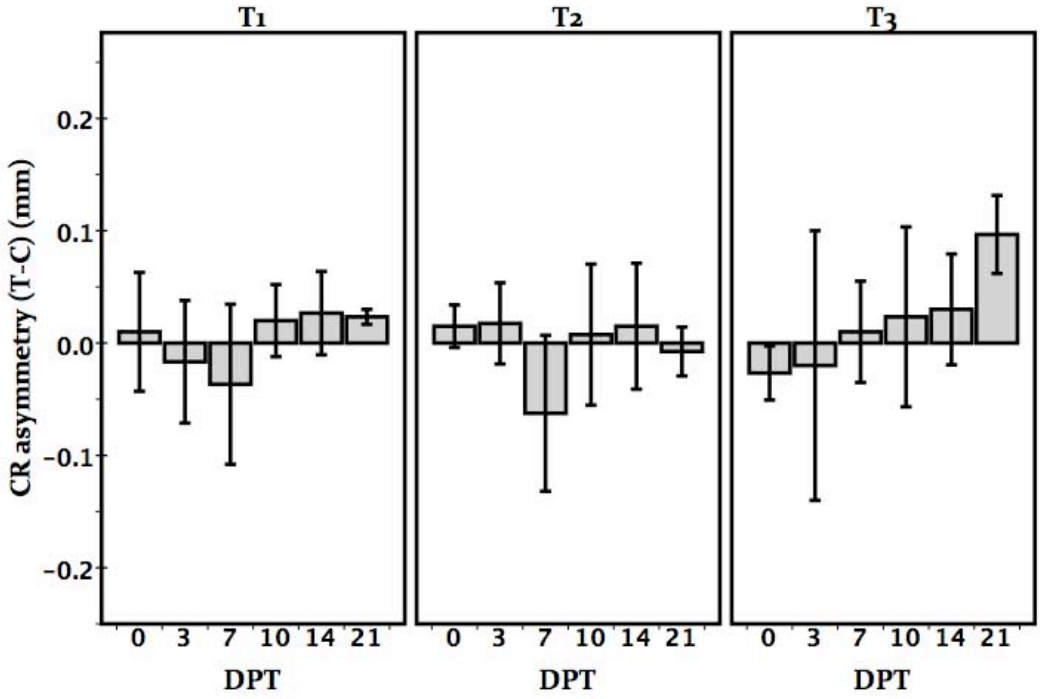

Fig. 8.10. Plus lens: Corneal radius of curvature (CR) asymmetry in tertile groups. By 21 DPT, the CR asymmetry (T-C) of chicks in the T3 group of lesion success showed significant within-subject CR asymmetry with the treated eyes exhibiting relatively flatter corneas. Mean CR shown for plus lens-treated chicks at 0, 3, 7, 10, 14 and 21 DPT time-points. *Error bars represent SE.*

Table 8.3. Refractive state and anisometropia (T-C), (±SD) in groups of differing ION/IOTr lesion success (%) for plus lens treated chicks and plano lens treated sham-operated controls.

	Refractive state (D)			
Pre-screen	**T1** (n=7)	**T2** (n=7)	**T3** (n=7)	**Plano sham**
Treated eye	4.61±0.73	4.68±0.99	4.57±0.51	4.22±0.87
Control eye	4.82±0.69	4.61±1.06	4.57±0.67	4.38±0.58
Anisometropia (T-C)	-0.21±0.47	0.07±0.35	0.00±0.32	-0.17±0.48
3 days post- initial lens fitting (3 DPT)				
Treated eye	11.18±1.01	11.39±1.47	11.18±1.36	3.53±0.21
Control eye	4.36±0.20	4.11±0.72	4.75±0.96	4.10±0.33
Anisometropia (T-C)	6.82±1.06***	7.29±1.41***	6.43±1.69***	-0.60±0.33***
7 days post- initial lens fitting (7 DPT)				
Treated eye	8.68±2.52	9.79±1.60	10.39±2.04	1.82±1.32
Control eye	3.68±0.43	3.68±0.69	3.46±0.68	2.90±0.62
Anisometropia (T-C)	5.00±2.77***	6.11±1.46***	6.93±1.56***	-1.10±1.14
End of lens wearing phase				
3 days post- lens removal (10 DPT)				
Treated eye	4.00±1.24	3.50±1.34	4.39±2.04	3.02±0.75
Control eye	3.04±0.60	2.54±0.40	3.14±0.56	2.85±0.62
Anisometropia (T-C)	0.96±1.51	0.96±1.51	1.25±2.38	0.17±0.81
7 days post- lens removal (14 DPT)				
Treated eye	2.54±0.51	2.32±0.64	2.11±0.67	2.10±0.48
Control eye	2.64±0.43	2.11±0.64	2.57±0.51	2.05±0.74
Anisometropia (T-C)	-0.11±0.28	0.21±0.53	-0.46±0.39*	0.05±0.32
14 days post- lens removal (21 DPT)				
Treated eye	2.13±0.56	1.61±0.55	1.24±0.60	1.80±0.48
Control eye	2.02±0.42	1.77±0.67	1.79±0.39	2.10±0.33
Anisometropia (T-C)	0.11±0.35	-0.16±0.36	-0.55±0.91	-0.32±0.17

Statistical test results relate to within group analyses (i.e. Is treated eye different to control eye). Between group comparisons are shown in Fig. 8.8. *p<0.05, **p<0.01, ***p<0.005 (paired t-tests).

Table 8.4. Ocular component dimensions asymmetry (T-C) (±SD) in groups of differing ION/IOTr lesion success (%) for plus lens treated chicks and plano lens treated sham-operated controls.

7 days post-initial lens fitting (7 DPT)	Ocular component asymmetry (T-C) (mm)			
	T1 (n=7)	**T2** (n=7)	**T3** (n=7)	**Plano** (n=8)
Anterior chamber depth	0.113±0.148	0.117±0.147	0.057±0.090	0.244±0.106***
Lens thickness	0.003±0.026	0.006±0.033	-0.005±0.035	-0.015±0.024
Vitreous chamber depth	-0.272±0.429	-0.478±0.162***	-0.401±0.362*	-0.091±0.155
Axial length	-0.156±0.481	-0.355±0.233**	-0.349±0.365*	0.138±0.102**
End of lens wearing phase				
7 days post- lens removal				
Anterior chamber depth	0.070±0.063*	0.085±0.094	0.023±0.022*	0.119±0.083**
Lens thickness	-0.023±0.042	-0.033±0.064	0.002±0.017	-0.053±0.046*
Vitreous chamber depth	0.022±0.128	0.030±0.124	0.134±0.089**	0.048±0.172
Axial length	0.068±0.090	0.083±0.104	0.159±0.101**	0.114±0.139
14 days post- lens removal				
Anterior chamber depth	0.051±0.029**	0.044±0.044*	0.023±0.014***	0.053±0.018***
Lens thickness	-0.031±0.036	-0.016±0.055	0.011±0.019	-0.025±0.018**
Vitreous chamber depth	0.053±0.055	0.071±0.034***	0.108±0.060***	0.107±0.064***
Axial length	0.073±0.053*	0.099±0.037***	0.141±0.066***	0.135±0.080***

Statistical test results relate to within group analyses (i.e. Is treated eye different to control eye). Between group comparisons are shown in Fig. 8.9. *p<0.05, **p<0.01, ***p<0.005 (paired t-tests).

8.3 Discussion

8.3.1 Lens wear effect

Compensation to lens imposed defocus is primarily achieved through an increase (minus lens wear) or decrease (plus lens wear) in VCD. For example, the mean VCD of minus lens treated chicks following 7 days of lens wear was *longer* (0.287 mm ± 0.286) than fellow untreated eyes. Conversely, the treated eyes of chicks that had worn plus lenses for 7 days had a mean VCD that were *shorter* (-0.303 mm ± 0.320) than fellow untreated eyes. Although the lens power of the minus and plus lenses used were -15 D and +10 D, respectively, for optical reasons the effective power of the lenses during treatment was less.

When the length of the silicone sleeve within which the lenses were fitted is taken into account (8-10 mm) and applied to the equation below (Keirl and Christie, 2007):

$Pe = P/(1 + d \times P)$

(Pe, effective lens power; P, actual lens power; d, tube holder distance)

the effective lens power at the eye was:

Minus lens (-15 D): -13.04 D to -13.39 D

Plus lens (+10 D): +10.87 D to +11.11 D

Even taking this adjusted power into account, neither the minus lens or plus lens treated chicks had fully compensated for the imposed defocus. The mean refractive state of minus lens treated eyes compared to fellow control eyes after 7 days lens wear was -11.05 D ± 2.17, showing 85% compensation to the -15 D lens. Similarly, the refractive state of plus lens treated eyes compared to fellow eye controls at the same time point was 6.01 D ± 2.08, showing a 56% compensation to the +10 D lens. Interestingly, in the T1 and T2 groups, the percentage compensation to plus lens wear was greater at 3 DPT (65%) than at 7 DPT (51%). Conversely, the compensation of the T3 group was progressive, from 59% at 3 DPT to 64% at 7 DPT.

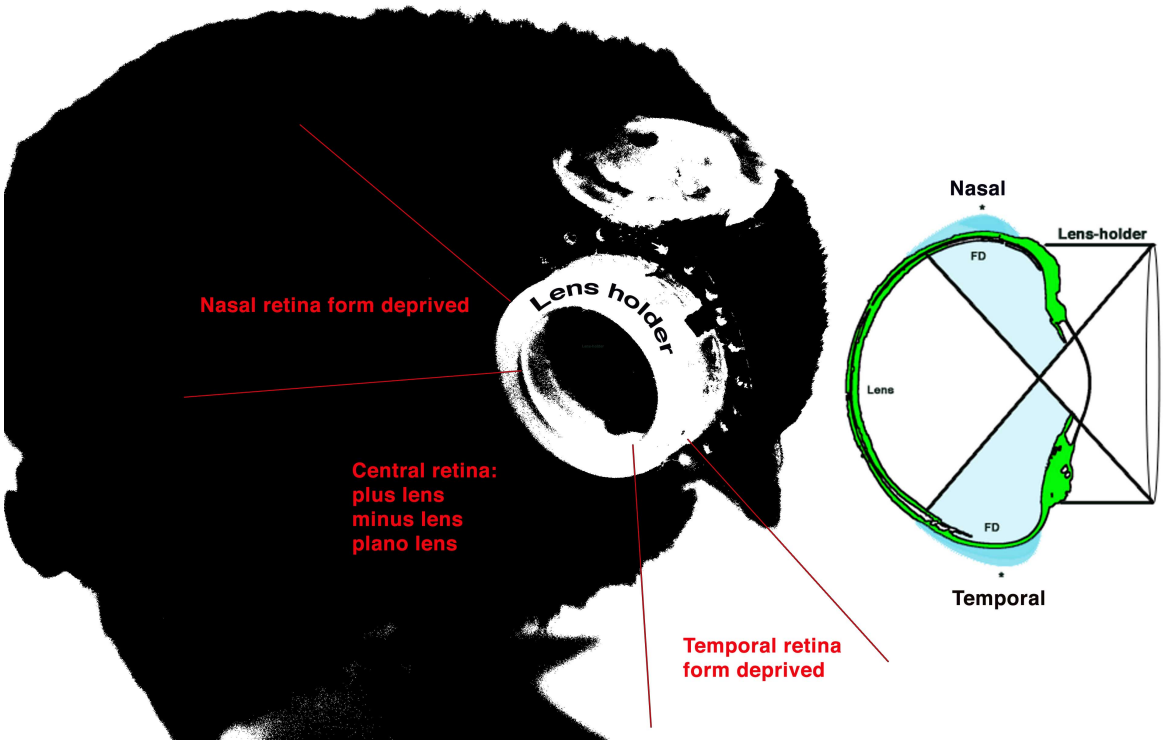

Fig. 8.11. Lens holder effect on visual fields. Form deprivation (FD) in the peripheral retina, from lens holder wear, could cause equatorial expansion (**asterisks**) and the eye to develop a more oblate shape (**blue shaded regions**). On the left image, the position of the lens holder in front of the treated eye, i.e. the eye contralateral to the lesion of the IOTr is shown. In addition note the position of the heat-molded plastic cap used to cover the scalp incision. The inset on the right shows in schematic form how the deprivation of the peripheral retina may have induced localised axial elongation and caused an abnormal ocular shape to result. Such an effect may have acted to mask any potential IOTr lesion effect.

Plano lens treated, sham-operated control eyes developed significantly deeper anterior chambers and elongated axial lengths when compared to their fellow untreated eyes (**Table 8.2**), which resulted in them becoming slightly myopic in comparison (7DPT; -1.10 D ± 1.14) (**Table 8.1**). Compared to control eyes of chicks in the first lesion study (**Chapter 6**), plano lens wearing eyes exhibited significantly longer ACD and shorter VCD (**Fig. 8.12**). No difference in ocular component dimensions existed between age matched controls (**Chapter 6**) and the fellow untreated eyes of plano-lens wearing chicks. These effects are in contrast

to the findings of studies that used a similar lens holder arrangement and reported a shorter ACD in plano lens wearing chicks (Chen et al., 2011a). Both complete and hemiretinal form deprivation have been shown to cause anterior chamber elongation (Gottlieb et al., 1987). Thus, one explanation for the above effect (and, indeed, for plus and minus lens treated chicks) is that partial (i.e. peripheral) form deprivation, which resulted from the silicone sleeve of the lens holder extending into the peripheral visual field of the treated eyes (**Fig. 8.11**), may have caused ACD elongation. In addition, the observed significant shortening of the VCD of plano lens treated eyes compared to age-matched controls (**Fig. 8.12**) could equally be explained as the result of compensation to myopic defocus imposed by the deeper anterior chamber and steeper corneal curvature. Having said that, in this instance, an increase in ACD was not reflected by a significant steepening of corneal curvature in plano lens treated eyes relative to fellow, or age-matched control eyes ($F_{2,34} = 0.487$, $p=0.619$). Alternatively, since eye growth is know to be controlled by local visual experience (Wallman et al., 1987), local peripheral form deprivation resulting from lens holder wear may have caused equatorial expansion (**Fig. 8.11**), causing the eye to develop a more oblate shape and relatively shorter VCD as observed in plano lens treated chicks (**Fig. 8.12**).

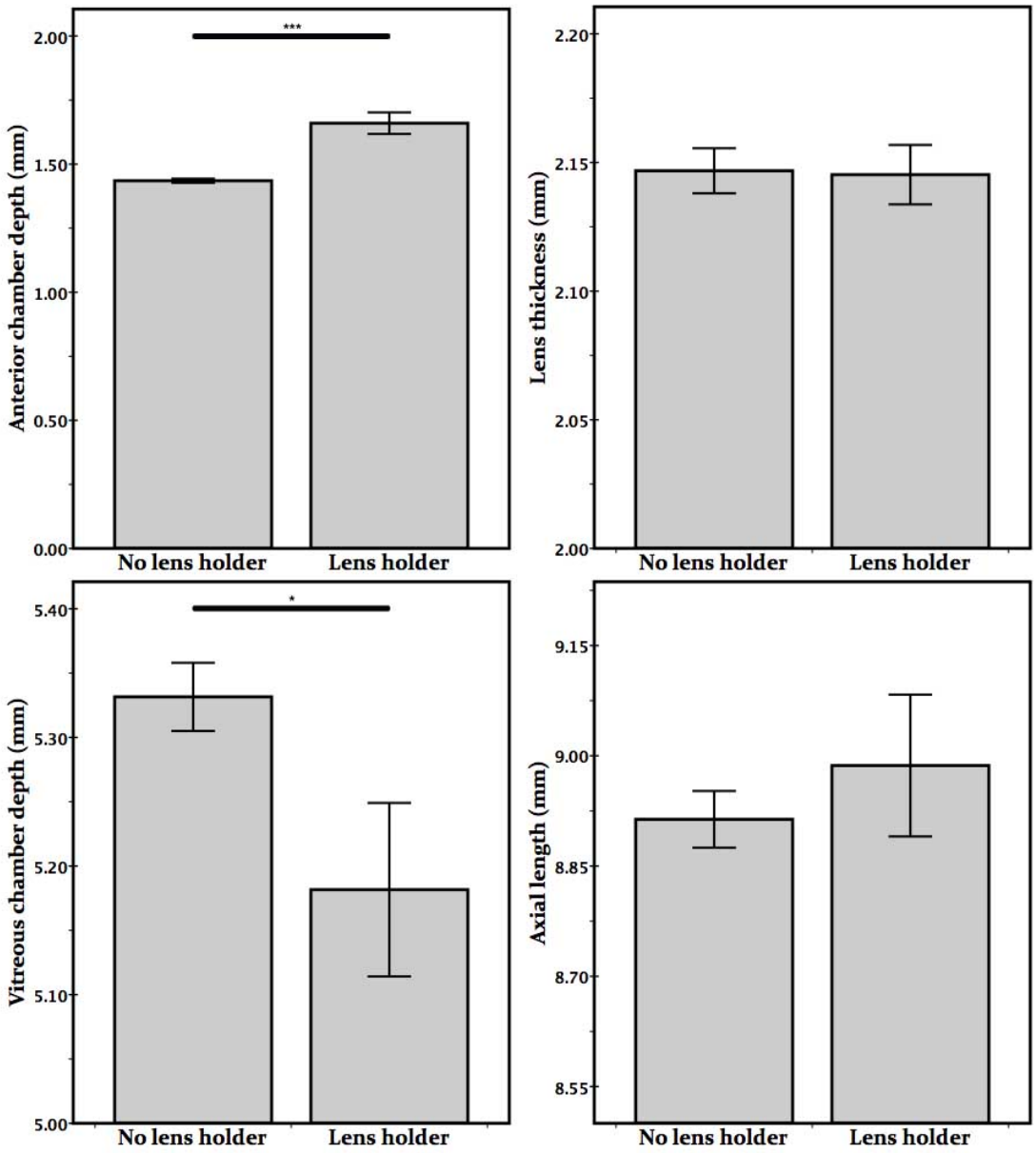

Fig. 8.12. Lens wear effect on ocular component dimensions. Absolute ocular component dimensions for plano lens treated eyes and age-matched control eyes (**Chapter 6**) at 7 DPT. Lens holder wear induced highly significant anterior chamber depth elongation combined with significant vitreous chamber shortening. Error bars represent SE. *p<0.05, **p<0.01, ***p<0.005 (independent t-tests).

8.3.2 IOTr lesion induced hyperopia in plano lens wearing chicks

The relative hyperopia that developed in the Q4 group of chicks in **Chapter 6** was not replicated in IOTr lesioned plano lens wearing chicks. Having said that, although plano

lens wearing eyes were *less* hyperopic than fellow control eyes during the lens wearing phase (**Table 8.3**), the treated eyes of chicks with higher lesion success were *more* hyperopic in comparison to those with lower percent lesion success by 7 DPT (**Fig. 8.13**). It should be noted, however, that the percentage lesion success in the plano lens wearing group was lower than expected, resulting in only 3 chicks with a >70% lesion. Nevertheless, a significant negative correlation existed between percentage lesion success and AXL asymmetry after 7 DPT suggesting that, in keeping with the findings of **Chapter 6**, those chicks with a greater lesion success percentage had relatively shorter treated eyes relative to fellow eyes (r= -0.610, p=0.046). There was also a trend towards a negative relationship between percentage lesion success and ACD asymmetry, suggesting that those chicks with a greater lesion success percentage showed a lesser degree of ACD asymmetry relative to fellow eyes r= -0.554, p=0.077).

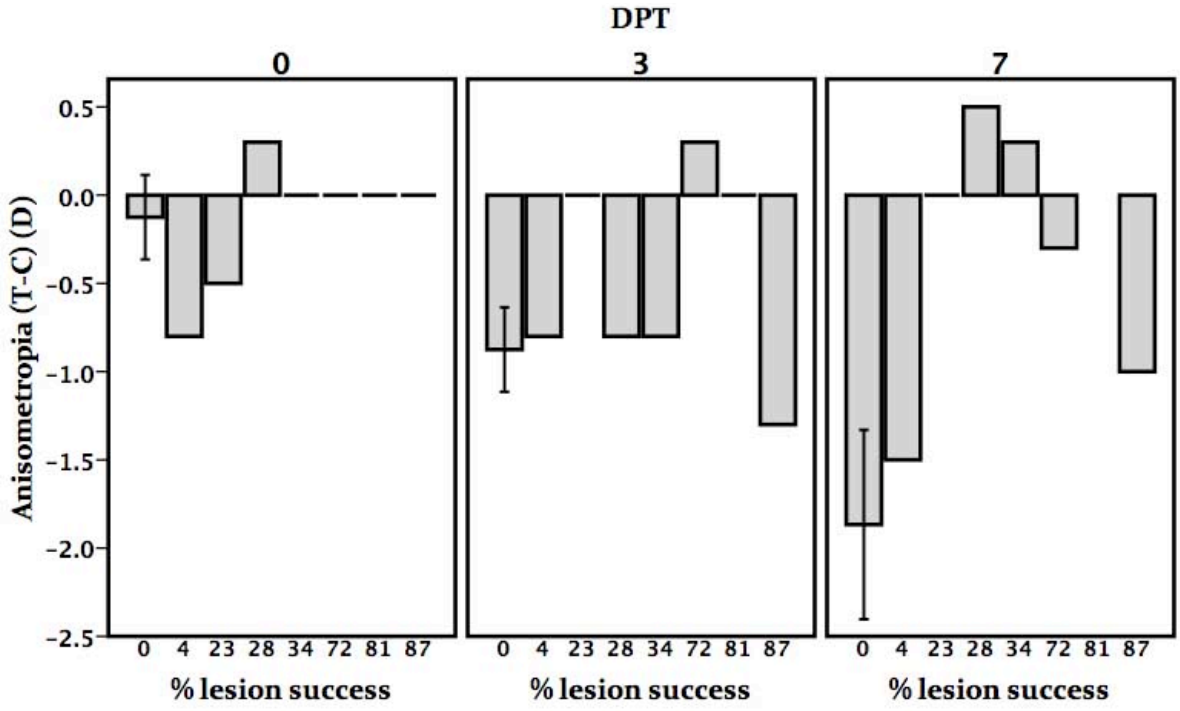

Fig. 8.13. Plano lens: Anisometropia vs. lesion success. Anisometropia (T-C) as a function of ION/IOTr lesion success in plano lens-wearing chicks at 0, 3 and 7 DPT time points. *Error bars represent SE.*

8.3.3 Centrifugal efferent disruption and lens compensation

These results indicate that disruption of centrifugal efferents to the retina does not affect the ability of either the treated or control eye to compensate to myopic or hyperopic defocus. Moreover, following removal of the lens treatment, the ability of eyes to recover from lens induced hyperopia or myopia, respectively, was largely unaffected.

Wildsoet (2003) showed that refractive compensation to minus lens treatment was not affected following ONS. Chicks develop a baseline hyperopic refractive state following ONS treatment. Although the absolute refractive state of ONS chicks following compensation to minus lens wear was found to be more myopic relative to chicks with intact optic nerves, the overall refractive compensation to the lens from baseline values was unchanged. Given that disruption of centrifugal efferents also induces an initial hyperopic shift in refractive state, one might have expected similar responses to occur when combining centrifugal disruption and hyperopic defocus. However, my results showed no difference in compensation to minus lens wear in IOTr lesioned birds.

Conversely, under the same logic, one could predict that compensation to plus lens wear would result in an even more hyperopic absolute refractive state in ONS or IOTr lesioned chicks. Although the T3 group of chicks did show the greatest amount of compensation to myopic defocus, a comparison across tertile groups showed there to be no statistical difference in the amount of anisometropia in plus lens-treated chicks. Nevertheless, across tertile groups of plus lens wearing chicks, a small but statistically significant overshoot in the recovery phase was apparent, which led to treated eyes becoming myopic relative to fellow control eyes in the T3 group of chicks (**Fig. 8.14**). This overshoot in refractive state was mirrored by VCD asymmetry, i.e. the mean treated vs. control eye difference in VCD of chicks in the T3 group was greater than that of the T1 and T2 groups (with the mean treated eye VCD longer than that of the control eyes). Despite these significant within-group

comparisons, there was no statistically significant difference between groups (VCD; $F_{2,18} = 2.092$, p=0.152).

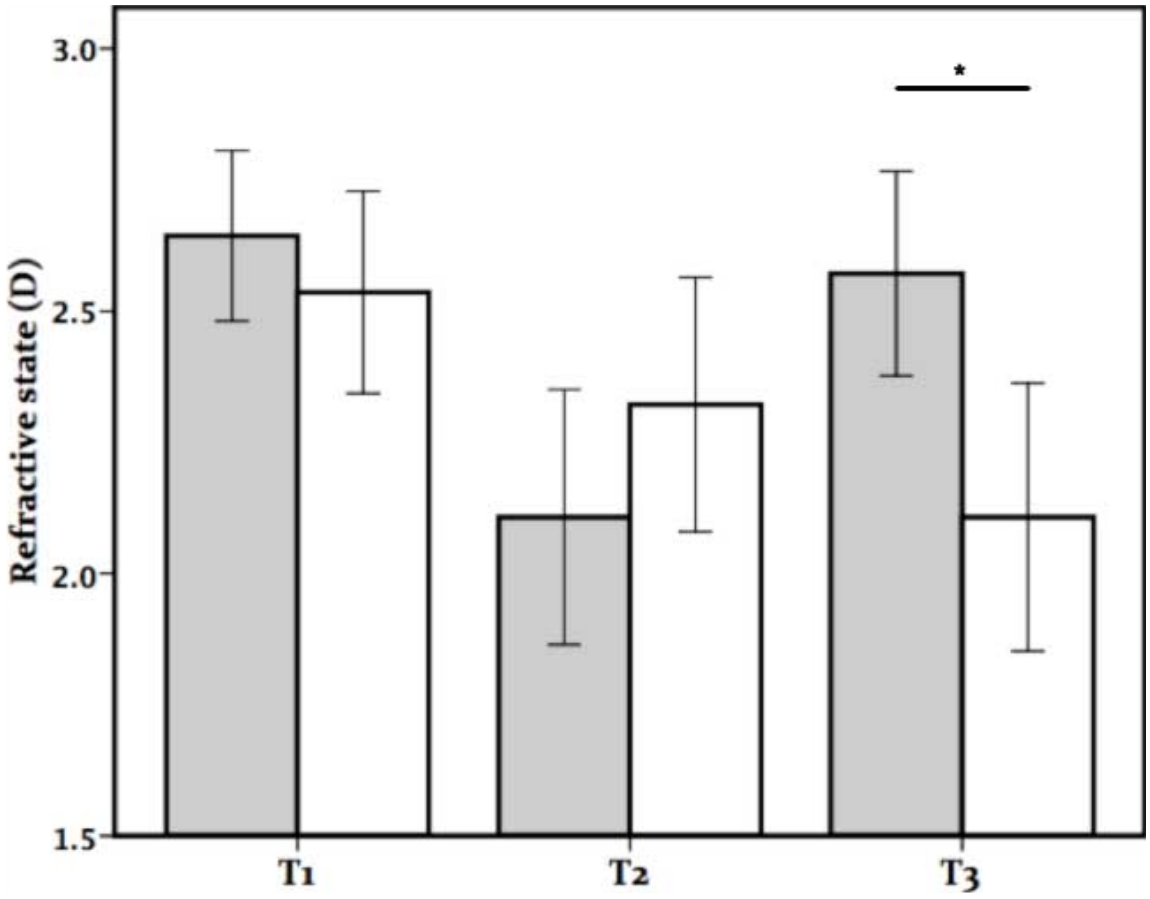

Fig. 8.14. Plus lens: Absolute refractive state 14 days post lens treatment (DPT). Absolute refractive state of treated (**white**) and control (**grey**) eyes 7 days following lens removal. A significant fellow eye difference in refractive state was evident in the T3 group of chicks suggesting a relative overshoot in correction from the plus lens induced hyperopia to relative myopia. *Error bars represent SE.* Error bars represent SE. *p<0.05, **p<0.01, ***p<0.005 (independent t-tests).

While the hyperopic shift in refractive state that is induced following ONS is stable, i.e. persisting up to, at least, 48 days post surgery (Troilo et al., 1987), the comparable response following lesion of the IOTr is a transient response, presumably due in part to the local retinal effect (i.e. only cells in the retina that receive centrifugal input) of the latter as opposed to the whole-retina retrograde degenerative effects induced by ONS, which eventually lead to RGC death (Muchnick and Hibbard, 1980). With this in mind, given that a

brain-retina connection is not required for compensation, in the absence of retinal disruption induced by ONS surgery it is perhaps not surprising that no effect was observed after only a lesion of IOTr.

An alternative possibility for the inconsistency in ONS and centrifugal disruption results is that the anterior chamber effects that result from lens wear, i.e. increased ACD (**Figs. 8.5** and **8.9**), which in turn induce axial elongation, may have acted to mask the altered set point induced by centrifugal efferent disruption. This suggestion is supported by the fact that, although the treated eyes of plano-lens wearing chicks with higher percentage lesion success were more *hyperopic* relative to plano lens wearing sham-operated controls, they were still more *myopic* than fellow control eyes (**Fig. 8.5**).

8.4 Conclusion

In conclusion, disruption of centrifugal efferents to the chick retina does not impair the ability of eyes to compensate for minus or plus lens wear. However, while recovery from minus lens treatment was normal, recovery from plus lens treatment led to a small, vitreous chamber-dependent overcorrection of the initial refractive error.

8.5 Summary

In this, and the two chapters that precede it, I have begun to characterise the role of the CVS in the regulation of emmetropisation. In the next chapter, **Chapter 9**, the focus will switch to the midbrain connectivity of the CVS that gives rise to an efferent projection to the retina. A detailed understanding of the anatomy of the system and specifically the afferent input to ION and EA, is crucial to the interpretation of the findings of this study and those of the previous two chapters. As such, the inter-relation of the anatomical and functional aspects of this thesis will be a focus of **Chapter 10**.

Chapter 09

Results: Neuroanatomy of the avian CVS

9.0 Introduction

Numerous studies have attempted to identify the sources of afferent input to the ION (e.g. Miceli et al., 1997) (**Chapter 1**), although none to my knowledge have been directed specifically to the EA. Studies of CVS connectivity within the brain initially involved techniques such as tracing retrograde degeneration following eye enucleation (Cowan et al., 1961; O'Leary and Cowan, 1982). However, with the onset of pathway tracers, the shift of focus moved towards intra-cranial injections of, for example horseradish peroxidase (HRP) into the ION/EA region. Problems associated with both of these approaches stem mainly from the anatomy of the CVS. Situated at the dorsal roof of the midbrain, beneath the large decussating trochlear nerve (dCNIV), and only about 1000 μm in its longest axis (Holden and Powell, 1972; Wolf-Oberhollenzer, 1987), the ION/EA **is** [20] a challenging target both to inject into, and also to consistently restrict the spread of tracer within the target region (Réperant et al., 2006). Miceli et al. (1993, 1997, 2002) countered these issues following the advent of trans-synaptic pathway tracers. In such studies, the bidirectional tracer RITC was injected intravitreally in conjunction with kainic acid to prevent uptake and transmission in the anterograde direction to retino-recipient brain centres. The trans-synaptic, retrograde properties of RITC mean that, when injected intra-vitreally, it is in essence equivalent to delivery of a localised injection of RITC into centrifugal neurons of the ION/EA directly. The studies of Miceli and others using this technique have elucidated a number of extratectal sources of afferent input, including nucleus linearis caudalis (LC), a serotonergic immunoreactive cell population which is reportedly analogous to the mammalian dorsal raphe complex and has been implicated in a number of non perceptual functions from neuroendocrine function to photic regulation of arousal and circadian rhythms (Fite et al., 1999; Réperant et al., 2000; Fite and Janusonis, 2001; Janusonis and Fite, 2001). The main aim of the experiments [21] described below, was to clarify what is an at times confused literature on the afferent connectivity of the ION/EA (**Chapter 1**), particularly that of EA. The

intention was to identify extratectal afferent sources through stereotaxic injections of retrograde pathway tracers into the ION/EA and, subsequently, to confirm and characterise the afferent input by injection of anterograde pathway tracers into the identified structure(s). Without any obvious candidates for extratectal afferent regions, the first and arguably most important question to be answered was: ***Do EA neurons receive tectal, i.e. visual, afferent input?***

9.1 Methods and experimental design

This investigation into the midbrain anatomy and connectivity of the CVS can be split into three subsections:

9.1.1 An investigation into EA distribution - The purpose of this study into the anatomical distribution of EA cells was two-fold. Firstly, it was my intention to build upon the work of Medina et al. (1998) and identify subpopulations of EA, which could be broadly defined based upon both position relative to ION and cell morphology. Subsequently, I wished to investigate the possibility that these subpopulations could be further defined by isolating their (potentially) distinct afferent input. Secondly, from a surgical perspective, familiarity with the distribution of EA populations was crucial in choosing suitable target areas for pathway tracer injections in **Sections 9.1.2** and **9.1.3.**

Anatomical division of the ectopic area into dorsal, lateral, medial and ventral/ventromedial was based upon a number of factors. The morphology of ectopic centrifugal neurons is distinct from that of centrifugal isthmo-optic neurons, with the former, while heterogeneous, exhibit, in general, a more complex multipolar phenotype, suggesting that afferent input may be local based upon the region relative to the ION within which they are situated. Thus, the subdivision of the ectopic area considered the neural architecture within which the centrifugal neurons were distributed. In addition, the work of Medina et al. (1998) provided a comprehensive neurochemical map of the region surrounding the ION. In fact

the neurochemistry of the ectopic area is both complex and heterogeneous, suggesting that the locus of a give ectopic neuron of neuron population may provide important physiological and functional clues. While ectopic neuron distribution may, at first glace, appear chaotic, there is in fact a good deal of intra-species conservation in terms of region-specific cell density and, in that sense, the boundaries of the subpopulations that are considered below are a product of the boundaries demarcated by regions of *low* cell density that separate the regions that are of consistently *high* centrifugal cell density.

The approach taken to investigate centrifugal ectopic neurons in this instance, was multifaceted and undertaken under the assumption that the preconceived single population of EA cells in fact consisted of a number of subpopulations with specific afferent connectivity, neurochemical properties and function. It is undisputed, however, that they share the common efferent pathway to the retina, wherein they influence large retinal regions and, unlike ION neurons, do not demonstrate topographic connectivity. The regions focused upon in the experiments of this chapter were those regions medial (M) and ventromedial (VM) to the ION.

A total of two pigeons as well as sham-operated control chicks (n=26) from intravitreal injections of WGA described in **Chapters 5 to 8** were used for the analysis of EA distribution. Intravitreal injections (**Section 3.8**) of the trans-synaptic pathway tracer WGA (**Section 4.9.1**) were used to label centrifugal neurons of the EA/ION. As I have alluded to previously, when discussing the choice of retrograde pathway tracer to use in the analysis of lesion success for the experiments described in **Chapters 6-8** (**Section 3.8**), wheat-germ agglutinin was chosen over cholera-toxin subunit B, in part because of the trans-synaptic properties that it demonstrates. Trans-synaptic transport, potentially allows identification of sources of afferent input to primary retrograde regions. Thus, sham lesioned cases of chicks in **Chapters 6-8** provided a valuable source of information for the anatomical subsection of

this work, which focused predominantly on the identification sources of afferent input to centrifugal neurons. An obvious shortcoming of this approach was that the available histological information was derived from retrograde WGA labeling in the *chick*, whilst *pigeons* were the choice species for this anatomical investigation. Pigeons were chosen in this instance, predominantly for their practicality. Adult pigeons are a smaller and quieter species than adult chickens, and while juvenile chicks would have been the ideal model for the sake of continuity across the subsections of the project, their rapid rate of growth and development would have meant that the surgical time-window during which predetermined stereotaxic co-ordinates were usable would have been small. In contrast, the adult pigeon has been the subject of a detailed stereotaxic atlas (Karten and Hodos, 1967), thus removing the necessity for complex and time-consuming stereotaxic co-ordinate determination along the lines described in **Section 3.3**). In favour of this divergence in the animal model used, the neural architecture of the two species is remarkably similar, especially so in terms of CVS organisation. As such, one can work with reasonable confidence, under the assumption that findings in the pigeon would also be applicable in the chicken.

9.1.2 Determination of ION/EA afferent input - In the second part of the study, a total of 10 pigeons were used. Discrete injections of a retrograde pathway tracer, i.e. Fast Blue (FB) (**Section 4.4**), were made into the ION and a specific population of EA (identified from the prior investigation into EA distribution) (e.g. **Fig. 9.6**) in order to identify potential sources of afferent innervation from retrograde labeling following a survival time of between 2 and 7 days. FB was chosen for these experiments because of its tendency not to spread too far from the injection site (**Fig. 9.8 A**) (e.g. compared to Fluoro-Gold).

9.1.3 Double tracer paradigm - A total of 6 pigeons were used in this part of the study. In order to ascertain whether identified region(s) of afferent innervation were projecting to the ION or to EA cells independently, a combination of tracers was employed. Two distinct

combinations of FB and a second tracer, CtB-488 (**Section 4.2**), both retrograde tracers (with emission wavelength spectra that would not overlap when imaged), were used to address 2 specific questions:

1. In the first instance, an intra-cranial injection of FB into the *left* EA was combined with an intravitreal injection of CtB-488 into the *left* eye in order to determine whether EA cells that project to the contralateral retina communicated with EA cells across the midline (**Fig. 9.11**).
2. The second permutation combined an intra-cranial injection of FB into the *left* EA with an intra-vitreal injection of CtB-488 into the *right* eye. The purpose of this combination was to determine whether EA cells that projected to the ipsilateral retina did so by initially decussating within the midbrain before decussating again at the optic chiasm as discussed in **Section 1.5.6 (Fig. 9.19)**.

For both of these permutations, the same injection time-points were used:

- **Injection 01 (Day 01)** - Intra-vitreal injection of CtB-488 was made into the appropriate eye in adult pigeons (**Section 4.2**). As the tracer involved was conjugated to a light sensitive fluorophore, all such surgeries were performed about an hour before the lights were turned off in the housing room.
- **Injection 02 (Day 04)** – Injection of FB into the medial EA (**Section 4.4**).
- **Perfusion (Day 07)** – Six days following CtB-488 injection and 2 days following FB injection, the animal was intra-cardially perfused (**Section 4.5**).

9.2 An investigation into EA distribution in the chicken

Unlike neurons of the ION, EA cells are not highly organised within a nuclear boundary. Their distribution does, however show a good degree of conservation between individuals of the same species. Morphologically, EA neurons are heterogeneous, although certain

populations exhibit a degree of morphological commonality, e.g. EA neurons dorsal to ION, i.e. within the tectal commisure, are predominantly flat bipolar neurons, which are oriented parallel to the course of crossing axonal fibers (Miceli et al., 1997). The highest density of neurons is found proximal to the ION border, with regions of particular preponderance ventromedially and ventrally with respect to ION (Miceli et al., 1997). In the sagittal plane, the highest density of EA neurons is found at the caudal and rostral poles of the ION, where the boundary between EA and ION border cells becomes particularly indistinct due to the interspersion of ION border cells with EA neurons. Although the description of the distribution of EA cells given below is based on that of the chicken, inter-species variation (i.e. with the pigeon) is also considered.

Dorsal (Fig. 9.1, red) - In the pigeon and, to a greater degree, the chicken, a distinct population of EA cells is situated within a narrow passage between the roof of the midbrain and the dorsal border of ION. A dense region of flattened bipolar EA cells, again often interspersed with the dorsal border isthmo-optic neurons, lies in the path of intra-mesencephalic fibers of the tectal commissure. This distribution of EA cells is, however, far more distinct in the chicken (**Fig. 9.4**) than in the pigeon. EA cell somata are generally larger than those of ION cells (EA - 15-20 μm, ION – 10-12 μm) with EA cells situated farthest from ION being generally larger and morphologically more heterogeneous.

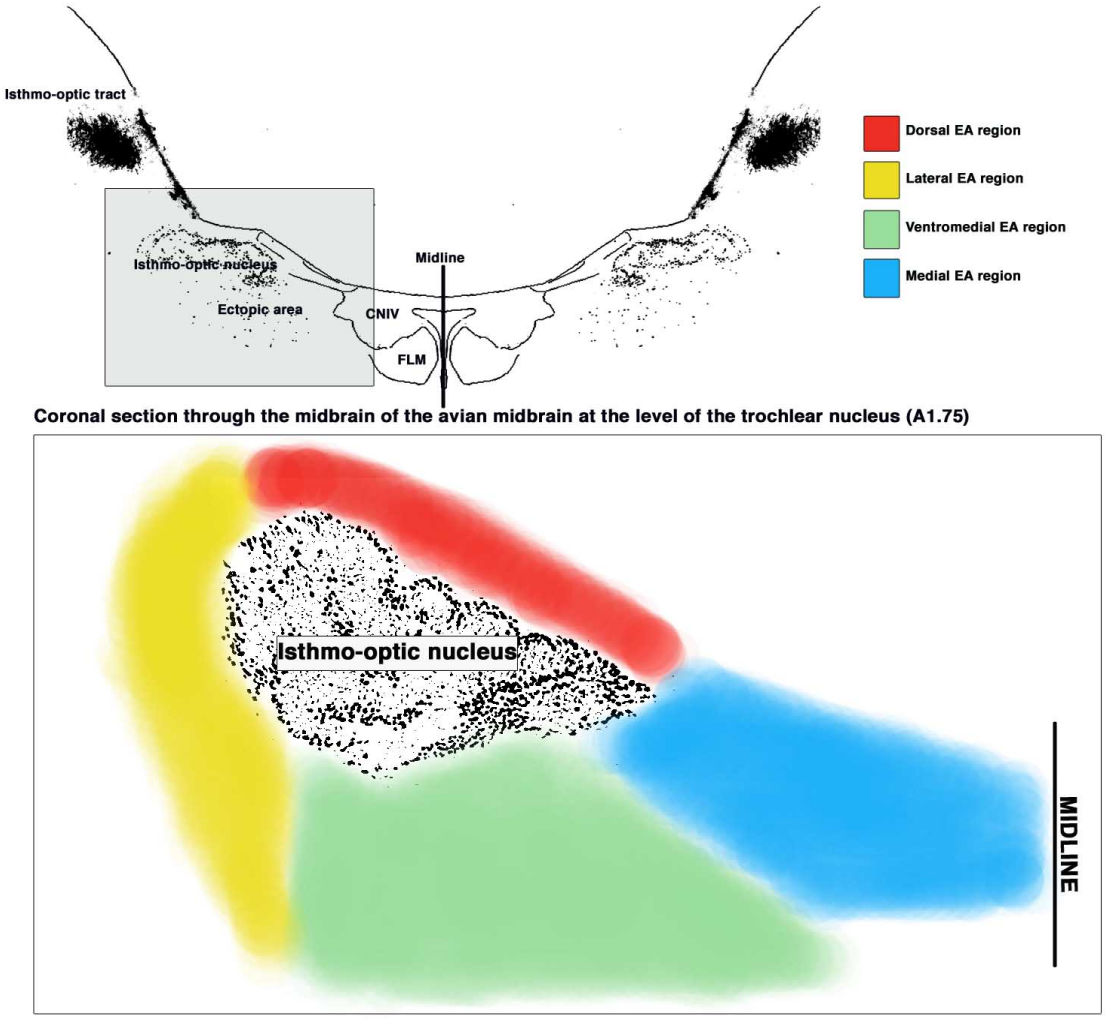

Fig. 9.1. Subpopulations of EA cells. Subdivision of the EA into regions surrounding ION: dorsal EA (**red**), medial EA (**blue**), ventral/ventromedial EA (**green**) and lateral EA (**yellow**). The region surrounding the isthmo-optic nucleus (ION) was divided, somewhat arbitrarily, into four subdivisions. Specific regions exhibit high cell densities interspersed with regions of lower cell densities, thus, to a degree, the division was guided anatomically. In addition, the borders of midbrain regions and nuclei that constitute the ectopic area (EA), as defined by the stereotaxic atlases for the chick (Masson and Kuenzel) and pigeon (Karten and Hodos) were also considered in this approach, e.g. the region in green, corresponding to the ventromedial EA, overlaps with the locus ceruleus. The low power schematic above shows the location of the ION and EA in a coronal section of the midbrain at the level of the trochlear nucleus (corresponding to A1.75 in both chick and pigeon atlases). Note that the above schematics are descriptive and not to scale.

Medial (M) (Fig. 9.1, blue) - The region medial to ION, corresponding to the GCt, i.e. within the region of the decussation of the NIV (Karten and Hodos, 1967), is an area of relative EA cell paucity (particularly so in comparison to the relatively high EA cell density of the neighbouring ventromedial region (**Fig 9.4**). However, in rostral and caudal extensions (relative to ION) of the medial EA, cell density is greater (**Fig. 9.2**).

Ventral/ventromedial (V/VM) (Fig. 9.1, green) - The density of EA neurons is particularly high in the VM region, with the distribution extending deep into the area corresponding to LoC (Karten and Hodos, 1967). EA density is at its greatest around the border cells of ION (**Fig. 9.4**). Morphologically, EA cells in this region are predominantly bipolar and are regularly oriented in the ventromedial plane (**Fig. 9.4 C, arrow**).

Lateral (Fig. 9.1, yellow) – EA density is relatively sparse in the region lateral to ION, however distinct populations are consistently labeled in the region of LLd and around the border of Ipc (**Fig. 9.5**).

Rostral/caudal (Fig. 9.2) – Dense regions of EA are consistently labeled at the rostral and caudal poles of ION. As with other regions, the density of EA cells decreases with distance from ION in the rostral and caudal directions from a peak density proximal to the nucleus (**Fig. 9.2**).

Ipsilateral – A small population of EA neurons is labeled ipsilateral to the injected eye following intravitreal injection of WGA. The total number of cells per brain in the chick ranges from ~10-60. The distribution of ipsilateral EA cells corresponds to those regions most densely labeled in the contralateral EA.)

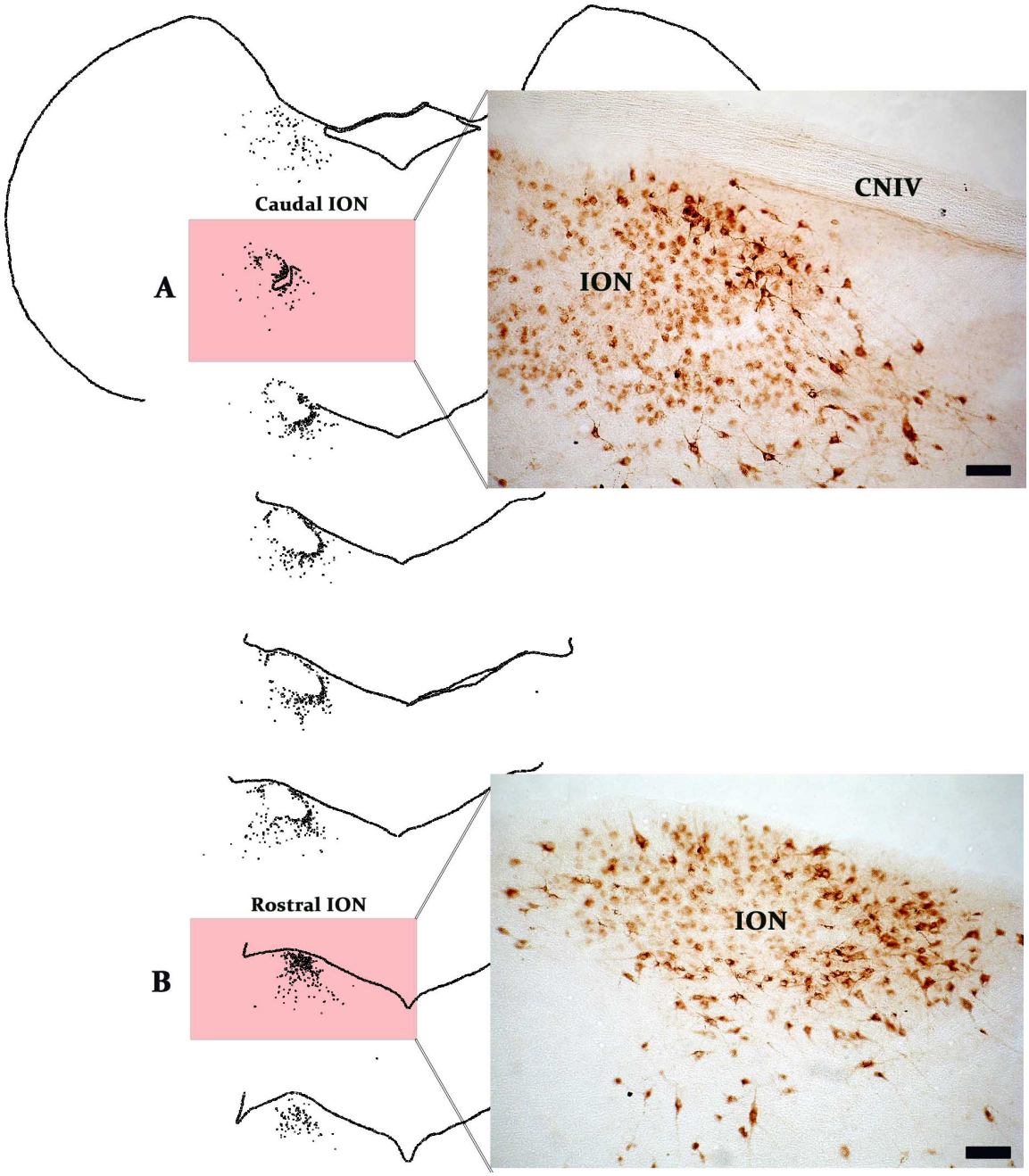

Fig. 9.2. EA cell distribution at the rostral and caudal poles of ION. Highlighting the relative cell density of EA cells at caudal (**A**) and rostral (**B**) poles of the ION. The more densely labeled cells, which are larger in size and possess distinct morphology are EA cells interspersed with the more lightly labeled ION border cells. Schematic on the left shows EA cell distribution in a 1:3 series of coronal sections in the 4-week old chick. **Scale bar = 100 μm**.

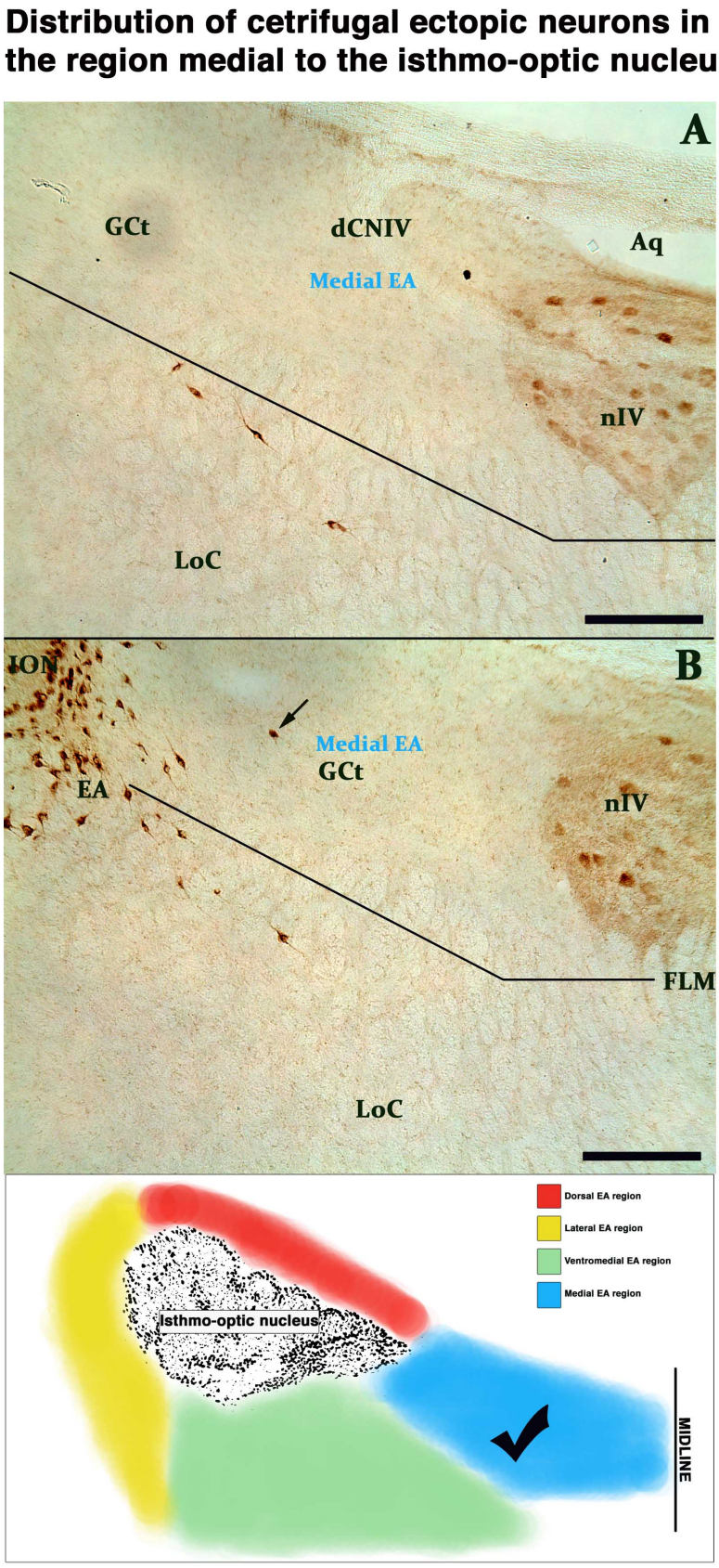

Fig. 9.3. (*See overleaf for figure legend*)

Fig. 9.3. Medial EA distribution. Examples of the distribution of WGA labeled cells in the medial EA region (denoted by outline). (**A, B**) Relative paucity of cell density in the medial EA region (**arrow**). (**C**) Higher magnification micrograph of the medial EA rostral to ION where EA cell density is greater. Aq, aqueduct; dCNIV, decussation of the trochlear nerve; EA, ectopic area, GCt, central grey; ION, isthmo-optic nucleus; LoC, locus ceruleus; LLd, nucleus lemnisci lateralis pars dorsalis; TC, tectal commissure; SLu, nucleus semilunaris. The schematic below shows the colour coordinated subdivision of the ectopic area into 4 sub regions, with a '**tick**' highlighting the region considered in this instance. Note that the above schematic is descriptive and not to scale. **Scale bar = 250 μm.**

Fig. 9.4. Ventromedial EA distribution. Examples of the distribution of WGA labeled cells in the medial EA region. (**A**) High region of EA density in the VM region. Note the common ventromedial orientation of bipolar EA cells in the VM region (**arrow**). (**B**) Flat bipolar EA cells in the dorsal region (**three arrows**) located within crossing fibers of the tectal commissure. (**C**) Higher magnification image of V/VM region EA cell distribution. Note the common orientation in EA cell processes (**right arrow**). Aq, aqueduct; EA, ectopic area, GCt, central grey; ION, isthmo-optic nucleus; LoC, locus ceruleus; LLd, nucleus lemnisci lateralis pars dorsalis; TC, tectal commissure; SLu, nucleus semilunaris. The schematic below shows the colour coordinated subdivision of the ectopic area into 4 sub regions, with a '**tick**' highlighting the region considered in this instance. Note that the above schematic is descriptive and not to scale. **Scale bar = 250 μm.**

Distribution of centrifugal ectopic neurons in the regions dorsal (red) and ventral/ventromedial (green) to the isthmo-optic nucleus

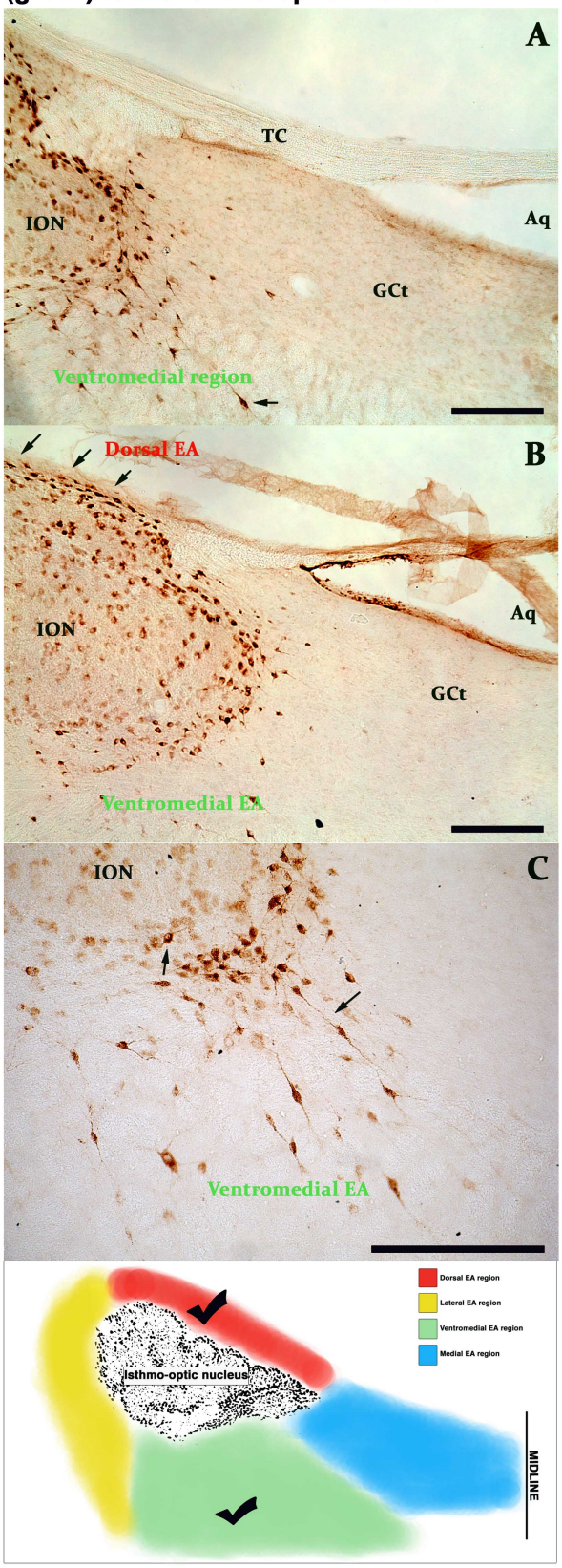

Fig. 9.4. (*See previous page for figure legend*)

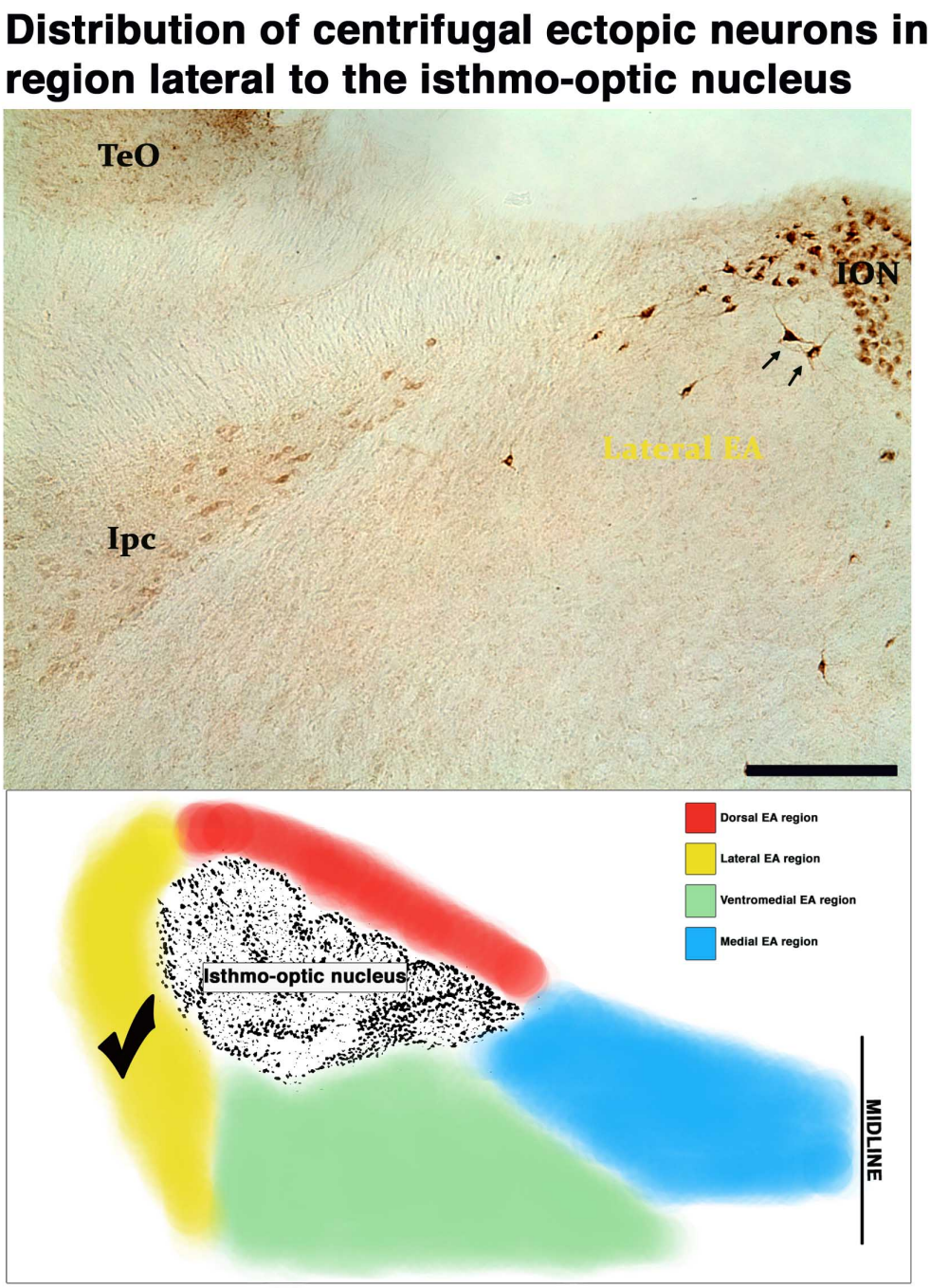

Fig. 9.5. An example of the distribution of WGA labeled cells in the lateral EA region. Morphologically lateral EA cells are often large and multipolar extending ventrolaterally towards the border of trans-synaptic labeled Ipc neurons. EA, ectopic area; ION, isthmo-optic nucleus; LLd, nucleus lemnisci lateralis pars dorsalis; LoC, locus ceruleus; SLu, nucleus semilunaris. The schematic below shows the colour coordinated subdivision of the ectopic area into 4 sub regions, with a '**tick**' highlighting the region considered in this instance. Note that the above schematic is descriptive and not to scale. **Scale bar = 250 μm.**

9.3 Determination of ION/EA afferent input

Following preliminary analysis of EA distribution in the pigeon, the area of highest cell density, i.e. VM EA relative to ION (**Fig. 9.4** and **9.6**) was targeted with intra-cranial injections of the pathway tracer Fast Blue (FB). While there is also consistently a high EA cell density ventral to ION, targeting this region would have involved passage of the needle through ION and in all likelihood, leakage into the nucleus itself. Thus, in order to confine an injection site entirely to the EA, independently of the ION, the VM region was most suitable.

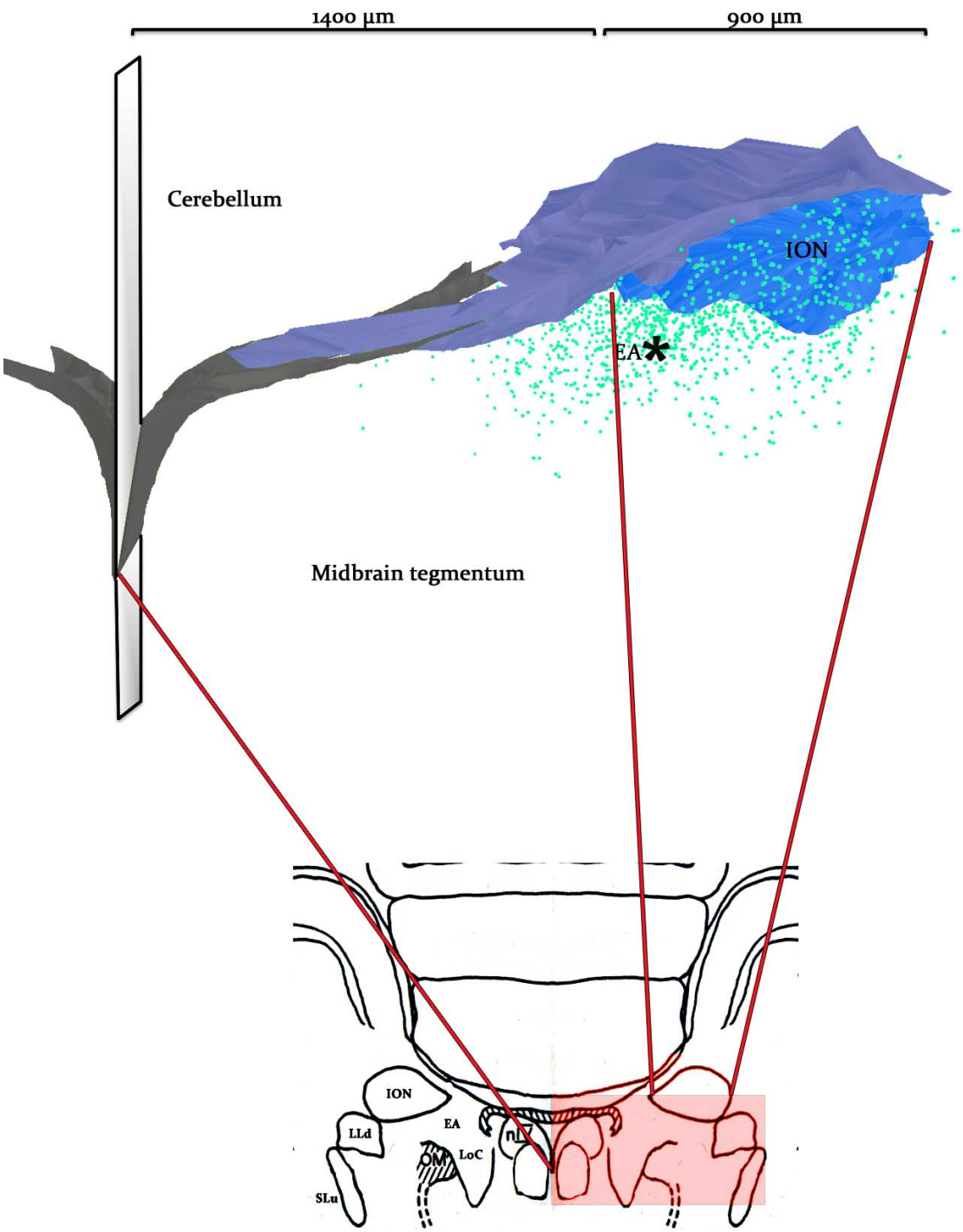

Fig. 9.6. 3-D reconstruction of coronal sections of the pigeon ION and surrounding EA cells. The shaded red region of the schematic (cropped from the stereotaxic atlas of the pigeon (Karten and Hodos 1967) at the level of the trochlear nucleus (A1.75)) corresponds to the area shown by the 3D reconstruction. The asterisk denotes the region of high EA cell density targeted with injections of Fast Blue. EA, ectopic area; ION, isthmo-optic nucleus. Note that the above schematic is descriptive and not to scale.

9.3.1 Optic tectum (TeO)

Injections of FB into the EA alone did not result in retrograde labeling of tecto-isthmic neurons of the TeO. However, those injections that included the medial aspect of ION resulted in retrograde labeling of tecto-isthmic neurons in layers 9/10, albeit labeled cells were restricted to ventral and ventromedial regions of TeO (**Fig. 9.7 C**).

9.3.2 Nucleus isthmi parvocellularis (Ipc)

In one case, following an injection of FB into the ventral/ventromedial EA that spread within the border of ION as well, a population of neurons restricted to the dorsomedial aspect of Ipc was retrogradely labeled (**Fig. 9.8 B**). The dorsal arm of Ipc extends medially along the AP axis of ION to take up a position around 200 μm from the lateral border of ION. Labeled neurons were observed to project branches dorsally into the dorsomedial aspect of TeO (**Fig. 9.8 C**). In this pigeon, FB appeared to be taken up by the dorsomedial aspect of TeO, presumably via fibers of the tectal commissure (**Fig. 9.8 C**).

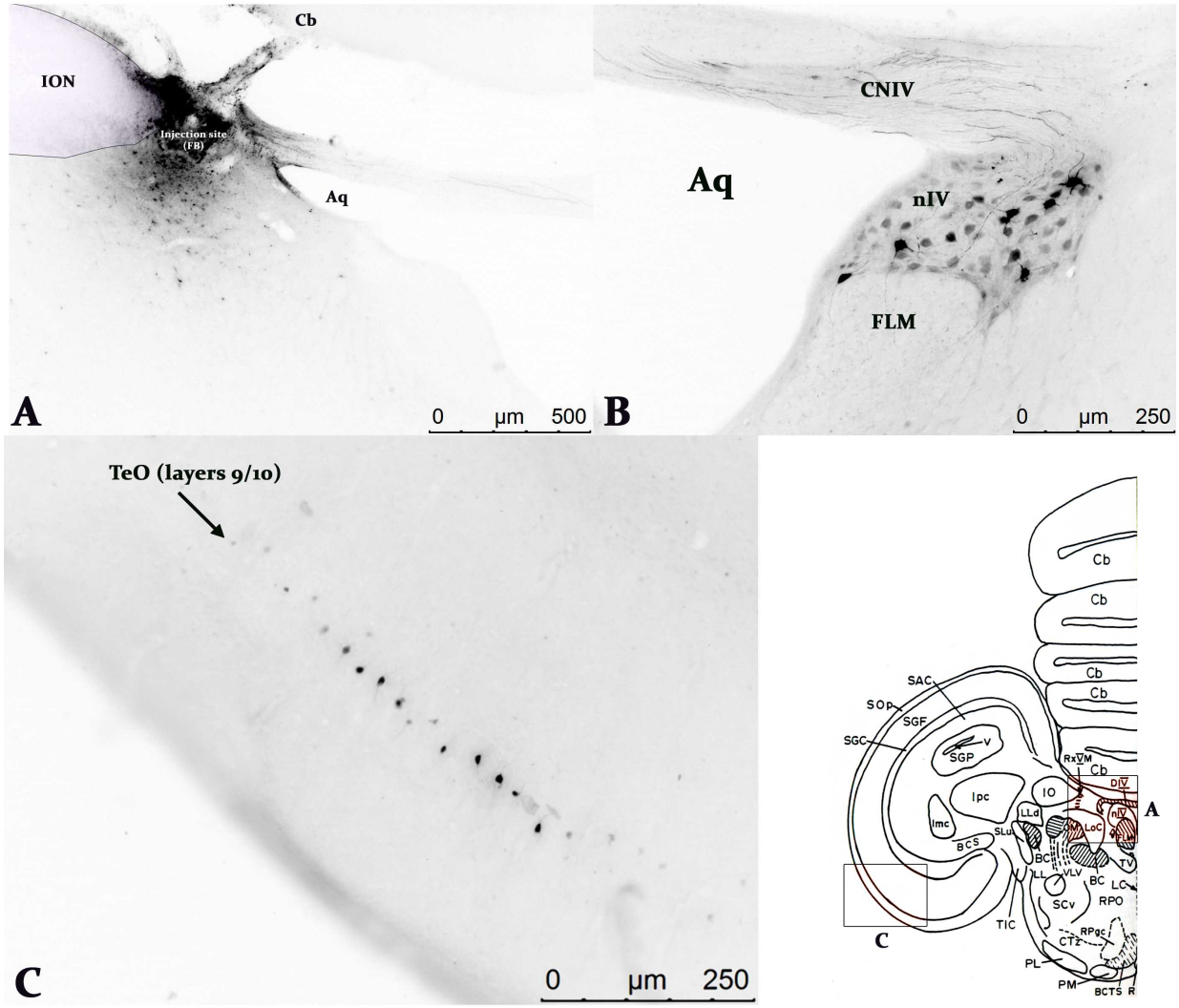

Fig. 9.7. Retrograde labeling following intra-cranial injection of Fast Blue. (A) The spread of tracer following an injection of FB into the medial aspect of ION and VM population of EA. **(B)** Neurons of the contralateral nIV are labeled following uptake of FB by fibers of passage of the CNIV that pass along the dorsal roof of the midbrain. **(C)** Injections that involved ION retrogradely labeled tecto-isthmic neurons (layers 9/10) (**arrow**) of the TeO. Schematic shows location of injection site (**A**) and retrogradely labeled tecto-isthmic cells (layers 9/10) (**C**). Aq, aqueduct; Cb, cerebellum; CNIV, trochlear nerve; FLM, fasciculus longitudinalis medialis; ION, isthmo-optic nucleus; nIV, trochlear nucleus; TeO, optic tectum. The lower right schematic shows location of injection site (**A**) and FB-labeled tectal neurons (**B**). Taken from Karten and Hodos (1967).

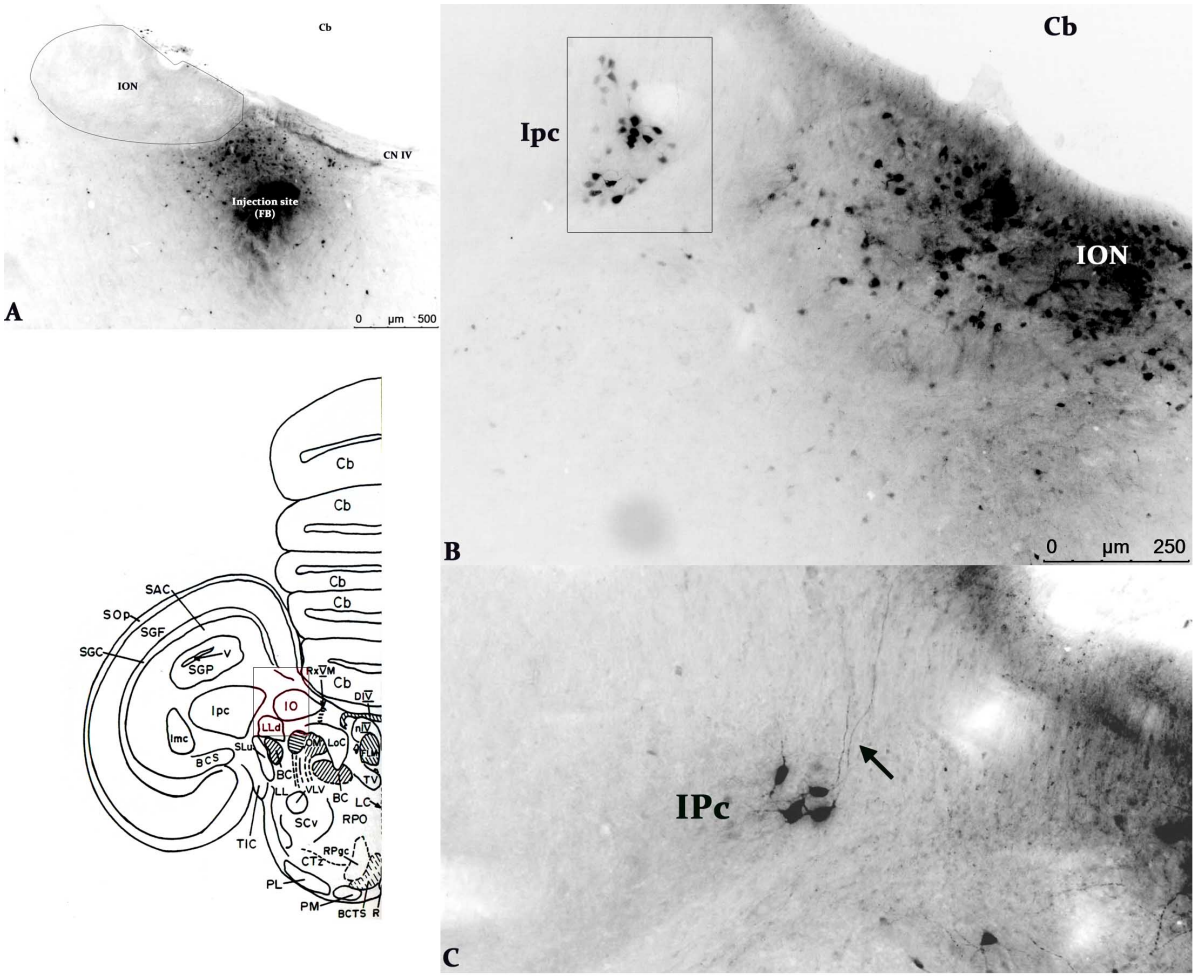

Fig. 9.8. Retrograde labeling of nucleus isthmi parvocellularis (Ipc). Following intra-cranial injection of the medial EA, retrograde labeling of soma in the dorsomedial extent of Ipc was observed (**rectangle in B**). **(A)** The Fast Blue injection site into the medial and ventromedial EA region. **(B)** FB-labeled neurons in the dorsomedial aspect of Ipc, proximal to ION. **(C)** Inset of box in **B**; Ipc neurons project dendritic branches towards the dorsomedial TeO (**arrow**). Cb, cerebellum; ION, isthmo-optic nucleus; Ipc, nucleus isthmi parvocellularis. Schematic shows location of injection site and Ipc labeled cells. Taken from Karten and Hodos (1967). **Scale bar in C apples to B also.**

9.3.3 Contralateral ectopic area neurons

Following intra-cranial injection of FB into the medial aspect of ION and the interspersed dense region of EA, a population of neurons was retrogradely labeled consistently in the corresponding EA region of the contralateral midbrain hemisphere (**Fig. 9.9**). The crossed fibers of the CNIV course along the dorsal roof of the midbrain (i.e. within the path of an

syringe needle) and as a result, tracer was regularly taken up by fibers of passage and subsequently transported retrogradely to label neurons of the contralateral nIV (**Fig. 9.7 B**). However, in a number of cases where the M/VM ION/EA was injected without involving the NIV (and nIV), retrograde labeling of contralateral EA neurons was still observed.

The distribution of contralateral EA neurons was, for the most part, confined to the contralateral V/VM EA region that mirrored the injection site on the other side, occupying the dorsomedial midbrain in between the ION laterally and the trochlear nucleus medially. The distribution of labeled cells was particularly dense proximal to the trochlear nucleus (alongside decussating fibers) (**Fig. 9.10 B**). High density regions of cells were consistently found around blood vessels in the medial EA region (**Fig. 9.10 A**). At the ventromedial aspect of the contralateral ION, EA neurons were distributed in a manner analogous to centrifugal EA neurons (**Section 9.2**), often interspersed within border cells of the ION itself (**Fig. 9.10 C**).

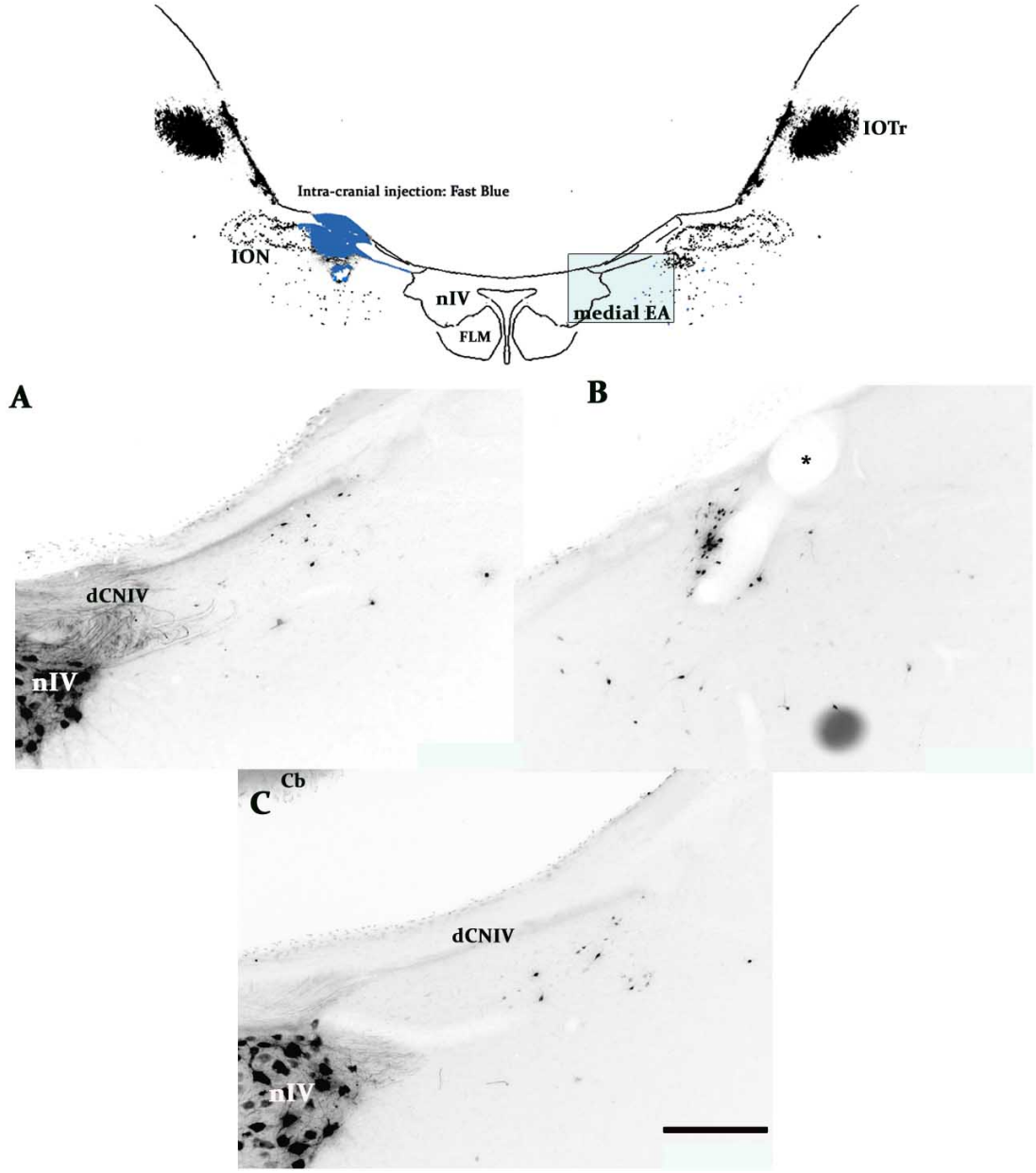

Fig. 9.9. Retrograde labeling of a FB-labeled EA population contralateral to the injection site. Following intra-cranial injection of FB (**blue**) into the medial ION/EA, a population of neurons in the EA region of the contralateral side of the midbrain was labeled. Contralateral FB-labeled cells distributed: (**A**) in the medial and ventromedial EA regions between ION and nIV, (**B**) around blood vessels (**asterisk**), (**C**) within and around decussating fibers of CNIV. Cb, cerebellum; CNIV, trochlear nerve; FLM, fasciculus longitudinalis medialis; ION, isthmo-optic nucleus; IOTr, isthmo-optic tract; nIV, trochlear nucleus. **Scale bar = 250 *μ*m.**

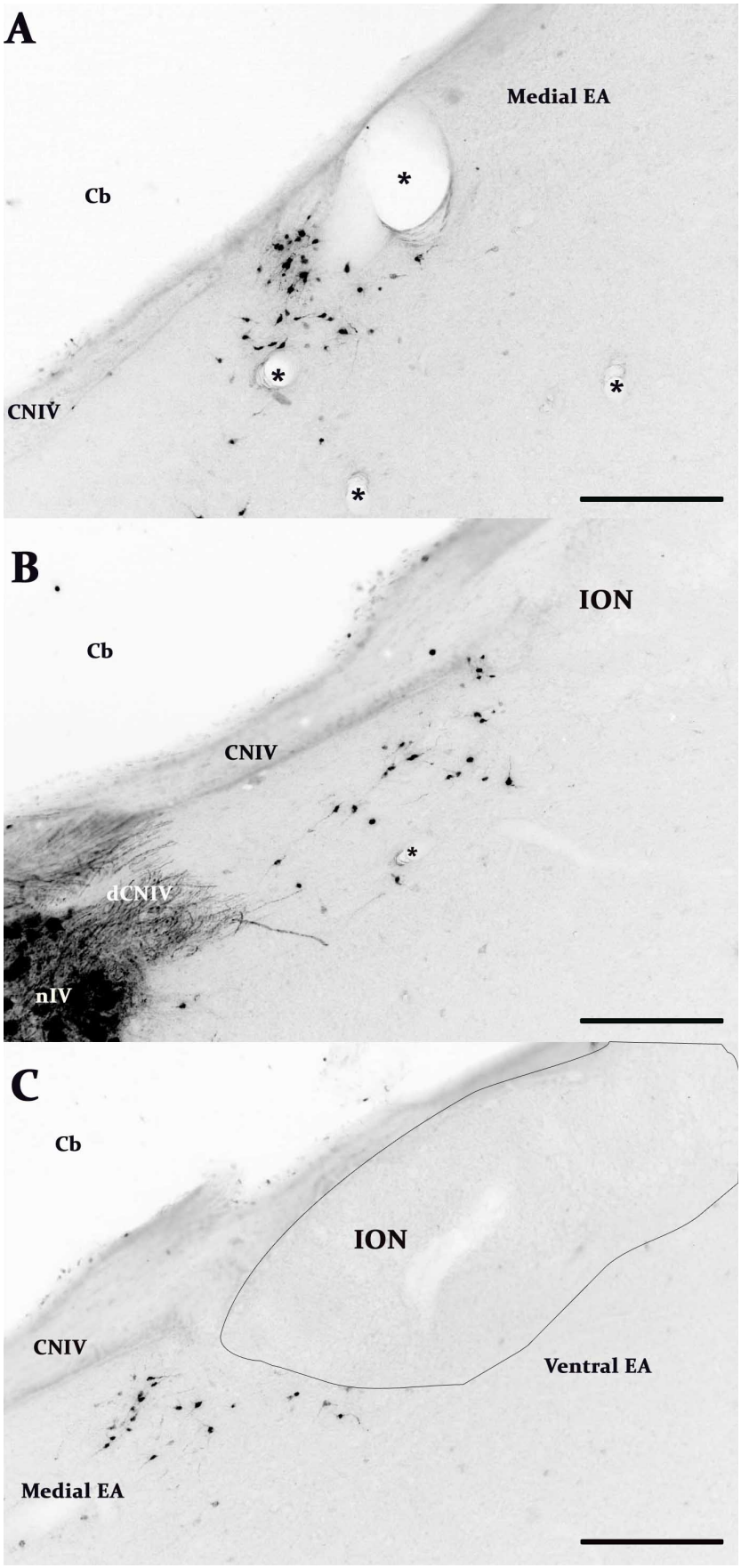

Fig. 9.10. (*see overleaf for figure legend)*

Fig. 9.10. Distribution of FB-labeled cells in the EA contralateral to the injection site. Following intra-cranial injection of FB into the medial and ventromedial EA, neurons were retrogradely labeled on the contralateral side of the midbrain again in the medial and ventromedial EA regions. **(A)** A high density of FB-labeled neurons around blood vessels (**asterisks**), **(B)** Distribution of FB labeled neurons within and around decussating fibers of CNIV, **(C)** FB labeled neurons medial to the contralateral ION. Cb, cerebellum; CNIV, trochlear nerve; dCNIV, decussation of the trochlear nerve; EA, ectopic area; GCt, central grey; ION, isthmo-optic nucleus; nIV, trochlear nucleus. **Scale bar = 250 μm.**

Following an initial investigation into the afferent connectivity of the M/VM EA region, two extratectal (i.e. regions other than the well defined afferent input from the TeO) regions were identified:

1. **Nucleus isthmi parvocellularis (Ipc)**
2. **Contralateral EA region (EA)**

Ipc has been identified as a potential source of ION/EA afferents in past studies (Miceli et al., 1997). For a number of reasons, which include other more likely routes outlined in **Section 9.8.3**, it is unlikely that the labeling of cells observed in this study, whether through either trans-synaptic pathway tracing or injection of Fast Blue into ION/EA, are a result of direct Ipc-ION/EA connectivity. As a result, the focus of the remaining experiments of this study were towards investigating the possibility of a novel interconnectivity between EA populations on opposite sides of the midbrain

9.4 Investigating EA interconnectivity

The finding that neurons in the same region as those that were retrogradely labeled by injection of FB into EA, but on the *opposite* side of the midbrain raised several intriguing possible explanations:

1. EA axon collaterals decussate within the midbrain and terminate upon EA neurons in the corresponding contralateral EA in an EA, i.e. a substrate for cross talk between the EA populations either side of the midline of the midbrain.
2. Labeled contralateral EA cells were ipsilaterally projecting EA neurons, suggesting a double crossed pathway terminating upon the ipsilateral retina (**Fig. 9.35**).
3. Labeled contralateral EA cells were unrelated to the CVS and were in fact the result of a crossed projection from nearby regions, e.g. GCT or LoC, within which EA neurons are distributed.

In order to address the first two possibilities, two experimental designs, using the same combination of pathway tracers (i.e. Fast blue (FB) and cholera toxin subunit-B conjugated to Alexa Fluor 488 (CtB-488)) were employed. Common to both permutations was an injection of FB into the medial EA region of the left midbrain (which retrogradely labeled neurons in the contralateral medial ectopic area). The designs differed in which eye was injected with CtB-488 and thus, whether contralateral or ipsilateral centrifugal neurons would be labeled in the region common to those neurons retrogradely labeled by injection of FB. It is crucial to the interpretation of these results not only to remember that an intravitreal injection of a retrograde pathway tracer labels the ION and EA of the *contralateral* midbrain but also that a small number of centrifugal neurons are retrogradely labeled in the ipsilateral midbrain. Thus, the two permutations used differed based upon which of these populations was labeled in the 'area of interest', i.e. the medial EA region contralateral to the injection of FB. In the following section, results of the design employed to investigate potential centrifugal EA cross-talk mechanisms will be addressed. Subsequently, in Section 9.6, the

9.5 Double tracer (Left ION (FB), *Left* eye (CtB-488))

As discussed above and in **Section 9.1.1**, the purpose of the combination of pathway tracer

injections used in this instance was to investigate the possibility that EA neurons within one hemisphere of the midbrain communicate with EA neurons in the contralateral EA population. The first injection of CtB-488 into the left vitreous chamber was used to label all centrifugal neurons in the right midbrain hemisphere, while the second injection of FB into the left medial EA to label neurons of the EA in the opposite side of the midbrain (i.e. the right midbrain) as in **Section 9.3.2**. Double labeling of EA neurons in the right hemisphere (**rectangle, Fig. 9.11**) would provide direct evidence for EA axonal collaterals crossing within the midbrain (presumably *via* the nearby CNIV decussation).

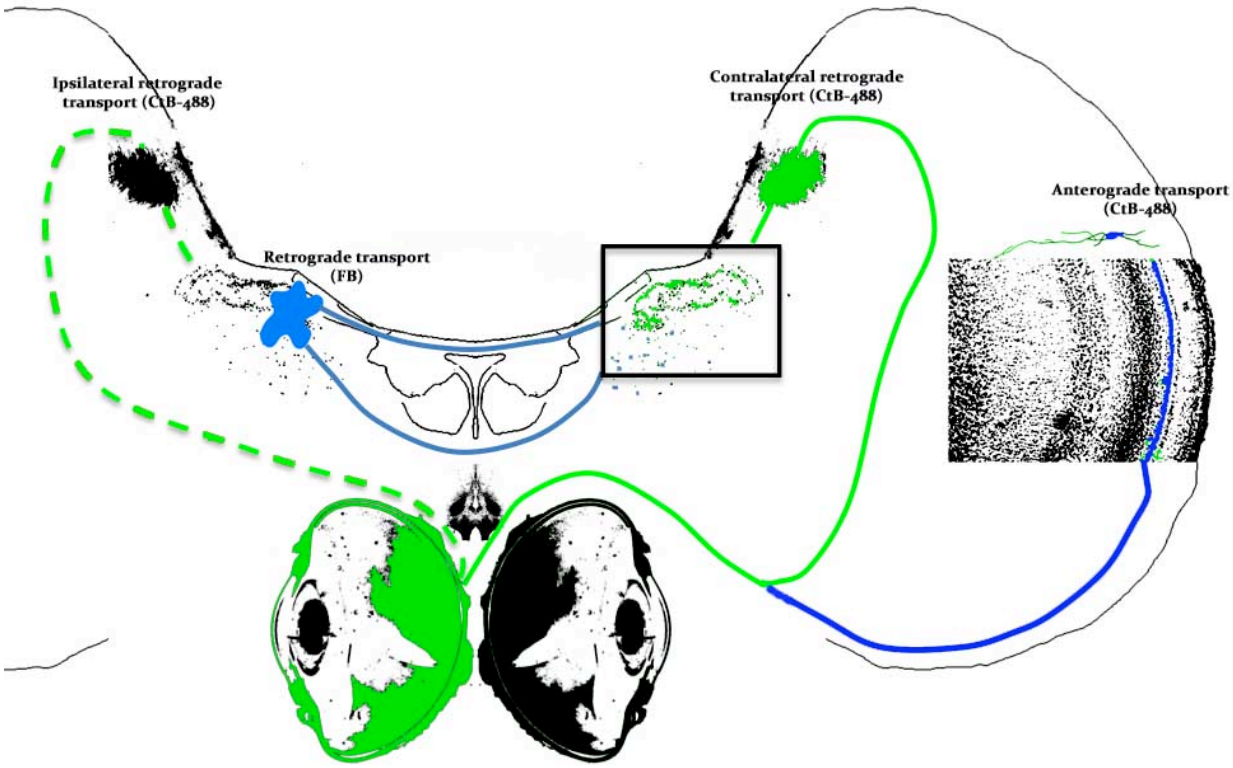

Fig. 9.11. (See overleaf for figure legend)

Fig. 9.11. Double tracer 01: investigating EA crosstalk. Schematic representation of the double tracer paradigm employed to investigate the possibility of a cross-talk projection between populations of centrifugal neurons**.** Intravitreal injection of CtB-488 into the left eye retrogradely labeled contralateral centrifugal cells (**solid green**) and ipsilateral centrifugal cells (**dashed green**) as well as anterogradely labeled terminals on cells of primary visual centres, e.g. TeO (**dark blue**). Two days later, injection of FB into the left medial EA region retrogradely labeled cells in the contralateral EA region (**light blue**). Double-labeled cells in the region of interest (**rectangle**) would provide direct evidence for communication between EA populations on either side of the midbrain. CtB-488, cholera-toxin subunit-B conjugated to Alexa-Fluor 488; FB, Fast Blue; EA, ectopic area; TeO, optic tectum.

9.5.1 Injection sites: Summary of cases

In case 01, the intra-cranial injection of FB was confined to the trochlear nerve itself (**Fig. 9.12**). However, retrogradely labeled neurons in the contralateral midbrain were still evident, albeit fewer than typically observed following an injection that incorporated the ventromedial EA region (**Fig. 9.4**). Extensive labeling of contralateral centrifugal neurons following intra-vitreal injection of CtB-488 was apparent (e.g. **Fig. 9.14**). In case 02 the injection site of FB here again included the trochlear nerve but also the medial ION and surrounding EA (**Fig. 9.12**). FB labeling of cells within the contralateral EA was consistent with that observed in the previous injection of the CNIV itself. Once again, labeling of centrifugal neurons following intravitreal injection of CtB-488 was comprehensive. Case 3 was a deeper injection site included medial and VM EA as well as medial ION but, in this case, did not label somata of the contralateral IV nucleus (**Fig. 9.12**). Contralateral FB labeled neurons were again observed, including a dense region of small bipolar neurons in the medial EA at the roof of the midbrain. However, CtB-488 labeling was sparse, labeling just a few ION border cells in each section.

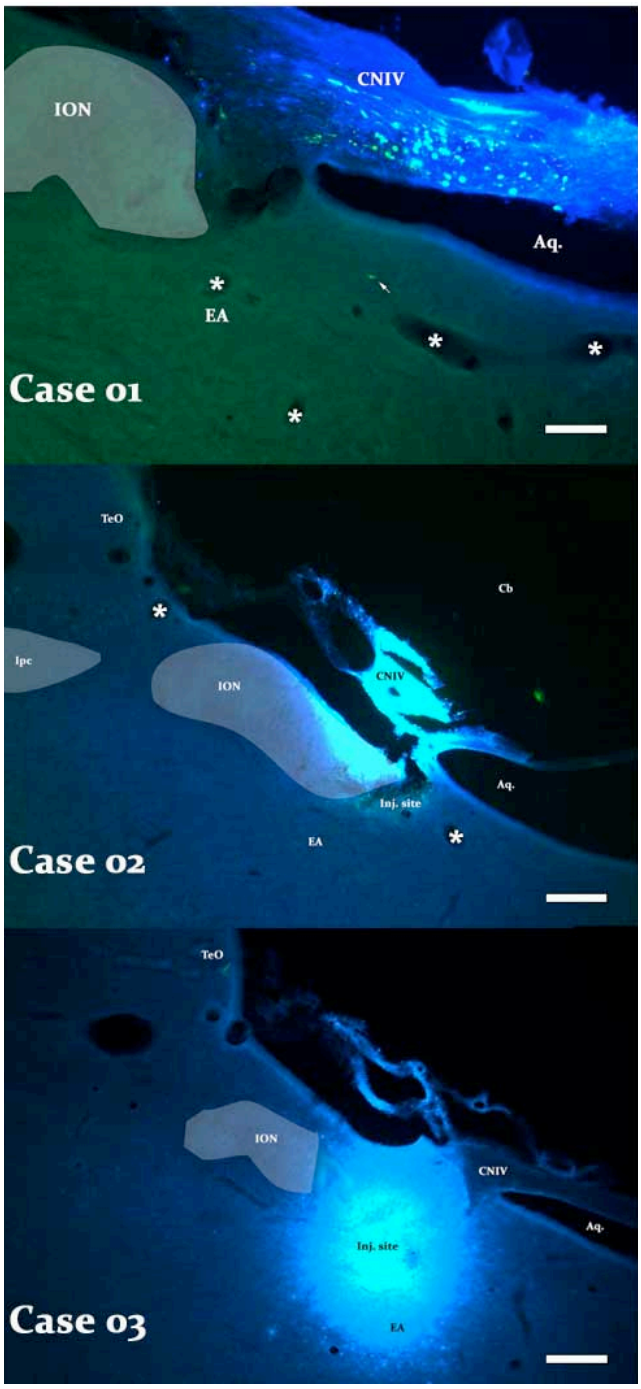

Fig. 9.12. Double tracer 01: Injection sites. FB injection sites. **Case 01**: Superficial injection taken up entirely by the CNIV. Note the ipsilateral EA neuron in the medial EA region from the intra-vitreal injection of CtB-488 (**arrow**). **Case 02**: Dorsomedial ION/EA and IV nerve. **Case 03**: ventromedial EA and ION. Tracer was taken up by CNIV fibers of passage. Aq, aqueduct; Cb, cerebellum; CNIV, trochlear nerve; ION, isthmo-optic nucleus (Asterisks show blood vessels). **Scale bar = 250 *μ*m.**

9.5.2 Double labeling

Other than a single ION neuron, none of the other retrogradely FB-labeled cells in the contralateral EA was found to be double-labeled for both CtB-488 and FB tracers (**Fig. 9.13**). That being said, there were numerous examples of the dendrites of retrogradely labeled FB neurons in the contralateral EA, which appeared to branch out to contact retrogradely CtB-488 labeled centrifugal neurons (**Fig. 9.17**) (**See section 9.5.1.3**) below. As a result of the uncharacteristically sparse labeling of centrifugal neurons following intravitreal injection of CtB-488 in case 03, it is perhaps unsurprising that no double labeled neurons were found.

9.5.3 Interconnectivity

As alluded to above, although only a single CtB-488 centrifugal neuron was double labeled with FB, there were numerous examples of apparent interconnectivity between FB labeled and CtB-488 labeled neurons. Retrogradely labeled FB neurons were often in very close proximity to CtB-488 labeled centrifugal neurons, including some that overlapped but were not double-labeled (as they were in different focal planes along the z-axis of the tissue sections) (**Fig. 9.15** and **9.16**). Apparent interaction between the two populations was regularly observed with retrogradely labeled FB neurons situated in amongst centrifugal subpopulations, extending branches towards both ION and EA neurons (**Fig. 9.17**). However, with the limitations of light microscopy, actual synaptic connections between the cell populations were not observed.

Interestingly, in one case (case 03), comprehensive bilateral retrograde FB-labeling of the nucleus lemnisci lateralis pars dorsalis (LLd; an nucleus of the ascending auditory pathway (**Fig. 9.27**)) was observed with projecting branches of LLd neurons extending into the injection site in the M and VM EA regions. On the contralateral side of the midbrain to the injection site of FB, equally dense labeling of the nucleus was observed with the dendrites of individual soma projecting up to the lateral border of ION, although the fibers could not be

followed to their termination (**Fig. 9.18**).

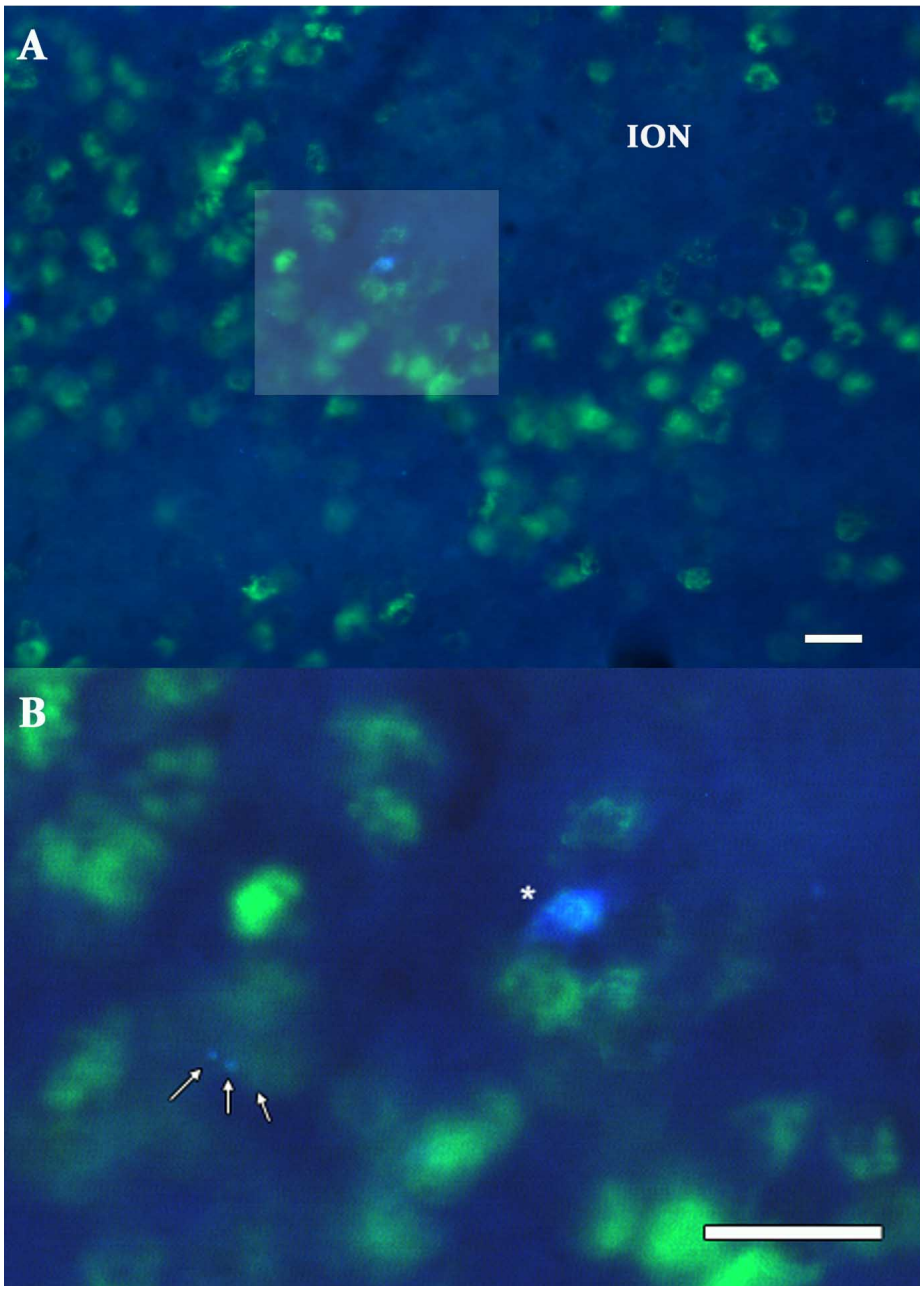

Fig. 9.13. Double labeling. Low (**A**) and high magnification (**B**) example of a double-labeled isthmo-optic neuron. **(A)** CtB-488 (**green**) and FB (**blue**) double labeled ION cell. **(B)** Inset of shaded rectangle in (**A**) showing the double labeled cell (**asterisk**) and double labeled terminals on nearby ION cells (**arrows**). ION, isthmo-optic nucleus. **Scale bar = 25 *μ*m.**

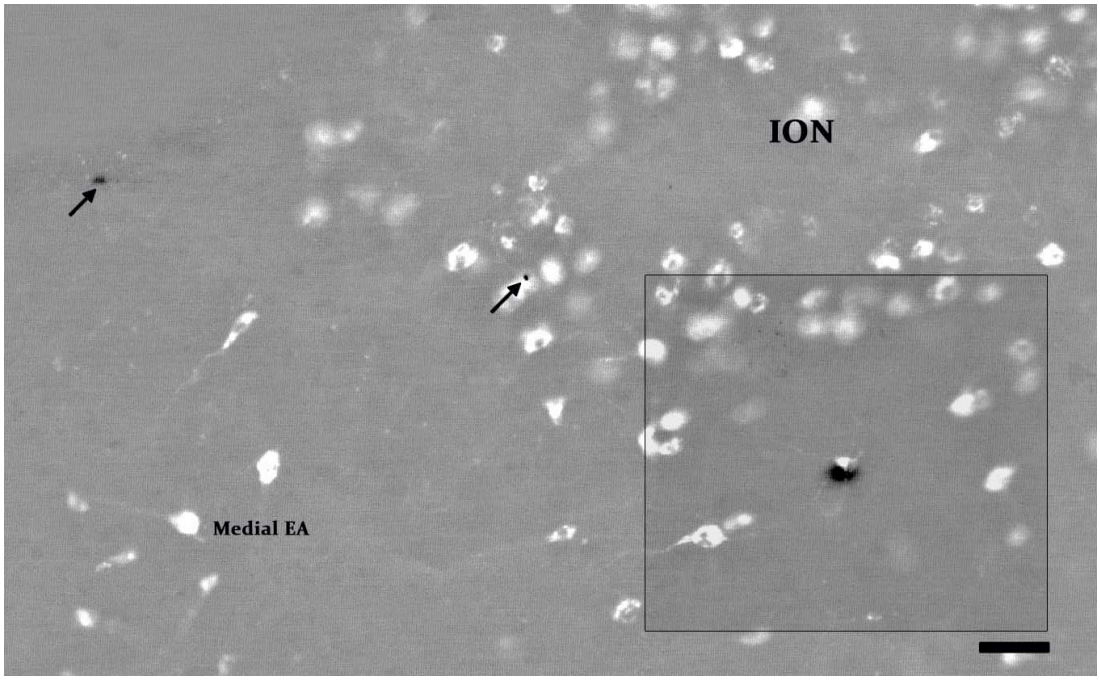

Fig. 9.14. Interaction between FB and CtB-488 labeled cells. Fast Blue labeled cells (**black (arrows)**) and CtB-488 labeled cells (**white)** including an example of the two overlapping one another but not double labeled (close to the ventromedial border of the rostral ION). See **Figure 9.16** for higher magnification micrographs of the highlighted region. **Scale bar = 25 *μ*m.**

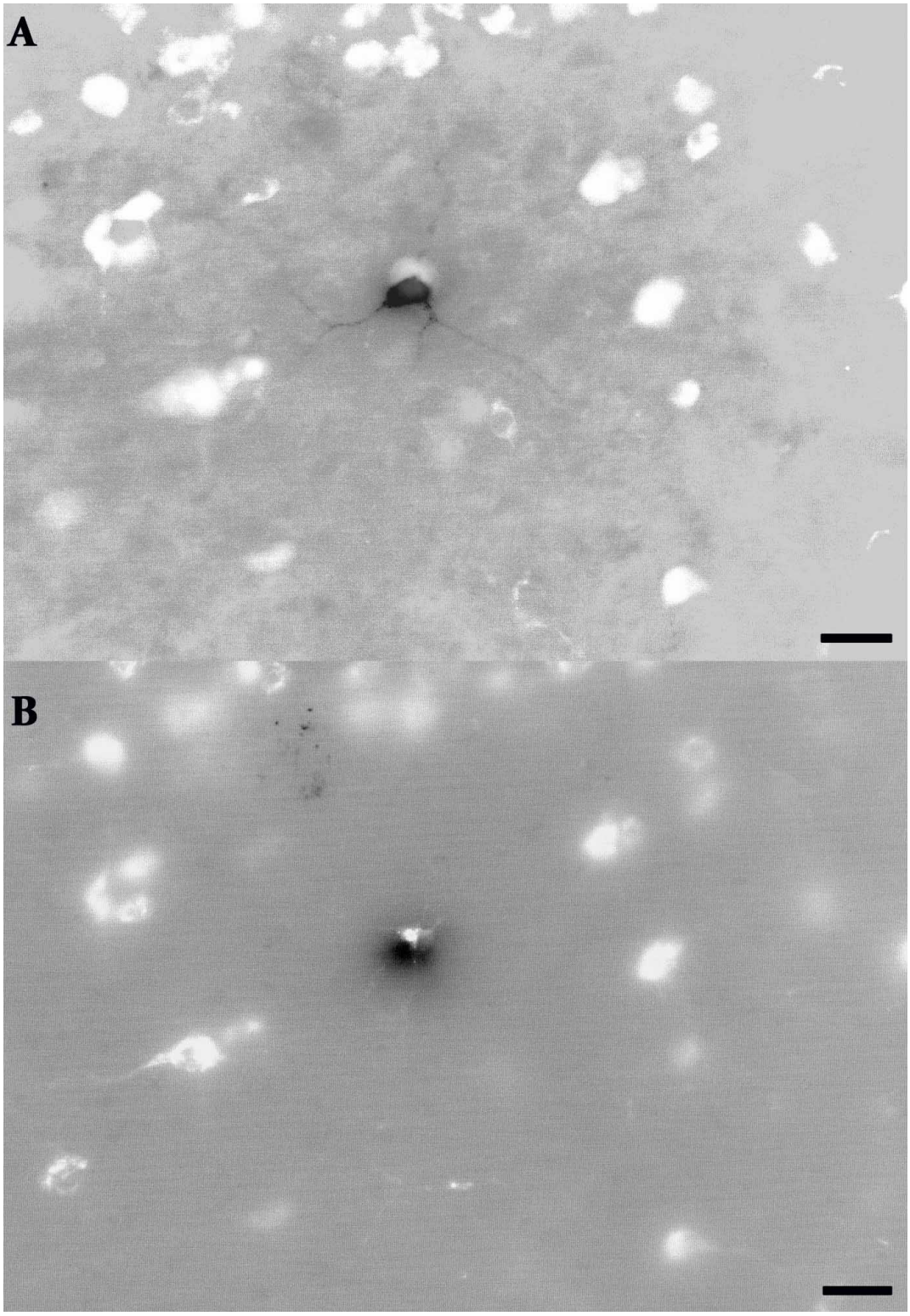

Fig 9.15. Overlapping FB and CtB-488 labeled cells. High magnification micrographs of the highlighted region in **Fig. 9.15**. A Fast Blue labeled cell (**black**) overlying, but in a different plane of focus to a CtB-488 labeled centrifugal EA cell (**white**). (**A**) Fast Blue cell in focus. (**B**) CtB-488 cell in focus. **Scale bar = 25 *μ*m.**

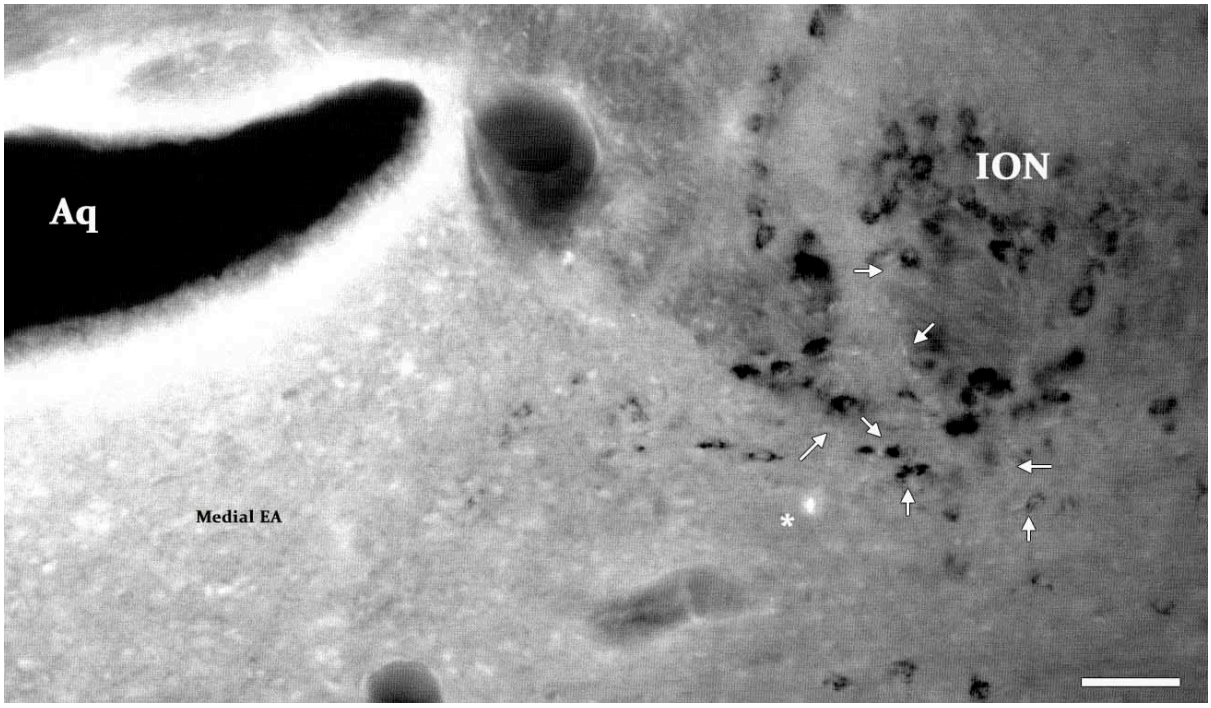

Fig. 9.16. Interaction between FB and CtB-488 labeled ION cells. FB labeled cell (**asterisk**) on the M/VM border of ION projecting dendrites towards numerous border cells of the ventromedial ION (**arrows**). **NB**. FB-labeled cells are **white** and CtB-488 labeled cells are **black** in this figure. Aq, aqueduct; EA, ectopic area; ION, isthmo-optic nucleus. **Scale bar = 50 *μ*m.**

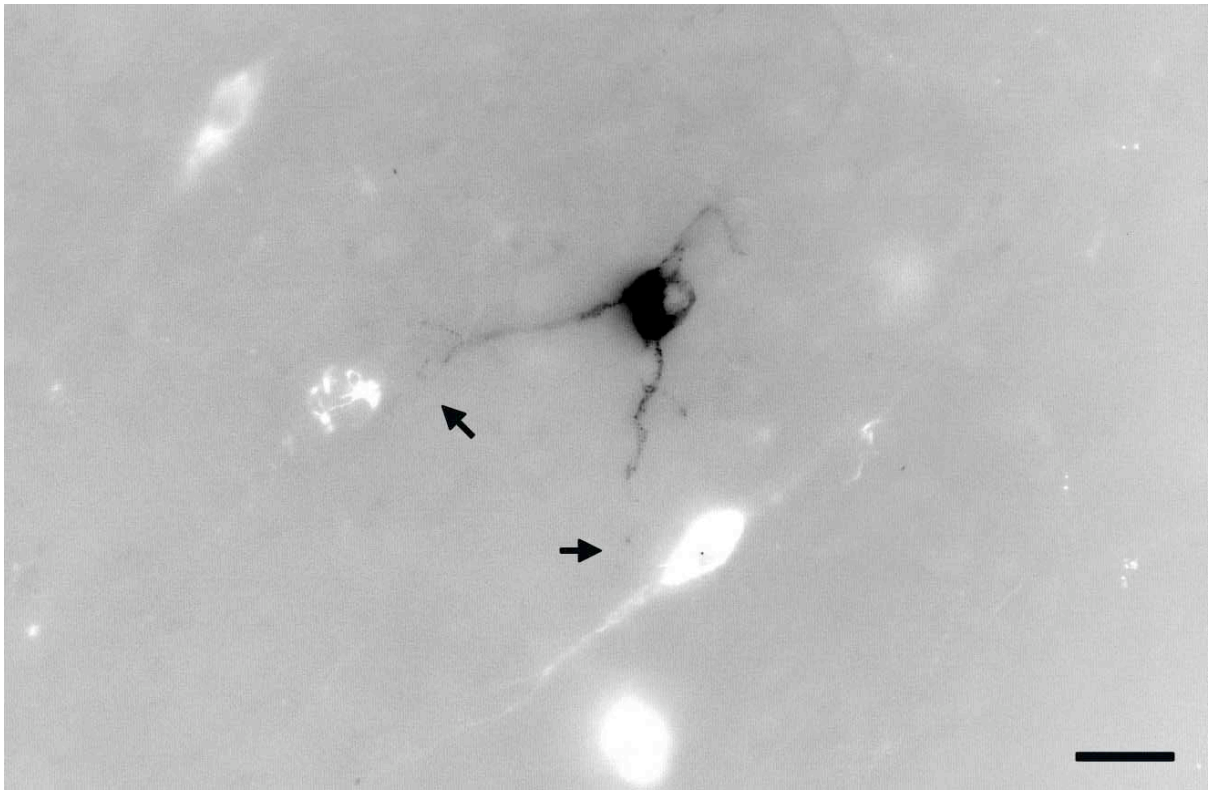

Fig. 9.17. A clear example of the close proximity of the two populations of labeled neurons in midbrain side contralateral to the injection of FB. FB labeled (**black**) multipolar cell in the ventromedial EA region projecting branches towards bipolar CtB-488 labeled centrifugal (**white**) EA cells (**arrows**). **Scale bar = 25 *μ*m.**

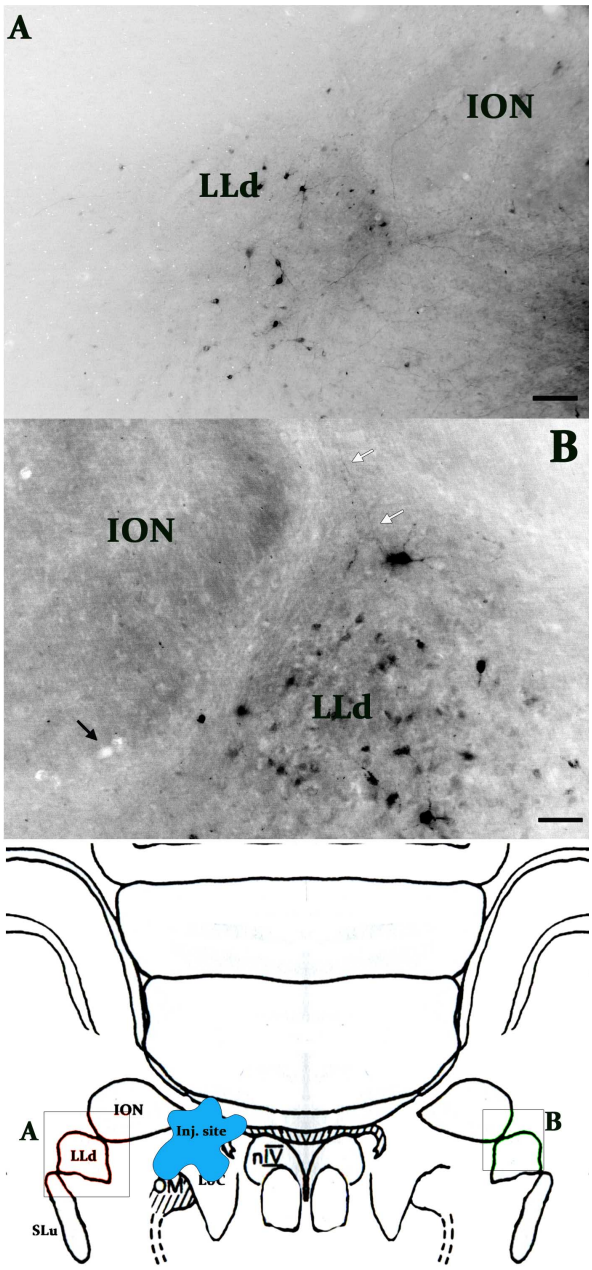

Fig. 9.18. Bilateral labeling of nucleus lemnisci lateralis pars dorsalis (LLD). Bilateral LLd labeling following injection of FB into the contralateral M and VM EA region and medial ION. Schematic below showing the location of the micrographs (**A**) ipsilateral and (**B**) contralateral to the injection site (**blue**). **Arrows** show axon branches extending up the lateral border of ION towards decussating fibers of the tectal commissure. Schematic taken from Karten and Hodos (1967). **Scale bar = 100 *μ*m** (**A**) **and 50 *μ*m** (**B**).

9.6 Double tracer (Left ION (FB), *Right* eye (CtB-488))

As discussed in **Section 9.1.1**, the purpose of this combination of pathway tracer injections was to investigate the possibility that centrifugal EA neurons innervate the ipsilateral retina via a double decussation pathway, whereby axons cross within the midbrain via the CNIV decussation and re-cross at the optic chiasm. The first injection of CtB-488 into the right vitreous chamber was used to label all centrifugal neurons in the left midbrain hemisphere, as well as, crucially, ipsilateral EA cells in the right side of the midbrain. The second injection of FB into the medial EA of the left side of the midbrain labeled neurons of the EA in the contralateral side of the midbrain (i.e. the right midbrain) as in **Section 9.3.2**. Double labeling of ipsilateral EA neurons in the right hemisphere (**Fig. 9.19**) would be direct evidence for such a pathway.

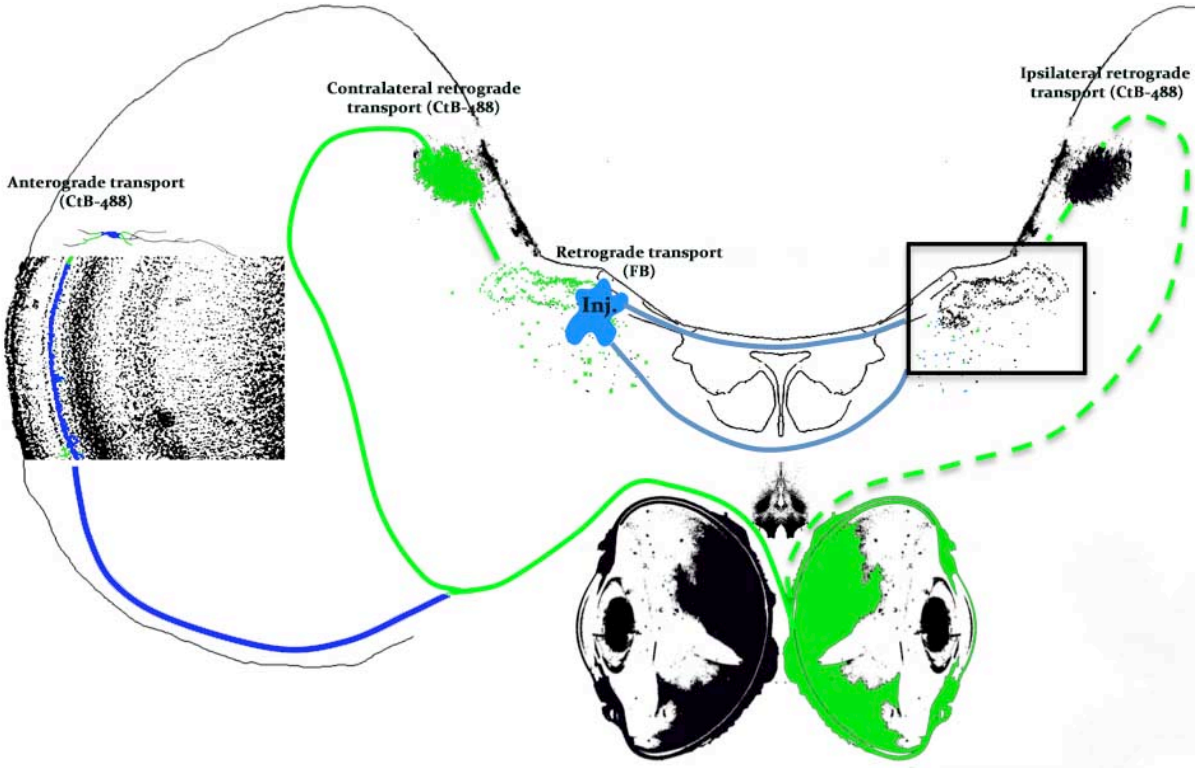

Fig. 9.19. Double tracer 02: investigating the ipsilateral EA pathway. Schematic representation of the double tracer paradigm employed to investigate the possibility of a novel double-crossed projection in the pathway taken by EA neurons to the ipsilateral retina. Intravitreal injection of CtB-488 into the right eye retrogradely labeled contralateral centrifugal cells (**solid green**) and ipsilateral centrifugal cells (**dashed green**) as well as anterogradely labeled terminals on cells of primary visual centres, e.g. TeO (**dark blue**). Two days later, injection of FB (**Inj.**) into the left medial EA region retrogradely labeled cells in the contralateral EA region (**light blue**). Double-labeled cells in the region of interest (**rectangle**) would provide direct evidence for a double-decussation ipsilateral EA cell efferent pathway. CtB-488, cholera-toxin subunit-B conjugated to Alexa-Fluor 488; FB, Fast Blue; EA, ectopic area; TeO, optic tectum. Note that this schematic is not to scale.

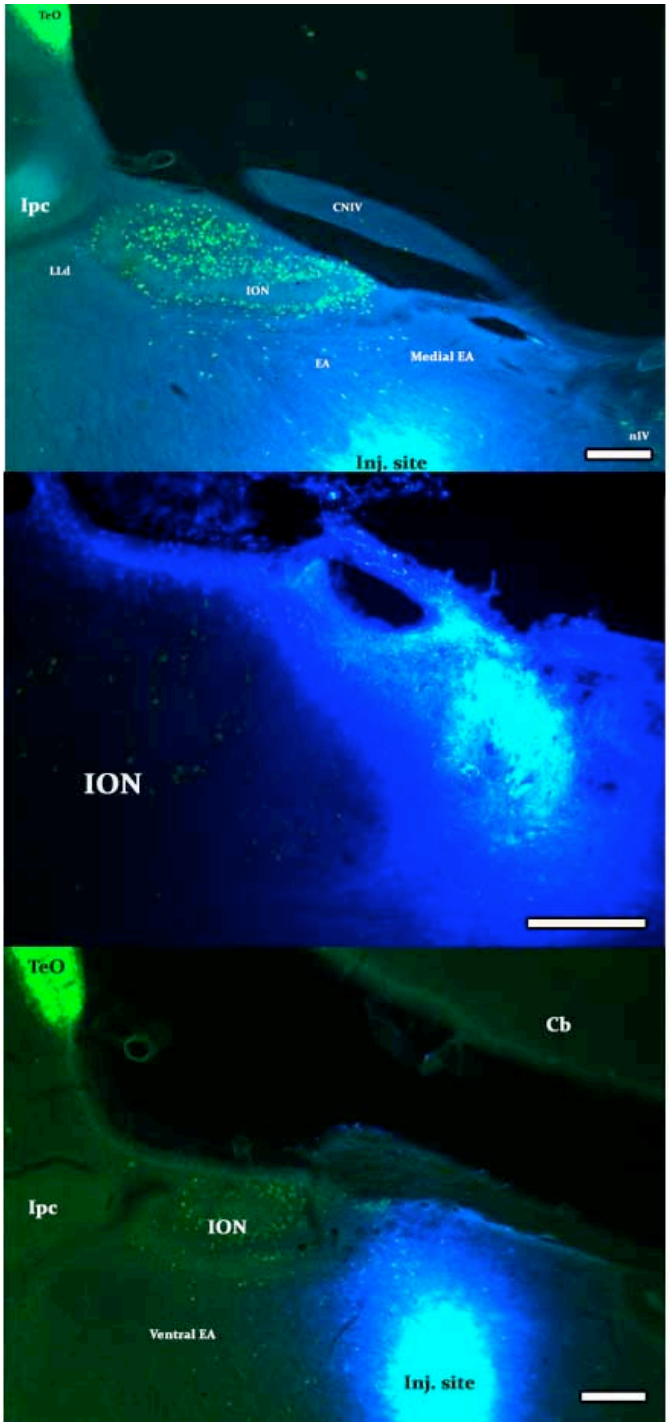

Fig. 9.20. Double tracer 02: Injection sites. FB injection sites. **Case 01**: Deep injection into the VM EA region. **Case 02**: Medial apex of ION and proximal EA region. **Case 03**: VM EA. Tracer was taken up by CNIV fibers of passage. Aq, aqueduct; Cb, cerebellum; CNIV, trochlear nerve; EA, ectopic area; ION, isthmo-optic nucleus; Ipc, nucleus isthmi parvocellularis; LLd, nucleus lemnisci lateralis pars dorsalis; nIV, trochlear nucleus. **Scale bar = 250 *μ*m.**

9.6.1 Injection sites: summary of individual cases

The FB injection site case 01 was in the V/VM EA region, deep into the region of LoC (**Fig. 9.21**). CtB-488 labeling of the contralateral ION/EA was comprehensive. Labeling of ipsilateral EA cells was minimal (2-3) and possibly, no double labeled cells were found as a result. Interestingly, cells double labeled for FB and CtB-488 were present lateral to the injection site, in the region around dorsomedial apex of Ipc, i.e. between Ipc and LLd (**Fig. 9.22**). In case 02 the FB injection site was in the medial ION and M/VM EA region. CtB labeling was robust and the number of ipsilateral EA labeled cells was much greater than in Case 01. In case 03, intra-cranial injection of FB was in the V and VM regions of EA but did not extend into ION (**Fig. 9.23**). CtB-488 labeling of centrifugal neurons of ION and EA was once again substantial.

9.6.2 Double labeling

Only in one case (case 03) was double labeling apparent. Four double labeled neurons were found proximal to the medial border of ION in the AP region where the fibers of CNIV and the TC, that form the roof of the aqueduct, meet the dorsal roof of the midbrain most proximal to ION (**Fig. 9.26**). A fourth double labeled cell was situated proximal to the ventromedial border cells of ION (**Fig. 9.27**).

9.6.3 Interconnectivity

Although double labeling was only evident in one of the 3 cases, numerous examples of close proximity and possible interaction between the two labeled populations of cells were apparent (**Fig. 9.24**).

In addition, a number of long retrogradely labeled FB axons were observed, extending beneath the ventral border of ION. The source of these axons, in one case, was found to be a unipolar cell in the medial EA region midway between ION and the IV nucleus. Its axon

bifurcated proximal to the soma and long axonal branches extended in opposite directions in the horizontal plane; one towards the ventral border of ION, or potentially LLd, and the other towards the midline (**Fig. 9.25 A**). Following injection of FB into the region of LoC, i.e. deeper into the VM EA region than previous examples, a large number of labeled fibers crossing the midline below the aqueduct were apparent (**Fig. 9.23**). The fibers could be traced to FB-labeled soma in the contralateral V/VM EA region. Retrogradely labeled FB cells were also present in the medial EA region proximal to the region where decussating fibers of the IV nerve leave the dorsal roof of the midbrain, however these cells did not appear to be contacted by the same crossing fibers.

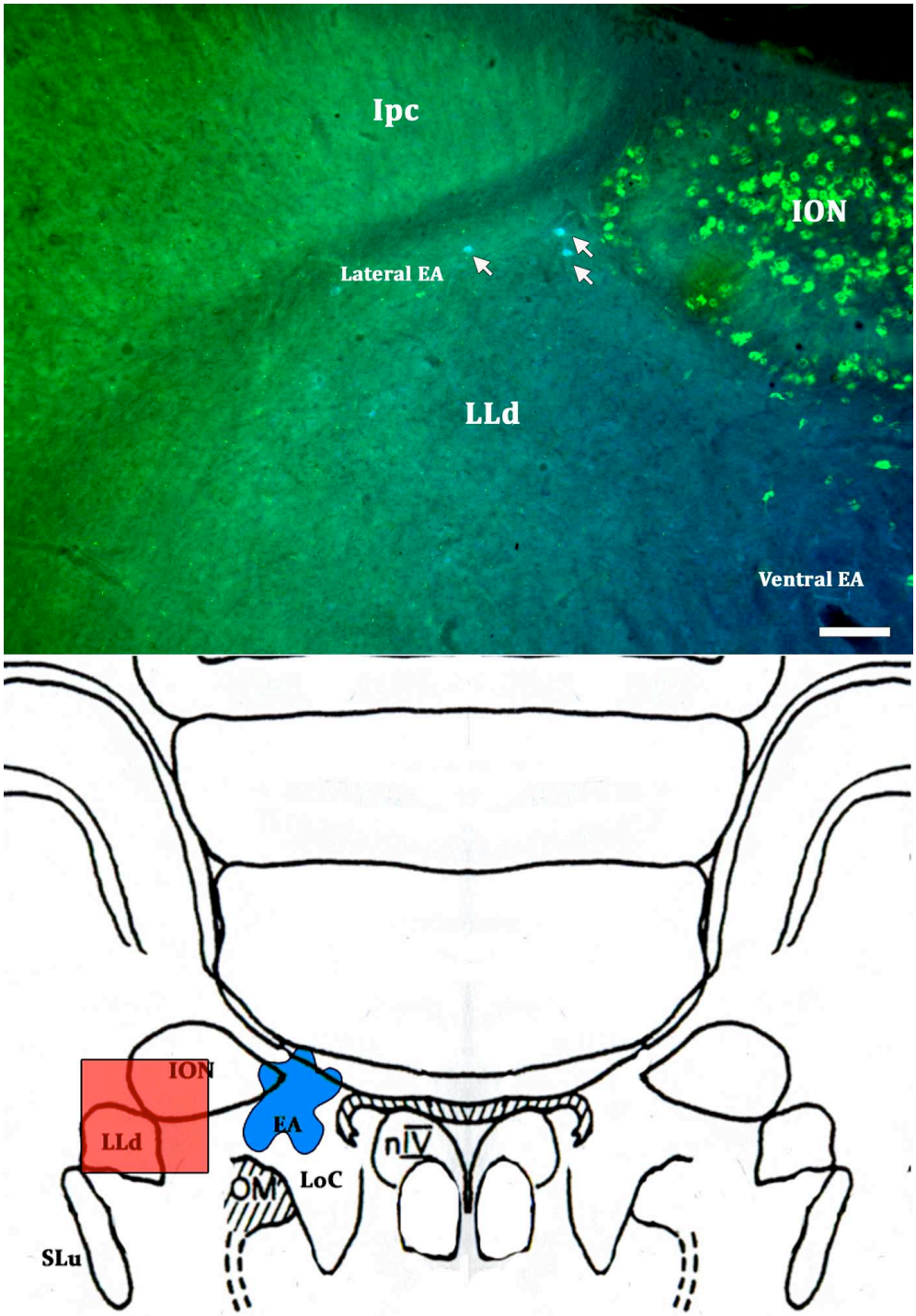

Fig. 9.21. Double labeling ipsilateral to the injection site. Double labeled cells *ipsilateral* to the FB injection site situated between the dorsomedial aspect of Ipc and LLd (**arrows**). Schematic below showing the location of the micrograph relative to the injection site (**blue**). EA, ectopic area; ION, isthmo-optic nucleus; Ipc, nucleus isthmi parvocellularis; LLd, nucleus lemnisci lateralis pars dorsalis. Modified from Karten and Hodos (1967). Note the schematic diagram is not to scale. **Scale bar = 50 μm.**

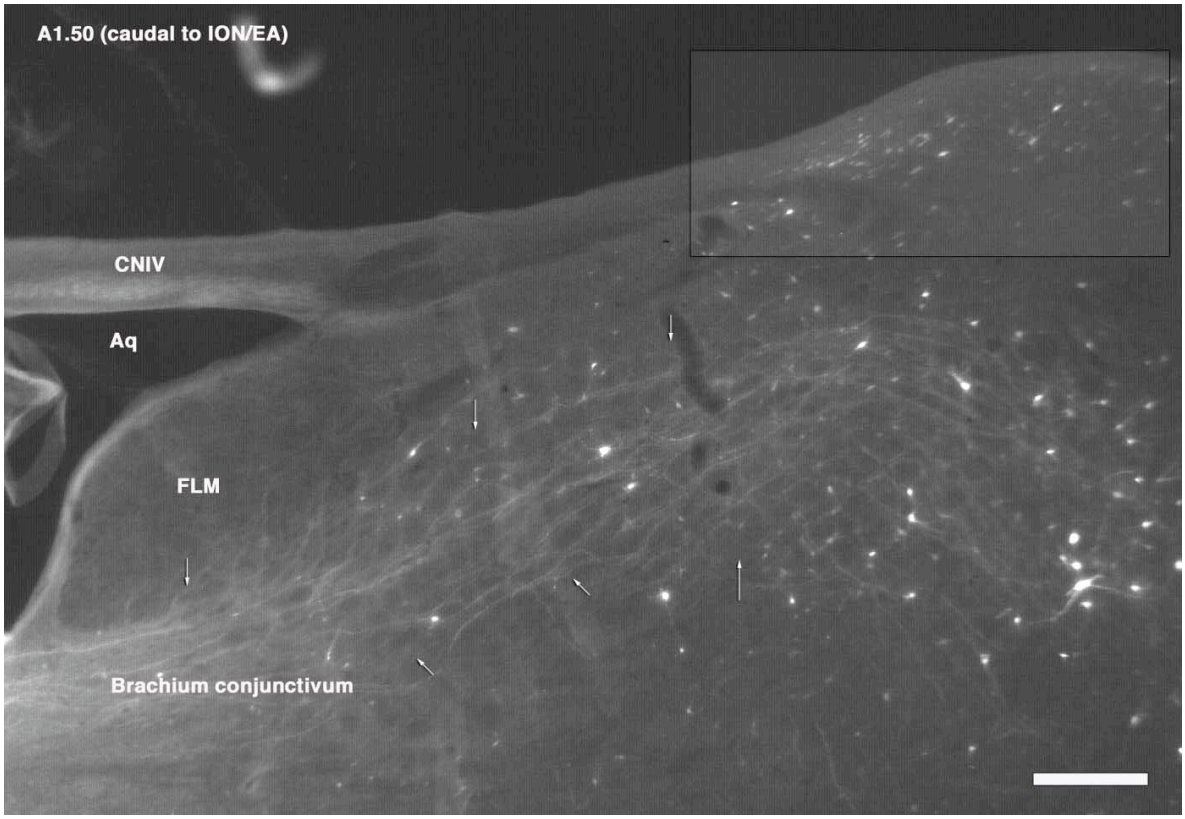

Fig. 9.22. Uptake by fibers of the brachium conjunctivum. FB labeled axons projecting from the injection site in the contralateral M and VM EA region across the midline to the contralateral EA region (**arrows**). Shaded region identifies a separate group of FB-labeled cells that do not appear to project via this pathway. See Fig. 9.28 for further description of the path taken by the brachium conjunctivum. Aq, aqueduct; CNIV, decussation of the trochlear nerve; FLM, fasciculus longitudinalis medialis. **Scale bars = 250 μm**.

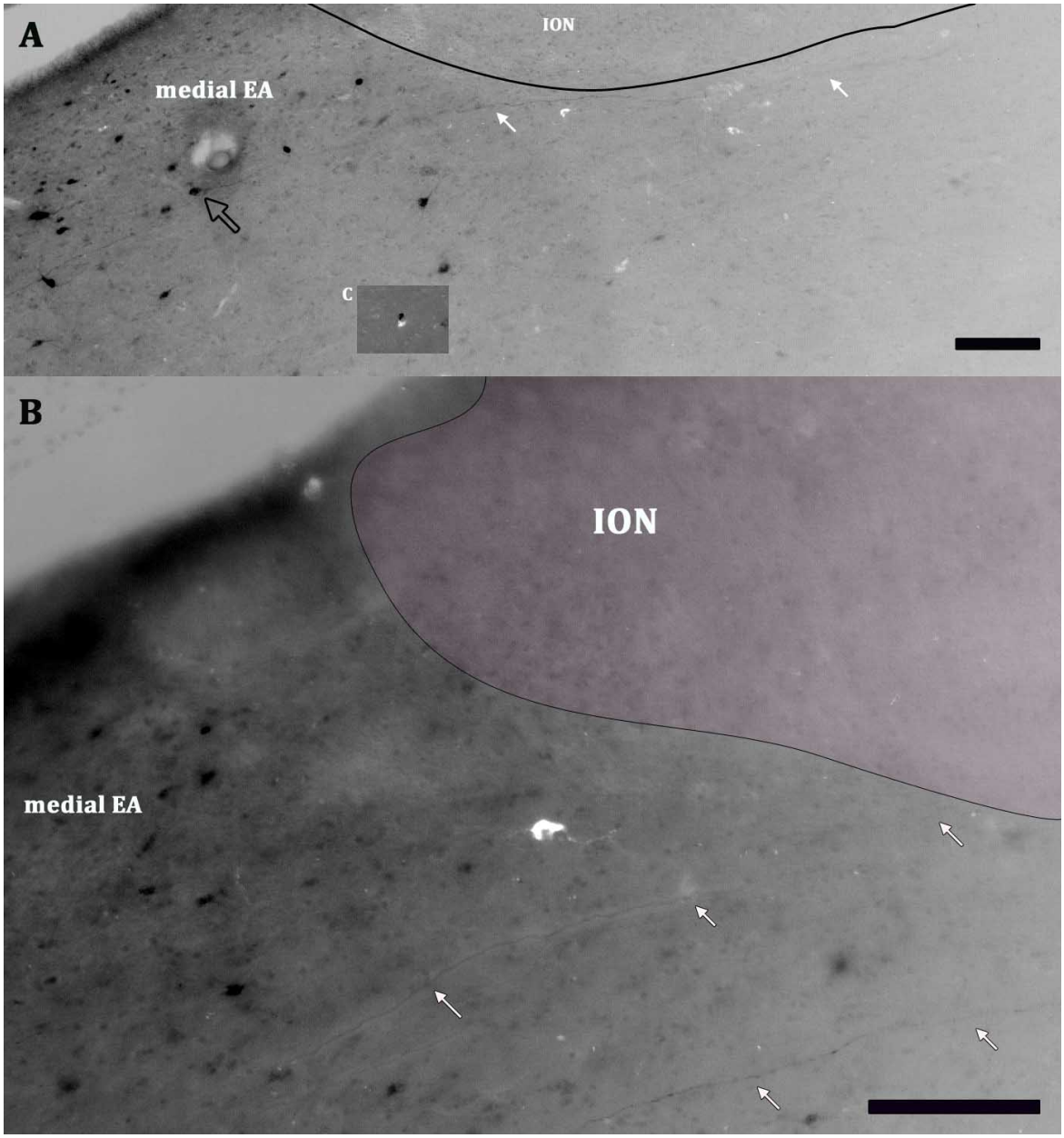

Fig. 9.23. Long axonal projections of FB-labeled cells in the contralateral medial EA. (**A**) An FB labeled unipolar cell (**hollow arrow**) whose axon bifurcates proximal to the soma, with each branch extending horizontally in the coronal plane. Highlighted region shows another example of the 2 populations overlapping in distribution. (**B**) Large ipsilateral EA cell on the ventromedial border of ION (**white cell**). Note the FB labeled long axons passing beneath the ventral border of ION in **A** and **B** (**white arrows**). EA, ectopic area; ION, isthmo-optic nucleus. **Scale bar = 100 μm.**

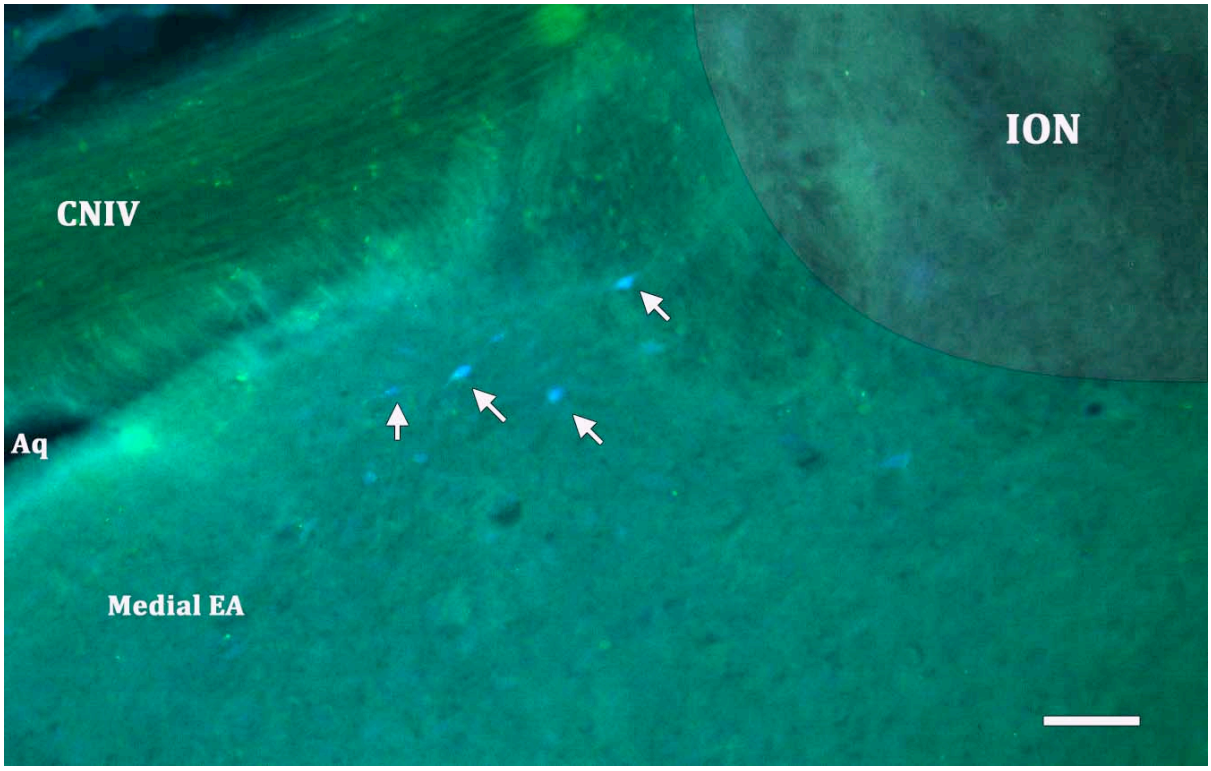

Fig. 9.24. (See overleaf for figure legend)

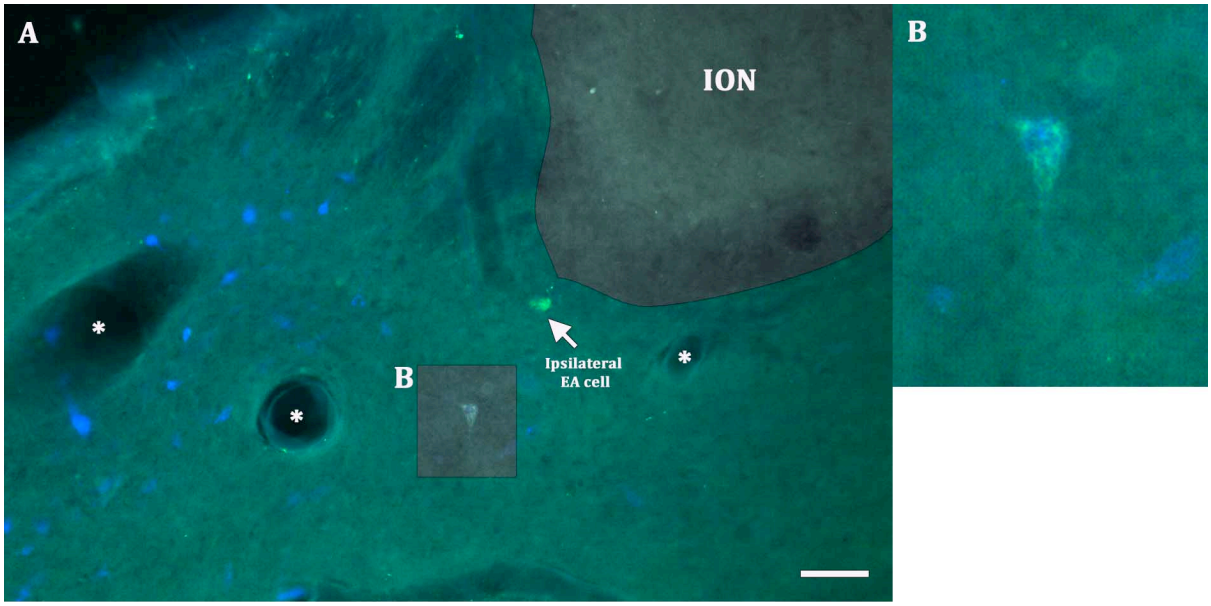

Fig. 9.25. (See overleaf for figure legend)

Fig. 9.24. Case 03: Double labeling contralateral to the injection site. FB and CtB-488 double labeled cells in the medial EA region on the side of the midbrain contralateral to the FB injection site (**arrows**). Aq, aqueduct; CNIV, trochlear nerve; EA, ectopic area; ION, isthmo-optic nucleus. **Scale bar = 50 μm**.

Fig. 9.25. Case 03: Double labeled cell contralateral to the injection site. (**A**) M/VM EA region with two ipsilateral EA cells, one of which is double labeled. (**B**) Inset of double labeled cell corresponding to highlighted region in **A**. EA, ectopic area; ION, isthmo-optic nucleus. **Scale bar = 50 μm**.

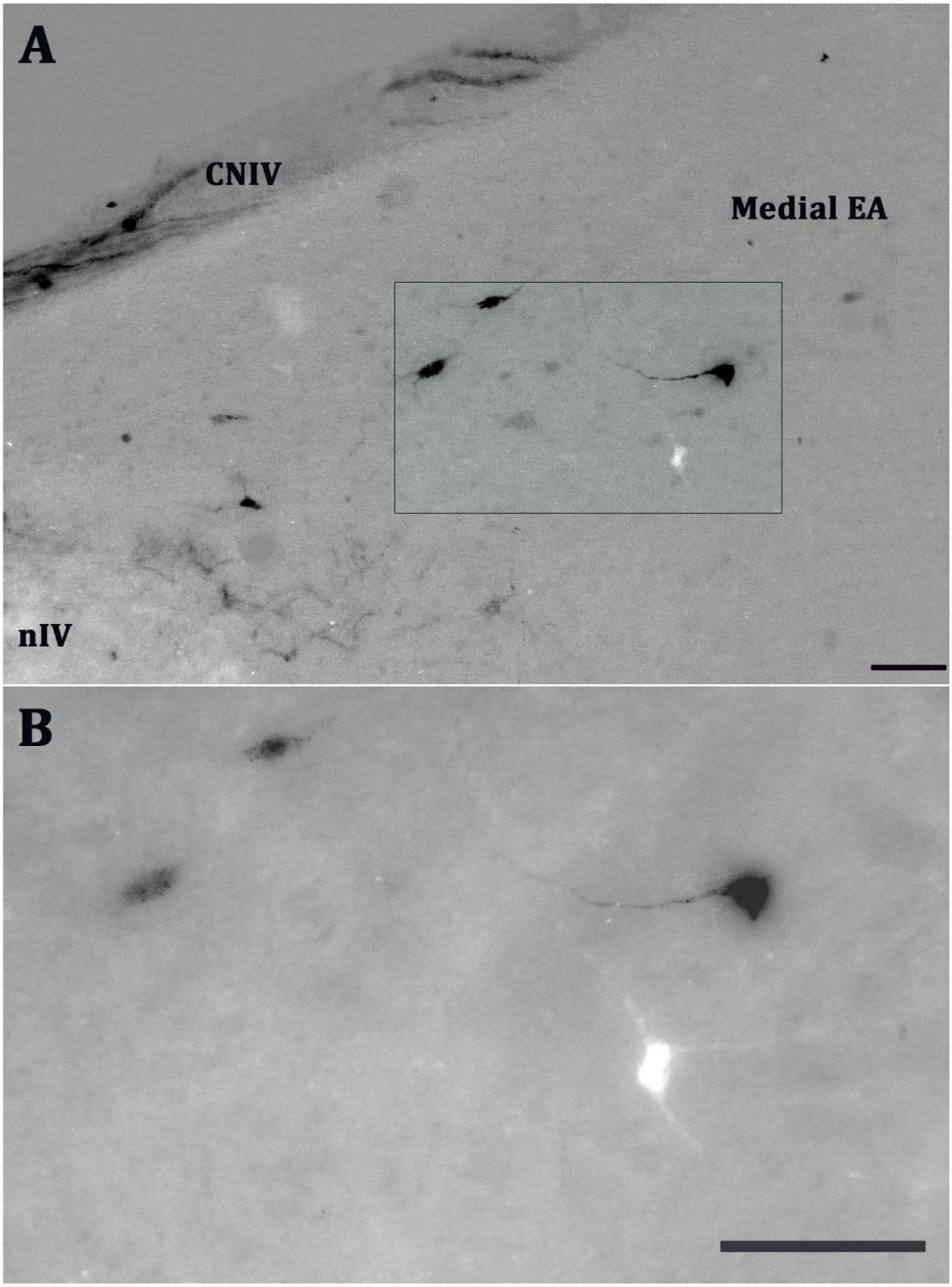

Fig. 9.26. Case 03: Interaction between FB and CtB-488 labeled cells. (**A**) Close proximity of CtB-488 and FB-labeled neurons in the medial EA region proximal to the IV nucleus. (**B**) High magnification inset of highlighted region in **A**. CNIV, trochlear nerve; EA, ectopic area; nIV, trochlear nucleus. **Scale bar = 50 μm**.

9.7 Discussion

These results, while not conclusive, raise a number of previously unasked questions relating to the organisation and connectivity of centrifugal EA cells [22]. The distribution of EA cells is not uniform, with particular localised regions surrounding the ION showing higher EA cell density than others. Moreover, specific areas, e.g. ventromedial to the ION border, have a consistently high EA cell density within species (in this case, the chicken). Logically, a conserved non-uniform distribution such as this implies that the location of a given population defines its role. All EA cells have a common feature, that is they all project an axon to the retina. Therefore, their location in the midbrain relative to the ION may determine a separate variable, e.g. afferent input. The initial aim of this study was to define subpopulations of EA cells and characterise them based upon afferent input.

9.7.1 *Do EA cells receive tectal (i.e. indirect visual) input?*

Although the ION is known to receive a predominantly indirect retinal input via the TeO, the question of whether EA cells receive a common input to ION had not been addressed. Here, we show that injection of a monosynaptic pathway tracer into a specific region of the EA (M and VM regions), that excludes ION, does not retrogradely label tecto-isthmic neurons. As expected, however, when there was tracer uptake by ION neurons, tecto-isthmic cells were labeled. Thus, although this finding does not exclude the possibility that other regions of EA receive afferent input from TeO, or that EA cells receive *indirect* TeO input, it does suggest that at least EA cells medial and ventromedial to ION receive predominantly, if not exclusively extratectal input. These findings are supported by the incidental results of Woodson et al. (1991) whose investigation into TeO-ION connectivity showed that control injections of tracer into tegmental regions surrounding ION, i.e. EA, which included medial, rostral and caudal EA regions, did not retrogradely label TeO. In the same study, a control injection into the ventrolateral EA region did label cells in superficial

layers of TeO. However, contrary to the view of Réperant et al. (2006), our findings in the pigeon (as well as chicken) are that this is not a region of high EA cell density and, in fact, the labeling in TeO could be explained by uptake of tracer by nearby isthmic structures, e.g. Ipc or SLu (Woodson et al., 1991; Hellmann et al., 2001).

9.7.2 Extratectal EA afferents

Having established EA cells do not receive visual input, i.e. from TeO, the next logical step was to investigate the actual afferents to EA cells. Technically, this raised a number of difficulties. For example, while trans-synaptic pathway tracing following intravitreal injection of RITC has proven a valuable tool in elucidating centrifugal cell afferent input, it does not distinguish ION from EA afferents. Moreover, injection of pathway tracers directly into the ION poses its own difficulties (such as confining the spread of the injection site to the ION and not surrounding structures such as EA). Nevertheless, if successful, one can then be confident in concluding that the resulting retrogradely labeled region (e.g. TeO) is an afferent source for centrifugal neurons. As EA neurons are intermingled with other non-centrifugal cells, even tracer injections directly into EA inevitably include cells that do not project to the retina. Therefore, one would have to consider the afferent input to regions with which the EA overlaps, i.e. GCt and LoC, in the interpretation of retrograde labeling. Following intracranial injection of the retrograde pathway tracer Fluoro-Gold into ION, Miceli et al. (1997) identified several extratectal sources of ION afferentation including the area ventralis of Tsai (AVT), the region surrounding the oculomotor complex, the mesencephalic and pontine reticular formation and nucleus linearis caudalis (LC). Here, we consider three further possible sources of afferent input, labeled following injections of FB into (but not restricted to) EA.

9.7.3 Interpretation of tracer labeling

Investigatory experiments into potential sources of EA afferents though injection of FB into

the M and VM EA region, i.e. the region of highest cell density, highlighted three regions of interest (**Section 9.3**). Retrograde labeling was identified ipsilaterally in Ipc (as well as in chicks following intravitreal injection of the transneuronal retrograde tracer, WGA), bilaterally in LLd and contralaterally in the M and VM EA regions (i.e. GCt and LoC, respectively).

9.7.3.1 n. isthmi parvocellularis (Ipc)

The first region, Ipc, is a member of the isthmic complex that receives a topographic reciprocal projection from layers 10/11 of TeO (Woodson et al., 1991). As well as the single pigeon case in which retrograde labeling was observed, Ipc is consistently labeled following intravitreal injection of WGA in the chick. As Ipc does not contain centrifugal neurons, the possibility exists that Ipc labeling was achieved by trans-neuronal transport via ION/EA and therefore represents a potential source of afferent input to centrifugal neurons.

By comparison of the potentially trans-neuronal retrograde labeling of WGA with the retrograde labeling of a tracer known to be transported only mono-synaptically, i.e. CtB, one can, with a degree of confidence, discern trans- from mono-synaptic labeling. In practice, WGA labeling in sham-operated control chicks from the experiments described in **Chapters 6** to **8** was available to be compared with online chick brain sections prepared following intra-vitreal injection of CtB (Karten, Brainmaps.org). Following CtB labeling, no Ipc labeling was found. While this finding is evidence for Ipc-ION/EA connectivity, the alternative possibility is that Ipc somata were labeled following indirect trans-neuronal retrograde transport via an ION-TeO-Ipc pathway exists. Miceli et al. (1993) observed similar Ipc labeling following intravitreal injection of RITC, however, when RITC was combined with KA (to prevent anterograde transport (**Section 9.0**)), Ipc labeling was absent. They suggested that a tracer that is transported anterogradely (e.g. RITC and WGA) to primary visual centres, e.g. TeO, may 'leak' out and be taken up by nearby TeO efferent cells

and/or afferent terminals before being subsequently transported retrogradely to Ipc in a presumably visual Retina-TeO-Ipc pathway.

Furthermore, caution is warranted in any interpretation of ION/EA-Ipc labeling following FB injection in the pigeon. Ipc labeling was only evident in one case in which the injection site spread to include both the ION and the tectal commissure. As mentioned above, Ipc exhibits reciprocal connectivity with TeO, thus uptake of FB by tectal neurons innervated by Ipc could explain the labeling observed. In summary, the lack of consistent labeling in Ipc between animals as well as the alternative possible explanations mentioned above raise sufficient doubt that a direct connection of Ipc with ION or EA exists.

9.7.3.2 n. lemnisci lateralis pars dorsalis (LLd)

In two pigeons, an FB injection into the medial EA/ION led to bilateral retrograde labeling of LLd. LLd receives input from ascending input that ascends from auditory nuclei of the caudal brainstem en route to n. mesencephalicus lateralis pars dorsalis (MLd), the avian homologue of the mammalian inferior colliculus (Karten, 1967). MLd is situated medial to the tectal ventricle and rostral to ION, and projects via the tectal commissure to the contralateral MLd. LLd also receives input from ascending fibers of the lateral lemniscus pathway that course in the mediolateral plane of ION (Conlee and Parks, 1986) (**Fig. 9.29**). As a result, ipsilateral labeling of LLd may have been a result of uptake by fibers of the lateral lemniscus that passed close to the injection site. LLd labeling was only found in two cases whose injection sites were positioned further lateral within the midbrain, i.e. they encompassed more of ION than those that did not label LLd. Labeling of the contralateral LLd is unexplained by the literature, however neurons within the nucleus appeared to project branches towards the decussating fibers of the tectal commissure, raising the possibility that a tract connecting the LLd on either side of the midbrain may have been present. It seems unlikely that ION/EA receive auditory information, however, given the

location of centrifugal neurons within the path of ascending auditory information and proximity to LLd, it is an interesting possibility.

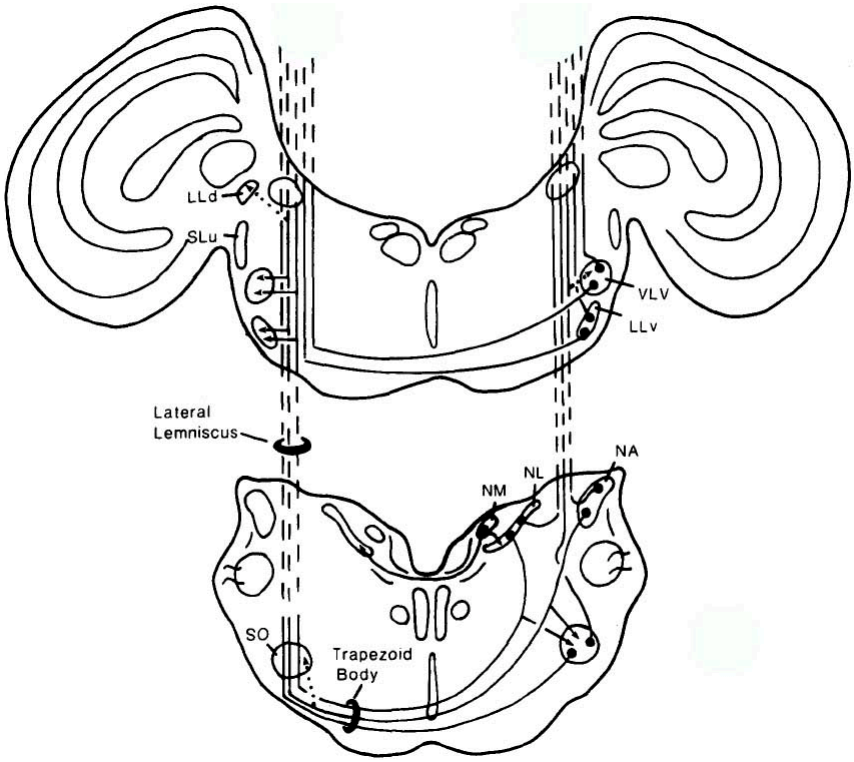

Fig. 9.27. Anatomy of the ascending auditory pathway. Bilateral retrograde FB labeling was observed in LLd following intra-cranial injection into IONEA. This figure shows the path of ascending auditory information from the caudal brainstem to the midbrain at the level of ION. Note the position of ION within the lateral lemniscus and its proximity to LLd. The proximity of the ION and the LLd suggests that tracer spread may have been the cause of the observed labeling. Taken from Conlee and Parks (1986).

9.7.3.3 Contralateral EA region (GCt, LoC)

The third region of interest, identified as being labeled after injection of FB into the medial EA, i.e. within the EA of the contralateral midbrain hemisphere (**Section 9.3.2**), was unexpected. Careful examination of some past studies reveals occasional reference to inter-ION or EA connectivity, including a report of a single EA cell whose axon looked as though it was projecting towards the contralateral ION/EA region (Hayes and Webster, 1981).

However, the idea that there may be cross talk between ION or EA has never been explicitly investigated. One of the more intriguing aspects of the initial finding reported here was that injection of tracer into the CNIV alone was sufficient to label the population of cells in the contralateral EA region. Crucially though, if the injection was independent of the CNIV (as confirmed by the absence of labeling in the contralateral nIV), the population of labeled neurons was still present in the contralateral EA region. This finding (**Section 9.6.1**) suggested that axons of crossing fibers (i.e. visualised containing FB), may take advantage of the nearby pathway of decussating CNIV fibers that combine with commissural fibers to form the roof of the aqueduct. That being said, a puzzling feature of the labeling pattern following injection of FB into CNIV alone was that retrograde labeling of cells in the EA region was only found contralaterally. Under the assumption that between-hemisphere EA interconnectivity is bidirectional, one would expect an injection of CNIV would be taken up by fibers travelling in both directions.

Given the intermingling of EA cells within a number of peri-ION regions (e.g. GCt, LoC, etc.), it is important to consider the connectivity of these regions in the interpretation of retrograde labeling after injection into EA regions. Following deeper injections of FB into the V/VM EA region, FB labeled fibers were observed to cross the midline beneath the aqueduct, immediately ventral to the fasciculus longitudinalis medialis (FLM), (a major fiber tract situated immediately beneath the IV nucleus). Fibers crossing beneath the FLM were identified as those of the brachium conjunctivum (BC) (Karten and Hodos, 1967). The BC contains, among others, deep cerebellar nuclei efferents that decussate at the level of ION ventral to the FLM before forming an ascending fiber bundle that projects fibers to GCt, LoC and nIV as well as a descending bundle that projects to the pontine and lateral reticular formation (Arends and Zeigler, 1991) (**Fig. 9.29**). Injections of FB deep into the VM EA led to uptake by fibers of passage of the BC and the distinctive labeling of large populations of cells throughout the contralateral midbrain found in **Fig. 9.22**. However, more superficial

injections (i.e. those that were not in the path of BC fibers) into the medial EA, i.e. GCt, or even the CNIV alone were still found to label cells of the contralateral EA. For this reason, BC fiber uptake does not fully explain the contralateral EA labeling in M and VM EA regions proximal to ION.

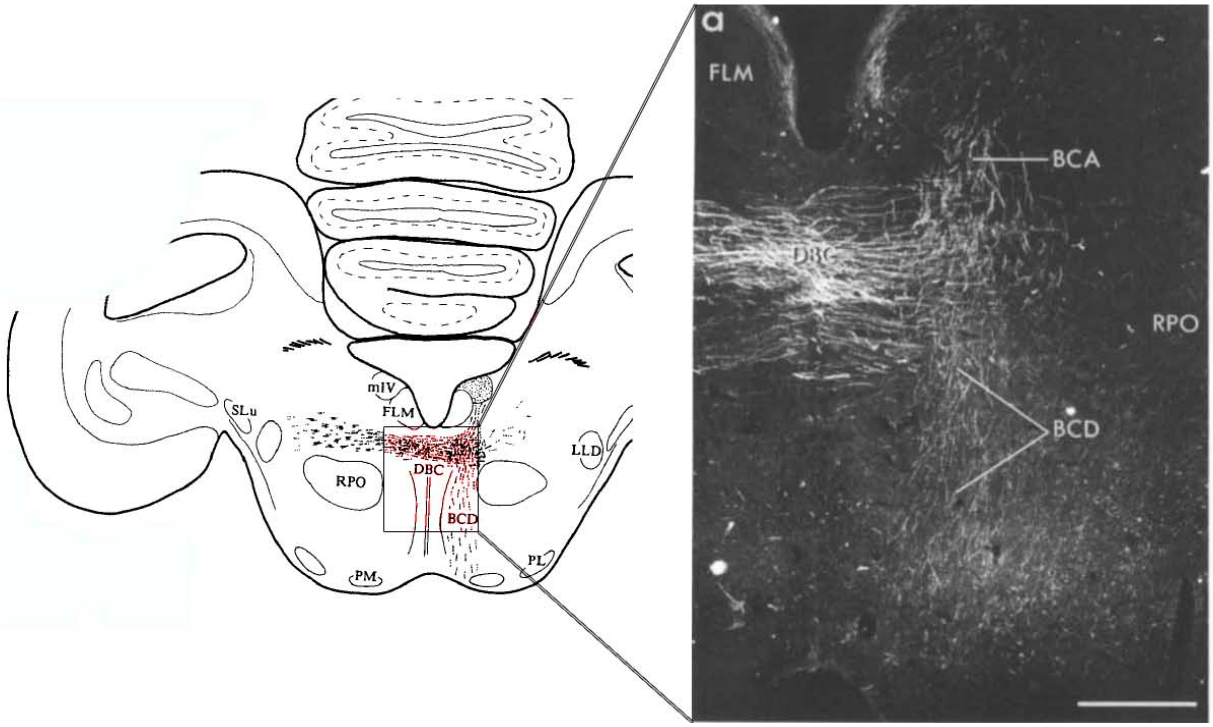

Fig. 9.28. Crossing fibers of the brachium conjunctivum (BC). Labeling of decussating fibers of the BC following injection of an anterograde pathway tracer into deep cerebellar nuclei. BCA, brachium conjunctivum ascending; BCD, brachium conjunctivum descending; RPO, pontine reticular formation; FLM, fasciculus longitudinalis medialis. Modified from Arends and Zeigler (1991). **Scale bar = 500 μm.**

Ascending projections to the visual wulst (VW) arise from midbrain regions including GCT, LoC, serotonergic cells of the nucleus linearis caudalis (LC), as well as AVT (Kitt and Brauth, 1986). The possibility exists that retrograde labeling in these regions followed tracer uptake by ascending fibers of passage from these brainstem areas. However, following injection of retrograde pathway tracer into VW, these regions are labeled entirely *ipsilaterally* (Bagnoli and Burkhalter, 1983). Thus uptake of tracer from these fibers of passage cannot explain the

retrograde labeling observed in this case, i.e. in the midbrain contralateral to the injection site. Having said that, in a separate parallel study, as well as concordant retrograde labeling in LoC and GCt, labeling of cells within and around the border of the *contralateral* nIV were observed (Wild, 1987) (**Fig. 9.32**). Thus, the possibility that tracer uptake by fibers of passage of ascending midbrain efferents contributed to contralateral EA region labeling cannot be excluded.

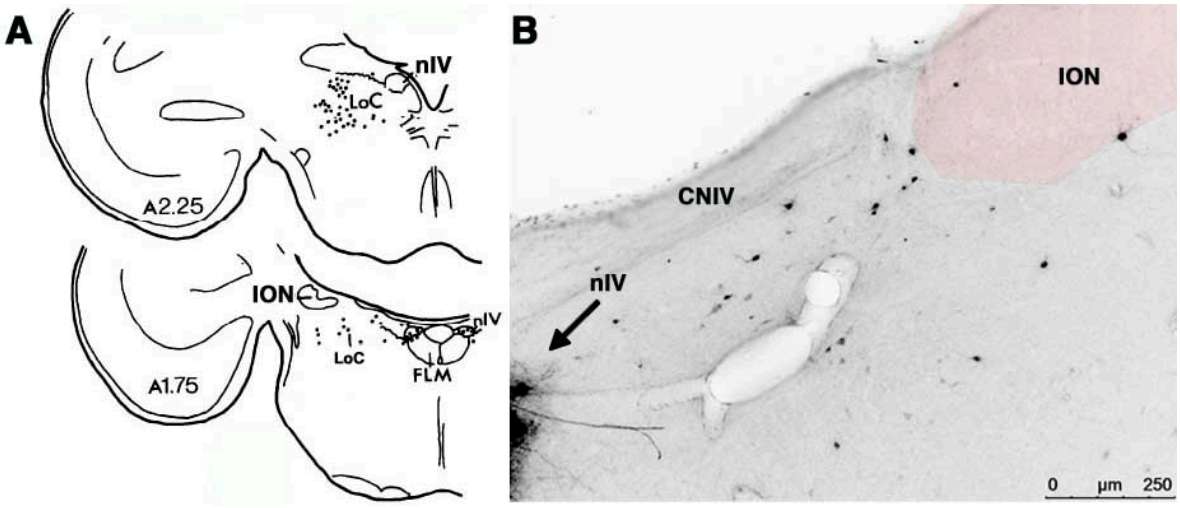

Fig. 9.29. Distribution of cells projecting to the thalamus in the pigeon midbrain. A) Distribution of retrogradely labeled cells following injection of the thalamus in the left hemisphere of the pigeon. All mesencephalic labeling was ipsilateral to the injection site. (Wild, 1987). **B)** Distribution of retrogradely FB-labeled neurons following injection of the media EA (for comparison). CNIV, trochlear nerve; FLM, fasciculus longitudinalis medialis; ION, isthmo-optic nucleus; LoC, locus ceruleus; nIV, trochlear nucleus.

9.7.4 Characterisation of a novel contralateral EA population

Following up on single tracer experiments, we employed a second tracer in an attempt to remove some of the uncertainty concerning the initial interpretation of the labeling of those cells labeled in the contralateral EA and to provide some insight into their role in CVS connectivity. Specifically, we wanted to investigate two possible explanations:

1. EA cells on one side of the midbrain project axon collaterals across the midline via the roof of the aqueduct to contact centrifugal EA cells in the contralateral midbrain.

To test this, in addition to an injection of FB into the medial EA, a second tracer, CtB-488 was injected intra-vitreally into the eye *ipsilateral* to the side of the intra-cranial injection of FB into EA. Thus, ION and EA neurons would be labeled by CtB-488 in the midbrain hemisphere *contralateral* to the FB injection.

The findings of this first paradigm were inconclusive. Taken together in 3 birds, only a single double labeled cell was found. However, numerous examples of the two labeled populations of cells in close proximity and even on top of one another within the same section were observed (**Fig. 9.17**). While it was not possible to visualise actual synapses between the two populations, single FB labeled cells were often seen to project 2-3 branches in the direction of 2-3 CtB-488 labeled ION or EA cells (**e.g. Fig. 9.17**), i.e. they appeared to be associated rather than obviously independent. Excluding the single double labeled ION cell and, assuming methodological issues that might interfere with double labeling did not play a role, it is likely that EA cells that project to the contralateral retina *do not* send axon collaterals to the contralateral EA within the midbrain.

2. A proportion of those cells labeled in the contralateral EA constituted the population of ipsilateral EA cells.

Up to 96 ipsilateral EA cells have been reported in the pigeon (Wolf-Oberhollenzer, 1987), and while far fewer have been encountered during this study (~30 cells), even the higher figure would not account for all of the labeled FB cells observed contralateral to the FB injection site in the M and VM EA regions. The approach used here was identical to the previous paradigm, except that in this case, the intravitreal injection of CtB-488 was made into the eye *contralateral* to the FB injection into EA. Thus, the population of ipsilateral EA cells would be labeled in the

region of interest (i.e. in the opposite side of the midbrain to which the FB injection was made).

The findings of the second tracer combination experiment were similarly ambiguous. In one bird, 4 double labeled ipsilateral EA cells were found while in the other 2 birds, no double labeled cells were observed. Once again, FB labeled cells were often found in close proximity to ipsilateral EA cells but, they were only rarely double labeled.

Two possible explanations exist for the few observed double labeled cells in the ipsilateral EA population. The first is that ipsilateral EA cells project axons bilaterally, innervating both eyes. However Wolf-Oberhollenzer (1987) found no evidence of this in the pigeon following bilateral intravitreal injection of two fluorescent tracers. The second explanation is that ipsilateral EA cells take a double-decussation pathway to the ipsilateral retina, i.e. decussating with fibers of the tectal commissure in the midbrain and recrossing at the optic chiasm. As mentioned in the introduction (**Chapter 1**), such a (possibly transient) pathway has been described in retrograde degeneration studies in the developing chick visual system (O'Leary et al., 1983) (**Fig. 9.30**). While no firm conclusions can be made as a result of the inconsistency in the occurrence of double labeled cells between birds, the possibility that ipsilateral EA axons take a double crossed pathway can not be ruled out based on these results.

Although the biological implications of a double crossed ipsilateral EA pathway are not immediately obvious, defining the ipsilateral EA pathway is crucial when considered in the context of interpreting the experiments reported here. As has been alluded to in previous chapters, the existence of the ipsilateral EA pathway in studies of the CVS is a complicating factor. In studies, such as those described in **Chapters 6** to **8**, a lesion of the IOTr disconnects the contralateral, *treated* retina from the ION/EA. However, under the assumption that the ipsilateral EA tract remains uncrossed at the optic chiasm, the *treated*

eye would still receive its normal ipsilateral EA input. Conversely, the *control* eye would have an intact contralateral ION/EA input, but its ipsilateral EA input would be disconnected. If, however, as we propose, ipsilateral EA axons cross within the midbrain via the tectal commissure to join the contralateral IOTr, the interpretation of an IOTr lesion would be different. The *treated* eye would have been disconnected from *both* contralateral ION/EA and ipsilateral EA pathways while the *control* retina would still have both pathways intact.

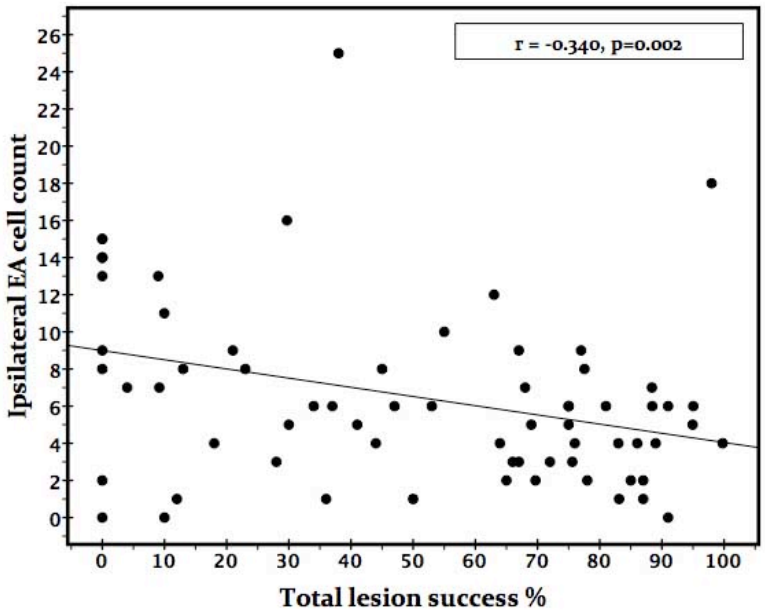

Fig. 9.30. The effect of IOTr lesion on the number of WGA-labeled ipsilateral EA cells. The above figure shows the relationship between lesion success from chicks in the preceding chapters and the number of ipsilateral EA cells that were retrogradely labeled. Theoretically, if the ipsilateral EA pathway simply remained uncrossed at the optic chiasm, there would be no effect on the number of neurons that were retrogradely labeled. Here we see a highly significant negative relationship, suggesting that lesion of the IOTr did affect the number of ipsilateral EA cells that were labeled. This provides evidence towards an alternate pathway for the ipsilateral EA pathway, potentially via the double decussation pathway discussed here. WGA labeled ipsilateral EA cell count (from a 1:3 series) plotted against total percentage lesion success in chicks from the experiments in **Chapters 6-8**.

Interestingly, following analysis of labeled ipsilateral EA cell numbers in the chick WGA brains obtained from the experiments described in **Chapters 6** to **8**, a highly significant negative correlation was found between ipsilateral EA cell number and total percentage lesion success ($F_{1,66}$ = 8.625, p=0.005) (**Fig. 9.30**). While under the previously assumed pathway (**Fig. 9.31**) one would not expect the ipsilateral EA cell number to be affected by a lesion of the contralateral IOTr, a significant decrease in the number of ipsilateral projecting EA cells contralateral to IOTr lesion suggests that an alternative pathway for ipsilateral EA axons (such as the double-decussation route) is a more likely scenario.

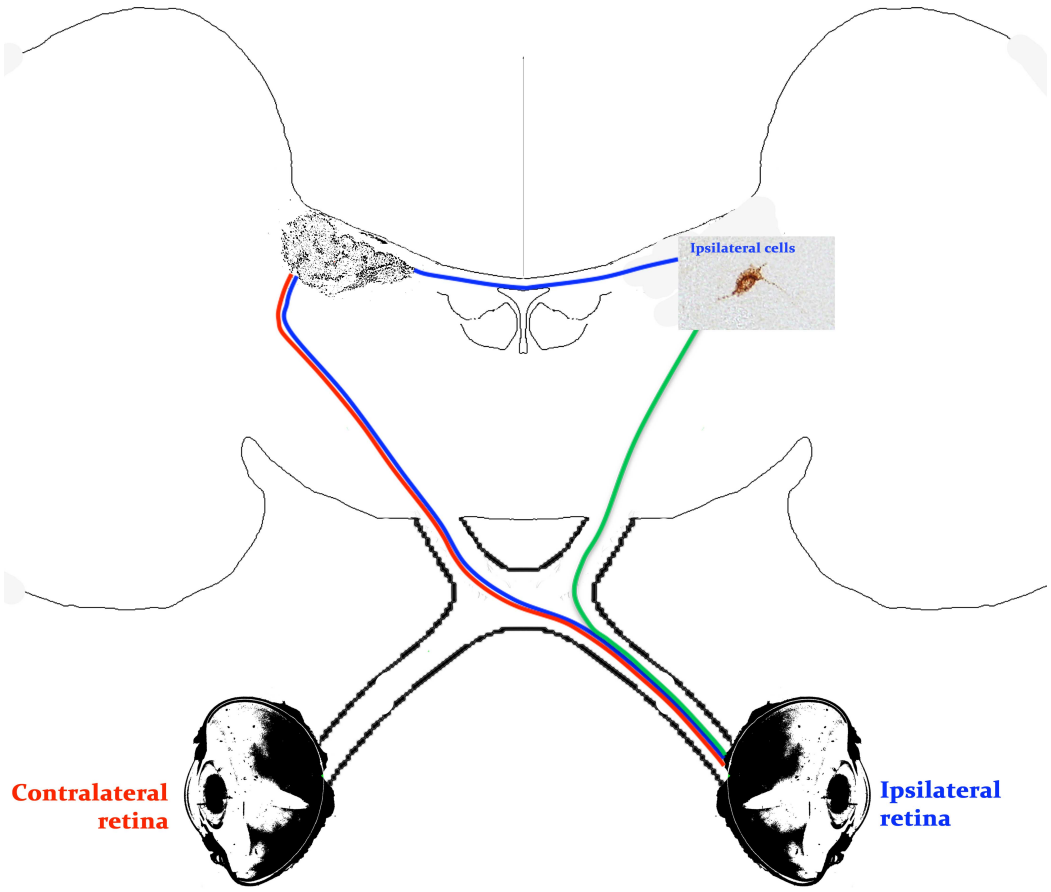

Fig. 9.31. Possible paths of the ipsilateral EA projection. (**Green**) The assumed pathway of EA cell axons to the *ipsilateral* retina. (**Blue**) The potential 'double decussation' pathway of ipsilateral axons, which cross the midline in the midbrain and join the axon fiber bundle of centrifugal cells projecting to the *contralateral* retina (**red**).

Finally, concerning the frequent apparent association between FB and CtB-488 labeled populations, the EA region, specifically that corresponding to LoC and GCt, receives numerous inputs, some of which have already been alluded to. Furthermore, the EA region as a whole shows highly complex neurochemical immunoreactivity. Medina et al. (1998) attempted to elucidate the neurochemical properties of EA centrifugal cells specifically by combining retrograde labeling with RITC and immuno-fluorescence for 23 different neuropeptides/neurotransmitters. They found that cells in the EA *region* were immunoreactive for 17 of the 23 antibodies tested, including: choline acetyl transferase (ChAT), nitric oxide synthase (NOS), tyrosine hydroxylase (TH) and serotonin (5-HT). However, no EA centrifugal *cells*, i.e. centrifugal neurons, were found to be double labeled!

Those neuropeptides most prominent, or exclusive, to the ventromedial EA region of interest in this study included 5-HT, TH and vasoactive intestinal peptide (VIP). Drawing parallels with the findings of this study, Medina et al. (1998) noted that, although no centrifugal EA cells were double labeled, they observed frequent interaction of EA centrifugal cells with a number of the various immuno-labeled populations.

9.7.5 Functional implications

The rich and diverse nature of the immunoreactivity in the EA region is in keeping with the 'widespread' terminal fields of EA cell efferents within the retina, i.e. divergent efferent fibers (Woodson et al., 1995; Medina et al., 1998). Thus, EA cells may have a more general role in the regulation of arousal, awareness and potentially sleep/wake cycles in the retina (Miceli, Medina and Réperant, 1995a). In this study we have identified a subpopulation of cells within the EA that exhibit connectivity between opposite sides of the midbrain and therefore might play a role in modulating control of ocular dominance through the direct midbrain-retina connection of centrifugal EA cells. Furthermore, if this were the case, EA may act to localise a broad region(s) of awareness (i.e. 'area codes') for the subsequent

topographic fine control of the restricted efferent fibers of ION cells.

9.8 Conclusion

In this chapter, the question of afferent input to centrifugal ectopic neurons has been addressed. One major finding of this work is that, while the isthmo-optic nucleus receives predominantly retinal input via the optic tectum, the EA does not. It is important to qualify this statement as only specific (ventro-medial and medial EA) regions were investigated. Thus it may be the case that other regions of the EA do receive tectal afferents. That being said, this finding is important in distinguishing the two populations of centrifugal neurons. Given the morphological and neuro-architectural difference in the two populations, i.e. ION and EA, I propose that while the ION receives predominantly visual input, EA cells receive local input that is specific to their position in the midbrain tegmentum. Medina et al, (1998) demonstrated the diversity in neurochemistry within the midbrain tegmentum, raising the possibility that EA distribution is not chaotic, as first thought, and is in fact highly organised such that a specific locus relative to ION pertains to specific local inputs and neurochemical signatures that govern specific intra-retinal mechanisms, perhaps regulating circadian fluctuation in neurotransmitter concentration within the retina for instance.

Following up on this hypothesis, an investigation into the specific connectivity of the medial/ventromedial EA raised the possibility of a cross talk projection between populations of centrifugal neurons on either side of the midbrain through retrograde labeling of a population of neurons in the EA on the contralateral side of the midbrain, effectively within the mirror image of the injection site. While the double-tracer paradigms did not show conclusively whether, or not, a cross-talk pathway exists, the overlapping distributions of retrogradely labeled FB neurons and centrifugal neurons described in Sections 7.5 and 7.6, did not refute the possibility entirely. The possibility remains that an interneuron population mediates what is presumably an inhibitory cross-talk pathway. If this were the

case, the mono-synaptic nature of the pathway tracers used would have precluded the possibility of double-labeling.

A second possibility was based around the idea that the ipsilateral EA pathway took a more convoluted, double crossed pathway to the ipsilateral retina. While double labeled ipsilateral EA neurons were present, this finding was inconsistent between cases and unconvincing. The fact that O'Leary (1987) had previously demonstrated that such double-crossed pathways existed during embryological development in the chick was intriguing. While the ipsilateral EA projection is numerically minor, it remains a particularly inconvenient consideration in the interpretation of lesion studies, for instance, i.e. it precludes a direct treated/control eye comparison. Indeed, the significance of the ipsilateral EA pathway may be underestimated. The finding that under constant light conditions, lesion of the IOTr led to a reduced rate of growth in the ipsilateral eye (**Chapter 7**) was one such example of the difficulties the pathway imparts upon interpreting lesion studies.

While the conclusions from this part of the study are not as clear as one would have hoped, it has raised a number of important questions that, in answering may provide important anatomical clues in the effort to establish the functional basis of the centrifugal pathways.

Chapter 10

General discussion and future work

10.0 General discussion

The centrifugal visual system (CVS) has been the focus of numerous studies over the course of 120 years, which for the most part have attempted to elucidate the anatomical (e.g. Miceli et al., 1997), physiological (e.g. Uchiyama et al., 1994) and/or evolutionary basis of CVS organisation (Réperant et al., 2007) and, subsequently, to relate their findings to (or generate) functional hypotheses. Exceptions to this generalisation are found in a comprehensive subsection of the literature on CVS development. Developmental studies have taken advantage of the unique properties and organisation of the system (i.e. a direct brain-retina connection), to investigate mechanisms of neural connection fine-tuning, i.e. elimination of axonal targeting errors (Fritzsch, Crapon de Caprona and Clarke, 1990), as well as changes in midbrain organisation following disruption of programmed neuronal death (i.e. apoptosis), during development, e.g. through eye enucleation (Clarke, 1976; Pequignot and Clarke, 1992) (**Section 1.5.6**).

10.1 *How do the findings of the experiments described here fit into the existing literature?*

10.1.1 CVS function – It is significant that, after 120 years of research, we have been able to identify a functional effect definitively, however it is unlikely that a role in the modulation of eye growth towards emmetropia is the main purpose of the CVS. Given that the development of the chick CVS is characterised by the degeneration of ~60% of centrifugal neurons between embryonic days 13 and 17 (Clarke, Rogers and Cowan, 1976), one would expect the surviving twelve thousand cells to maintain functional significance beyond the critical phase of post hatch development. Moreover, as it is well established that the mechanisms of visually-driven ocular growth are predominantly intra-retinal (e.g. as demonstrated by local ocular growth persisting following ONS) (**Section 2.2**), the highly topographic organisation of the CVS loop, and the characteristics of the efferent projection itself (i.e. the thick myelination of the axons) are not consistent with a modulatory role in

development alone. In addition, the finding that ION/EA somata receive afferent input from multiple, distinct sources, (as demonstrated by the identification of 8 terminal types on ION cell soma (Miceli et al., 1995b) and that only ~50% of afferent input to ION/EA is extratectal (McGill et al., 1966)), it is likely that the CVS plays a modulatory role in more than one visual function.

10.1.2 Emmetropisation – One of the major findings of this project was that IOTr lesion induced-disruption of centrifugal efferents induced a transient hyperopia in the developing eye contralateral to the lesion. This finding is, perhaps, most logically considered in the context of ONS emmetropisation studies, as severance of the optic nerve not only transects retinal efferent axons, but also centrifugal efferents (retinal afferent input from the CVS). Without a brain-retina/retina-brain connection, chicks develop progressive moderate hyperopia (**Section 2.5**). Here I demonstrate that, following transection of the 1% of the optic nerve that comprise efferent fibers (through lesion of the IOTr), a comparable, but transient, response occurs.

These findings warrant a re-interpretation of past ONS studies, specifically, a consideration of the effects of retrograde degeneration of RGCs following axotomy. As mentioned above, hyperopia induced by ONS surgery is progressive and has been shown to persist for at least 4 weeks, although 75% of the hyperopia present after 4 weeks had developed after only 1 week (Troilo et al., 1987). Two obvious possible explanations exist for the progressive/transient difference in the nature of the hyperopia induced by ONS and IOTr lesion, respectively: **1**) more than one emmetropisation mechanism (i.e. in addition to centrifugal modulation) is dependent on a brain-retina/retina-brain connection; **2**) ONS surgery induced retrograde degeneration of RGCs prevents recovery of the hyperopia that is the direct result of the loss of the CVS efferents.

While it is plausible that other retina-brain mechanisms regulate emmetropisation, it may be the case that the progressive, severe hyperopia reported following ONS surgery is likely to be largely due to the effects of retrograde degeneration on intra-retinal mechanisms (Troilo et al., 1987; Wildsoet, 2003). If modulation of eye growth by centrifugal efferents constitutes the only extra-retinal influence on emmetropisation, the findings of **Chapter 6** represent the true, albeit less severe effects of brain-retina disconnectivity. It is worthy of note that there is a degree of disagreement in the two long-term ONS studies that have been performed. Troilo, Gottlieb and Wallman (1987) reported vitreous chamber shortening, which resulted in progressive hyperopia, but with no anterior chamber effects. However, Li and Howland (2000) found, 4 weeks following ONS surgery, a significant fellow (control) eye difference in refractive state was *not* evident and the eyes were emmetropic. Furthermore, the treated eyes had relatively steeper corneas and shorter vitreous chambers than fellow untreated eyes. It may be the case that the ONS surgery induced corneal steepening which, in turn, led to normal compensatory VCD shortening to the hyperopia. Given this discrepancy, further investigation into the long-term effects of ONS surgery on ocular growth is required.

Only one study has investigated the combined effects of CL treatment and ONS surgery on emmetropisation (Li and Howland, 2000). However, this combination of treatment provides an interesting basis for comparison with the results of **Chapter 7** (the effects of IOTr lesion on eye growth in CL conditions). In their study, chicks were raised in CL for 7 days before undergoing unilateral ONS surgery. Four weeks following surgery, both treated and control eyes showed no differences from previously reported CL effects in chicks with intact optic nerves (Li et al., 1995b). Importantly, no significant differences between eyes were reported, i.e. treated vs. control eye asymmetry in refractive state, CR, VCD, etc. was not apparent

The results of **Chapter 7** show that, 3 weeks following IOTr lesion in chicks raised in CL, the eye ipsilateral to the lesion had developed a significantly shorter VCD relative to both fellow *treated* and sham operated control chicks which were equivalent. Moreover, the shorter VCD of control eyes was accompanied by an increase (1.08 D ± 1.33) in the amount of hyperopia, relative to contralateral eyes, although this was not significant. In addition, at the 7 days post surgery time point, the treated, contralateral eyes of individuals showed a significant relationship between lesion success and refractive state (i.e. the same effect reported in NL conditions). In parallel with the results of **Chapter 6** (IOTr lesion in chicks raised in NL conditions), the treated eye effect had recovered by the 3 week time point. Thus, through the introduction of CL conditions, in addition to the treated eye effect in **Chapter 6**, the control eye had become (and remained) significantly shorter than normal.

CL conditions have been shown to disrupt circadian rhythms (Weiss and Schaeffel, 1993) and, as discussed in **Chapter 7**, to cause disruption of the diurnal fluctuation and interaction of neuromodulators such as dopamine, melatonin and nitric oxide. Dopamine, for example, is expressed at its highest levels during the day, during which it inhibits the expression of an enzyme that converts serotonin to melatonin (Bernard et al., 1997). Conversely, melatonin, which is synthesised at its greatest levels during the dark, suppresses dopamine production. Thus, light-evoked dopamine release regulates antagonistic dopamine/melatonin diurnal rhythms (Nowak, Żurawska and Zawilska, 1989). Also, as discussed previously (**Section 7.3.1**), melatonin inhibits nitric oxide synthesis. My results show that, under CL conditions, an IOTr lesion appears to exert a 'stop' signal for ocular elongation in the ipsilateral eye (**Chapter 7**). Although the obvious explanation for this effect centres around the ipsilateral EA pathway, it may not be the case that the ipsilateral EA pathway is responsible. An alternate possibility is that the observed asymmetry resulted from the disruption of inter EA-population communication within the midbrain as suggested by the findings of **Chapter 9**.

Having said that, the effect of ipsilateral EA pathway disruption remains a highly plausible explanation. Ipsilateral EA cells are situated in amongst midbrain regions (i.e. GCt and LoC), which are populated by cells that exhibit immunoreactivity to a vast array of neurochemicals (Medina et al., 1998), some of which are regulated by diurnal rhythms. These include serotonin and tyrosine hydroxylase (the rate-limiting enzyme involved in dopamine synthesis). In addition, GCt and LoC receive afferent input from telencephalic visual centres (**Section 9.7.3.3**). Thus a potential explanation for the effects in the control eye observed is that the disruption of ipsilateral EA efferents resulting from a lesion of the IOTr prevented conduction of a light-dependent signal, potentially controlled by telencephalic afferents to the midbrain, from reaching the retina. Presumably, if intact, such a pathway would be a 'start' signal for ocular elongation. Importantly, however, this explanation is dependent upon ipsilateral EA cells acting *via* an independent mechanism to that of contralateral EA cells, i.e. they must receive independent afferent input or terminate upon an independent target cell type within the retina.

A number of studies have reported effects on control eyes following experimental treatments. For example, changes in ZENK expression were predominantly found in control eyes following unilateral plus or minus lens wear (Bitzer and Schaeffel, 2002). In addition, while it is well established that unilateral form deprivation induces ocular elongation and *myopia*, in one study in the chicken form deprivation was found to induce *hyperopia* when applied to both eyes (Schaeffel and Howland, 1991). Furthermore, when chicks were form deprived unilaterally, the normal diurnal growth rhythm (i.e. growth during the day and slight shrinkage at night) of the control eye was disrupted, and although the eye remained emmetropic, growth was consistently slow and did not exhibit a diurnal pattern (Weiss and Schaeffel, 1993). The above findings are very relevant in the context of the results presented in **Chapter 7** and provide circumstantial evidence that a retina-brain/brain-retina connection is necessary for normal ocular growth patterns associated with circadian

rhythms. Moreover, these results provide additional evidence for the hypothesis that symmetrical growth of fellow eyes is dependent upon inter-ocular communication.

In **Chapter 2**, I alluded to the idea that ipsilateral EA pathway efferents made the centrifugal projection an interesting candidate for a role in the modulation of eye growth, and in particular the development of ocular symmetry through inter-ocular communication. The findings of this study strongly support this possibility, and therefore the role of the EA centrifugal neurons in diurnal growth rhythms warrants further investigation.

10.1.3 Anatomy

It is striking that the majority of the literature on the CVS is comprised of work using an avian model (**Section 1.5**). The species most often used are the chicken (*Gallus gallus*), pigeon (*Columba livia*) and the Japanese quail (*Coturnix japonica*). However, a number of thought provoking comparative studies have demonstrated significant variation in CVS organisation between, for example, ground feeding and predatory bird species (**Section 1.5.7.2**). Nevertheless, different species within the avian class share a common general organisation, i.e. a well defined ION and surrounding EA cells, while a comparison of CVS organisation *between* orders, e.g. avian vs. mammalian reveal far fewer features in common. In fact, the mammalian (e.g. monkey) CVS (Gastinger et al., 2006) arguably exhibits more anatomical commonality with the CVS of the visually primitive horse-shoe crab (*Limulus polyphemus*) (Powers and Barlow, 1985; Gastinger et al., 2006), than that of birds (e.g. Miceli et al., 1999) (**Section 1.5.7**). The evolutionary basis of CVS organisation has been discussed in depth by Réperant et al. (2006), who proposed eight distinct subsystems that share a common centrifugal projection, while Uchiyama et al. (1989) suggests a simpler 'ION' or 'non-ION' categorisation. Réperant proposed that the avian CVS fits into the same category (i.e. the *dorsal isthmo-retinal system)* as that of the *Chelonia* (turtles), *Crocodilia* (large reptiles), *Lacertilia* (lizards) and *Eutheria* (mammals) groups. However, no distinction is

made between the ION and EA components of the avian CVS and whether they comprise a single subsystem or whether ION and EA populations represent two distinct centrifugal subsystems that have arisen together within the avian class. Perhaps the ION component represents Réperant's *dorsal* isthmo-retinal system and the EA represents the *ventral* isthmo-retinal system. The latter subsystem is characterised by serotonergic neurons that are situated around the midline raphe nuclei. Miceli (2002) identified cells that provide a source of serotonergic afferent input to centrifugal neurons of the ION from a population of neurons that constitute a lateral extension of the serotonergic midline raphe nuclei. These cells are found in close proximity to the centrifugal cells of the EA, and although they do not project to the retina, their distribution coincides with the region of highest centrifugal EA cell density (i.e. ventromedial to ION) wherein they contribute to the vast range of neurochemical diversity that makes up the ION. Afferentation input to centrifugal EA cells was the focus of **Chapter 9,** in which I identified a population of cells that project across the midline of the midbrain (potentially via the commissural fibers at the level of the CNIV). The results raise a number of interesting possibilities, that include communication between EA populations on different sides of the midbrain as well as an alternative to the assumed pathway taken by axons of ipsilateral EA cells.

Inter-communication of cells in opposite medial and ventromedial EA regions (i.e. GCt and LoC) (**Section 9.5**) could provide the basis of the regulation of symmetrical eye growth. These regions are reported to receive telencephalic visual input, and thus, the ocular growth rhythm described by Weiss and Schaeffel (1993) may be driven by higher visual input and, in turn, modulated by interhemispheric connectivity at the level of the midbrain. Subsequently, this binocular signal could be conveyed to retinal target cells *via* EA efferents.

A second possibility, which also relates to the experiments described in **Chapters 6** to **8,** is that ipsilateral EA neurons project to the ipsilateral retina *via* a double decussation pathway

(**Section 9.7**). As alluded to in **Sections 5.5.5** and **6.4,** interpretation of lesion studies of the CVS is complicated by the ipsilateral EA pathway, whose existence precludes a treated/control eye distinction following unilateral lesion. The pathway taken by ipsilateral EA axons to the retina has, until now, been assumed to remain uncrossed at the optic chiasm. While this may well be the case, it is a major assumption and the importance of identifying the route of the ipsilateral EA pathway is particularly evident when interpreting the results of **Chapter 7** (in which a control eye effect was observed). The pathway tracer paradigm used to investigate the possibility of an alternative double-crossed pathway in this case provided inconclusive results (**Chapter 9**). However, in spite of this, I have attempted to take into account both possibilities in the interpretation of the results from the lesion studies described here.

10.2 Future work

10.2.1 Emmetropisation

Several questions remain following this initial investigation into the role of the CVS on eye growth. As discussed at length, above, and in **Chapter 6**, the discrepancy between the effects of ONS and IOTr lesion effects are unknown, although, I have attempted to put forward the most likely explanations. Future work into the intra-retinal effects of IOTr lesions, e.g. on nitric oxide synthase expression at sequential time points following lesion, in a manner analogous to that used by Lee et al (2003), following ONS in the rat (**Chapter 6**), would not only clarify these results but also provide insight into the potential mechanisms of centrifugal control on eye growth. In addition, the contradiction in findings reported following ONS treatment on eye growth requires clarification. With the benefit of hindsight, this contradiction would have been most effectively resolved by a parallel ONS study in the same strain of chick, i.e. Shaver Black, thus removing the potential for inter-strain variability (**Chapter 5**).

10.2.2 Anatomy

In terms of the CVS itself, the major goal of identifying its function(s) still remains. Recent work has continued to improve our understanding of the intra-retinal connectivity of centrifugal efferents (e.g. Wilson and Lindstrom, 2011), while in the present series of studies, I have attempted to address the questions that remain as regards the midbrain connectivity of ION and EA neurons. Identification of the target cells of EA efferents may provide important clues as to CVS function and could help to clarify whether ION and EA exert influence over a common function or whether they represent different centrifugal subsystems. Furthermore, the controversy surrounding the possible termination of EA cells on dRGCs has yet to be resolved. Repetition of the unpublished work of Woodson and Britto, in which dRGCs were labeled in the retina through retrograde transport from a tracer injection into nBOR, in combination with an injection of an anterograde tracer into EA is crucial for settling this issue by providing direct evidence for, or against, such connectivity.

Finally, the results of **Chapter 7** raise the interesting possibility that centrifugal neurons may have a role in the regulation of retinal diurnal rhythms. Further investigation may look to establish the mechanisms involved, i.e. how does disruption of centrifugal efferents influence intra-retinal levels of neurochemicals, e.g. dopamine, glucagon, etc.

Bibliography

Ahnelt P K, Hokoc J N, and Rohlich P (1995) Photoreceptors in a primitive mammal, the south american opossum, didelphis marsupialis aurita: Characterization with anti-opsin immunolabeling. *Visual neuroscience* 12: 793-804.

Ahnelt P K, and Kolb H (2000) The mammalian photoreceptor mosaic-adaptive design. *Progress in retinal and eye research* 19: 711-777.

Arends J J, and Zeigler H P (1991) Organization of the cerebellum in the pigeon (*Columba livia*): II. Projections of the cerebellar nuclei. *The Journal of comparative neurology* 306: 245-272.

Bagnoli P, and Burkhalter A (1983) Organization of the afferent projections to the wulst in the pigeon. *The Journal of comparative neurology* 214: 103-113.

Barlow H B, and Hill R M (1963) Selective sensitivity to direction of movement in ganglion cells of the rabbit retina. *Science* 139: 412-414.

Barlow H B, and Ostwald T J (1972) Pecten of the pigeon's eye as an inter-ocular eye shade. *Nature: New biology* 236: 88-90.

Bartmann M, Schaeffel F, Hagel G, and Zrenner E (1994) Constant light affects retinal dopamine levels and blocks deprivation myopia but not lens-induced refractive errors in chickens. *Visual neuroscience* 11: 199-208.

Bennett A G, and Rabbetts R B (1998) *Bennett and Rabbetts' Clinical Visual Optics*. Butterworth-Heinemann.

Bernard M, Iuvone P M, Cassone V M, Roseboom P H, Coon S L, and Klein D C (1997) Avian melatonin synthesis: Photic and circadian regulation of serotonin n-acetyltransferase mrna in the chicken pineal gland and retina. *Journal of neurochemistry* 68: 213-224.

Bitzer M, and Schaeffel F (2002) Defocus-induced changes in ZENK expression in the chicken retina. *Investigative ophthalmology & visual science* 43: 246-252.

Bloch S, and Martinoya C (1982) Comparing frontal and lateral viewing in the pigeon. I. Tachistoscopic visual acuity as a function of distance. *Behavioural brain research* 5: 231-244.

Bowmaker J K (1977) The visual pigments, oil droplets and spectral sensitivity of the pigeon. *Vision research* 17: 1129-1138.

Boycott B B, and Wassle H (1991) Morphological classification of bipolar cells of the primate retina. *The European journal of neuroscience* 3: 1069-1088.

Bradley D V, Fernandes A, and Boothe R G (1999) The refractive development of untreated eyes of rhesus monkeys varies according to the treatment received by their fellow eyes. *Vision research* 39: 1749-1757.

Brecha N C, and Karten H J (1981) Organization of the avian accessory optic system. *Annals of the New York academy of sciences* 374: 215-229.

Briggman K L, Helmstaedter M, and Denk W (2011) Wiring specificity in the direction-selectivity circuit of the retina. *Nature* 471: 183-188.

Briggs F, and Usrey W M (2009) Corticothalamic Connections: Structure and Function. *Encyclopedia of Neuroscience*. Oxford: Academic Press, pp. 215-219.

Briggs F, and Usrey W M (2011) Corticogeniculate feedback and visual processing in the primate. *The Journal of physiology* 589: 33-40.

Britto L R, Keyser K T, Hamassaki D E, and Karten H J (1988) Catecholaminergic subpopulation of retinal displaced ganglion cells projects to the accessory optic nucleus in the pigeon (columba livia). *The Journal of comparative neurology* 269: 109-117.

Brown N P, Koretz J F, and Bron A J (1999) The development and maintenance of emmetropia. *Eye* 13 (Pt 1): 83-92.

Budzynski C A, Gagliardo A, Ioale P, and Bingman V P (2002) Participation of the homing pigeon thalamofugal visual pathway in sun-compass associative learning. *The European journal of neuroscience* 15: 197-210.

Butler A B (1994) The evolution of the dorsal pallium in the telencephalon of amniotes - cladistic-analysis and a new hypothesis. *Brain research reviews* 19: 66-101.

Cajal S R (1972) *The Structure of the Retina*. C. C. Thomas.

Cajal S R, and Greeff R (1894) *Die Retina der Wirbelthiere: Untersuchungen mit der golgi-cajal'schen chromsilbermethode und der ehrlich'schen methylenblaufürbung*. Bergmann.

Catsicas S, Catsicas M, and Clarke P G (1987) Long-distance intraretinal connections in birds. *Nature* 326: 186-187.

Chen Y P, Hocking P M, Wang L, Povazay B, Prashar A, To C H, Erichsen J T, Feldkaemper M, Hofer B, Drexler W, Schaeffel F, and Guggenheim J A (2011a) Selective breeding for susceptibility to myopia reveals a gene-environment interaction. *Investigative ophthalmology & visual science* 52: 4003-4011.

Chen Y P, Prashar A, Erichsen J T, To C H, Hocking P M, and Guggenheim J A (2011b) Heritability of ocular component dimensions in chickens: Genetic variants controlling susceptibility to experimentally induced myopia and pretreatment eye size are distinct. *Investigative ophthalmology & visual science* 52: 4012-4020.

Choh V, Padmanabhan V, Li W S, Sullivan A B, and Wildsoet C F (2008) Colchicine attenuates compensation to negative but not to positive lenses in young chicks. *Experimental eye research* 86: 260-270.

Clarke P G, and Cowan W M (1975) Ectopic neurons and aberrant connections during neural development. *Proceedings of the National academy of sciences of the United States of America* 72: 4455-4458.

Clarke P G, Rogers L A, and Cowan W M (1976) The time of origin and the pattern of survival of neurons in the isthmo-optic nucleus of the chick. *The Journal of comparative neurology* 167: 125-142.

Clarke P G H (1976) Neuronal death as an error-correcting mechanism in development of chicks isthmo-optic nucleus. *Journal of physiology* 256: 44-45.

Clarke P G H, Gyger M, and Catsicas S (1996) A centrifugally controlled circuit in the avian retina and its possible role in visual attention switching. *Visual neuroscience* 13: 1043-1048.

Conlee J W, and Parks T N (1986) Origin of ascending auditory projections to the nucleus mesencephalicus lateralis pars dorsalis in the chicken. *Brain research* 367: 96-113.

Cook R C, and Glasscock R E (1951) Refractive and ocular findings in the newborn. *American journal of ophthalmology* 34: 1407-1413.

Coombs J, van der List D, Wang G Y, and Chalupa L M (2006) Morphological properties of mouse retinal ganglion cells. *Neuroscience* 140: 123-136.

Cowan W M, Adamson L, and Powell T P (1961) An experimental study of the avian visual system. *Journal of anatomy* 95: 545-563.

Cowan W M, and Clarke P G H (1976) Development of the isthmo-optic nucleus. *Brain behavior and evolution* 13: 345-375.

Cowan W M, and Powell T P (1962) Centrifugal fibres to the retina in the pigeon. *Nature* 194: 487.

Cowan W M, and Powell T P (1963) Centrifugal fibres in the avian visual system. *Proceedings of the Royal Society of London. Series B, containing papers of a biological character* 158: 232-252.

Crick F (1984) Function of the thalamic reticular complex: The searchlight hypothesis. *Proceedings of the national academy of sciences of the United States of America* 81: 4586-4590.

Crossland W J, and Hughes C P (1978) Observations on the afferent and efferent connections of the avian isthmo-optic nucleus. *Brain research* 145: 239-256.

Dacey D (2004) Origins of perception: Retinal ganglion cell diversity and the creation of parallel visual pathways. *Cognitive neurosciences, Third Edition*: 281-301.

Dacey D M (1999) Primate retina: Cell types, circuits and color opponency. *Progress in Retinal and eye research* 18: 737-763.

Dacey D M, and Lee B B (1994) The 'blue-on' opponent pathway in primate retina originates from a distinct bistratified ganglion cell type. *Nature* 367: 731-735.

Derobert Y, Medina M, Rio J P, Ward R, Réperant J, Marchand M J, and Miceli D (1999) Retinal projections in two crocodilian species, *Caiman crocodilus* and C*rocodylus niloticus*. *Anatomy and embryology* 200: 175-191.

Diether S, and Schaeffel F (1997) Local changes in eye growth induced by imposed local refractive error despite active accommodation. *Vision research* 37: 659-668.

Dong W, Sun W Z, Zhang Y Y, Chen X R, and He S G (2004) Dendritic relationship between starburst amacrine cells and direction-selective ganglion cells in the rabbit retina. *Journal of physiology* 556: 11-17.

Dowling J E (1968) Synaptic organization of the frog retina: An electron microscopic analysis comparing the retinas of frogs and primates. *Proceedings of the Royal Society of London. Series B, containing papers of a biological character* 170: 205-228.

Dubocovich M L (1983) Melatonin is a potent modulator of dopamine release in the retina. *Nature* 306: 782-784.

Erchenkov V G, Gusel'nikov V I, and Zaborskis A A (1972) Efferent influences on responses of the pigeon retinal ganglion cells. *Fiziologicheskii zhurnal SSSR imeni I. M. Sechenova* 58: 385-392.

Erichsen J T, Haamedi S N, Kuenzel W J, and Hodos W (2002) Myopia is induced by lesions of the isthmo-optic nucleus in chicks. *Investigative ophthalmology & visual science* 43: U35-U35.

Euler T, and Wassle H (1995) Immunocytochemical identification of cone bipolar cells in the rat retina. *The Journal of comparative neurology* 361: 461-478.

Feldkaemper M P, and Schaeffel F (2002) Evidence for a potential role of glucagon during eye growth regulation in chicks. *Visual neuroscience* 19: 755-766.

Feyerabend B, Malz C R, and Meyer D L (1994) Birds that feed-on-the-wing have few isthmo-optic neurons. *Neuroscience letters* 182: 66-68.

Field G D, and Chichilnisky E J (2007) Information processing in the primate retina: Circuitry and coding. *Annual review of neuroscience* 30: 1-30.

Fischer A J, McGuire J J, Schaeffel F, and Stell W K (1999a) Light- and focus-dependent expression of the transcription factor zenk in the chick retina. *Nature neuroscience* 2: 706-712.

Fischer A J, Morgan I G, and Stell W K (1999b) Colchicine causes excessive ocular growth and myopia in chicks. *Vision research* 39: 685-697.

Fischer A J, Omar G, Walton N A, Verrill T A, and Unson C G (2005) Glucagon-expressing neurons within the retina regulate the proliferation of neural progenitors in the circumferential marginal zone of the avian eye. *Journal of neuroscience* 25: 10157-10166.

Fischer A J, Ritchey E R, Scott M A, and Wynne A (2008) Bullwhip neurons in the retina regulate the size and shape of the eye. *Developmental biology* 317: 196-212.

Fischer A J, and Stell W K (1999) Nitric oxide synthase-containing cells in the retina, pigmented epithelium, choroid, and sclera of the chick eye. *The Journal of comparative neurology 405: 1-14.*

Fite K V (1973) Anatomical and behavioral correlates of visual acuity in the great horned owl. *Vision Research* 13: 219-230.

Fite K V, Brecha N, Karten H J, and Hunt S P (1981) Displaced ganglion cells and the accessory optic system of pigeon. *The Journal of comparative neurology* 195: 279-288.

Fite K V, and Janusonis S (2001) Retinal projection to the dorsal raphe nucleus in the chilean degus (*Octodon degus*). *Brain research* 895: 139-145.

Fite K V, Janusonis S, Foote W, and Bengston L (1999) Retinal afferents to the dorsal raphe nucleus in rats and mongolian gerbils. *The Journal of comparative neurology* 414: 469-484.

Franz-Odendaal T A (2006) Intramembranous ossification of scleral ossicles in *Chelydra serpentina*. *Zoology* 109: 75-81.

Fritzsch B, Crapon de Caprona M D, and Clarke P G (1990) Development of two morphological types of retinopetal fibers in chick embryos, as shown by the diffusion along axons of a carbocyanine dye in the fixed retina. *The Journal of comparative neurology* 300: 405-421.

Fujikado T, Kawasaki Y, Fujii J, Taniguchi N, Okada M, Suzuki A, Ohmi G, and Tano Y (1997) The effect of nitric oxide synthase inhibitor on form-deprivation myopia. *Current eye research* 16: 992-996.

Galifret Y (1968) The various functional areas of the retina of pigeons. *Zeitschrift fur Zellforschung und mikroskopische Anatomie* 86: 535-545.

Galifret Y, Condé-Courtine F, Repérant J, and Servière J (1971) Centrifugal control in the visual system of the pigeon. *Vision research* 11, Supplement 3: 185-IN128.

Gamlin P D, and Cohen D H (1988) Projections of the retinorecipient pretectal nuclei in the pigeon (*Columba livia*). The j*ournal of comparative neurology* 269: 18-46.

Gamlin P D, Reiner A, Erichsen J T, Karten H J, and Cohen D H (1984) The neural substrate for the pupillary light reflex in the pigeon (*Columba livia*). The *Journal of comparative neurology* 226: 523-543.

Garamszegi L Z, Moller A P, and Erritzoe J (2002) Coevolving avian eye size and brain size in relation to prey capture and nocturnality. *Proceedings of the Royal Society of London. Series B, containing papers of a biological character* 269: 961-967.

Gastinger M J, Tian N, Horvath T, and Marshak D W (2006) Retinopetal axons in mammals: Emphasis on histamine and serotonin. *Current eye research* 31: 655-667.

Gee S S, and Tabbara K F (1988) Increase in ocular axial length in patients with corneal opacification. *Ophthalmology* 95: 1276-1278.

Glasser A, Troilo D, and Howland H C (1994) The mechanism of corneal accommodation in chicks. *Vision research* 34: 1549-1566.

Glickstein M, and Millodot M (1970) Retinoscopy and eye size. *Science* 168: 605-606.

Goddard G V, McIntyre D C, and Leech C K (1969) A permanent change in brain function resulting from daily electrical stimulation. *Experimental neurology* 25: 295-330.

Goodge W R (1960) Adaptations for amphibious vision in the dipper (C*inclus mexicanus*). *Journal of Morphology* 107: 79-91.

Gottlieb M D, Fugate-Wentzek L A, and Wallman J (1987) Different visual deprivations produce different ametropias and different eye shapes. *Investigative ophthalmology & visual science* 28: 1225-1235.

Grunert U, Martin P R, and Wassle H (1994) Immunocytochemical analysis of bipolar cells in the macaque monkey retina. *The Journal of comparative neurology* 348: 607-627.

Guerrero J M, Pablos M I, Ortiz G G, Agapito M T, and Reiter R J (1996) Nocturnal decreases in nitric oxide and cyclic-gmp contents in the chick brain and their prevention by light. *Neurochemistry international* 29: 417-421.

Guillery R W, Feig S L, and Lozsádi D A (1998) Paying attention to the thalamic reticular nucleus. *Trends in neurosciences* 21: 28-32.

Gultiken M E, Yildiz D, Onuk B, and Karayigit M O (2011) The morphology of the pecten oculi in the common buzzard (B*uteo buteo*). *Veterinary ophthalmology*.

Gundlach R H, Chard R D, and Skahen J R (1945) The mechanism of accommodation in pigeons. *The Journal of comparative psychology* 38: 27-42.

Güntürkün O (1985) Lateralization of visually controlled behavior in pigeons. *Physiology & behavior* 34: 575-577.

Güntürkün O (1987) A golgi study of the isthmic nuclei in the pigeon (*Columba livia*). *Cell and tissue research* 248: 439-448.

Güntürkün O, and Bohringer P G (1987) Lateralization reversal after intertectal commissurotomy in the pigeon. *Brain research* 408: 1-5.

Güntürkün O, and Remy M (1990) The topographical projection of the nucleus isthmi pars parvocellularis (ipc) onto the tectum opticum in the pigeon. *Neuroscience Letters* 111: 18-22.

Guo S S, Sivak J G, Callender M G, and Diehl-Jones B (1995) Retinal dopamine and lens-induced refractive errors in chicks. *Current eye research* 14: 385-389.

Gutierrez-Ibanez C, Iwaniuk A, Kolominsky J, Linsey T J, and Wylie D R (2011) Comparative study of the relative size of the isthmo-optic nucleus (ion and its association to other visual brain structures in birds (*Aves*) *Investigative opthalmology and visual science* Abstract nr. 734.05/AAA11.

Hahmann U, and Gunturkun O (1992) Visual-discrimination deficits after lesions of the centrifugal visual system in pigeons (*Columba livia*). *Visual neuroscience* 9: 225-233.

Hall M I, and Ross C F (2007) Eye shape and activity pattern in birds. *Journal of zoology* 271: 437-444.

Harmening W M, and Wagner H (2011) From optics to attention: Visual perception in barn owls. *Journal of comparative physiology. A, Neuroethology, sensory, neural, and behavioral physiology* 197: 1031-1042.

Harris W (1904) Binocular and stereoscopic vision in man and other vertebrates, with its relation to the decussation of the optic nerves, the ocular movements, and the pupil light reflex. *Brain* 27: 107-147.

Hartline H K, Wagner H G, and Macnichol E F, Jr. (1952) The peripheral origin of nervous activity in the visual system. *Cold Spring Harbor symposia on quantitative biology* 17: 125-141.

Hartline H K, Wagner H G, and Ratliff F (1956) Inhibition in the eye of limulus. *The Journal of general physiology* 39: 651-673.

Hayes B P (1982) Chapter 7 the structural organization of the pigeon retina. *Progress in retinal research* 1: 197-226.

Hayes B P, and Holden A L (1983a) The distribution of centrifugal terminals in the pigeon retina. *Experimental brain research. Experimentelle Hirnforschung. Experimentation cerebrale* 49: 189-197.

Hayes B P, and Holden A L (1983b) The distribution of displaced ganglion cells in the retina of the pigeon. *Experimental brain research. Experimentelle hirnforschung. Experimentation cerebrale* 49: 181-188.

Hayes B P, and Webster K E (1981) Neurones situated outside the isthmo-optic nucleus and projecting to the eye in adult birds. *Neuroscience letters* 26: 107-112.

Hellmann B, Manns M, and Gunturkun O (2001) Nucleus isthmi, pars semilunaris as a key component of the tectofugal visual system in pigeons. *The Journal of comparative neurology* 436: 153-166.

Hirano A A, Brandstatter J H, Vila A, and Brecha N C (2007) Robust syntaxin-4 immunoreactivity in mammalian horizontal cell processes. *Visual neuroscience* 24: 489-502.

Hodos W, and Kuenzel W J (1984) Retinal-image degradation produces ocular enlargement in chicks. *Investigative ophthalmology & visual science* 25: 652-659.

Holden A L (1978) Centrifugal actions on pigeon retinal ganglion cells *The Journal of physiology* 282: 8-9.

Holden A L (1990) Centrifugal pathways to the retina: Which way does the "searchlight" point? *Visual neuroscience* 4: 493-495.

Holden A L, and Powell T P (1972) The functional organization of the isthmo-optic nucleus in the pigeon. *The Journal of physiology* 223: 419-447.

Honrubia F M, and Elliott J H (1968) Efferent innervation of the retina. I. Morphologic study of the human retina. *Archives of ophthalmology* 80: 98-103.

Howland H C, Merola S, and Basarab J R (2004) The allometry and scaling of the size of vertebrate eyes. *Vision research* 44: 2043-2065.

Hubel D H, and Wiesel T N (1962) Receptive fields, binocular interaction and functional architecture in the cat's visual cortex. *The Journal of physiology* 160: 106-154.

Huberman A D, Feller M B, and Chapman B (2008) Mechanisms underlying development of visual maps and receptive fields. *Annual review of neuroscience* 31: 479-509.

Huberman A D, and Niell C M (2011) What can mice tell us about how vision works? *Trends in neurosciences* 34: 464-473.

Husband S A, and Shimizu T (1999) Efferent projections of the ectostriatum in the pigeon (*Columba livia*). *The Journal of comparative neurology* 406: 329-345.

Irving E L, Sivak J G, and Callender M G (1992) Refractive plasticity of the developing chick eye. *Ophthalmic & physiological optics : The Journal of the British college of ophthalmic opticians* 12: 448-456.

Iuvone P M, Tigges M, Stone R A, Lambert S, and Laties A M (1991) Effects of apomorphine, a dopamine receptor agonist, on ocular refraction and axial elongation in a primate model of myopia. *Investigative ophthalmology & visual science* 32: 1674-1677.

Iwaniuk A N, Heesy C P, Hall M I, and Wylie D R (2008) Relative wulst volume is correlated with orbit orientation and binocular visual field in birds. *Journal of comparative physiology. A, Neuroethology, sensory, neural, and behavioral physiology* 194: 267-282.

Iwaniuk A N, and Wylie D R (2006) The evolution of stereopsis and the wulst in caprimulgiform birds: A comparative analysis. *Journal of comparative physiology. A, Neuroethology, sensory, neural, and behavioral physiology* 192: 1313-1326.

Janusonis S, and Fite K V (2001) Diurnal variation of c-fos expression in subdivisions of the dorsal raphe nucleus of the mongolian gerbil (*Meriones unguiculatus*). *The Journal of comparative neurology* 440: 31-42.

Jeffery G (1985) Retinotopic order appears before ocular separation in developing visual pathways. *Nature* 313: 575-576.

Jerison H J (1973) *Evolution of the Brain and Intelligence*. Academic Press.

Karten H J (1967) The organization of the ascending auditory pathway in the pigeon (columba livia) i. Diencephalic projections of the inferior colliculus (nucleus mesencephali lateralis, pars dorsalis). *Brain research* 6: 409-427.

Karten H J (1969) Organization of avian telencephalon and some speculations on phylogeny of amniote telencephalon. *Annals of the New York academy of sciences* 167: 164-&.

Karten H J, and Hodos W (1967) *A Stereotaxic Atlas of the Brain of the Pigeon: Columba livia*. Johns Hopkins Press.

Karten H J, and Hodos W (1970) Telencephalic projections of the nucleus rotundus in the pigeon (*Columba livia*). *The Journal of comparative neurology* 140: 35-51.

Karten H J, Hodos W, Nauta W J H, and Revzin A M (1973) Neural connections of visual-wulst of avian telencephalon - experimental studies in pigeon (*Columba livia*) and owl (S*peotyto-cunicularia*). *The Journal of comparative neurology* 150: 253-277.

Kee C S, Marzani D, and Wallman J (2001) Differences in time course and visual requirements of ocular responses to lenses and diffusers. *Investigative ophthalmology & visual science* 42: 575-583.

Keirl A, and Christie C (2007) *Clinical Optics and Refraction: A guide for optometrists, contact lens opticians and dispensing opticians*. Elsevier Science Health Science Division.

Kitt C A, and Brauth S E (1986) Telencephalic projections from midbrain and isthmal cell groups in the pigeon. I. Locus coeruleus and subcoeruleus. *The Journal of comparative neurology* 247: 69-91.

Knipling R R (1978) No deficit in near-field visual acuity of pigeons after transection of the isthmo-optic tract. *Physiology & behavior* 21: 813-816.

Knudsen E I (2011) Control from below: The role of a midbrain network in spatial attention. *European journal of neuroscience* 33: 1961-1972.

Koch C, and Davis J L (1994) *Large-scale Neuronal Theories of the Brain*. Mit Press.

Kolb H (1995) *Gross Anatomy of the Eye*. In: Kolb H, Fernandez E, and Nelson R [eds.] *Webvision: The organization of the retina and visual system*. Salt Lake City (UT).

Kolb H (1997) Amacrine cells of the mammalian retina: Neurocircuitry and functional roles. *Eye* 11 (Pt 6): 904-923.

Kolb H, Mariani A, and Gallego A (1980) A second type of horizontal cell in the monkey retina. *The Journal of comparative neurology* 189: 31-44.

Kuenzel W J, and Masson M (1988) *A Stereotaxic Atlas of the Brain of the Chick (Gallus domesticus)*. Johns Hopkins University Press.

Kuffler S W (1953) Discharge patterns and functional organization of mammalian retina. *Journal of neurophysiology* 16: 37-68.

Kuffler S W (1973) The single-cell approach in the visual system and the study of receptive fields. *Investigative ophthalmology* 12: 794-813.

Lauber J K, and Oishi T (1990) Kainic acid and formoguanamine effects on environmentally-induced eye lesions in chicks. *Journal of ocular pharmacology* 6: 151-156.

Laverghetta A V, and Shimizu T (2003) Organization of the ectostriatum based on afferent connections in the zebra finch (*Taeniopygia guttata*). *Brain research* 963: 101-112.

Lee E J, Kim K Y, Gu T H, Moon J I, Kim I B, Lee M Y, Oh S J, and Chun M H (2003) Neuronal nitric oxide synthase is expressed in the axotomized ganglion cells of the rat retina. *Brain research* 986: 174-180.

Levy B, and Sivak J G (1980) Mechanisms of accommodation in the bird eye. *The Journal of comparative physiology* 137: 267-272.

Li J L, Xiao Q, Fu Y X, and Wang S R (1998) Centrifugal innervation modulates visual activity of tectal cells in pigeons. *Visual neuroscience* 15: 411-415.

Li T, and Howland H C (2000) Modulation of constant light effects on the eye by ciliary ganglionectomy and optic nerve section. *Vision research* 40: 2249-2256.

Li T, and Howland H C (2006) Role of the pineal gland in ocular development of the chick in normal and constant light conditions. *Investigative ophthalmology & visual science* 47: 5132-5136.

Li T, Troilo D, Glasser A, and Howland H C (1995) Constant light produces severe corneal flattening and hyperopia in chickens. *Vision research* 35: 1203-1209.

Li W C, Hu J, and Wang S R (1999) Tectal afferents monosynaptically activate neurons in the pigeon isthmo-optic nucleus. *Brain research bulletin* 49: 203-208.

Lindstrom S H, Azizi N, Weller C, and Wilson M (2010) Retinal input to efferent target amacrine cells in the avian retina. *Visual neuroscience* 27: 103-118.

Lindstrom S H, Nacsa N, Blankenship T, Fitzgerald P G, Weller C, Vaney D I, and Wilson M (2009) Distribution and structure of efferent synapses in the chicken retina. *Visual neuroscience* 26: 215-226.

MacNeil M A, Heussy J K, Dacheux R F, Raviola E, and Masland R H (1999) The shapes and numbers of amacrine cells: Matching of photofilled with golgi-stained cells in the rabbit retina and comparison with other mammalian species. *The Journal of comparative neurology* 413: 305-326.

Mariani A P (1982) Association amacrine cells could mediate directional selectivity in pigeon retina. *Nature* 298: 654-655.

Marin G, Letelier J C, and Wallman J (1990) Saccade-related responses of centrifugal neurons projecting to the chicken retina. *Experimental brain research. Experimentelle Hirnforschung. Experimentation cerebrale* 82: 263-270.

Martin G R, Wilson K J, Wild J M, Parsons S, Kubke M F, and Corfield J (2007) Kiwi forego vision in the guidance of their nocturnal activities. *PloS one* 2.

Martin P R, White A J, Goodchild A K, Wilder H D, and Sefton A E (1997) Evidence that blue-on cells are part of the third geniculocortical pathway in primates. *The European journal of neuroscience* 9: 1536-1541.

Martin R D, and Martin A E (1990) *Primate Origins and Evolution: A Phylogenetic Reconstruction*. Princeton University Press.

Maturana H R, and Frenk S (1963) Directional movement and horizontal edge detectors in the pigeon retina. *Science* 142: 977-979.

Maturana H R, and Frenk S (1965) Synaptic connections of centrifugal fibers in pigeon retina. *Science* 150: 359-&.

McBrien N A, and Adams D W (1997) A longitudinal investigation of adult-onset and adult-progression of myopia in an occupational group. Refractive and biometric findings. *Investigative ophthalmology & visual science* 38: 321-333.

McBrien N A, Moghaddam H O, Cottriall C L, Leech E M, and Cornell L M (1995) The effects of blockade of retinal cell action potentials on ocular growth, emmetropization and form deprivation myopia in young chicks. *Vision research* 35: 1141-1152.

McBrien N A, and Norton T T (1992) The development of experimental myopia and ocular component dimensions in monocularly lid-sutured tree shrews (*Tupaia belangeri*). *Vision research* 32: 843-852.

McGill J I (1964) Organization within the central and centrifugal fibre pathways in the avian visual system. *Nature* 204: 395-396.

McGill J I, Powell T P S, and Cowan W M (1966) Retinal representation upon optic tectum and isthmo-optic nucleus in pigeon. *Journal of anatomy* 100: 5-&.

Medina M, Réperant J, Miceli D, Bertrand C, and Bennis M (1998) An immunohistochemical study of putative neuromodulators and transmitters in the centrifugal visual system of the quail (coturnix japonica). *Journal of chemical neuroanatomy* 15: 75-95.

Mertz J R, and Wallman J (2000) Choroidal retinoic acid synthesis: A possible mediator between refractive error and compensatory eye growth. *Experimental eye research* 70: 519-527.

Miceli D, Medina M, and Réperant J (1995a) A neurochemical study of retinal projection neurons and their afferent connections in the quail. *Investigative ophthalmology & visual science* 36: S291-S291.

Miceli D, Réperant J, Bavikati R, Rio J P, and Volle M (1997) Brain-stem afferents upon retinal projecting isthmo-optic and ectopic neurons of the pigeon centrifugal visual system demonstrated by retrograde transneuronal transport of rhodamine β-isothiocyanate. *Visual neuroscience* 14: 213-224.

Miceli D, Réperant J, Bertrand C, and Rio J P (1999) Functional anatomy of the avian centrifugal visual system. *Behavioural brain research* 98: 203-210.

Miceli D, Repérant J, Medina M, Volle M, and Rio J-P (2006) Distribution of ganglion cells in the pigeon retina labeled via retrograde transneuronal transport of the fluorescent dye rhodamine β-isothiocyanate from the telencephalic visual wulst. *Brain research* 1098: 94-105.

Miceli D, Réperant J, Rio J P, and Medina M (1995b) Gaba immunoreactivity in the nucleus isthmo-opticus of the centrifugal visual system in the pigeon - a light and electron microscopic study. *Visual neuroscience* 12: 425-441.

Miles F A (1972a) Centrifugal control of the avian retina. 3. Effects of electrical stimulation of the isthmo-optic tract on the receptive field properties of retinal ganglion cells. *Brain research* 48: 115-129.

Miles F A (1972b) Centrifugal control of the avian retina. Ii. Receptive field properties of cells in the isthmo-optic nucleus. *Brain research* 48: 93-113.

Miles F A (1972c) Centrifugal control of the avian retina. Iv. Effects of reversible cold block of the isthmo-optic tract on the receptive field properties of cells in the retina and isthmo-optic nucleus. *Brain research* 48: 131-145.

Miles F A, and Wallman J (1990) Local ocular compensation for imposed local refractive error. *Vision research* 30: 339-349.

Monakow C v (1889) Experimentelle und pathologisch-anatomische untersuchungen über die optischen centren und bahnen. *European archives of psychiatry and clinical neuroscience* 20: 714-787.

Morgan I G, Miethke P, and Li Z K (1994) Is nitric-oxide a transmitter of the centrifugal projection to the avian retina. *Neuroscience letters* 168: 5-7.

Morrell F (1961) Microelectrode studies in chronic epileptic foci. *Epilepsia* 2: 81-88.

Muchnick N, and Hibbard E (1980) Avian retinal ganglion cells resistant to degeneration after optic nerve lesion. *Experimental neurology* 68: 205-216.

Müller H (1872) *Gesammelte und hinterlassene schriften zur anatomie und physiologie des auges*. Engelmann.

Nickla D L, Damyanova P, and Lytle G (2009) Inhibiting the neuronal isoform of nitric oxide synthase has similar effects on the compensatory choroidal and axial responses to myopic defocus in chicks as does the non-specific inhibitor l-name. *Experimental eye research* 88: 1092-1099.

Nickla D L, Gottlieb M D, Marin G, Rojas X, Britto L R, and Wallman J (1994) The retinal targets of centrifugal neurons and the retinal neurons projecting to the accessory optic system. *Visual neuroscience* 11: 401-409.

Nickla D L, and Wallman J (2010) The multifunctional choroid. *Progress in retinal and eye research* 29: 144-168.

Nolte J, and Angevine J B (2000) *The Human Brain: In Photographs and Diagrams*. Mosby.

Nowak J Z, Żurawska E, and Zawilska J (1989) Melatonin and its generating system in vertebrate retina: Circadian rhythm, effect of environmental lighting and interaction with dopamine. *Neurochemistry international* 14: 397-406.

O'Keefe J, and Nadel L (1979) Precis of O'Keefe and nadel the hippocampus as a cognitive map. *Behavioral and brain sciences* 2: 487-494.

O'Leary D D, and Cowan W M (1982) Further studies on the development of the isthmo-optic nucleus with special reference to the occurrence and fate of ectopic and ipsilaterally projecting neurons. *The Journal of comparative neurology* 212: 399-416.

O'Leary D M, Gerfen C R, and Cowan W M (1983) The development and restriction of the ipsilateral retinofugal projection in the chick. *Brain research* 312: 93-109.

Ohno H, and Uchiyama H (2006) Activity of neurons in the isthmo-optic nucleus and its relationship with head movements. *Neuroscience research* 55: S222-S222.

Oishi T, and Lauber J K (1988) Chicks blinded with formoguanamine do not develop lid suture myopia. *Current eye research* 7: 69-73.

Papastergiou G, Schmid G, Laties A, Pendrak K, Lin T, and Stone R (1998) Induction of axial eye elongation and myopic refractive shift in one-year-old chickens. *Vision research* 38: 1883-1888.

Pearlman A L, and Hughes C P (1976a) Functional role of efferents to the avian retina. I. Analysis of retinal ganglion cell receptive fields. *The Journal of comparative neurology* 166: 111-122.

Pearlman A L, and Hughes C P (1976b) Functional role of efferents to the avian retina. II. Effects of reversible cooling of the isthmo-optic nucleus. *The Journal of comparative neurology* 166: 123-131.

Pequignot Y, and Clarke P G (1992) Maintenance of targeting errors by isthmo-optic axons following the intraocular injection of tetrodotoxin in chick embryos. *The Journal of comparative neurology* 321: 351-356.

Perry V H, Oehler R, and Cowey A (1984) Retinal ganglion cells that project to the dorsal lateral geniculate nucleus in the macaque monkey. *Neuroscience* 12: 1101-1123.

Pettigrew J D, Wallman J, and Wildsoet C F (1990) Saccadic oscillations facilitate ocular perfusion from the avian pecten. *Nature* 343: 362-363.

Pocock G, and Richards C D (2004) *Human Physiology: The basis of medicine*. Oxford University Press.

Powers M K, and Barlow R B (1985) Behavioral-correlates of circadian-rhythms in the limulus visual-system. *Biological bulletin* 169: 578-591.

Rabin J, Van Sluyters R C, and Malach R (1981) Emmetropization: A vision-dependent phenomenon. *Investigative ophthalmology & visual science* 20: 561-564.

Rada J A S, and Wiechmann A F (2006) Melatonin receptors in chick ocular tissues: Implications for a role of melatonin in ocular growth regulation. *Investigative ophthalmology & visual science* 47: 25-33.

Raisman G (1969) Neuronal plasticity in the septal nuclei of the adult rat. *Brain research* 14: 25-48.

Reiner A, Brecha N C, and Karten H J (1982) Basal ganglia pathways to the tectum: The afferent and efferent connections of the lateral spiriform nucleus of pigeon. *The Journal of comparative neurology* 208: 16-36.

Remington L A (2005) *Clinical Anatomy of the Visual System*. Elsevier.

Remy M, and Gunturkun O (1991) Retinal afferents to the tectum opticum and the nucleus opticus principalis thalami in the pigeon. *The Journal of comparative neurology* 305: 57-70.

Réperant J (1973) [new data on visual projections in the pigeon (*Columba livia*). *J Hirnforsch* 14: 151-187.

Réperant J, Araneda S, Miceli D, Medina M, and Rio J P (2000) Serotonergic retinopetal projections from the dorsal raphe nucleus in the mouse demonstrated by combined [(3)h] 5-ht retrograde tracing and immunolabeling of endogenous 5-ht. *Brain research* 878: 213-217.

Réperant J, Medina M, Ward R, Miceli D, Kenigfest N B, Rio J P, and Vesselkin N P (2007) The evolution of the centrifugal visual system of vertebrates. A cladistic analysis and new hypotheses. *Brain research reviews* 53: 161-197.

Réperant J, Miceli D, Vesselkin N P, and Molotchnikoff S (1989) The centrifugal visual-system of vertebrates - a century-old search reviewed. *International review of cytology - A survey of cell biology* 118: 115-171.

Réperant J, Vesselkin N P, Rio J P, Ermakova T V, Miceli D, Peyrichoux J, and Weidner C (1981) Do centrifugal visual pathways only exist in birds? *Revue Canadienne De Biologie* 40: 29-46.

Réperant J, Ward R, Miceli D, Rio J P, Medina M, Kenigfest N B, and Vesselkin N P (2006) The centrifugal visual system of vertebrates: A comparative analysis of its functional anatomical organization. *Brain research reviews* 52: 1-57.

Rodieck R W, Binmoeller K F, and Dineen J (1985) Parasol and midget ganglion cells of the human retina. *The Journal of comparative neurology* 233: 115-132.

Rogers L J, and Miles F A (1972) Centrifugal control of the avian retina. V. Effects of lesions of the isthmo-optic nucleus on visual behaviour. *Brain research* 48: 147-156.

Schaeffel F, Hagel G, Bartmann M, Kohler K, and Zrenner E (1994) 6-hydroxy dopamine does not affect lens-induced refractive errors but suppresses deprivation myopia. *Vision research* 34: 143-149.

Schaeffel F, Hagel G, Kohler K, and Zrenner E (1992) Deprivation myopia and ametropia induced by spectacle lenses result from 2 different mechanisms in chicks. *Investigative ophthalmology & visual science* 33: 1052-1052.

Schaeffel F, and Howland H C (1991) Properties of the feedback loops controlling eye growth and refractive state in the chicken. *Vision research* 31: 717-734.

Schmid K L, and Wildsoet C F (2004) Inhibitory effects of apomorphine and atropine and their combination on myopia in chicks. *Optometry and vision science : official publication of the American Academy of Optometry* 81: 137-147.

Schoenfeld T A, and Hamilton L W (1977) Secondary brain changes following lesions: A new paradigm for lesion experimentation. *Physiology & behavior* 18: 951-967.

Schultze M (1866) Zur anatomie und physiologie der retina. *Archiv für Mikroskopische Anatomie* 2: 175-286.

Seko Y, Tanaka Y, and Tokoro T (1994) Apomorphine inhibition of scleral chondrocyte proliferation is increased by coculture with rpe cells. *Investigative ophthalmology & visual science* 35: 1802-1802.

Seko Y, Tanaka Y, and Tokoro T (1997) Apomorphine inhibits the growth-stimulating effect of retinal pigment epithelium on scleral cells in vitro. *Cell biochemistry and function* 15: 191-196.

Sharpless S K (1964) Reorganization of function in the nervous system--use and disuse. *Annual review of physiology* 26: 357-388.

Sherman S M (2009) Thalamic Mechanisms in Vision. *Encyclopedia of neuroscience*. Oxford Academic Press, pp. 929-944.

Shimizu T, and Bowers A N (1999) Visual circuits of the avian telencephalon: Evolutionary implications. *Behavioural brain research* 98: 183-191.

Shimizu T, and Hodos W (1989) Reversal learning in pigeons: Effects of selective lesions of the wulst. *Behavioral neuroscience* 103: 262-272.

Shimizu T, Patton T B, and Husband S A (2010) Avian visual behavior and the organization of the telencephalon. *Brain, behavior and evolution* 75: 204-217.

Shortess G K, and Klose E F (1975) The area of the nucleus isthmo-opticus in the american kestrel (*Falco sparverius*) and the red-tailed hawk (*Buteo jamaicensis*). *Brain research* 88: 525-531.

Siegwart J T, Jr., and Norton T T (1998) The susceptible period for deprivation-induced myopia in tree shrew. *Vision research* 38: 3505-3515.

Sivak J G (1980) Avian mechanisms for vision in air and water. *Trends in neurosciences* 3: 314-317.

Smith E L, 3rd, Bradley D V, Fernandes A, and Boothe R G (1999) Form deprivation myopia in adolescent monkeys. *Optometry and vision science : official publication of the American Academy of optometry* 76: 428-432.

Smith E L, 3rd, Huang J, Hung L F, Blasdel T L, Humbird T L, and Bockhorst K H (2009) Hemiretinal form deprivation: Evidence for local control of eye growth and refractive development in infant monkeys. *Investigative ophthalmology & visual science* 50: 5057-5069.

Smith E L, 3rd, Hung L F, Kee C S, and Qiao Y (2002) Effects of brief periods of unrestricted vision on the development of form-deprivation myopia in monkeys. *Investigative ophthalmology & visual science* 43: 291-299.

Stavraky G W (1961) Effects of partial denervation on spinal neurones and their possible relation to parkinsonism. *Revue canadienne de biologie / editee par l'Universite de Montreal* 20: 159-166.

Stein D G, Rosen J J, Graziadei J, Mishkin D, and Brink J J (1969) Central nervous system: Recovery of function. *Science* 166: 528-530.

Stone R A, Lin T, Laties A M, and Iuvone P M (1989) Retinal dopamine and form-deprivation myopia. *Proceedings of the national academy of sciences of the United States of America* 86: 704-706.

Strauss O (1995a) The Retinal Pigment Epithelium. In: Kolb H, Fernandez E, and Nelson R [eds.] *Webvision: The organization of the retina and visual system*. Salt Lake City (UT).

Strauss O (1995b) The retinal pigment epithelium. *Webvision: The Organization of the retina and visual system*.

Szel A, Rohlich P, Caffe A R, Juliusson B, Aguirre G, and Van Veen T (1992) Unique topographic separation of two spectral classes of cones in the mouse retina. *The Journal of comparative neurology* 325: 327-342.

Szel A, Rohlich P, Caffe A R, and van Veen T (1996) Distribution of cone photoreceptors in the mammalian retina. *Microscopy research and technique* 35: 445-462.

Szel A, van Veen T, and Rohlich P (1994) Retinal cone differentiation. *Nature* 370: 336.

Temple S E (2011) Why different regions of the retina have different spectral sensitivities: A review of mechanisms and functional significance of intraretinal variability in spectral sensitivity in vertebrates. *Visual neuroscience* 28: 281-293.

Tepelus T C, and Schaeffel F (2010) Individual set-point and gain of emmetropization in chickens. *Vision research* 50: 57-64.

Troilo D, Gottlieb M D, and Wallman J (1987) Visual deprivation causes myopia in chicks with optic nerve section. *Current eye research* 6: 993-999.

Troilo D, and Judge S J (1993) Ocular development and visual deprivation myopia in the common marmoset (*Callithrix jacchus*). *Vision research* 33: 1311-1324.

Troilo D, Li T, Glasser A, and Howland H C (1995) Differences in eye growth and the response to visual deprivation in different strains of chicken. *Vision research* 35: 1211-1216.

Troilo D, and Nickla D L (2005) The response to visual form deprivation differs with age in marmosets. *Investigative ophthalmology & visual science* 46: 1873-1881.

Troilo D, and Wallman J (1991) The regulation of eye growth and refractive state: An experimental study of emmetropization. *Vision research* 31: 1237-1250.

Uchiyama H (1989) Centrifugal pathways to the retina: Influence of the optic tectum. *Visual neuroscience* 3: 183-206.

Uchiyama H, and Ito H (1993) Target-cells for the isthmo-optic fibers in the retina of the japanese quail. *Neuroscience letters* 154: 35-38.

Uchiyama H, and Stell W K (2005) Association amacrine cells of Ramon y Cajal: Rediscovery and reinterpretation. *Visual neuroscience* 22: 881-891.

Uchiyama H, Yamamoto N, and Ito H (1996) Tectal neurons that participate in centrifugal control of the quail retina: A morphological study by means of retrograde labeling with biocytin. *Visual neuroscience* 13: 1119-1127.

Wallman J, and Adams J I (1987) Developmental aspects of experimental myopia in chicks: Susceptibility, recovery and relation to emmetropization. *Vision research* 27: 1139-1163.

Wallman J, Adams J I, and Trachtman J N (1981) The eyes of young chickens grow toward emmetropia. *Investigative ophthalmology & visual science* 20: 557-561.

Wallman J, Gottlieb M D, Rajaram V, and Fugate-Wentzek L A (1987) Local retinal regions control local eye growth and myopia. *Science* 237: 73-77.

Wallman J, and Winawer J (2004) Homeostasis of eye growth and the question of myopia. *Neuron* 43: 447-468.

Walls G L (1942) *The Vertebrate Eye and its Adaptive Radiation*. Cranbrook Institute of Science.

Wang Y, Major D E, and Karten H J (2004) Morphology and connections of nucleus isthmi pars magnocellularis in chicks (*Gallus gallus*). *The Journal of comparative neurology* 469: 275-297.

Wang Y C, Jiang S, and Frost B J (1993) Visual processing in pigeon nucleus rotundus: Luminance, color, motion, and looming subdivisions. *Visual neuroscience* 10: 21-30.

Wassle H (2004) Parallel processing in the mammalian retina. *Nature reviews. Neuroscience* 5: 747-757.

Watanabe M, and Rodieck R W (1989) Parasol and midget ganglion cells of the primate retina. *The Journal of comparative neurology* 289: 434-454.

Wei W, and Feller M B (2011) Organization and development of direction-selective circuits in the retina. *Trends in neurosciences* 34: 638-645.

Weidner C, Réperant J, Desroches A M, Miceli D, and Vesselkin N P (1987) Nuclear-origin of the centrifugal pathway in birds of prey. *Brain research* 436: 153-160.

Weidner C, Réperant J, Miceli D, Haby M, and Rio J P (1985) An anatomical study of ipsilateral retinal projections in the quail using radioautographic, horseradish peroxidase, fluorescence and degeneration techniques. *Brain research* 340: 99-108.

Weiss S, and Schaeffel F (1993) Diurnal growth rhythms in the chicken eye: Relation to myopia development and retinal dopamine levels. *Journal of comparative physiology. A, Sensory, neural, and behavioral physiology* 172: 263-270.

Weller C, Lindstrom S H, De Grip W J, and Wilson M (2009) The area centralis in the chicken retina contains efferent target amacrine cells. *Visual neuroscience* 26: 249-254.

Wiechmann A F, and Summers J A (2008) Circadian rhythms in the eye: The physiological significance of melatonin receptors in ocular tissues. *Progress in retinal and eye research* 27: 137-160.

Wiesel T N, and Hubel D H (1974) Ordered arrangement of orientation columns in monkeys lacking visual experience. *The Journal of comparative neurology* 158: 307-318.

Wiesel T N, and Raviola E (1979) Increase in axial length of the macaque monkey eye after corneal opacification. *Investigative ophthalmology & visual science* 18: 1232-1236.

Wild J M (1987) Thalamic projections to the paleostriatum and neostriatum in the pigeon (columba livia). *Neuroscience* 20: 305-327.

Wildsoet C (2003) Neural pathways subserving negative lens-induced emmetropization in chicks: Insights from selective lesions of the optic nerve and ciliary nerve. *Current eye research* 27: 371-385.

Wildsoet C, and Wallman J (1995) Choroidal and scleral mechanisms of compensation for spectacle lenses in chicks. *Vision research* 35: 1175-1194.

Wildsoet C F (1997) Active emmetropization - evidence for its existence and ramifications for clinical practice. *Ophthalmic and physiological optics : The Journal of the British College of Ophthalmic Opticians* 17: 279-290.

Wildsoet C F, and Schmid K L (2000) Optical correction of form deprivation myopia inhibits refractive recovery in chick eyes with intact or sectioned optic nerves. *Vision research* 40: 3273-3282.

Wilson M, and Lindstrom S H (2011) What the bird's brain tells the bird's eye: The function of descending input to the avian retina. *Visual neuroscience* 28: 337-350.

Winawer J, Zhu X, Choi J, and Wallman J (2005) Ocular compensation for alternating myopic and hyperopic defocus. *Vision research* 45: 1667-1677.

Wingstrand K G, and Munk O (1965) *The Pecten Oculi of the Pigeon with Particular Regard to its Function*.

Witkovsky P (2004) Dopamine and retinal function. *Documenta ophthalmologica* 108: 17-40.

Wizenmann A, and Thanos S (1990) The developing chick isthmo-optic nucleus forms a transient efferent projection to the optic tectum *Neuroscience letters* 113: 241-246.

Wolf-Oberhollenzer F (1987) A study of the centrifugal projections to the pigeon retina using two fluorescent markers. *Neuroscience letters* 73: 16-20.

Woodson W, Reiner A, Anderson K, and Karten H J (1991) Distribution, laminar location, and morphology of tectal neurons projecting to the isthmo-optic nucleus and the nucleus isthmi, pars parvocellularis in the pigeon (columba livia) and chick (*Gallus domesticus*): A retrograde labelling study. *The Journal of comparative neurology* 305: 470-488.

Woodson W, Shimizu T, Wild J M, Schimke J, Cox K, and Karten H J (1995) Centrifugal projections upon the retina - an anterograde tracing study in the pigeon (*Columba livia*). *The Journal of comparative neurology* 362: 489-509.

Yamagata M, and Sanes J R (1995) Lamina-specific cues guide outgrowth and arborization of retinal axons in the optic tectum. *Development* 121: 189-200.

Yinon U, Rose L, and Shapiro A (1980) Myopia in the eye of developing chicks following monocular and binocular lid closure. *Vision research* 20: 137-141.

Zeigler H P, and Bischof H J (1993) *Vision, Brain, and Behavior in Birds*. Mit Press.

Zeigler H P, and Miller M (1975) Trigeminal nerve and eating in the pigeon (*Columba livia*): Neurosensory control of the consummatory responses. *The Journal of comparative and physiological psychology* 89: 845-858.

Zhu X, Park T W, Winawer J, and Wallman J (2005) In a matter of minutes, the eye can know which way to grow. *Investigative ophthalmology & visual science* 46: 2238-2241.

Zhu X, Winawer J A, and Wallman J (2003) Potency of myopic defocus in spectacle lens compensation. *Investigative ophthalmology & visual science* 44: 2818-2827.

Zucker C L, and Dowling J E (1987) Centrifugal fibres synapse on dopaminergic interplexiform cells in the teleost retina. *Nature* 330: 166-168.